



**THE SYNTHESIS AND CHARACTERIZATION OF RUTHENIUM  
COMPLEXES FOR DYE SENSITIZED SOLAR CELLS  
APPLICATION**

**YURANAN THATHONG**

**A THESIS SUBMITTED IN PARTIAL FULFILLMENT OF THE REQUIREMENTS  
FOR THE DEGREE OF MASTER OF SCIENCE  
MAJOR IN CHEMISTRY  
FACULTY OF SCIENCE  
UBON RATCHATHANI UNIVERSITY  
YEAR 2013  
COPYRIGHT OF UBON RATCHATHANI UNIVERSITY**



**THESIS APPROVAL**  
**UBON RATCHATHANI UNIVERSITY**  
**MASTER OF SCIENCE**  
**MAJOR IN CHEMISTRY FACULTY OF SCIENCE**

**TITLE** THE SYNTHESIS AND CHARACTERIZATION OF RUTHENIUM COMPLEXES  
FOR DYE SENSITIZED SOLAR CELLS APPLICATION

**NAME** MISS YURANAN THATHONG

**THIS THESIS HAS BEEN ACCEPTED BY**

*Rukkiat Jitchati*  
..... CHAIR

(ASST.PROF.DR.RUKKIAT JITCHATI)  
*Tienthong Thongpanchang*  
..... COMMITTEE  
(ASST.PROF.DR.TIENTHONG THONGPANCHANG)

*[Signature]*  
..... COMMITTEE  
(DR.KITTIYA WONGKHAN)

*P. Saejueng*  
..... COMMITTEE  
(DR.PRANORM SAEJUENG)

*[Signature]*  
..... DEAN  
(ASST.PROF.DR.JANPEN INTARAPRASERT)

**APPROVAL BY UBON RATCHATHANI UNIVERSITY**

*Utith Inprasit*  
.....  
(ASSOC.PROF.DR.UTITH INPRASIT)

VICE PRESIDENT FOR ACADEMIC AFFAIRS

FOR THE PRESIDENT OF UBON RATCHATHANI UNIVERSITY

ACADEMIC YEAR 2013

## ACKNOWLEDGEMENTS

First and foremost, I would like to deeply express my appreciation to my advisor Asst.Prof.Dr. Rukkiat Jitchati, without whom I would never have started and finished this thesis, for his excellent guidance and advices during the doing and writing of this thesis.

I would like give a special thanks to Asst.Prof.Dr. Tienthong Thongpanchang for his excellent suggestions, Dr. Kittiya Wongkhan and Dr. Pranorn Saejueng for constructive comment and valuable suggestion for this thesis. I am also thankful to Asst.Prof.Dr. Taweesak Sudyoadsuk and Assoc.Prof.Dr. Sayant Saengsuwan for available machine to DSSCs devices and thank to my friends, sisters and brothers in my laboratory, center of organic electronic and alternative energy (COEA), for their helpful advices.

I would like to thank Prof. Yoshiro Yamashita, Tokyo Institute of Technology (Japan) for available instruments. I am especially grateful to Science Achievement Scholarship of Thailand. Lastly, and most importantly, I feel appreciate and grateful to my family for their supporting on my education.

T. Yuranan  
(Miss Yuranan Thathong)

Researcher

## บทคัดย่อ

- ชื่อเรื่อง : การสังเคราะห์และพิสูจน์เอกลักษณ์สาร โลหะเชิงซ้อนรูทีเนียม เพื่อประยุกต์ใช้เป็นสีย้อมไวแสงในโซลาร์เซลล์
- โดย : ยุระนันท์ ทาทอง
- ชื่อปริญญา : วิทยาศาสตรมหาบัณฑิต
- สาขาวิชา : เคมี
- ประธานกรรมการที่ปรึกษา : ผู้ช่วยศาสตราจารย์ ดร. รักเกียรติ จิตคดี
- ศัพท์สำคัญ : โซลาร์เซลล์ สีย้อมไวแสง สารโลหะเชิงซ้อนรูทีเนียม

งานวิจัยนี้ กลุ่มผู้วิจัยรายงานการสังเคราะห์ สารประกอบโลหะเชิงซ้อนรูทีเนียม 3 ชนิด ได้แก่ ชนิด โอโมเลพติก YN-N3 (syn) ซึ่งไม่มีเกลือเตตระโบรไมด์แอมโมเนียมเป็นส่วนประกอบ สารประกอบโลหะเชิงซ้อนรูทีเนียมชนิดเฮเทอโรเลพติก ไพริดีน มีเกลือเตตระโบรไมด์แอมโมเนียมเป็นส่วนประกอบ (YN-pber และ YN-06) และสารประกอบโลหะเชิงซ้อนรูทีเนียมชนิดโอโมเลพติกและเฮเทอโรเลพติก โดยมีเกลือเตตระโบรไมด์แอมโมเนียมเป็นส่วนประกอบ (YN-719, YN-07 และ YN-08 ตามลำดับ) สารโลหะเชิงซ้อนรูทีเนียมทั้งหมดได้พิสูจน์เอกลักษณ์ด้วยเทคนิค นิวเคลียร์แมกเนติกเรโซแนนซ์ (NMR) ฟลูออโรทรานสฟอร์ม อินฟราเรดสเปกโทรสโกปี (FT-IR) แมสสเปกโทรสโกปี (MS) ไซคลิกโวลแทมเมตรี (CV) และเทคนิคสเปกโทรสโกปี ประสิทธิภาพการเปลี่ยนแปลงพลังงานแสงเป็นพลังงานไฟฟ้าพบว่า อุปกรณ์สีย้อมไวแสงที่ใช้ YN-719 ร่วมกับสารละลายอิเล็กโทรไลต์ชนิดของเหลว 0.05 โมลาร์ ไทโอซีน 0.4 โมลาร์ 4-เทอเทียรี-บิวทิลโพธิลีน 0.1 โมลาร์ ลิเทียมไอโอไดด์ 0.6 โมลาร์ เตตระไพริดีนแอมโมเนียม ไอโอไดด์ แสดงประสิทธิภาพการเปลี่ยนแปลงพลังงานแสงเป็นพลังงานไฟฟ้าสูงสุดร้อยละ 4.57 ภายใต้ความเข้มแสงมาตรฐานที่ AM 1.5 ความเข้มแสงเท่ากับ 100 มิลลิวัตต์ต่อตารางเซนติเมตร

## ABSTRACT

TITLE : THE SYNTHESIS AND CHARACTERIZATION OF RUTHENIUM  
COMPLEXES FOR DYE SENSITIZED SOLAR CELLS APPLICATION  
BY : YURANAN THATHONG  
DEGREE : MASTER OF SCIENCE  
MAJOR : CHEMISTRY  
CHAIR : ASST.PROF. RUKKLAT JITCHAU, Ph.D.

KEYWORDS : SOLAR CELLS / DYE SENSITIZER / RUTHENIUM COMPLEXES

In this research, we reported the synthesis of the three series ruthenium(II) complexes, for example; homoleptic ruthenium(II) complex without tetrabutylammonium salt, named YN-N3 (syn), heteroleptic pyridyl ruthenium(II) complexes with tetrabutylammonium salt (YN-phen, YN-06) and homoleptic and heteroleptic ruthenium(II) complexes with tetrabutyl ammonium salt (YN-719, YN-07 and YN-08), respectively. All ruthenium(II) complexes were characterized by nuclear magnetic resonance spectroscopy (NMR), fourier transform infrared spectroscopy (FT-IR), mass spectroscopy (MS), cyclic voltammetry (CV) as well as absorption spectroscopy techniques. The ruthenium(II) complexes were tested the solar light to conversion efficiency using the liquid electrolyte (0.05 M I<sub>2</sub>, 0.4 M 4-tert-butylpropylene, 0.1 M LiI, 0.6 M tetrapyridylammonium iodide). The device sensitized by YN-719 shows the highest photovoltaic efficiency of 4.57% under a standard AM 1.5 irradiation (100 mW/cm<sup>2</sup>).

## CONTENTS

	<b>PAGES</b>
<b>ACKNOWLEDGEMENTS</b>	<b>I</b>
<b>THAI ABSTRACT</b>	<b>II</b>
<b>ENGLISH ABSTRACT</b>	<b>III</b>
<b>CONTENTS</b>	<b>IV</b>
<b>LIST OF TABLES</b>	<b>VII</b>
<b>LIST OF FIGURES</b>	<b>VIII</b>
<b>LIST OF ABBREVIATIONS</b>	<b>XIV</b>
<b>CHAPTER</b>	
<b>1 INTRODUCTION</b>	
1.1 Importance in research and development	1
1.2 Dye sensitized solar cells (DSSCs)	2
1.3 Component of dye sensitized solar cells	3
1.4 Principle of dye-sensitized solar cells	6
1.5 Key efficiency parameters of the DSSCs	7
1.6 Type of dye sensitized solar cells (DSSCs)	9
1.6.1 Organic sensitizers	9
1.6.2 Porphyrin sensitizers	11
1.6.3 Ruthenium sensitizers	12
1.7 Aims of thesis	14
<b>2 LITERATURE REVIEWS</b>	
2.1 Literature reviews	16
<b>3 EXPERIMENTAL</b>	
3.1 Chemicals	25
3.2 Instruments and general chemical characterization techniques	28
3.2.1 General instruments	28

## CONTENTS (CONTINUED)

	PAGES
3.2.2 General chemical characterization techniques	28
3.3 Experimental section	30
3.3.1 Ligand and ruthenium precursor synthesis	31
3.3.2 Homoleptic ruthenium(II) complex without tetrabutylammonium salt synthesis	33
3.3.3 Heteroleptic pyridyl ruthenium(II) complexes with tetrabutylammonium salt synthesis	34
3.3.4 Homoleptic and heteroleptic ruthenium(II) complexes with tetrabutylammonium salt synthesis	36
3.4 DSSCs device fabrication	
3.4.1 Main chemical reagents	39
3.4.2 Ingredient of electrolyte solution	39
3.4.3 Preparation of FTO glass	39
3.4.4 Fabrication of dye sensitized solar cells	40
3.4.5 Measuring instrument techniques	41
<b>4 RESULTS AND DISCUSSIONS</b>	
4.1 The synthesis homoleptic ruthenium(II) complex without tetrabutylammonium salt	43
4.1.1 The synthesis of di- $\mu$ -chloro-bis[( $\eta^6$ - benzene)chlororuthenium(II)] (YN-05)	44
4.1.2 The synthesis of 4,4'-dicarboxy-2,2'-bipyridine (YN-04)	45
4.1.3 The synthesis of homoleptic ruthenium(II) YN-N3 (syn)	49
4.1.4 Characterization of homoleptic ruthenium(II) complex dye without tetrabutylammonium salt	51

## CONTENTS (CONTINUED)

	PAGES
4.2 The synthesis of heteroleptic pyridyl ruthenium(II) complexes with tetrabutyl ammonium salt	57
4.2.1 The synthesis of dipyrido[3,2-a:2',3'-c]phenazine (YN-01)	57
4.2.2 The synthesis of heteroleptic ruthenium(II) (YN-phen)	59
4.2.3 Characterization of heteroleptic pyridyl ruthenium(II) complex dyes	62
4.3 Synthesis homoleptic and heteroleptic ruthenium(II) complexes with tetrabutyl ammonium salt	66
4.3.1 Characterization homoleptic and heteroleptic ruthenium(II) complex dyes	68
<b>5 CONCLUSIONS</b>	<b>75</b>
<b>REFERENCES</b>	<b>76</b>
<b>APPENDICES</b>	
A Results of characterized studies	87
B Mass spectra of ligand and ruthenium(II) complexes	99
C Publication papers	110
<b>VITAE</b>	<b>134</b>

## LIST OF TABLES

TABLE		PAGES
3.1	Chemicals for synthesis	25
3.2	Chemicals for DSSCs devices	27
3.3	Instruments	28
4.1	The absorption of <b>YN-N3 (syn)</b> and <b>N3 (std)</b> solution in dry DMF	52
4.2	Cyclic voltammetric results for <b>YN-N3 (syn)</b> and <b>N3 (std)</b>	54
4.3	Solar light to electricity conversion efficiency with the <b>YN-N3 (syn)</b> and <b>N3 (std)</b> ruthenium(II) complexes	56
4.4	The absorption of <b>YN-phen</b> and <b>YN-06</b> in DMF solution	62
4.5	Cyclic voltammetric result for <b>YN-phen</b> and <b>YN-06</b>	64
4.6	Solar light to electricity conversion efficiency with the <b>YN-phen</b> and <b>YN-06</b> ruthenium(II) complexes	66
4.7	The absorption of <b>YN-719</b> , <b>YN-07</b> and <b>YN-08</b> in DMF solution	70
4.8	Cyclic voltammetric result for <b>YN-719</b> , <b>YN-07</b> and <b>YN-08</b>	71
4.9	Solar light to electricity conversion efficiency with the <b>YN-719</b> , <b>YN-07</b> and <b>YN-08</b> ruthenium(II) complexes	74
5.1	Solar light to electricity conversion efficiency with ruthenium(II) complexes	76

## LIST OF FIGURES

FIGURE		PAGES
1.1	Incident photon to current conversion efficiency as a function of the wavelength for the standard N3 (red line), Black dye (black line), and the bare nanocrystalline TiO <sub>2</sub> film (blue line)	2
1.2	Composition of dye sensitized solar cells	3
1.3	Principle of operation and energy level scheme of the dye sensitized nanocrystalline solar cells	6
1.4	Chemical structure of C219 dye	9
1.5	Chemical structure of XS29, HKK-BTZ4, SB3, NKX-2700 and NKX-2586 dyes	10
1.6	Chemical structure of JK2 and UB3 dyes	11
1.7	Chemical structure of Zn-1a and Zn-TCPP dyes	11
1.8	Chemical structure of YD0, YD2 and DTBC dyes	12
1.9	Chemical structure of N3, BLACK Dye and N719 dyes	13
1.10	Possible binding modes for carboxylic group on TiO <sub>2</sub>	14
2.1	Molecular structure of N3 sensitizer	17
2.2	Molecular structure of JK-92 and S8 dyes	18
2.3	Molecular structure of ruthenium sensitizer CYC-B5	19
2.4	Molecular structure of N719 sensitizer	19
2.5	Molecular structure of K77 dye	20
2.6	Molecular structure of T18 dye	21
2.7	Molecular structure of CYC-B12 dye	22
2.8	Molecular structure of Ru(II)pp and Ru(II)pdpa dyes	23
2.9	A series of heteroleptic ruthenium(II) (Ar 20, Ar 24, Ar 25 and Ar 27)	23
2.10	Molecular structure of YS5 dye	24
3.1	Experimental chart of this work	30

## LIST OF FIGURES (CONTINUED)

FIGURE		PAGES
3.2	The finishing FTO glasses (working electrode (WE) and counter electrode (CE))	40
3.3	A completed dye sensitized solar cells device	41
4.1	The synthesis of ruthenium(II) complex dye (YN-N3 (syn))	43
4.2	Synthetic method of YN-05 ruthenium(II) precursor	44
4.3	<sup>1</sup> H NMR in CDCl <sub>3</sub> of precursor ruthenium complex (YN-05)	44
4.4	The synthetic route to 4,4'-dicarboxy-2,2'-bipyridine (YN-04)	45
4.5	The propose mechanism of Sandmeyer reaction	46
4.6	The synthetic method of 4,4'-dimethyl-2,2'-bipyridine (YN-03)	46
4.7	The propose mechanism of homocoupling reaction	47
4.8	Synthetic method of 4,4'-dicarboxylic-2,2'-bipyridine (YN-04)	48
4.9	The propose mechanism of oxidation reaction	48
4.10	<sup>1</sup> H NMR in DMSO-d <sub>6</sub> of 4,4'-dicarboxylic-2,2'-bipyridine (YN-04)	49
4.11	The synthetic route of ligand substitution reaction to YN-N3 (syn)	50
4.12	<sup>1</sup> H NMR of YN-N3 (syn) in CD <sub>3</sub> OD	51
4.13	UV-Vis absorption spectra of 1×10 <sup>-5</sup> M YN-N3 (syn) and N3 (std) solution in DMF at room temperature	52
4.14	Cyclic voltammogram for YN-N3 (syn) and N3 (std) in 1×10 <sup>-4</sup> M solution DMF at scan rate 100 mV/s with 0.1 M [Bu <sub>4</sub> N]PF <sub>6</sub> supporting electrolyte	53
4.15	Energy diagram for the YN-N3 (syn) and N3 (std) sensitized TiO <sub>2</sub> solar cells with iodine redox electrolyte	54
4.16	A: IV characteristic of N3 (std) and YN-N3 (syn) under AM 1.5 G radiation (100 mW/cm <sup>2</sup> ) and B: incident photo to current conversion efficiency spectra for dye sensitized solar cells based on N3 (std) and YN-N3 (syn)	56
4.17	Molecular structure of heteroleptic pyridyl ruthenium(II) complexes	57

## LIST OF FIGURES (CONTINUED)

FIGURE		PAGES
4.18	Synthesis of dipyrido[3,2-a:2',3'-c]phenazine (YN-01)	58
4.19	The propose mechanism of cyclization reaction	58
4.20	<sup>1</sup> H NMR of YN-01 ligand in CDCl <sub>3</sub>	59
4.21	The propose synthetic route of ligand substitution reaction of YN-phen	60
4.22	<sup>1</sup> H NMR in CDCl <sub>3</sub> of heteroleptic pyridyl ruthenium(II) (YN-phen)	61
4.23	The structure of ruthenium(II) complex dye (YN-06)	61
4.24	UV-Vis absorption spectra of 1×10 <sup>-5</sup> M YN-phen and YN-06 solution in DMF at room temperature	62
4.25	Cyclic voltammogram for YN-phen and YN-06 in 1×10 <sup>-4</sup> M DMF solution at scan rate 100 mV/s with 0.1 M [Bu <sub>4</sub> N]PF <sub>6</sub> supporting electrolyte	63
4.26	Energy diagram for the YN-phen and YN-06 sensitized TiO <sub>2</sub> solar cells with iodine redox electrolyte	64
4.27	A: IV characteristic of YN-phen and YN-06 under AM 1.5 G radiation (100 mW/cm <sup>2</sup> ) and B: incident photo to current conversion efficiency spectra for dye sensitized solar cells based on YN-phen and YN-06.	65
4.28	Molecular structure of homoleptic and hereroleptic ruthenium(II) complexes	66
4.29	The YN-719 ruthenium(II) complex structure	67
4.30	<sup>1</sup> H NMR in DMSO-d <sub>6</sub> of homoleptic ruthenium(II) (YN-719)	67
4.31	Molecular structure of heteroleptic ruthenium(II) complex (YN-07)	68
4.32	Structure of homoleptic ruthenium(II) complex (YN-08)	68
4.33	UV-Vis absorption spectra of 1×10 <sup>-5</sup> M YN-719, YN-07 and YN-08 solution in DMF at room temperature	69
4.34	Cyclic voltammogram of 1×10 <sup>-4</sup> M YN-719, YN-07 and YN-08 in DMF at scan rate 100 mV/s with 0.1 M [Bu <sub>4</sub> N]PF <sub>6</sub> supporting electrolyte	71

## LIST OF FIGURES (CONTINUED)

FIGURE		PAGES
4.35	Energy diagram for the YN-719, YN-07 and YN-08 sensitized TiO <sub>2</sub> solar cells with iodine redox electrolyte	72
4.36	A: IV characteristic of YN-719, YN-07 and YN-08 under AM 1.5 G radiation (100 mW/cm <sup>2</sup> ) and B: incident photo to current conversion efficiency spectra for dye sensitized solar cells based on YN07, YN-08 and YN-719	73
A.1	<sup>1</sup> H NMR, <sup>13</sup> C NMR in CDCl <sub>3</sub> at room temperature and FT-IR spectra of dipyrido[3,2-a:2',3'-c]phenazine (YN-01)	88
A.2	<sup>1</sup> H NMR, <sup>13</sup> C NMR in CDCl <sub>3</sub> at room temperature and FT-IR spectra of 2-bromo-4-methylpyridine (YN-02)	89
A.3	<sup>1</sup> H NMR, <sup>13</sup> C NMR in CDCl <sub>3</sub> at room temperature and FT-IR spectra of 4,4'-dimethyl-2,2'-bipyridine (YN-03)	90
A.4	<sup>1</sup> H NMR, <sup>13</sup> C NMR in DMSO-d <sub>6</sub> at room temperature and FT-IR spectra of 4,4'-dicarboxylic-2,2'-bipyridine (YN-04)	91
A.5	<sup>1</sup> H NMR, <sup>13</sup> C NMR in CDCl <sub>3</sub> at room temperature and FT-IR spectra of di-μ-chloro bis [(η <sup>6</sup> -benzene)chlororuthenium(II)] (YN-05)	92
A.6	<sup>1</sup> H NMR, <sup>13</sup> C NMR in CD <sub>3</sub> OD at room temperature and FT-IR spectra of bis(4,4'-dicarboxy-2,2'-bipyridine)dithiocyanatoruthenium(II), YN-N3 (syn)	93
A.7	<sup>1</sup> H NMR, <sup>13</sup> C NMR in DMSO-d <sub>6</sub> at room temperature and FT-IR spectra of tetrabutylammonium (1,10-phenanthroline)(4-carboxy-2,2'-bipyridine-4'-carboxylate)dithiocyanatoruthenium(II) ion (YN-phen)	94
A.8	<sup>1</sup> H NMR, <sup>13</sup> C NMR in DMSO-d <sub>6</sub> at room temperature and FT-IR spectra of tetrabutylammonium dipyrido[3,2-a:2',3'-c]phenazine(4-carboxy-2,2'-bipyridine-4'-carboxylate)dithiocyanatoruthenium(II) ion (YN-06)	95

## LIST OF FIGURES (CONTINUED)

FIGURE		PAGES
A.9	<sup>1</sup> H NMR, <sup>13</sup> C NMR in DMSO-d <sub>6</sub> at room temperature and FT-IR spectra of bis(tetrabutylammonium)(bis(4-carboxy-2,2'-bipyridine-4'-carboxylate)dithiocyanatoruthenium(II) ion (YN-719)	96
A.10	<sup>1</sup> H NMR, <sup>13</sup> C NMR in DMSO-d <sub>6</sub> at room temperature and FT-IR spectra of tetrabutylammonium (2,2'-biquinoline-4,4'-dicarboxylic acid)(4-carboxy-2,2'-bipyridine-4'-carboxylate)dithiocyanato ruthenium(II) ion (YN-07)	97
A.11	<sup>1</sup> H NMR, <sup>13</sup> C NMR in DMSO-d <sub>6</sub> at room temperature and FT-IR spectra of bis(tetrabutylammonium)bis(4-carboxy-2,2'-biquinoline-4'-carboxylate)dithiocyanatoruthenium(II) ion (YN-08)	98
B.1	Mass spectrum of dipyrido[3,2-a:2',3'-c]phenazine (YN-01)	100
B.2	Mass spectrum of 4,4'-dimethyl-2,2'-bipyridine	101
B.3	Mass spectrum of 4,4'-dicarboxy-2,2'-bipyridine (YN-04)	102
B.4	Mass spectrum of di- <i>μ</i> -chloro-bis(η <sup>6</sup> -benzene)chlororuthenium(II) (YN-05)	103
B.5	Mass spectrum of bis(4,4'-dicarboxy-2,2'-bipyridine)dithiocyanato ruthenium(II) (YN-N3)	104
B.6	Mass spectrum of tetrabutylammonium(1,10-phenanthroline)(4-carboxy-2,2'-bipyridine-4'-carboxylate)dithiocyanatoruthenium(II) ion (YN-phen)	105
B.7	Mass spectrum of tetrabutylammoniumdipyrido[3,2-a:2',3'-c]phenazine (4-carboxy-2,2'-bipyridine-4'-carboxylate)dithiocyanatoruthenium(II) ion (YN-06)	106
B.8	Mass spectrum of bis(tetrabutylammonium)(bis(4-carboxy-2,2'-bipyridine-4'-carboxylate)dithiocyanatoruthenium(II) ion (YN-719)	107

## LIST OF FIGURES (CONTINUED)

FIGURE		PAGES
B.9	Mass spectrum of tetrabutylammonium(4,4'-dicarboxy-2,2'-biquinoline) (4-carboxy-2,2'-bipyridine-4'-carboxylate)dithiocyanatoruthenium(II) ion (YN-07)	108
B.10	Mass spectrum of bis(tetrabutylammonium)bis(4-carboxy-2,2'-biquinoline- 4'-carboxylate)dithiocyanatoruthenium(II) ion (YN-08)	109

## LIST OF ABBREVIATIONS

<b>Abbreviation</b>	<b>Full word</b>
A	Ampere
AR	Analysis reagent
aq.	Aqueous
AM	Air mass
anh.	Anhydrous
Ar	Aromatic
bipy	Bypyridine
conc.	Concentrated
cm <sup>-1</sup>	Reciprocal centimeter (unit of wave number)
<sup>13</sup> C NMR	Carbon 13 nuclear magnetic resonance
°C	Degree celsius
CB	Conduction band
cm	Centimeter
cm <sup>3</sup>	Centimeter cubic unit
D	Deuterium
d	Doublet (for NMR spectral data)
dd	Double of doublet (for NMR spectral data)
DCM	Dichloromethane
dcbiq	4,4'-Dicarboxy-2,2'-biquinoline
dcphen	Dicarboxy phenanthroline
dil.	Diluted
DMF	Dimethyl formamide
DMSO	Dimethyl sulfoxide
DSSCs	Dye sensitized solar cells
E <sub>g</sub>	Energy gap

## LIST OF ABBREVIATIONS (CONTINUED)

Abbreviation	Full word
EN	Electronegativity
eV	Electron volt
EtOAc	Ethyl acetate
FAB-MS	Fast atomic bombardment mass spectrometry
FT-IR	Fourier transform infrared spectroscopy
FTO	Fluoride doped tin oxide
g	Gram
h	Hour
HOMO	Highest occupied molecular orbital
<sup>1</sup> H NMR	Proton nuclear magnetic resonance
Hz	Hertz
$I_{max}$	Maximum current
IPCE	Incident photon to current conversion efficiency
IR	Infrared
$J$	Coupling constant (for NMR spectral data)
$J_x$	Short circuit current density
L	Liter
LUMO	Lowest unoccupied molecular orbital
M	Molarity
m	Multiplet (for NMR spectral data)
mA	Milli ampere
m <sup>2</sup>	Square meter
MHz	Mega hertz
ml	Milliliter
MLCT	Metal to ligand charge transfer
mM	Milli molar

## LIST OF ABBREVIATIONS (CONTINUED)

Abbreviation	Full word
mmol	Millimol
m.p.	Melting point
mV	Milli volt
NHE	Normal hydrogen electrode
nm	Nanometer
Ox	Oxidation
phen	1,10-Phenanthroline
ppm	Part per million
Pt	Platinum
q	Quartet (for NMR spectral data)
Red	Reduction
Ru	Ruthenium
s	Singlet (for NMR spectral data)
s	Second
$S^*$	Excited state form of dye electron
$S^0$	Ground state form of dye electron
TBAOH	Tetrabutylammonium hydroxide
TBP	4-Tert-butylpyridine
TCO	Transparent conducting oxides
TLC	Thin layer chromatography
TMS	Tetramethyl silane
TW	Tera watts
t	Triplet (for NMR spectral data)
UV-Vis	Ultra violet-visible
V	Volume
VB	Valence band
$V_{max}$	Maximum voltage

## LIST OF ABBREVIATIONS (CONTINUED)

Abbreviation	Full word
$V_{oc}$	Open circuit voltage
W	Watt
$\alpha$	Alpha
$\mu$	Bridging ligand
$\delta$	Chemical shift (for NMR spectral data)
$f$	Fill factor
$\mu\text{m}$	Micro meter
$\epsilon$	Molar absorptivity
$p$	Para
$\eta^6$	Hexa hapto
$\eta$	Solar light to electricity conversion efficiency
$\lambda$	Wavelength

# CHAPTER I

## INTRODUCTION

### 1.1 Importance in research and development

Energy is a primary importance factor to develop our world. Currently, the energy requirement for seven billion people worldwide is estimated about 13 terawatts (TW) and this is expected to go up to 23 TW in a next 40 years. Hence, the scientists realize that we need to find alternative energy sources. Three viable options are being discussed: carbon-fuel-based sources, nuclear power and renewable energy sources. The first option is carbon-fuel-based energy that impacts to the environment. When we choose this option, it will lead to a substantial increase in the CO<sub>2</sub> levels. For the nuclear power option, the production process of nuclear power caused dispose of the dangerous nuclear fuel wastes. Thus, the renewable energy source is the best choice for several reasons, such as no worry about CO<sub>2</sub> levels in the atmosphere, clean and safe. There are many renewable energy sources, for examples, wind energy, water energy, biomass energy and solar energy [1].

The sun becomes the good choice of renewable energy. It is a natural source of clean energy, sustainable energy and friendly environment. Many research groups have been interested to use of solar energy to produce electrical power. One specific emerging technology will permit direct conversion of sunlight to electricity, called photovoltaic solar cell [2]. In 1954, photovoltaic solar cell and photovoltaic P-N type semiconductor single crystal silicon have developed to provide the first high performance by Chapin et al., Bell Laboratories, USA [3, 4]. After that, several researchers have developed P-N type semiconductor materials to improve efficiency until now. However, the manufacturing process to produce P-N solar cell need advanced technology and high purity of semiconductor material. For that reason, another type of solar cell was developed in 1991 by Grätzel's group [5, 6], as we called dye sensitized solar cell (DSSCs). This type of solar cell has similar efficiency with P-N type semiconductor silicon solar cell but it is easier to fabricate. It has lower production costs as well as flexible [7].

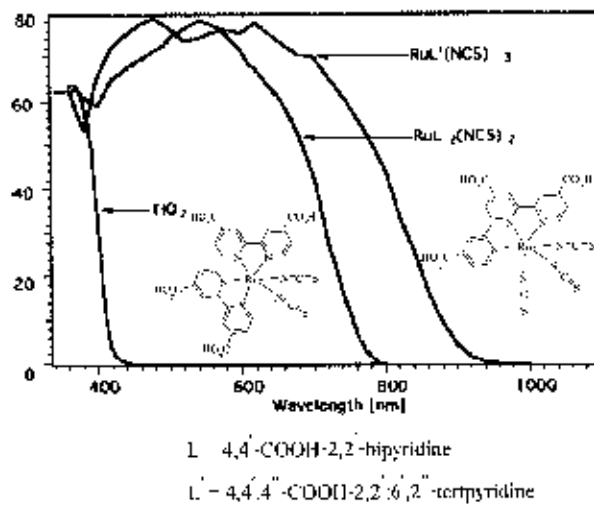


**Figure 1.1** Incident photon to current conversion efficiency as a function of the wavelength for the standard **N3** (red line), **Black dye** (black line), and the bare nanocrystalline  $TiO_2$  film (blue line)

### 1.2 Dye sensitized solar cells (DSSCs)

Dye sensitized solar cells (DSSCs) are the new class of photo electrochemical cells. Over the past decades, DSSCs have attracted a widespread in both academic and commercial for the conversion of sunlight into electricity. The DSSCs device, in Figure 1.2, composes of five major parts; 1) dye sensitizer, 2) nanocrystalline metal oxide semiconductor film ( $TiO_2$ ), 3) transparent electrode (FTO), 4) redox electrolyte ( $3I/I_3^-$ ) and 5) the counter electrode. The most important part of DSSCs device is a dye sensitizer which should absorb all region of the sun light. Many types of dye sensitizers have been studied [8-12]. Until now, the best sensitizer reported so far is a ruthenium complex dye, named **N719**, producing an overall efficiency of 11%.

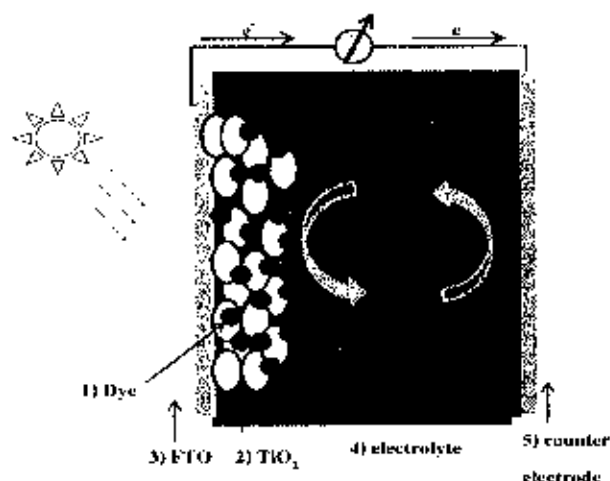


**Figure 1.2** Composition of dye sensitized solar cells

### 1.3 Component of dye sensitized solar cells

To construct the photovoltaic solar cell, the components needed are dye sensitizer, nano-crystalline metal oxide semiconductor film ( $\text{TiO}_2$ ), transparent electrode (FTO), redox electrolyte and the counter electrode as mentioned previously. Each component is described below;

**(1) Dye sensitizer:** It must show good property for absorbed solar energy, transferred electron to metal oxide particles, having long length optical absorption spectrum in the visible to near infrared, high extinction coefficient, high stability in the oxidation state and good adhesive on surface of metal oxide particles. There are many types of dye sensitized solar cells, for example organic dyes [13, 14], porphyrin dyes [15, 16] and ruthenium complex dyes [17-19]. Our research group interested to study and synthesize ruthenium complex dyes due to their high voltage redox and high stability. It also shows good electron transfer into nano-crystalline and metal oxide as well as the structure can be easily modified.

**(2) Metal oxide particles layer:** The semiconducting oxide film is one of the most important factors determining the photovoltaic performance of DSSCs. Semiconductor oxides used in dye sensitized solar cells include  $\text{TiO}_2$ ,  $\text{ZnO}$ ,  $\text{SnO}_2$ ,  $\text{Nb}_2\text{O}_5$  and so forth [20], which served as the carrier for the monolayer of the sensitizer using their huge surface and the medium of electron transfer to the conducting substrate. The oxide film holds the dye molecules, collected the photogenerated electrons from the LUMO level of the dye molecules, provide the path for the

transport of the electrons to the FTO. Therefore, the oxide materials have to satisfy several requisites; e.g., high surface area to load a large amount of dye molecules, conduction band energy level locating between the LUMO level of dye and the redox level of the electrolyte, more than 3 eV, high electron mobility, and chemical stability. To date,  $\text{TiO}_2$  becomes the best choice in semiconductor for several researchers including our group, due to its low-cost, abundance in the market, nontoxicity, biocompatibility, and it is also used widely in health care products as well as in paints.

**(3) Transparent electrodes:** It consists of anode electrode using fluoride doped tin oxide (FTO) and cathode electrode or counter electrode. Transparent electrodes can compensate electron to electrolyte system.

**(4) Electrolyte system:** The electrolyte is one of the key components for dye sensitized solar cells and its properties have much effect on the conversion efficiency and stability of the solar cells. It can be compensated electron for dye sensitized solar cells or received the positive charge from the cathode electrode and easily to oxidation reaction. The electrolyte used in DSSCs is divided into three types: liquid electrolyte, quasi-solid state electrolyte, and solid electrolyte.

The major redox couple contains  $\text{I}^-/\text{I}^{\cdot-}$  couple [21, 22] and electrolyte solution. Wang et al. used  $\text{Br}^-/\text{Br}_2$  as redox couple in Eosin Y sensitized solar cells [23].  $\text{SCN}^-/(\text{SCN})_2$  couple were also shown in the literature [24]. Sapp et al. reported the substituted bipyridyl cobalt (III/II) couple as redox couple in DSSCs [25]. However, the performance of these couples can hardly match with that of  $\text{I}^-/\text{I}^{\cdot-}$  couple. To date, the organic solvent based liquid electrolyte containing  $\text{I}^-/\text{I}_3^-$  as a redox couple give the best record DSSCs efficiency [26]. In this electrolyte type, the electron transfer from  $\text{TiO}_2$  to  $\text{I}_3^-$  governed by the weak dissociative chemisorption of the iodine is a slow process. In contrast, the regeneration rate of  $\text{I}^-$  from  $\text{I}_3^-$  at the counter electrode is very high and fast due to the effective catalytic reaction at the counter electrode and fast diffusion of  $\text{I}^-/\text{I}_3^-$  in the liquid media. Therefore, only preferred reactions occur in both anode and cathode, which satisfies the most important requirement of the ideal redox couple.

Organic solvent electrolytes were widely used and investigated in dye sensitized solar cells for their low viscosity, fast ion diffusion, high efficiency, easy to be designed and high pervasion into nanocrystalline film electrode [27]. The composition of the electrolytes composed of organic solvent, redox couple, and additive. Organic solvent used in organic liquid electrolyte including nitrile, such as acetonitrile, verlonitrile, 3-methoxypropionitrile, and esters (ethylene carbonate (CE), propylene carbonate (PC),  $\gamma$ -butyrolactone). In this work, we used acetonitrile and verlonitrile as organic liquid electrolyte.

The commonly additive used in the electrolytes for dye-sensitized solar cells contain 4-*tert*-butylpyridine (TBP) and *N*-methylbenzimidazole (NMBI) [28]. The addition of these additives could suppress the dark current and improve the photoelectric conversion efficiency. The function of TBP is to reduce the recombination of electrons in the conduction band of the semiconductor and the electron acceptor in the electrolyte through the coordination between N atom and the Ti ion to incomplete coordination state on the surface of TiO<sub>2</sub> film. Then, the photovoltage fill factor and the conversion efficiency can be increased dramatically.

#### (5) Counter electrode

To balance the charge and regenerate the key components, the oxidized form of the mediator needs to be reduced by electron flowing through the external circuit then passing through the counter electrode. For the iodide-I<sub>2</sub> mixture, the oxidized form corresponds to tri-iodide and reduction involves 2 electrons:



To reduce losses, the counter electrode material should show good electrocatalytic properties. The material of choice is platinum (Pt). As an electrode material, Pt shows excellent chemical stability and very low over potential for the tri-iodide reduction reaction (equation 1.1). In our group, we prepared Pt metal clusters by thermal decomposition of chloroplatinic acid (H<sub>2</sub>PtCl<sub>6</sub>) from 2-methoxy ethanol on a fluoride doped tin oxide (FTO) [29, 30].

#### 1.4 Principle of dye sensitized solar cells working [31]

The mechanism of the working DSSCs (Figure 1.3) is described as followed.

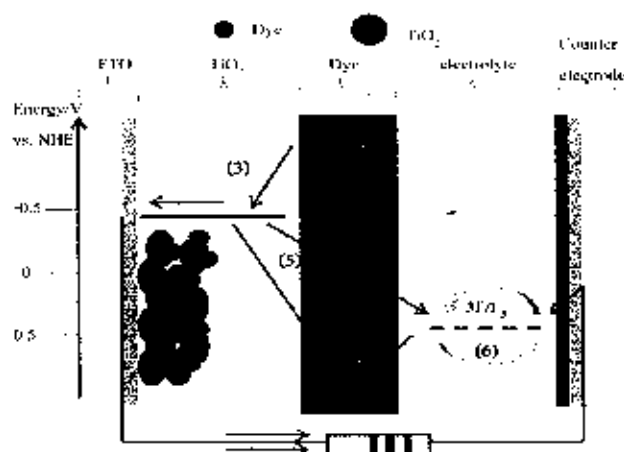
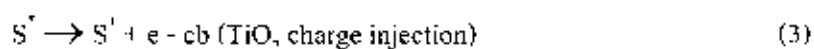


**Figure 1.3** Principle of operation and energy level scheme of the dye sensitized nanocrystalline solar cells

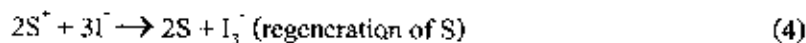
(1) Consider electron reaction that take place at the anode, where the absorption of the light by the dye ( $S^0$ ) lead to formation of its electronically state ( $S^*$ )



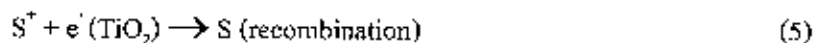
(2) The molecule in the excited state can decay back to the ground state or undergo oxidative quenching then inject electrons into the conduction band of  $TiO_2$ .



(3) The injected electrons travel through the mesoporous network of particle to reach the back-collector electrode to pass through the external circuit. The oxidized dye is reduced rapidly to the ground state by the donor (iodide) presented in the electrolyte:



(4) In the absence of a redox mediator to intercept and rapidly reduce the oxidized dye ( $S^+$ ), recombination with the electrons of the titania layer take place, without any measurable photocurrent:



(5) The electrons reaching the counter-electrode through the external circuit reduce in turn the oxidized iodide ( $I^-$ ), so that the entire sequences of electron transfer reactions involving the dye and the redox mediator ( $I_3^-/I^-$ ) render the cyclic:



(6) If cited reactions alone take place, the overall effect of irradiation with sunlight is to drive the electrons through the external circuit, i.e., direct conversion of sunlight to electricity.

### 1.5 Key efficiency parameters of the DSSCs

The spectral response of the dye sensitized solar cells depends on the absorption properties of the dye. Characterization of the cell depends on a number of experimentally accessible parameters, including the photocurrent and photo potential measured under different conditions (open and closed circuit, under monochromatic light or sunlight illumination):  $I_{oc}$ ,  $V_{oc}$ ,  $I_{sc}$ ,  $V_{sc}$ . The term incident photon to electrical conversion efficiency (IPCE) is a quantum yield term for the overall charge injection collection process measured using monochromatic light (single wavelength source).

The photocurrent measured under closed circuit  $I_{sc}$  is the integrated sum of IPCE measured over the entire solar spectrum:

$$I_{sc} = \int_0^{\infty} IPCE(\lambda) \cdot I_{sun}(\lambda) d\lambda \quad (1.2)$$

Thus IPCE ( $\lambda$ ) can be expressed as;

$$\text{IPCE } (\lambda) = 1240 \left( \frac{I_{sc}}{\lambda \phi} \right) \quad (1.3)$$

Where  $\lambda$  is the wavelength,  $I_{sc}$  is the current at short circuit ( $\text{mA}/\text{cm}^2$ ) and  $\phi$  is the incident radiative flux ( $\text{W}/\text{m}^2$ )

The overall sunlight to electric power conversion efficiency of the DSSCs is given by the following expression:

$$\eta = \frac{P_{max}}{P_{in}} = \frac{I_{sc} \cdot V_{oc} \cdot ff}{P_{in}} \quad (1.4)$$

Maximum power obtainable in the photovoltaic devices is the product of two terms  $I_{max}$  and  $V_{max}$ . The value of  $I_{max}$  gives the maximum photocurrent obtainable at some "maximum power point". The fill factor  $ff$  is defined as the ratio of  $(I_{max} V_{max} / I_{sc} V_{oc})$ . The four values  $I_{sc}$ ,  $V_{oc}$ ,  $ff$  and  $\eta$  are the key performance parameters of the solar cells.

The overall efficiency ( $\eta$ ) of the photovoltaic cell can be calculated from the integral photocurrent density ( $I_{ph}$ ), the open circuit photovoltage ( $V_{oc}$ ), the fill factor of the cell ( $ff$ ) and the intensity of the incident light ( $I_s = 1000 \text{ W}/\text{m}^2$ )

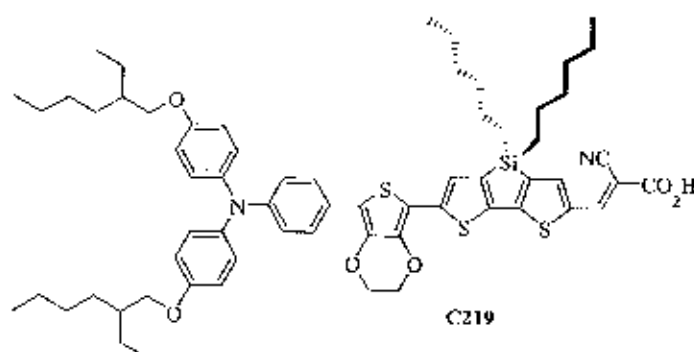
$$\eta = \frac{I_{ph} \cdot V_{oc} \cdot ff}{I_s} \quad (1.5)$$

The measured photocurrent will depend on the light intensity; the efficiency of charge injection in the excited state quenching process; the degree of recombination of electrons with the oxidized dye ( $S^+$ ); and the efficiency of charge transport in the titania films to the counter electrodes. Maximum photo voltage obtainable in such sensitized solar cells is the energy gap between the chemical potential level of the mediating redox electrolyte and the conduction band level of  $\text{TiO}_2$ .

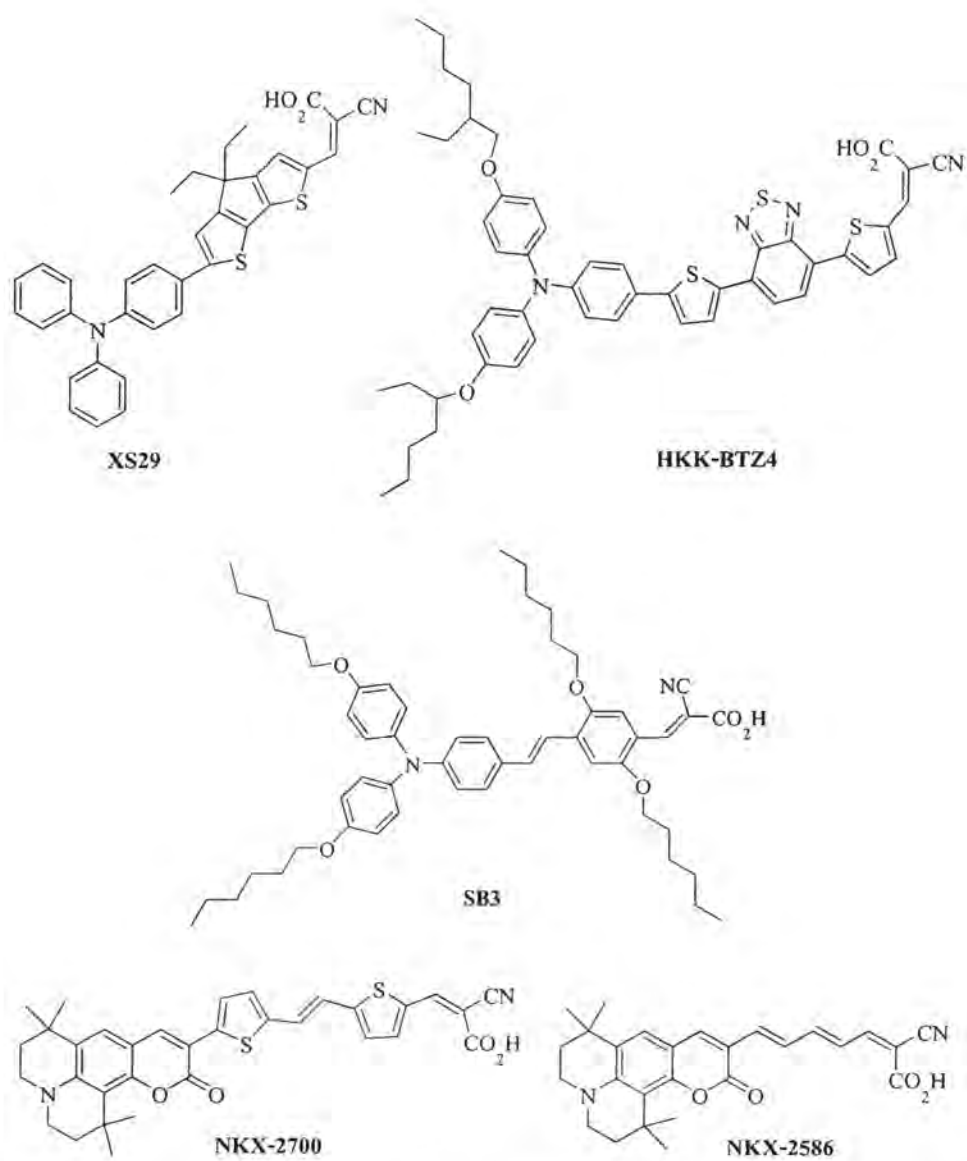
## 1.6 Type of dye sensitized solar cells (DSSCs)

### 1.6.1 Organic sensitizers

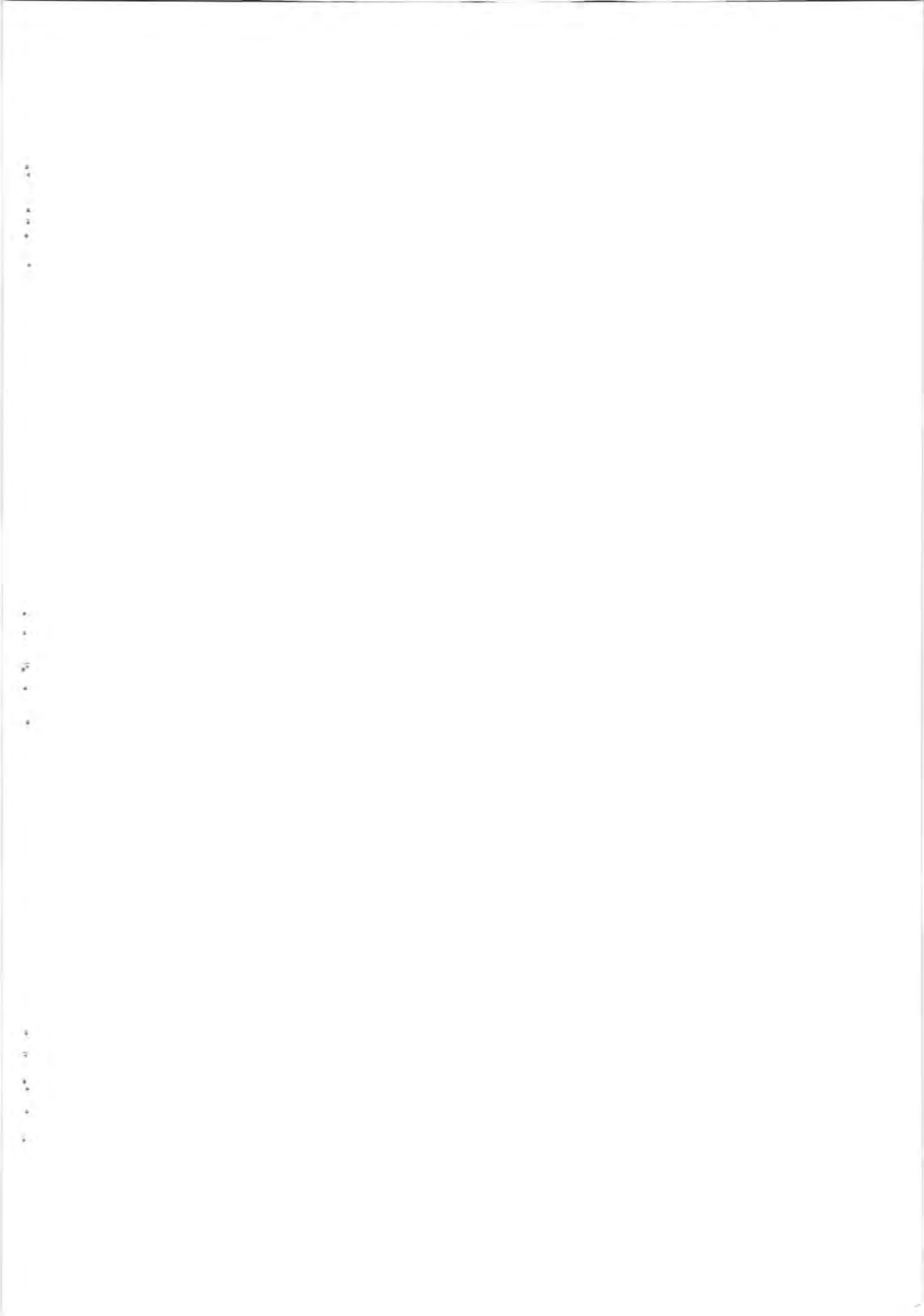
Organic dye is the molecule that was prepared by synthesis chemist. Almost all molecule contains conjugated double bond and containing high polar functional. The organic dyes generally consist of electron donor, electron acceptor, conjugated spacer between donor and acceptor, and surface anchoring group [32]. The anchoring groups are carboxylate, phosphonate, and sulfonate. The example of organic dye is **C219** ( $\eta = 10\%$ ) (Figure 1.4), **XS29** ( $\eta = 6.3\%$ ), **HKK-BTZ4** ( $\eta = 7.3\%$ ) and **SB3** ( $\eta = 6.1\%$ ) [33-35], comprising triphenylamine (TPA) moieties as the electro donor and the cyano acrylic acid moieties as the electron acceptor/anchoring groups. Both **NKX-2700** ( $\eta = 8.2\%$ ) and **NKX-2586** ( $\eta = 7.5\%$ ) [36, 37] are derivative of coumarin (Figure 1.5). In addition, several groups have reported the organic dye composed of the fluorine moieties as electron donor groups (Figure 1.6), **JK2** ( $\eta = 6.02\%$ ) [38] and D-D- $\pi$ -A type organic dye, **UB3** ( $\eta = 5.12\%$ ) [39] which was synthesized by Promarak's group.



**Figure 1.4** Chemical structure of **C219** dye.



**Figure 1.5** Chemical structure of XS29, HKK-BTZ4, SB3, NKX-2700 and NKX-2586 dyes



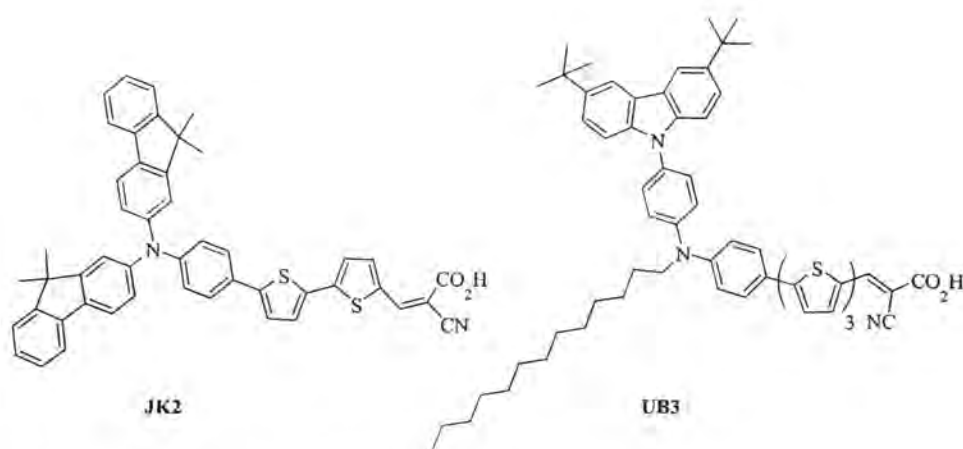


Figure 1.6 Chemical structure of JK2 and UB3 dyes

### 1.6.2 Porphyrin sensitizer

Porphyrin dyes is the main structure of chlorophyll which plays an important role in biological process of plants. This dye can also be synthesized in laboratory, and easily modified the functional group with other metals. In 2004, Campbell synthesized meso-linkes porphyrin dye, **Zn-1a** ( $\eta = 4.2\%$ ) [15], in Figure 1.7. After that the various structure of Zn metal was synthesized with porphyrin dye; for example **Zn-TCPP** ( $\eta = 1.1\%$ ) [40], **YD0** ( $\eta = 3.5\%$ ) and **YD2** ( $\eta = 7.4\%$ ) [41], **DTBC** ( $\eta = 5.2\%$ ) [42], Figure 1.8. However, the overall efficiency of the all porpyrin dyes is lower than that of the ruthenium complex and organic dyes. However, many research groups have been investigating in order to improve the efficiency of these dyes [16, 43].

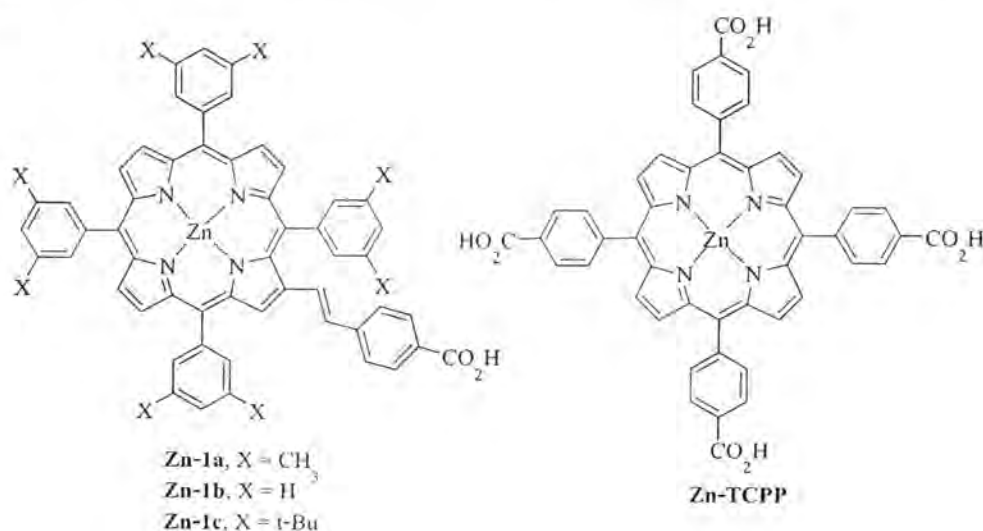
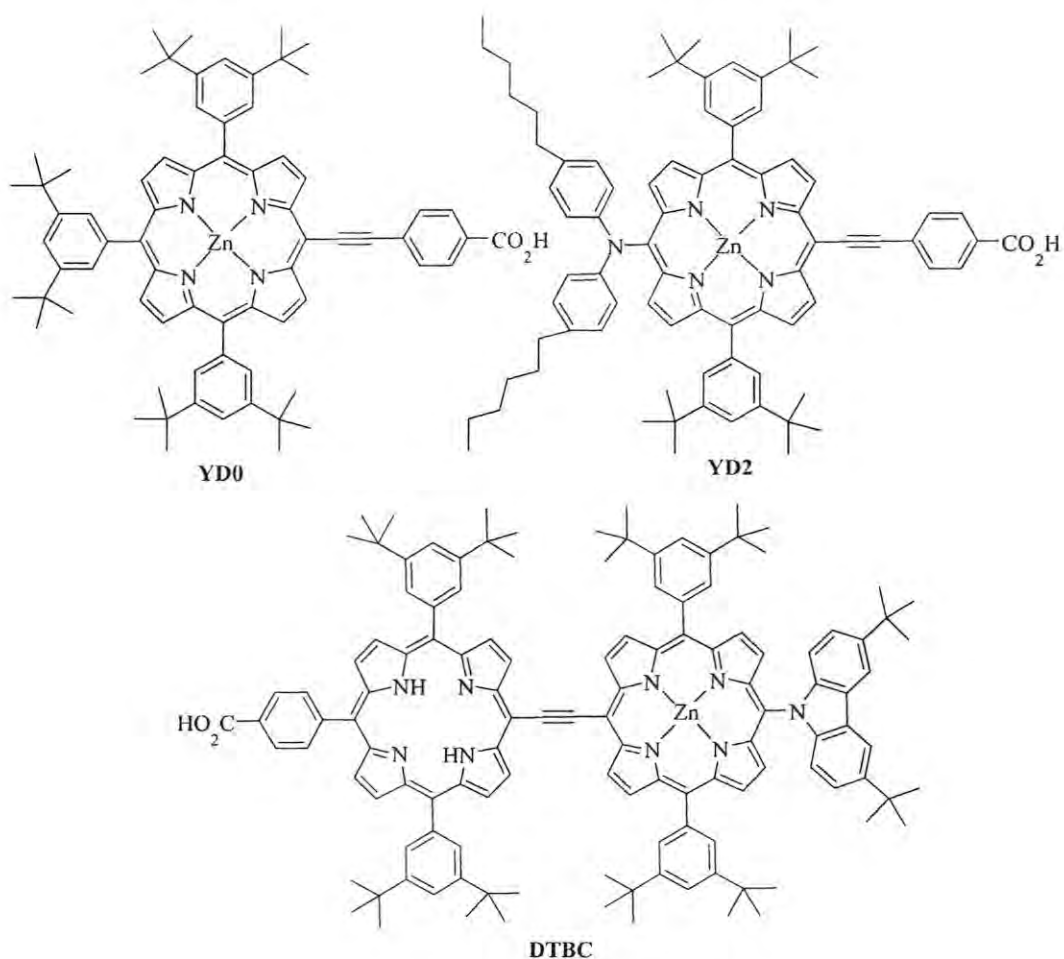


Figure 1.7 Chemical structure of Zn-1a and Zn-TCPP dyes

10  
11  
12  
13  
14

15  
16  
17  
18  
19  
20

21  
22  
23  
24  
25



**Figure 1.8** Chemical structure of YD0, YD2 and DTBC dyes

### 1.6.3 Ruthenium sensitizer

Ruthenium(II) complex dye is the most popular of metal complex dyes, because it shows the highest solar light to conversion efficiency. This type of dye has been developed and continuously studied by Grätzel's group. The advantages of ruthenium dyes are; 1) high stability and voltage redox potential, so it is good for transferring electron into nano crystalline and metal oxide and 2) this molecular structure can also be easily modified. The structure of ruthenium complexes contains in a variety of ligand. For example, **CYC-B1** composes of pyridine carboxylic acid, thiocyanate and pyridine which combined thiophene synthesized by Chai-Yuan Chen group. In 1993, the ruthenium complex  $\text{cis-RuL}_2(\text{NCS})_2(\text{L}:2,2'\text{-bipyridyl-4,4'-dicarboxylic acid})$ , called as **N3** dye, was found to dramatically increase the performance of DSSCs [44]. It is mainly due to metal to ligand charge transfer (MLCT) transition that moves the electrons from d orbital of Ru to

the  $\pi$  orbital of diimine which is directly attached to  $\text{TiO}_2$  [45, 46]. In a subsequently developed **N719** dye, two protons of **N3** were replaced by a tetrabutylammonium cation group (TBA). The deprotonation of **N3** changes the polarity at the interface, positively shifts the conduction band edge of  $\text{TiO}_2$  and increases  $V_{oc}$  in DSSCs employing **N719** dye [47, 48]. The structure of several ruthenium(II) complex dyes are shown in Figure. 1.9.

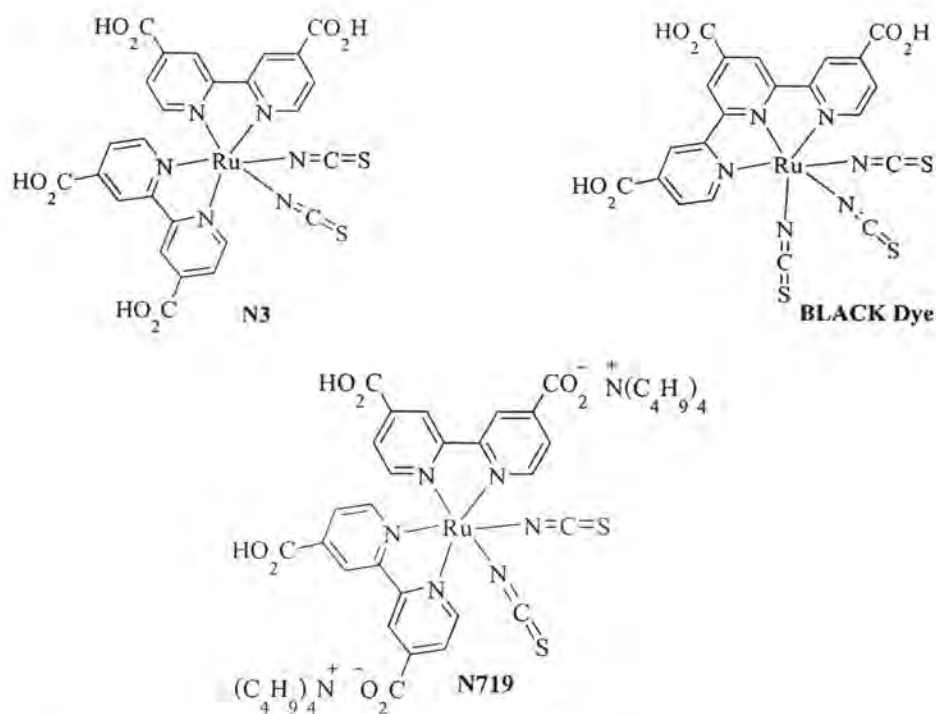


**Figure 1.9** Chemical structure of **N3**, **BLACK Dye** and **N719** dyes.

Anchoring to  $\text{TiO}_2$  has been achieved through a number of functional groups, such as salicylate ( $\text{C}_6\text{H}_4(\text{OH})(\text{CO}_2^-)$ ), carboxylic acid ( $\text{R}-\text{CO}_2\text{H}$ ), sulphonic acid ( $\text{R}-\text{SO}_3\text{H}$ ), phosphonic acid ( $\text{R}-\text{P}(\text{OH})_2$ ) and acetylacetonate ( $\text{M}(\text{acac})_3$ ) derivatives. However, the most widely used and successful to date are the carboxylic acid [49, 50]. Some of the possible modes of chelation/derivatisation, ranging from chemical bonding (chelating or bridging mode) to H-bonding, are shown in Figure 1.10.

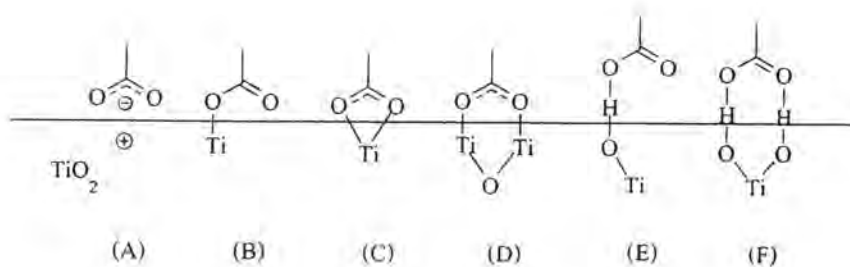


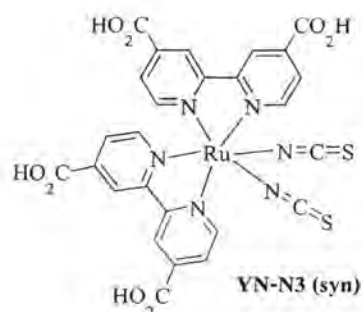
**Figure 1.10** Possible binding modes for carboxylic group on  $\text{TiO}_2$  [15]

## 1.7 Aims of thesis

### 1.7.1 To synthesize the ruthenium complexes

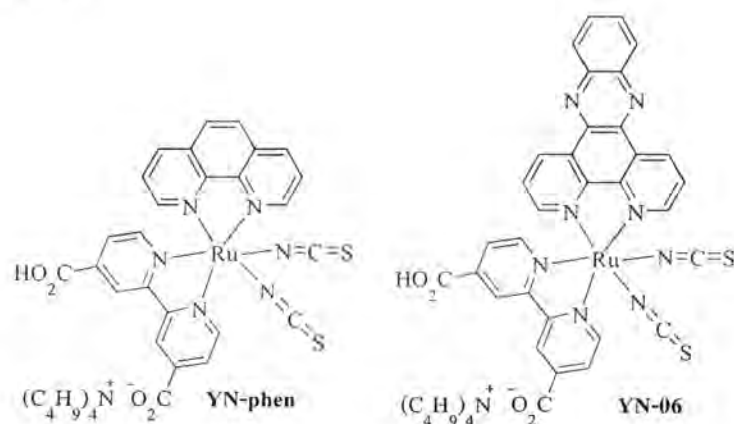
#### 1.7.1.1 Homoleptic ruthenium(II) without tetrabutylammonium salt

##### (YN-N3 (syn))



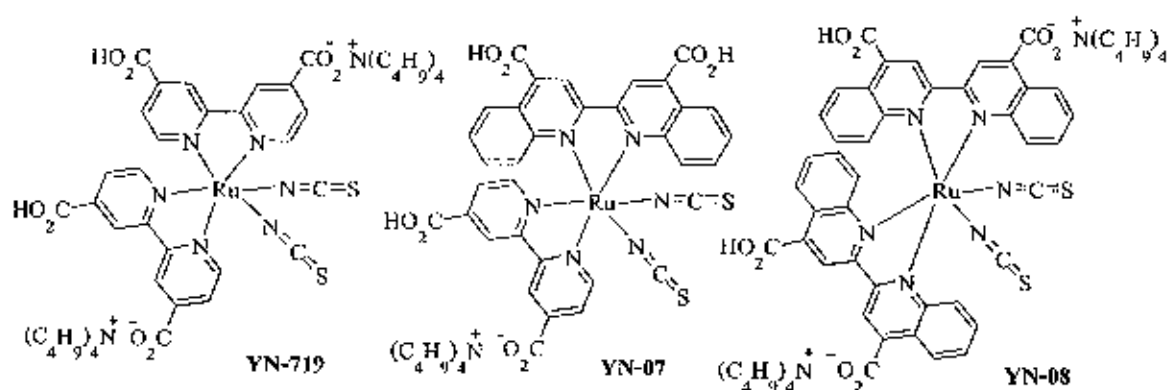
#### 1.7.1.2 Heteroleptic pyridinyl ruthenium(II) with tetrabutylammonium salt

##### (YN-phen and YN-06)



## 1.7.1.3 Homoleptic and heteroleptic ruthenium(II) with tetrabutylammonium salt

(YN-719, YN-07 and YN-08)

1.7.2 To characterize the molecular structure of the target complexes by  $^1\text{H}$  and  $^{13}\text{C}$ 

NMR, fourier transform infrared spectroscopy (FT-IR) and mass spectroscopy (MS)

1.7.3 To study a photo physic of ruthenium complexes by UV-Vis spectroscopy

1.7.4 To study of electrochemical property of ruthenium complexes by cyclic voltammetry

1.7.5 To fabricate and investigate the DSSCs devices using our ruthenium complexes



## CHAPTER 2

### LITERATURE REVIEWS

#### 2.1 Literature reviews

Dye sensitized solar cells (DSSCs) based on nanocrystalline semiconductor such as  $\text{TiO}_2$  and ruthenium(II) complexes are of great interest as an alternative to the conventional solar cells because of their high performance, low-cost production. DSSCs based on metal-free organic sensitizers possessing very high extinction coefficients have been reported to exhibit power conversion efficiencies surpassing 9% [51, 52]. In comparison, several polypyridyl ruthenium(II) based DSSCs have even higher efficiencies of >11% under standard AM 1.5 sunlight. Up to now, many research groups have been studied and developed ruthenium(II) complexes for dye sensitized solar cells.

The dyes absorbed on  $\text{TiO}_2$  substrate play a key role for harvesting the solar energy. In addition to the light absorption ability within an appropriate range, the dye sensitizers should fulfill several demanding conditions. Strong anchoring of dye on surface of metal oxide ( $\text{TiO}_2$ ) particles is one of the most important factors to enhance overall conversion efficiency. Over the last 20 years, ruthenium complexes with carboxylic acid anchoring group have been designed. Ruthenium complexes such as cis-dithiocyanatobis(4,4'-dicarboxy-2,2'-bipyridine)ruthenium(II), named as N3 (Figure 2.1), reported in 1993, have been found to be efficient sensitizers for DSSCs. This ruthenium(II) complex has high solar energy conversion efficiency, high photo and chemical stability. It is considered as a standard dye for comparison against others new sensitizers in DSSCs devices [53].

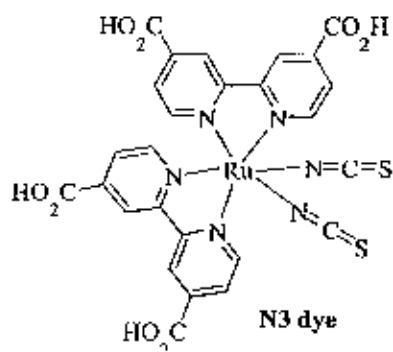


**Figure 2.1** Molecular structure of **N3** sensitizer

The ruthenium(II) complex, **JK-92** [54] (see Figure 2.2, left) has developed by expanding the  $\pi$ -conjugation of bipyridine ligand using phenyl triazole moieties and endowing it with electron donating alkoxy groups. The dioctyl 2,2'-bipyridine-4,4'-dicarboxylate moieties of complex **S8** [55] (Figure 2.2, right) and 4,4'-bis(1-(4-(hexyloxy)phenyl)-1H-1,2,3-triazol-4-yl)-2,2'-bipyridine moieties of **JK-92** are similar purpose to enhance molar extinction coefficient of sensitizers, and provide directionality in the excited state by fine tuning the LUMO level of the ligands with the electron donating alkoxy group. Both complexes contain anchoring carboxylic acid bipyridyl groups with some modification compared to **N3** dye. The **JK-92** and **S8** dyes have several advantages over the conventional **N3** dye; 1) higher binding capacity onto the  $\text{TiO}_2$  surface and 2) the hydrophobic group, such as aliphatic chain group in the complex increasing the stability of cells towards water induced desorption.

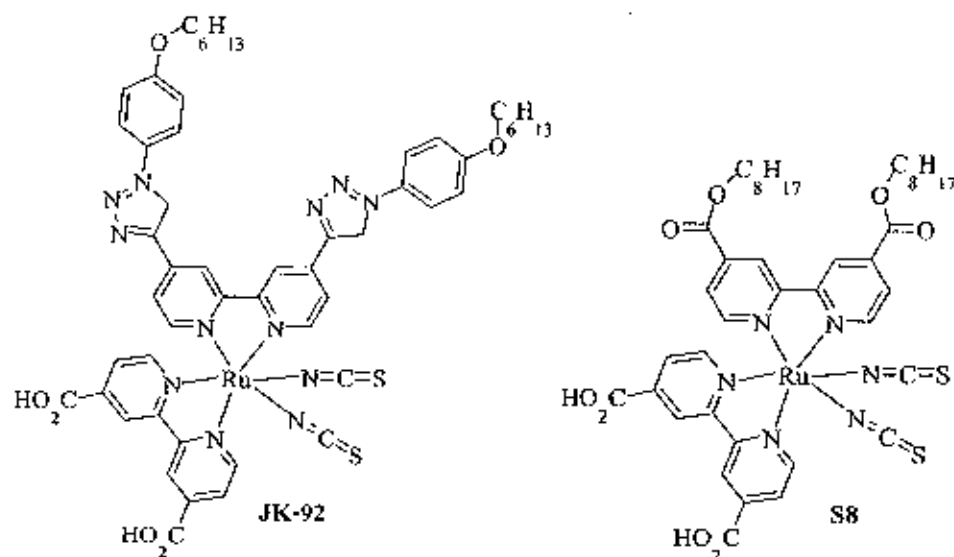
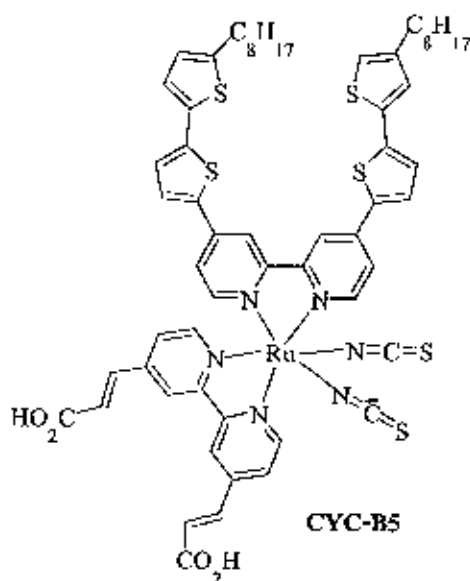


Figure 2.2 Molecular structure of JK-92 and S8 dyes

In 2010, Wu and coworkers [56] synthesized heteroleptic ruthenium complex dye, named **CYC-B5** (Figure 2.3), in which the conjugation length of both ancillary and anchoring ligands were extended with a conjugated moiety. The photovoltaic data of **CYC-B5** sensitized DSSCs have demonstrated that the existence of a vinyl group between the bipyridine and carbonyl segments of the anchoring ligand enhance both light-harvesting ability of the sensitizer and increase the amount of the sensitizer adsorbed on TiO<sub>2</sub>. Furthermore, due to the super high light harvesting ability, **CYC-B5** sensitized cell shows conversion efficiency higher than 7.50% at the light intensity as high as 198 mW/cm<sup>2</sup> using thin TiO<sub>2</sub> electrodes.



**Figure 2.3** Molecular structure of ruthenium sensitizer **CYC-B5**

In addition to the homoleptic ruthenium(II) based on structure of N3 sensitizer have been studied to increase the overall efficiency, for example, bis(tetrabutylammonium)bis(4-carboxy-2,2'-bipyridine-4'-carboxylate)dithiocyanato ruthenium(II) ion, named N719 [57]. The structure of N719 is shown in Figure 2.4. Unlike N3, the two carboxylic group of N719 ruthenium(II) complex was deprotonated and replaced with two tetrabutylammonium salt. The N719 dye shows overall conversion efficiency at  $\eta = 11\%$  which is higher than that N3 dye.

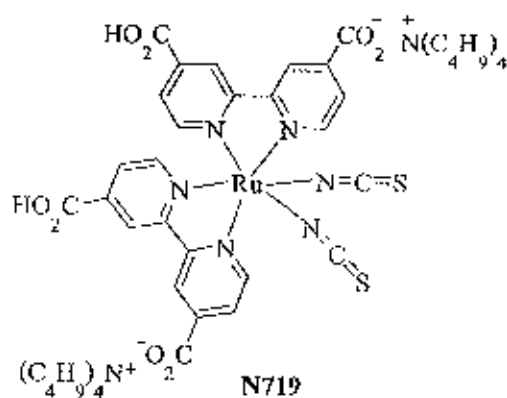


**Figure 2.4** Molecular structure of N719 sensitizer

To further improve the photovoltaic performance and stability of the several heteroleptic ruthenium sensitizers, extensive efforts have been focused on the synthesis of new highly efficient sensitizers contained tetrabutyl ammonium cation group ( $N^+(C_4H_9)_4$ ). For example, **K77**, **T18** and **CYC-B12**, Figure 2.5-2.7, have been developed by expanding the  $\pi$ -conjugation of the ancillary ligand and endowing it with electron donating alkyl group. In the ruthenium complex **K77** [58] (Figure 2.5), the purpose of 4,4'-bis(2-(4-tert-butyloxyphenyl)ethenyl)-2,2'-bipyridine ligand containing extended  $\pi$ -conjugation with substituted butoxy group are introduced in order to improve the hydrophobic properties and enhance the molar extinction coefficient. In a subsequently developed DSSCs dye, one proton of carboxylic group was replaced by ammonium cation group. The deprotonation of carboxyl group changes the polarity at the interface; positively shift the conduction band edge of  $TiO_2$  and increases  $V_{oc}$ . **K77** dye gave highly power efficiency of the corresponding dye sensitized solar cells,  $\eta = 9.12\%$  under AM 1.5 ( $100\text{ mW/cm}^2$ ) irradiation. This device exhibits excellent stability at  $80\text{ }^\circ\text{C}$  in the dark or under visible light soaking at  $60\text{ }^\circ\text{C}$  during 1000 h of accelerated tests.

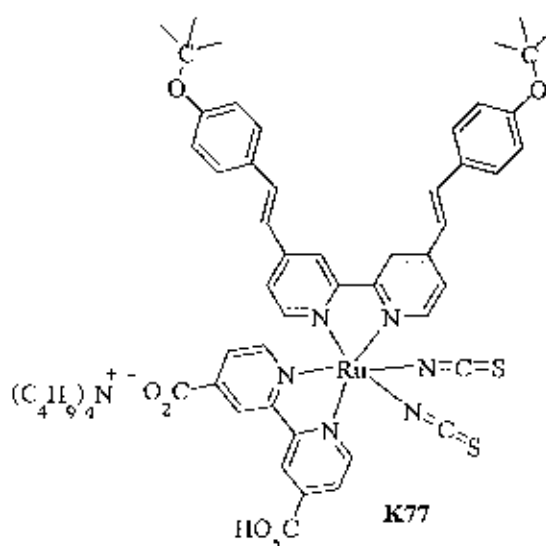


**Figure 2.5** Molecular structure of **K77** dye

For **T18** [59], the complex was synthesized by extended the conjugation with ketene thioacetal modified bipyridyl as an ancillary ligand electron rich groups (see Figure 2.6). To developed DSSCs dye, one proton of carboxylic group was replaced by ammonium cation group. The efficient performance of **T18** as a sensitizing dye is attributed to its high absorption extinction coefficient and extended absorption in the visible region of the solar spectrum when compared to **N719** dye.

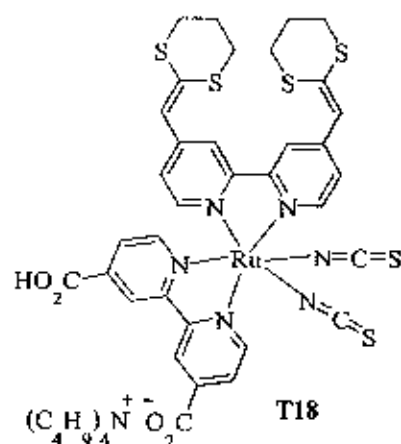


**Figure 2.6** Molecular structure of **T18** dye

The complex **CYC-B12** [60], structure shown in Figure 2.7, contains a branch of heteroleptic ruthenium(II) sensitizers endowed with the ancillary ligand consisting a thienothiophene conjugated bridge and carbazole hole-transport moiety as the molecular terminal. This dye has been developed toward enriching the light capturing ability to match the solar radiation and retarding the charge recombination between the dye sensitized semiconductor and electrolyte.

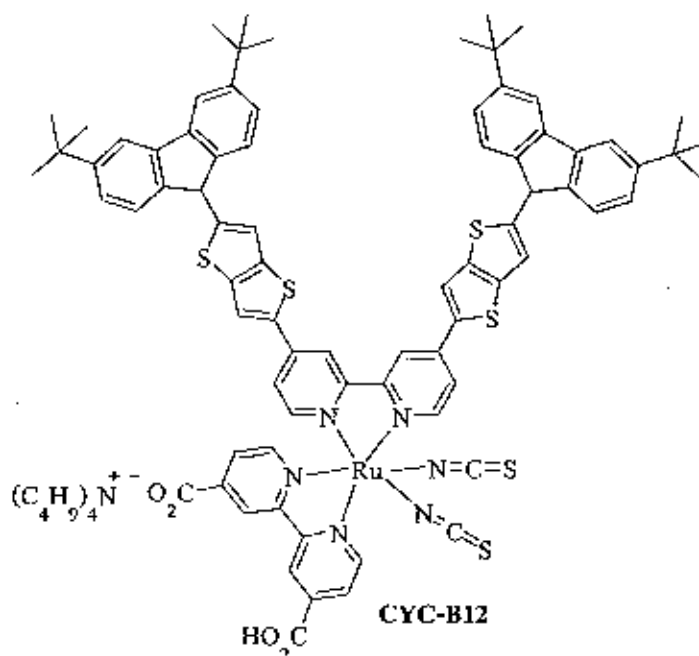


**Figure 2.7** Molecular structure of **CYC-B12** dye

In addition, many groups have reported a family of heteroleptic pyridyl ruthenium without tetrabutylammonium salt,  $\text{Ru}(\text{bpy})(\text{L})(\text{NCS})_2$  with various ancillary ligand  $\text{L}'$ . The carboxyl groups on **bpy** in the complexes are responsible for dye adsorption onto the semiconductor surface. The ancillary ligand  $\text{L}'$  is not directly attached onto the semiconductor but can be used for tuning the overall properties of the complexes. The **Ru(Hpip)** and **Ru(Hipdpa)** [8], see Figure 2.8, are one of the heteroleptic pyridyl ruthenium complexes, where  $\text{L}'$  is imidazole phenanthroline ligand grafted with benzene and triphenylamine group, **Hpip** and **Hipdpa**, respectively. When the  $\pi$ -conjugation was extended from **Ru(Hpip)** to **Ru(Hipdpa)**, the open circuit voltage, short circuit photocurrent density and overall light to electric power conversion efficiency are significantly enhanced.



In recently year, Sun's group have applied another new branch of heteroleptic pyridyl ruthenium(II) sensitizers endowed with the ancillary ligand consisting a phenyl graft on phenanthroline as the molecular terminal, represented as YS5 shown in Figure 2.10 [62]. The complex YS5 is the singly deprotonated surface anchoring derivative of 4,4'-dicarboxy-2,2'-bipyridine (dc bpyH<sub>2</sub>). The photovoltaic performance of YS5 complex produced a power conversion efficiency of 6.05%.

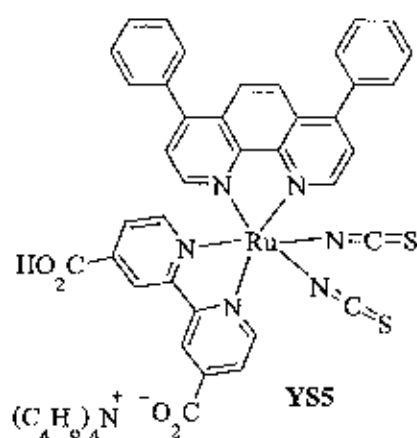


**Figure 2.10** Molecular structure of YS5 dye

To date, several dyes have been reported. In this thesis, we reported the ruthenium(II) complex dyes based on phenanthroline and bipyridine ligand part and carboxylic acid as anchoring group are reported. The ruthenium(II) dye structures were modified by introducing tetrabutyl ammonium salt substitutions, extending the  $\pi$ -conjugation and investigate their influence on the extinction coefficient as well as solar light to conversion efficiency of the DSSCs devices.

**CHAPTER 3**  
**EXPERIMENTAL**

**3.1 Chemicals**

All the chemicals used in this thesis are shown in Table 3.1 and Table 3.2

**Table 3.1** Chemicals for the synthesis

Chemicals	Formula	Grade	Manufacturer
2-Amino-4-methylpyridine	$C_6H_8N_2$	99%	Acros
Ammonium thiocyanate	$NH_4SCN$	ACS reagent, 97.5%	Acros
Bromine	$Br_2$	99% PS	Panreac
2-Bromo-4-methylpyridine	$C_8H_8BrN$	98%	Acros organics
2,2'-Biquinone-4,4'-dicarboxylic acid	$C_{20}H_{12}N_2O_4$	97% (TLC)	Fluca
Calcium hydride	$CaH_2$	93%	Acros
Dimethyl formamide	$C_3H_7NO$	Organic synthesis	Acros
Diethyl ether	$(C_2H_5)_2O$	PA-ACS-ISO	Panreac
Ethanol	$C_2H_6O$	ACS-for analysis	CARLO ERBA
Hydrochloric acid	$HCl$	37%, for analysis	CARLO ERBA
Hydrobromic acid	$HBr$	48%, ACS reagent	Acros organics
Isopropanol	$C_3H_8O$	ACS-for analysis	CARLO ERBA
Magnesium sulfate	$MgSO_4$	Industrial Grade	Panreac

Table 3.1 Chemicals for the synthesis (continued)

Chemicals	Formula	Grade	Manufacturer
Methanol	CH <sub>3</sub> OH	ACS-for analysis	CARLO ERBA
Nitric acid	HNO <sub>3</sub>	67%, for analysis	CARLO ERBA
Palladium acetate	Pd(OAc) <sub>2</sub>	99%	Acros organics
<i>o</i> -Phenanthroline	C <sub>12</sub> H <sub>8</sub> N <sub>2</sub>	ACS-for analysis	CARLO ERBA
1,10-Phenanthroline-5,6-dione	C <sub>12</sub> H <sub>6</sub> N <sub>2</sub> O <sub>2</sub>	97%	Aldrich
$\alpha$ -Phellandrene	C <sub>10</sub> H <sub>16</sub>	-	SAFC
<i>o</i> -Phenyldiamine	C <sub>6</sub> H <sub>8</sub> N <sub>2</sub>	98%	Acros
Potassium carbonate	K <sub>2</sub> CO <sub>3</sub>	ACS-for analysis	CARLO ERBA
Ruthenium(III) trichloride trihydrate	RuCl <sub>3</sub> ·3H <sub>2</sub> O	Hygroscopic	Pressure Chem. Co.
Sulfuric acid	H <sub>2</sub> SO <sub>4</sub>	96% AR. Grade	CARLO ERBA
Sodium dichromate	Na <sub>2</sub> CrO <sub>7</sub>	99.5%	Aldrich
Sodium hydroxide	NaOH	ISO-ACS-for analysis	CARLO ERBA
Sodium nitrite	NaNO <sub>2</sub>	Analytical reagent	Ajax Finechem
Sodium sulfate	Na <sub>2</sub> SO <sub>4</sub>	ACS-for analysis	CARLO ERBA
Sodium thiosulphate	Na <sub>2</sub> S <sub>2</sub> O <sub>3</sub>	ACS-for analysis	CARLO ERBA
Tetrabutylammonium hexafluorophosphate	(C <sub>4</sub> H <sub>9</sub> ) <sub>4</sub> N(PF <sub>6</sub> )	Organics	Acros
Tetrabutylammonium hydroxide	(C <sub>4</sub> H <sub>9</sub> ) <sub>4</sub> NOH	1 M solution in methanol	Acros

**Table 3.2** Chemicals for DSSCs devices

Chemicals	Formula	Grade	Manufacturer
Acetonitrile	CH <sub>3</sub> CN	ACS-for analysis	CARLO ERBA
Bis(4,4'-dicarboxy-2,2'-bipyridine)dithiocyanato ruthenium(II) (N3)	C <sub>26</sub> H <sub>16</sub> N <sub>6</sub> O <sub>8</sub> RuS <sub>2</sub>	95% NMR	Aldrich
Chloroplatinic acid	H <sub>2</sub> PtCl <sub>6</sub>	40% Pt	Acros
Ethanol	C <sub>2</sub> H <sub>6</sub> O	ACS-for analysis	CARLO ERBA
Isopropanol	C <sub>3</sub> H <sub>8</sub> O	ACS-for analysis	CARLO ERBA
Iodine	I <sub>2</sub>	ACS-for analysis	CARLO ERBA
Lithium iodide	LiI	99%, Pure analysis	Acros
3-Methoxy ethanol	C <sub>3</sub> H <sub>8</sub> O <sub>2</sub>	99.8% Anhydrous	CARLO ERBA
Tetra propyl ammonium iodine	C <sub>12</sub> H <sub>28</sub> NI	98%	Acros
Titanium(IV) oxide	TiO <sub>2</sub>	Titanium nanoxide 20T/SP, D/SP	Solaronix
Titanium tetrachloride	TiCl <sub>4</sub>	0.09 M in 20% HCl	Sigma-Aldrich
4-Tertbutyl pyridine (TBP)	C <sub>9</sub> H <sub>13</sub> N	96%	Acros
Valernitrile	CH <sub>3</sub> (CH <sub>2</sub> ) <sub>3</sub> CN	98%	Acros

### 3.2 Instruments and general chemical characterization techniques

#### 3.2.1 General instruments

Table 3.3 Instruments

Instruments	Model	Company
Fourier Transform Infrared Spectrometer (FT-IR)	Spectrum RX 1	Perkin Elmer
UV-Visible Spectrometer (UV)	V-650 spectrophotometer	Jasco
Nuclear Magnetic Resonance (NMR)	Bruker ADVANCE, 300 MHz	Perkin Elmer
Cyclic Voltammetry (CV)	Autolab Metrohm PG11	Metrohm
Mass Spectroscopy (MS)	JMS-700	JEOL
Melting point (m.p.)	630	Buchi
Photocurrent voltage ( <i>I-V</i> ) and incident photon to electron conversion efficiency (IPCE)	Kiethley 2400	Oriel instruments

#### 3.2.2 General chemical characterization techniques

The structural of phenanthroline, bipyridine ligands and ruthenium(II) complexes were characterized by  $^1\text{H}$  NMR,  $^{13}\text{C}$  NMR, melting point and FT-IR techniques. The optical and electrochemical properties of the ruthenium(II) complexes were characterized by UV-visible spectroscopy and cyclic voltammetry, respectively. The DSSCs fabrication methods with ruthenium(II) complex dyes were presented in section 3.4.4. The ruthenium complex dyes were purified by column chromatography technique using a LH-20 Sephadex<sup>TM</sup> as stationary phase using methanol as eluent.

### 3.2.2.1 Fourier Transform Infrared Spectroscopy (FT-IR)

Infrared (FT-IR) spectra were recorded on NaCl pellets technique (100 mg of dried NaCl and 2 mg of samples) with a Perkin-Elmer Spectrum RX.I one fourier transform infrared spectrophotometer over the 4000 - 400  $\text{cm}^{-1}$  range, at the rate of 16  $\text{nm/s}$ . Data for FT-IR spectra are reported as follows: frequency ( $\text{cm}^{-1}$ ).

### 3.2.2.2 UV-visible spectroscopy

UV-visible spectra were measured in a 1 cm path length quartz cell using a V-650 spectro high resolution UV-Vis for ruthenium(II) complex dyes. The samples were dissolved in DMF and diluted to a concentration of  $1 \times 10^{-5}$  M.

### 3.2.2.3 Nuclear magnetic resonance (NMR)

$^1\text{H}$  NMR and  $^{13}\text{C}$  NMR spectra were performed in  $\text{CDCl}_3$ ,  $\text{DMSO-d}_6$  or  $\text{CD}_3\text{OD}$  recorded on Bruker AVANCE 300 MHz spectrometer, using TMS (0.00 ppm) as the internal reference. Data for NMR spectra are reported as followed: chemical shift ( $\delta$  ppm), multiplicity, coupling constant ( $J$ ), and integration (Hz).

### 3.2.2.4 Cyclic voltammetry (CV)

Cyclic voltammetry was conducted on a Autolab Metrohm PG11. The  $1 \times 10^{-4}$  M solutions of the corresponding complexes were prepared in DMF containing 0.1 M tetrabutylammonium hexafluorophosphate ( $[\text{Bu}_4\text{N}]\text{PF}_6$ ) as supporting electrolyte and purged with nitrogen gas for 60 min prior to use at a scan rate of 100  $\text{mV/s}$  at room temperature. The working electrode was a glassy carbon electrode. The auxiliary electrode was a Pt disk electrode, and  $\text{Ag}/\text{AgCl}$  (3 M  $\text{KCl}$ ) electrode was used as reference electrode.

### 3.2.2.5 Mass spectroscopy

Molecular weight of ruthenium(II) complex dyes was measured on JEOL, JMS-700 by fast atomic bombardment mass spectrometry techniques.

### 3.2.2.6 Melting point (m.p.)

Melting points was measured on Buchi 530 scientific melting point apparatus in open capillary method and are uncorrected and reported in degree Celsius.

### 3.3 Experimental section

This experimental section gives a detailed description of the synthesis of the ruthenium(II) complexes for dye sensitized solar cells (DSSCs). It is divided in five main steps, where step 1 is the ligand and ruthenium(II) precursor synthesis. Step 2 is the ruthenium(II) complex dyes synthesis. Steps 3 to 5 are the characterization, electrochemical studied and photovoltaic performance of DSSCs devices, respectively. The overall experimental flow chart is shown in Figure 3.1.

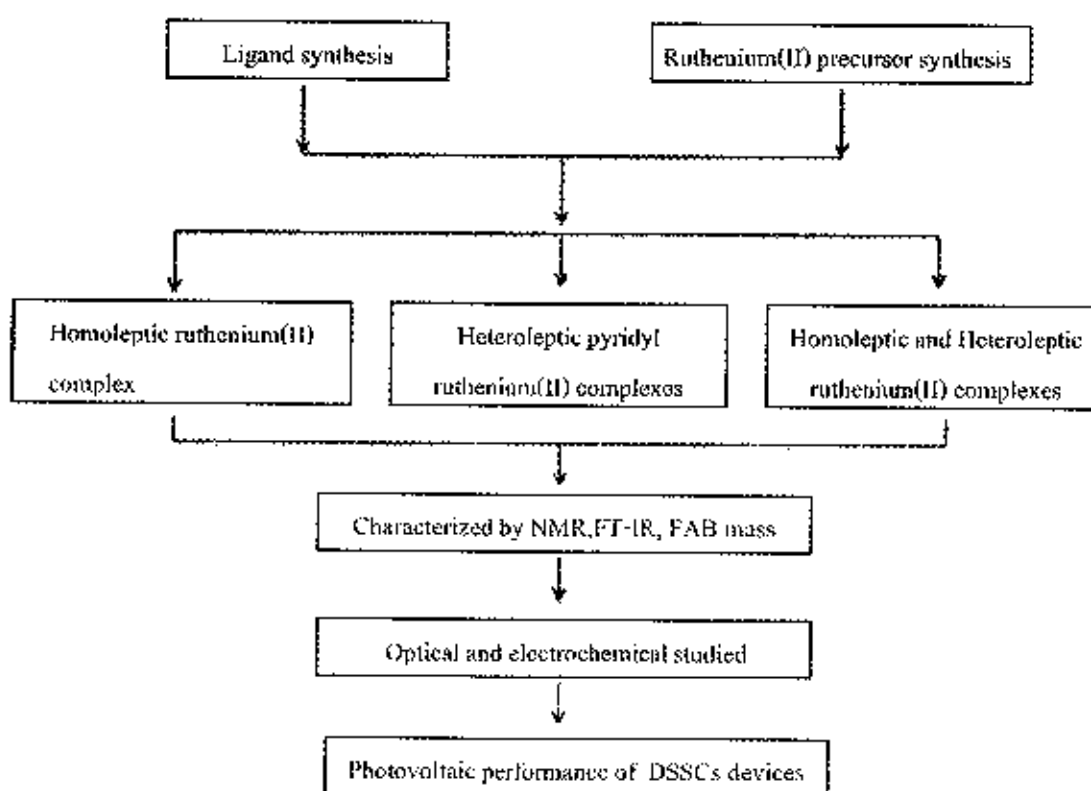
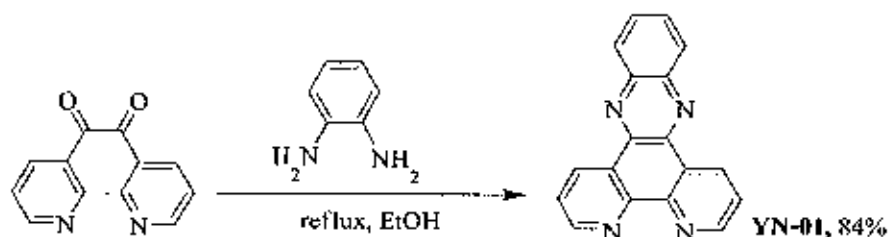


Figure 3.1 Experimental chart of this work

### 3.3.1 Ligand and ruthenium precursor synthesis

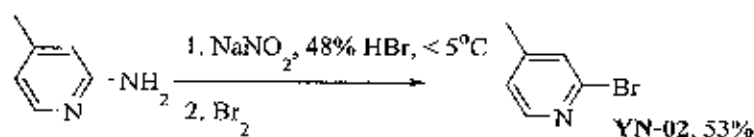
All reagents were obtained from the commercial sources, whereas dimethyl formamide (DMF) was dried over CaH<sub>2</sub> before used.

#### 3.3.3.1 The synthesis of dipyrido[3,2-a:2',3'-c]phenazine (YN-01) [63]



The mixture of *o*-phenyldiamine (0.26 g, 2.41 mmol), 10 ml ethanol and 1,10-phenanthroline-5,6-dione (0.25 g, 1.19 mmol) in 50 ml round bottom flask was heated to reflux for 1 h. Then the reaction mixture was allowed to cool in room temperature and filtered under vacuum. The collected brown solid was obtained after washing with 10 ml ethanol (0.28 g, 84%); m.p. 225 - 230 °C; MS (FAB<sup>+</sup>, *m/z*) C<sub>18</sub>H<sub>10</sub>N<sub>4</sub> 282 (M+1); <sup>1</sup>H NMR (300 MHz, CDCl<sub>3</sub>) δ 9.64 (dd, *J* = 8.1, 1.6 Hz, 2H), 9.27 (dd, *J* = 4.4, 1.6 Hz, 2H), 8.36 (dd, *J* = 6.5, 3.4 Hz, 2H), 8.01 - 7.92 (m, 2H), 7.92 - 7.73 (m, 2H); <sup>13</sup>C NMR (75 MHz, CDCl<sub>3</sub>): δ 152.4, 148.4, 142.5, 133.7, 130.6, 129.5, 127.6, 124.1, 120.3, 116.7; IR (NaCl) 3044, 1631, 1488, 1360, 1134 cm<sup>-1</sup>

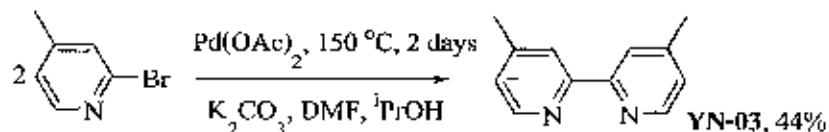
#### 3.3.3.2 The synthesis of 2-bromo-4-methylpyridine (YN-02) [64]



2-Amino-4-methylpyridine (2.70 g, 20 mmol) and 48% hydrobromic acid (5 ml, 90 mmol) were placed in an ice-salt bath with stirring. Then, 4 ml bromine (70 mmol) was added dropwise while the temperature was kept at 0 °C followed by aqueous solution of sodium nitrite (4 g in 6 ml). The controlling temperature of the reaction did not rise above 5 °C. After stirring for an additional 30 minutes to complete the reaction, yielding the dark brown solution, sodium hydroxide (2 ml, 10 M) was added dropwise to the reaction mixture. The yellow reaction was extracted by ethyl acetate followed by removal of the solvent. Then, the crude reaction was passed through silica column chromatography using 10% (v/v) ethyl acetate - hexane as eluent.

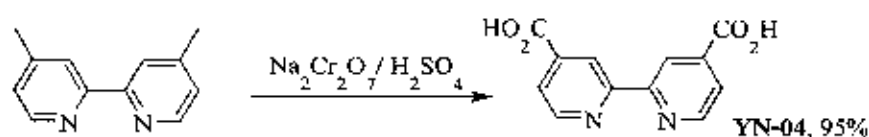
The product was obtained as the yellow liquid (2.29 g, 53%);  $^1\text{H NMR}$  (300 MHz,  $\text{CDCl}_3$ )  $\delta$  8.20 (d,  $J = 3\text{ Hz}$ , 1H), 7.30 (s, 1H), 7.07 (d,  $J = 6\text{ Hz}$ , 1H), 2.32 (s, 3H);  $^{13}\text{C NMR}$  (75 MHz,  $\text{CDCl}_3$ ):  $\delta$  149.6, 142.1, 128.7, 124.9, 123.8, 20.7; IR (NaCl) 2921, 2857, 1451, 1363, 1262, 1009, 736  $\text{cm}^{-1}$

### 3.3.3.3 The synthesis of 4,4'-dimethyl-2,2'-bipyridine (YN-03) [17, 65]



2-Bromo-4-methylpyridine (3.76 g, 20 mmol),  $\text{K}_2\text{CO}_3$  (3.04 g, 20 mmol) and  $\text{Pd(OAc)}_2$  (0.49 g, 1.80 mmol) was introduced in 30 ml anhydrous DMF in a two necked round bottom flask. Then, 1 ml portion of anhydrous isopropanol was syringed at once to the reaction flask. The reaction mixture was then heated to reflux under nitrogen atmosphere at 150  $^\circ\text{C}$  for 2 days. After that it was cooled to room temperature and extracted into dichloromethane (10 ml $\times$ 3). The crude reaction was evaporated to dryness and then passed through silica column chromatography using 5% (v/v) methanol - DCM to get the target product as a white solid (0.89 g, 44%); m.p. 174 - 176  $^\circ\text{C}$ ; MS (FAB $^+$ ,  $m/z$ )  $\text{C}_{12}\text{H}_{12}\text{N}_2$  184 (M);  $^1\text{H NMR}$  (300 MHz,  $\text{CDCl}_3$ )  $\delta$  8.53 (d,  $J = 6\text{ Hz}$ , 2H), 8.22 (s, 2H), 7.13 (d,  $J = 6\text{ Hz}$ , 2H), 2.43 (s, 6H);  $^{13}\text{C NMR}$  (75 MHz,  $\text{CDCl}_3$ ):  $\delta$  158.6, 148.9, 148.2, 124.7, 122.4, 21.2; IR (NaCl) 3040, 1931, 1594, 1454, 1365, 1247, 820  $\text{cm}^{-1}$

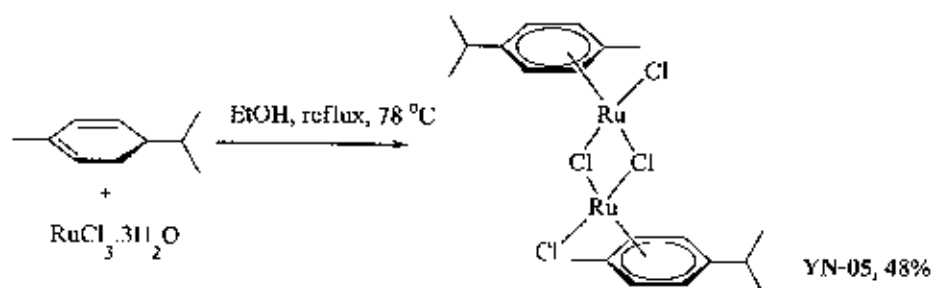
### 3.3.3.4 The synthesis of 4,4'-dicarboxy-2,2'-bipyridine (YN-04) [66]



$\text{Na}_2\text{Cr}_2\text{O}_7$  (1.35 g, 8.69 mmol) was added to 25 ml of conc.  $\text{H}_2\text{SO}_4$  in 100 ml round bottom flask. During the vigorous stirring, slowly added 4,4'-dimethyl-2,2'-bipyridine (0.40 g, 2.17 mmol) for 30 min (color changed from red to green) and then poured the mixture solution into 200 ml ice water and kept at 5  $^\circ\text{C}$  for 1 h. The yellow precipitate was filtered, then washed with ice water (10 ml $\times$ 3) and dissolved with 10% NaOH. The initial pH was adjusted to 2 by 10% HCl and filtered again. The compound was obtained as white solid in quantitatively yield (0.50 g, 95%); m.p. > 250  $^\circ\text{C}$ ;  $^1\text{H NMR}$  ( $\text{DMSO}-d_6$ , 300 MHz):  $\delta$  8.90 (d,  $J = 6\text{ Hz}$ , 2H), 8.80

(s, 2H), 7.89 (d,  $J = 6$  Hz, 2H);  $^{13}\text{C}$  NMR (75 MHz,  $\text{DMSO-d}_6$ ):  $\delta$  166.4, 155.9, 151.1, 140.0, 120.0, 119.8; IR (NaCl) 3413, 3108, 2448, 1717, 1456, 1368, 1292, 1068, 1011  $\text{cm}^{-1}$

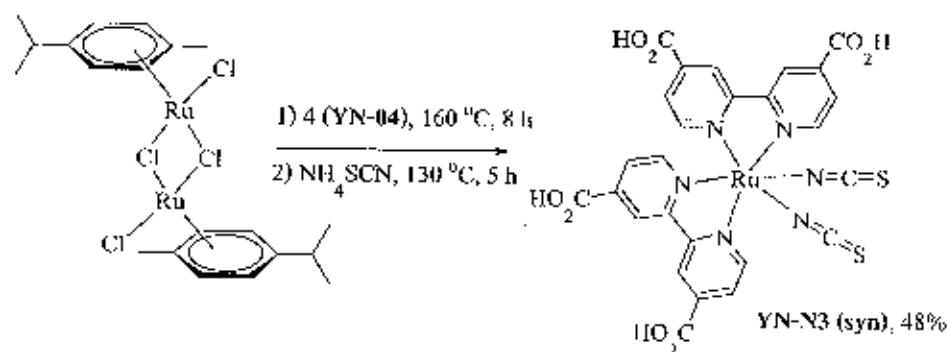
### 3.3.3.5 The synthesis of di- $\mu$ -chloro-bis[( $\eta^6$ -benzene)chloro ruthenium(II)] (YN-05) [67]



The  $\alpha$ -phellandrene (6 ml, 34.56 mmol) and ruthenium(III) trichloride trihydrated (1.13 g, 4.32 mmol) were dissolved by 10 ml ethanol in a two necked round bottom flask. The reaction mixture was refluxed overnight under  $\text{N}_2$  atmosphere. After the solvent was removed by rotary evaporator, it was filtered and washed the precipitate crude product with hexane. The product was obtained as the red solid (1.15 g, 48%); m.p. 190  $^\circ\text{C}$  (decomposed); MS (FAB $^+$ ,  $m/z$ )  $\text{C}_{20}\text{H}_{26}\text{Cl}_2\text{Ru}_2$ , 577 (M);  $^1\text{H}$  NMR ( $\text{CDCl}_3$ , 300 MHz):  $\delta$  5.49 (d,  $J = 6$  Hz, 2H), 5.35 (d,  $J = 6$  Hz, 2H) 2.93 (q,  $J = 6$  Hz, 1H), 2.71 (s, 3H) 1.29 (d,  $J = 6$  Hz, 6H);  $^{13}\text{C}$  NMR ( $\text{CDCl}_3$ , 75 MHz):  $\delta$  101.2, 96.7, 81.3, 80.5, 30.6, 22.1, 18.9; IR (NaCl) 3053, 2957, 2873, 2364, 1472, 1387, 878  $\text{cm}^{-1}$

### 3.3.2 Homoleptic ruthenium(II) complex synthesis

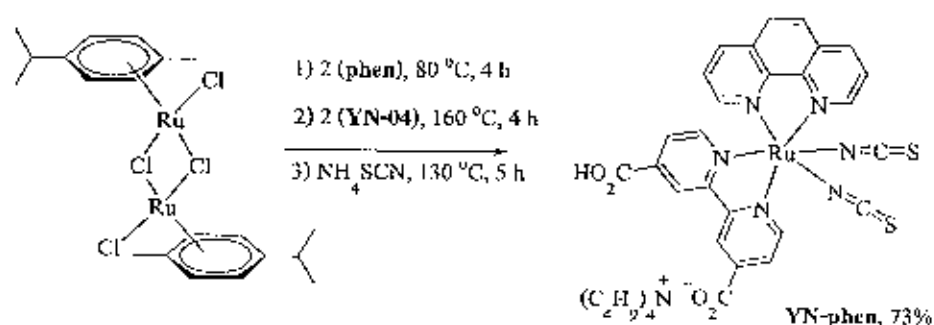
#### 3.3.2.1 The synthesis of bis(4,4'-dicarboxy-2,2'-bipyridine)dithiocyanato ruthenium(II) (YN-N3) [44]



Di- $\mu$ -chloro-bis[( $\eta^6$ -benzene)chloro ruthenium(II)] (0.10 g, 0.15 mmol) and 4,4'-dicarboxy-2,2'-bipyridine (0.15 g, 0.63 mmol) were dissolved in 25 ml dry DMF under reduced light condition. The reaction mixture was heated at 160 °C for 8 h in N<sub>2</sub> atmosphere and then NH<sub>4</sub>SCN (0.12 g) was added to the solution with continue heated at 130 °C for 5 h. The solvent was removed using a rotary evaporator and the resulting solid was redissolved with water and filtered on a sintered glass crucible. The precipitate was then washed well with water, followed by 1 : 4 acetone - ether. The dark resulting solid was dissolved by basic MeOH (1 M NaOH) and further purified on a sephadex LH-20 column using MeOH as an eluent. The main fraction was concentrated and redissolved with water. The initial pH was adjusted to 3 by adding 0.02 M HNO<sub>3</sub> to obtain a solid target complex then filtered on a sinter glass. The YN-N3 (syn) complex was achieved as a dark purple solid (0.05 g, 48%); MS (FAB<sup>+</sup>, m/z) C<sub>26</sub>H<sub>12</sub>N<sub>6</sub>O<sub>8</sub>RuS<sub>2</sub> 706 (M); <sup>1</sup>H NMR (CD<sub>3</sub>OD, 300 MHz):  $\delta$  9.62 (d, *J* = 5.9 Hz, 2H), 9.09 (s, 2H), 8.93 (s, 2H), 8.35 (d, *J* = 5.8 Hz, 2H), 7.84 (d, *J* = 5.7 Hz, 2H), 7.68 (d, *J* = 5.1 Hz, 2H); <sup>13</sup>C NMR (75 MHz, CD<sub>3</sub>OD):  $\delta$  165.9, 165.4, 159.0, 157.5, 153.4, 153.0, 140.6, 140.0, 134.8, 126.6, 125.7, 123.3, 122.9; IR (NaCl) 3450, 2866, 2118, 1698, 1609, 1401, 1317, 1258, 1228, 1015, 793 cm<sup>-1</sup>

### 3.3.3 Heteroleptic pyridyl ruthenium(II) complexes synthesis

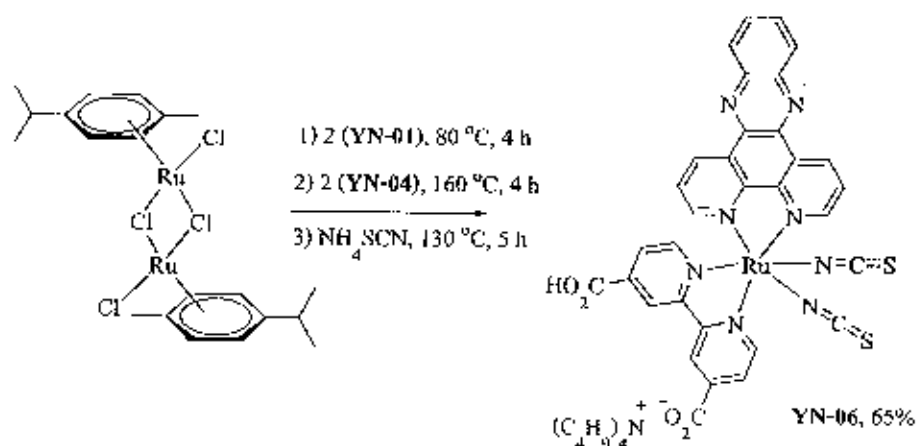
3.3.3.1 The synthesis of tetrabutylammonium(1,10-phenanthroline)(4-carboxy-2,2'-bipyridine-4'-carboxylate)dithiocyanatoruthenium(II) ion (YN-phen)



Di- $\mu$ -chloro-bis[( $\eta^6$ -benzene)chloro ruthenium(II)] (0.10 g, 0.15 mmol) and 1,10-phenanthroline (0.06 g, 0.31 mmol) were dissolved in 25 ml dry DMF under N<sub>2</sub> atmosphere. The mixture was heated in the dark for 4 h at 80 °C and then 4,4'-dicarboxy-2,2'-bipyridine (0.08 g, 0.31 mmol) was added with heating at 160 °C for 4 h. After that the NH<sub>4</sub>SCN 0.12 g (excess) was added into the reaction mixture with further heated for 5 h at 130 °C to

complete the reaction. The resulting complex was purified using a similar procedure as described for the **YN-N3 (syn)** synthesis. However, the basic MeOH (1 M TBAOH) was used instead of 1 M NaOH. The **YN-phen** complex was achieved as a dark purple solid (0.10 g, 73%); MS (FAB<sup>+</sup>, *m/z*) C<sub>42</sub>H<sub>51</sub>N<sub>7</sub>O<sub>4</sub>RuS<sub>2</sub> 884 (M+1), C<sub>16</sub>H<sub>15</sub>N 242 (M); <sup>1</sup>H NMR (DMSO-d<sub>6</sub>, 300 MHz): δ 9.76 (d, *J* = 4.8 Hz, 1H), 9.58 (d, *J* = 5.7 Hz, 1H), 9.03 (s, 1H), 8.84 (s, 1H), 8.72 (d, *J* = 7.9 Hz, 1H), 8.36 (d, *J* = 8.0 Hz, 1H), 8.28 - 8.02 (m, 4H), 7.93 (d, *J* = 4.9 Hz, 1H), 7.57 - 7.45 (m, 2H), 7.40 (d, *J* = 4.6 Hz, 1H), 3.26 (t, *J* = 16.7 Hz, 8H), 1.75 - 1.60 (m, 8H), 1.43 (dd, *J* = 14.5, 7.1 Hz, 8H), 1.04 (t, *J* = 7.3 Hz, 12H); <sup>13</sup>C NMR (75 MHz, DMSO-d<sub>6</sub>): δ 168.8, 168.5, 159.1, 158.1, 153.3, 153.0, 152.2, 151.6, 149.3, 148.2, 145.5, 144.9, 135.3, 134.6, 133.1, 132.9, 130.4, 130.3, 127.4, 127.3, 125.5, 125.3, 124.8, 124.6, 122.2, 122.0, 58.1, 23.4, 19.3, 12.5; IR (NaCl) 3418, 2960, 2862, 2102, 1722, 1602, 1406, 1228, 1024, 826 cm<sup>-1</sup>

3.3.3.2 The synthesis of tetrabutylammoniumdipyrido[3,2-a:2',3'-c]phenazine (4-carboxy-2,2'-bipyridine-4'-carboxylate)dithiocyanatoruthenium(II) ion (**YN-06**)



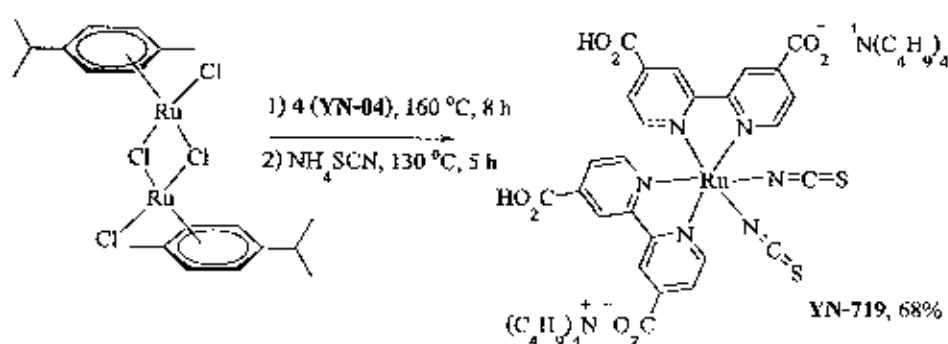
Di- $\mu$ -chloro-bis[( $\eta^6$ -benzene)chloro ruthenium(II)] (0.11 g, 0.17 mmol) and dipyrido[3,2-a:2',3'-c]phenazine (**YN-01**) (0.09 g, 0.34 mmol) were dissolved in 25 ml dry DMF under reduced light. To this solution was heated for 4 h at 80 °C under N<sub>2</sub> atmosphere and then 4,4'-dicarboxy-2,2'-bipyridine (**YN-04**) (0.08 g, 0.34 mmol) with continue heated for 4 h at 160 °C. The NH<sub>4</sub>SCN 0.12 g (excess) was added into the reaction mixture and heated for 5 h at 130 °C. After the reaction completed, the same procedure was used as described for the synthesis of **YN-phen**. The designed **YN-06** complex was achieved as a dark purple solid (0.11 g, 65%); MS (FAB<sup>+</sup>, *m/z*) C<sub>32</sub>H<sub>17</sub>N<sub>8</sub>O<sub>4</sub>RuS<sub>2</sub> 744 (M+1), C<sub>16</sub>H<sub>15</sub>N 242 (M); <sup>1</sup>H NMR (DMSO-d<sub>6</sub>, 300 MHz): δ

9.65 (d,  $J = 5.1$  Hz, 2H), 9.51 (d,  $J = 5.5$  Hz, 1H), 9.27 (s, 1H), 9.11 (d,  $J = 19.4$  Hz, 1H), 8.94 (d,  $J = 15.6$  Hz, 1H), 8.45 (d,  $J = 5.8$  Hz, 2H), 8.34 (d,  $J = 5.7$  Hz, 2H), 8.10 (s, 2H), 8.01 (s, 1H), 7.73 (s, 2H), 7.45 (s, 1H), 3.15 (s, 8H), 1.54 (s, 8H), 1.28 (d,  $J = 6.5$  Hz, 8H), 0.91 (t,  $J = 6.9$  Hz, 12H);  $^{13}\text{C}$  NMR (75 MHz, DMSO- $d_6$ ):  $\delta$  166.0, 165.5, 159.1, 158.1, 154.5, 153.6, 153.2, 151.9, 150.6, 142.2, 142.2, 140.3, 140.1, 134.8, 134.5, 132.6, 129.8, 129.5, 127.7, 126.8, 126.6, 125.6, 123.2, 58.0, 23.5, 19.6, 13.8; IR (NaCl) 3423, 2955, 2093, 1717, 1606, 1415, 1228, 1019, 797  $\text{cm}^{-1}$

### 3.3.4 Homoleptic and heteroleptic ruthenium(II) complex with tetrabutyl

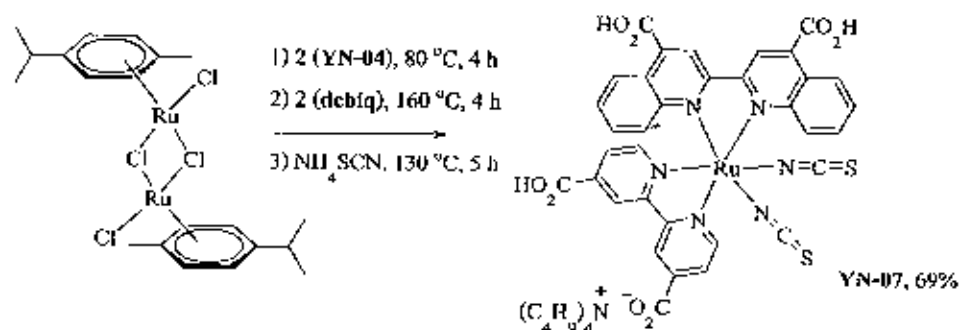
#### ammonium salt synthesis

3.3.4.1 The synthesis of bis(tetrabutylammonium)(bis(4-carboxy-2,2'-bipyridine-4'-carboxylate)dithiocyanatoruthenium(II) ion (YN-719) [47]



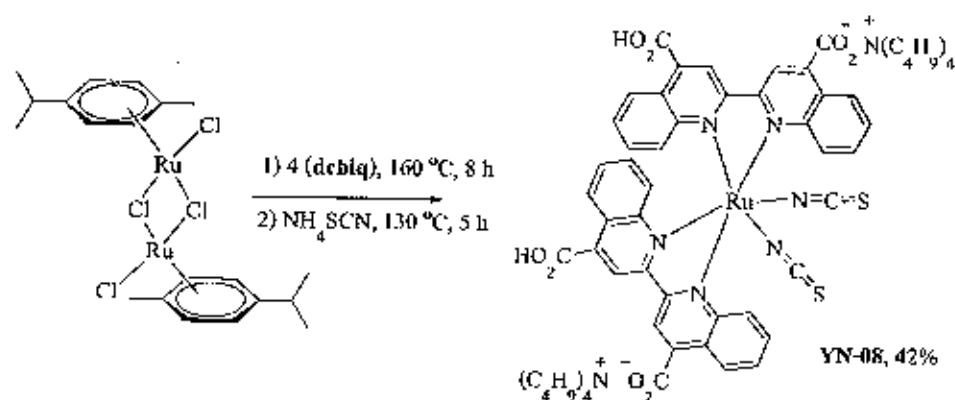
The YN-719 complex was synthesized by the same procedure as was employed to synthesize YN-N3, but using YN-04 (0.15 g, 0.63 mmol). The basic MeOH (TBAOH) was used instead of 1 M NaOH in the reaction workup procedure. The YN-719 complex was achieved as a dark purple solid (0.10 g, 68%); MS (FAB $^+$ ,  $m/z$ )  $\text{C}_{28}\text{H}_{12}\text{N}_6\text{O}_8\text{RuS}_2$  706 (M),  $\text{C}_{10}\text{H}_8\text{N}_2$  242 (M);  $^1\text{H}$  NMR (DMSO- $d_6$ , 300 MHz):  $\delta$  9.58 (d,  $J = 5.8$  Hz, 2H), 9.06 (s, 2H), 8.90 (s, 2H), 8.31 (d,  $J = 5.8$  Hz, 2H), 7.77 (d,  $J = 5.8$  Hz, 2H), 7.64 (d,  $J = 5.8$  Hz, 2H), 3.18 (t,  $J = 21.5$  Hz, 16H), 1.66 (dt,  $J = 15.9, 7.8$  Hz, 16H), 1.49 - 1.26 (m, 16H), 1.01 (t,  $J = 7.3$  Hz, 24H);  $^{13}\text{C}$  NMR (75 MHz, DMSO- $d_6$ ):  $\delta$  165.9, 165.4, 159.0, 157.5, 153.4, 153.0, 140.6, 140.0, 134.8, 126.6, 125.7, 123.3, 122.9, 58.0, 23.5, 19.7, 13.6; IR (NaCl) 3456, 2954, 2868, 2097, 1716, 1608, 1413, 1360, 1226, 1065, 801  $\text{cm}^{-1}$

3.3.4.2 The synthesis of tetrabutylammonium(4,4'-dicarboxy-2,2'-biquinoline)  
(4-carboxy-2,2'-bipyridine-4'-carboxylate)dithiocyanatoruthenium(II) ion (YN-07)



Di- $\mu$ -chloro-bis[( $\eta^6$ -benzene)chloro ruthenium(II)] (0.08 g, 0.13 mmol), 4,4'-dicarboxy-2,2'-bipyridine (YN-04) (0.06 g, 0.26 mmol) was dissolved in 25 ml dry DMF under  $N_2$  atmosphere. The mixture was heated in the dark for 4 h at 80 °C and then 4,4'-dicarboxy-2,2'-biquinoline (dcbiq) (0.05 g, 0.16 mmol) was added with continue heated at 160 °C for 4 h. After the  $NH_4SCN$  0.12 g (excess) was added into the reaction mixture and heated at 130 °C for 5 h. The reaction workup methods are similar to that the synthesis of YN-719. The YN-07 complex was achieved as a green solid (0.09 g, 69%); MS (FAB<sup>+</sup>,  $m/z$ )  $C_{33}H_{19}N_5O_8RuS$  749 ( $M+1$ ),  $C_{16}H_{16}N$  242 ( $M$ );  $^1H$  NMR (DMSO- $d_6$ , 300 MHz):  $\delta$  9.29 (s, 1H), 9.19 (d,  $J = 8.9$  Hz, 1H), 9.12 (d,  $J = 6.5$  Hz, 1H), 9.07 (s, 1H), 8.81 (d,  $J = 8.8$  Hz, 2H), 8.54 (d,  $J = 8.7$  Hz, 1H), 8.32 (d,  $J = 8.1$  Hz, 1H), 8.26 (d,  $J = 5.8$  Hz, 1H), 8.14 (d,  $J = 5.9$  Hz, 1H), 7.96 (s, 1H), 7.88 (d,  $J = 8.0$  Hz, 1H), 7.79 (s, 1H), 7.60 (s, 1H), 7.28 (d,  $J = 8.2$  Hz, 1H), 6.52 (d,  $J = 8.7$  Hz, 1H), 3.23 - 2.94 (m, 8H), 1.54 (s, 8H), 1.28 (dd,  $J = 14.4, 7.3$  Hz, 8H), 0.91 (t,  $J = 7.3$  Hz, 12H);  $^{13}C$  NMR (75 MHz, DMSO- $d_6$ ):  $\delta$  168.1, 167.5, 167.3, 165.6, 165.3, 162.1, 160.3, 159.8, 158.0, 155.3, 154.7, 154.3, 152.1, 151.4, 148.5, 139.7, 139.2, 138.9, 138.8, 137.7, 135.8, 131.6, 131.4, 131.0, 130.6, 130.3, 129.8, 129.4, 127.1, 126.1, 125.3, 124.7, 123.9, 119.7, 57.9, 23.5, 19.3, 13.9; IR (NaCl) 3423, 2960, 2107, 1711, 1549, 1458, 1379, 1231, 1153, 812  $cm^{-1}$

3.3.4.3 The synthesis of bis(tetrabutylammonium)bis(4-carboxy-2,2'-biquinoline-4'-carboxylate)dithiocyanatoruthenium(II) ion (YN-08)



The synthesis of YN-08 is similar to that was described in the YN-719 synthesis procedure, but the ligand 4,4'-dicarboxy-2,2'-biquinoline (debiq) (0.21 g, 0.60 mmol) was used instead of YN-04 ligand. The YN-08 complex was achieved (0.09 g, 42%) as a dark green solid; MS (FAB<sup>+</sup>, m/z) C<sub>40</sub>H<sub>22</sub>N<sub>4</sub>O<sub>8</sub>Ru<sub>2</sub>·CH<sub>3</sub>OH 824 (M), 242 (M); <sup>1</sup>H NMR (DMSO-d<sub>6</sub>, 300 MHz): δ 9.17 (s, 4H), 8.78 (d, J = 8.4 Hz, 4H), 8.32 (d, J = 8.4 Hz, 4H), 7.92 (t, J = 6 Hz, J = 9 Hz, 4H), 7.79 (t, J = 6 Hz, J = 9 Hz, 4H), 3.15 (s, 16H), 1.53 (s, 16H), 1.27 (d, J = 5.9 Hz, 16H), 0.91 (s, 24H); <sup>13</sup>C NMR (75 MHz, DMSO-d<sub>6</sub>): δ 168.0, 154.8, 148.6, 138.4, 130.9, 130.5, 129.2, 126.2, 125.3, 119.7, 58.0, 58.0, 23.5, 19.7, 13.6; IR (NaCl) 3429, 2965, 2097, 1973, 1602, 1550, 1306, 1277, 1242, 1156, 778 cm<sup>-1</sup>

### 3.4 DSSCs Device fabrication

**3.4.1 Main chemical reagents:** The chemical used for device fabrication in this thesis are listed [63]:

3.4.1.1 7 mM  $H_2PtCl_6$  in 3-methoxyethanol solution

3.4.1.2  $TiCl_4$

3.4.1.3 The homoleptic ruthenium(II) without tetrabutylammonium salt; **N3 (std)** and **YN-N3 (syn)**

3.4.1.4 The heteroleptic pyridinyl ruthenium(II) with tetrabutylammonium salt; **YN-phen** and **YN-06**

3.4.1.5 The homoleptic and heteroleptic ruthenium(II) with tetrabutylammonium salt; **YN-719**, **YN-07** and **YN-08**

3.4.1.6  $TiO_2$  nanoparticles; transparent (Ti-Nanoxide 20T/SP, transparent)

3.4.1.7  $TiO_2$  nanoparticles, scattering (Ti-Nanoxide D/SP, scattering)

#### 3.4.2 Ingredient of electrolyte solution [68]

3.4.2.1 0.05 M iodine ( $I_2$ )

3.4.2.2 0.4 M 4-tertbutylpropylene (TBP)

3.4.2.3 0.1 M lithium iodide (LiI)

3.4.2.4 0.6 M tetra pyridylammonium iodide

3.4.2.5 85 : 15 (v/v) mixtures of acetonitrile and valeronitrile

#### 3.4.3 Preparation of FTO glass

A pair of FTO glasses was cut into 2.0×1.3 cm size. These will be used as the working electrode (WE) and counter electrode (CE). Then, the CE electrode part was drilled by PROXXON, TBM 220 (hole size 0.5 mm). Both were cleaned in a detergent solution using an ultrasonic bath for 15 min/step with the following solvents; distilled water, dishwashing liquid, distilled water, ethanol and acetone, respectively. The finishing FTO glasses were shown in Figure 3.2.

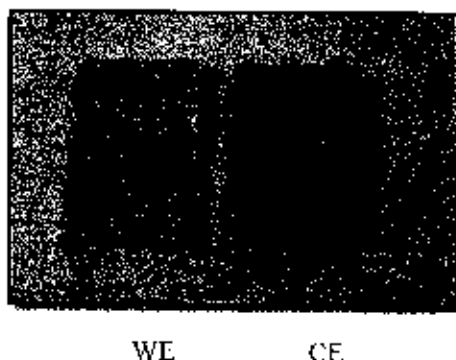


**Figure 3.2** The finishing FTO glasses (working electrode (WE) and counter electrode (CE))

### 3.4.4 Fabrication of Dye-Sensitized Solar Cells [69]

After the FTO glasses were prepared discussed in previously section, the fabrication for DSSCs devices as followed;

3.4.4.1 The  $\text{TiO}_2$  films (active area: ca.  $0.25 \text{ cm}^2$ ) were treated with a solution of titanium tetrachloride solution ( $\text{TiCl}_4$ ) and heated to  $70^\circ\text{C}$  for 30 min before being allowed to cool and dried in room temperature.

3.4.4.2 The 25 nm transparent  $\text{TiO}_2$  particle layer film was first printed on the working electrode (WE) followed by heated to  $200^\circ\text{C}$  for 15 min,  $500^\circ\text{C}$  15 min allowed to cool down to  $80^\circ\text{C}$ . This step was repeated twice and then the last layer was coated with 100 nm of  $\text{TiO}_2$  light scattering particle. The active  $\text{TiO}_2$  film was activated by treated with a solution of titanium tetrachloride and heated to  $70^\circ\text{C}$  for 30 min.

3.4.4.3 The dye solution ( $3 \times 10^{-4} \text{ M}$ ) was adsorbed with activated  $\text{TiO}_2$  at room temperature for 24 h in the dark.

3.4.4.4 The excess amount of dye was removed by rinsing off with ethanol.

3.4.4.5 The 36  $\mu\text{l}$  of 7 mM  $\text{H}_2\text{PtCl}_6$  in 3-methoxyethanol solution was drop on a counter electrode (CE) then heated to  $385^\circ\text{C}$  for 30 min allowed to cool down to  $110^\circ\text{C}$ .

3.4.4.6 The dye adsorbed  $\text{TiO}_2$  electrode and Pt counter electrode were assembled into a sealed sand-wich type cell by heating a hot melt ionomer film (Surlyn 1702, 25  $\mu\text{m}$  thickness, Solaronix) as a spacer between the electrodes.

3.4.4.7 An electrolyte solution was injected by vacuum backfilling method. Finally, the hole was sealed by using ionomer film and a glass cover slide (0.1 mm thickness). The finishing devices ready for the photophysic measurement are shown in Figure 3.3.

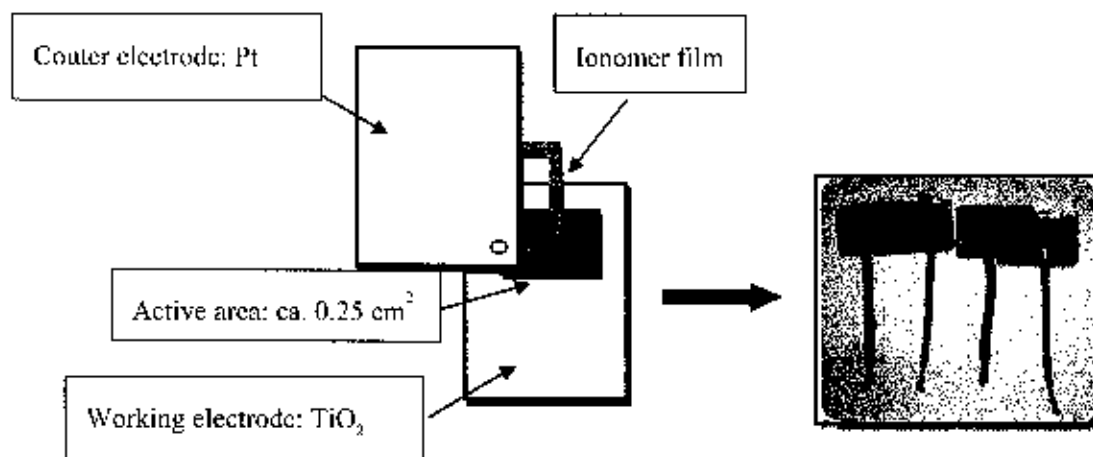


**Figure 3.3** A completed dye sensitized solar cells device

### 3.4.5 Measuring instrument techniques

To investigate the efficiency of ruthenium(II) complexes, a standardization of the measurement is needed. The photocurrent voltage characteristics ( $I$ - $V$ ) and incident photon to electron conversion efficiency (IPCE) were performed with a Kiethley 2400, Oriel instrument.

#### 3.4.5.1 Photocurrent voltage characteristics ( $I$ - $V$ )

The current-voltage ( $I$ - $V$ ) measurements were carried out with an active area of  $0.16 \text{ cm}^2$  by a Kiethley 2400 source meter, Kiethley 617 programmable electrometer measured unit under AM 1.5 global simulated sunlight ( $100 \text{ mW/cm}^2$ ) which was produced by a 500 W Oriel Solar Simulator (new port BB-L, USA). The incident light intensity was calibrated to 1 sun by a photovoltaic reference cell system (0.610 mA, Oriel instruments, USA). The conversion efficiency ( $\eta$ ) of the solar cell is calculated (see equation 1) from the short-circuit photocurrent density ( $J_{sc}$ ), the open-circuit photovoltage ( $V_{oc}$ ), the fill factor ( $ff$ ), and the intensity of the incident light ( $I_{ph}$ ).

$$\eta = \frac{J_{sc} \cdot V_{oc} \cdot ff}{I_{ph}} \quad (1)$$

#### 3.4.5.2 The incident photon to electron conversion efficiency (IPCE)

The incident photon to electron conversion efficiency (IPCE) of a DSSCs was measured at the short-circuit condition with a computerized apparatus consisting of a Oriel solar simulator (new port BB-L, USA), coupled to a 1/8 m monochromator (Oriel, USA), a Keithley 2400 digital source meter. The wavelength scanning range was from 350 nm to 800 nm with the interval of 5 nm. At each wavelength, three seconds were needed to stabilize the incident monochromatic light.

## CHAPTER 4

### RESULTS AND DISCUSSIONS

#### 4.1 The synthesis homoleptic ruthenium(II) complex without tetrabutyl ammonium salt

Bis(4,4'-dicarboxy-2,2'-bipyridine)dithiocyanatoruthenium(II), called **N3** dye, was synthesized by Grätzel's groups in 1993 [44]. This dye exhibits 10% of power to conversion efficiency, and widely uses as ruthenium complex standard dye. In this work, we reported the synthesis and study the optical and electrochemical properties as well as the overall conversion efficiency of bis(4,4'-dicarboxy-2,2'-bipyridine)dithiocyanatoruthenium(II), see Figure 4.1, coded **YN-N3 (syn)** dye, compared with a cell fabricated using the **N3 (std)** (95% NMR, Aldrich).

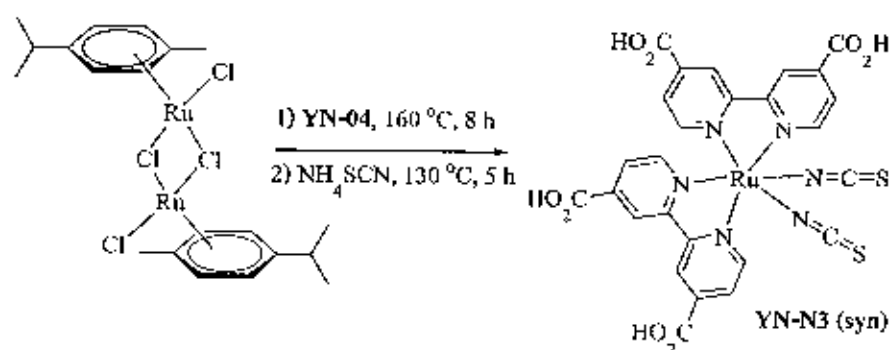


**Figure 4.1** The synthesis of ruthenium(II) complex dye (**YN-N3 (syn)**)

The molecular structure of homoleptic ruthenium(II) complex, **YN-N3 (syn)**, is comprised of dithiocyanate, bis(bipyridine) ligand grafted with carboxylic acid anchoring group and ruthenium metal center which was prepared from the **YN-05** precursor ruthenium(II) in Figure 4.2. The synthesis of **YN-04** ligand, **YN-05** precursor ruthenium(II) and **YN-N3 (syn)** are described as followed;

#### 4.1.1 The synthesis of di- $\mu$ -chloro-bis[( $\eta^6$ -benzene)chlororuthenium(II)] (YN-05)

The YN-05 was synthesized by addition reaction of the  $\text{RuCl}_3 \cdot 3\text{H}_2\text{O}$  with  $\alpha$ -phellandrene ligand to get the resulting complex product as red solid, 48% yield. The complex was characterized by FT-IR (Figure A.5, appendix A) and NMR techniques, shown in Figure 4.3.

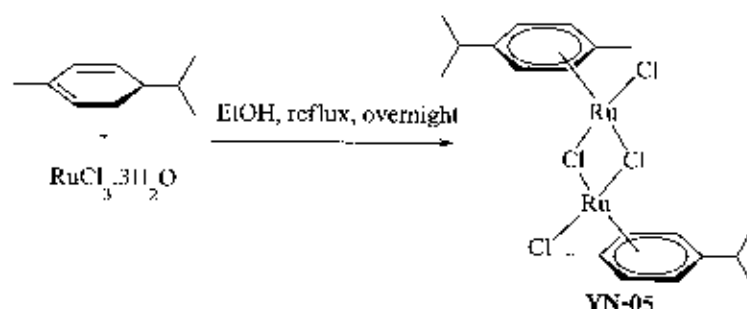


**Figure 4.2** Synthetic method of YN-05 ruthenium(II) precursor

YN-05 is a symmetric molecule. The  $^1\text{H}$  NMR spectrum of YN-05 shows the signal at  $\delta$  5.49 (4H) and 5.35 (4H) assigned as proton of phellandrene ring. Where the chemical shift at 2.91 (2H), 2.16 (6H) and 1.28 (12H) were assigned as the protons of the alkyl group.

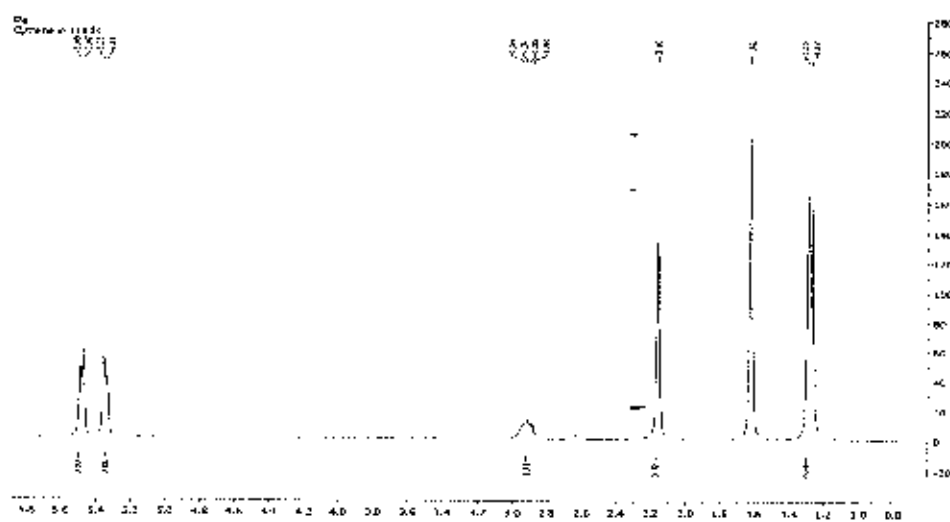


**Figure 4.3**  $^1\text{H}$  NMR in  $\text{CDCl}_3$  of the precursor ruthenium complex (YN-05)

#### 4.1.2 The synthesis of 4,4'-dicarboxy-2,2'-bipyridine (YN-04)

To begin the synthesis of the homoleptic YN-N3 (syn) ruthenium complex, the 4,4'-dicarboxy-2,2'-bipyridine (YN-04) ligand was synthesized in 3 steps as shown in Figure 4.4. YN-02 was prepared according to the previously reported (experimental section) via Sandmeyer reaction [64]. Then the homocoupling reaction of YN-02, using stable palladium(II) catalyst for carbon-carbon bond formation lead to YN-03 product. In the last step of the ligand synthesis, the dimethyl of YN-03 was oxidized by  $\text{H}_2\text{SO}_4/\text{Na}_2\text{Cr}_2\text{O}_7$  to get the target product YN-04 in quantitatively yield.

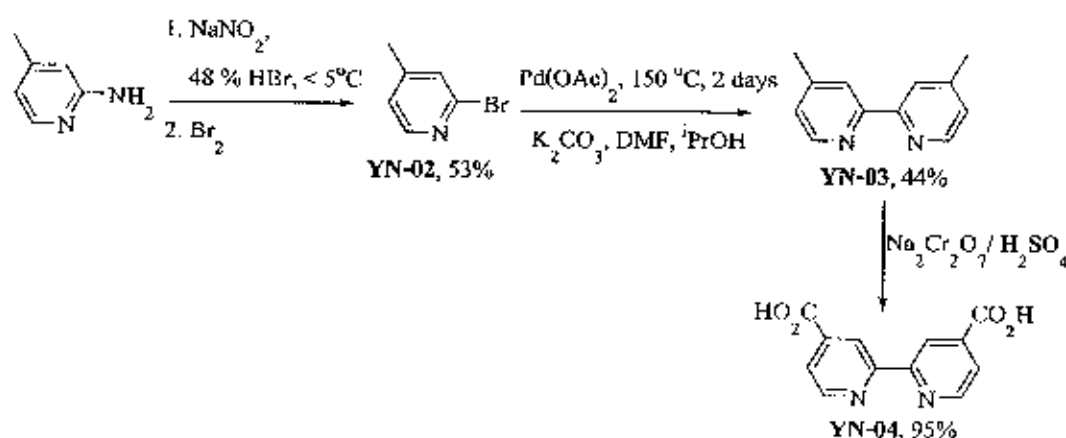


**Figure 4.4** The synthetic route to 4,4'-dicarboxy-2,2'-bipyridine (YN-04)

##### 4.1.2.1 The synthesis of 2-bromo-4-methyl pyridine (YN-02)

YN-02 was synthesized by the Sandmeyer reaction. Figure 4.5 shows the proposed mechanism of the reaction of 2-amino-4-methylpyridine with sodium nitrite in 48%  $\text{HBr}$  acidic condition at the temperature not over than  $5^\circ\text{C}$  to get the yellow liquid product. The reaction mechanism involved two-reaction steps. Step 1: in the acidic condition, nitrite ion changes to nitronium ion by losing one hydrate molecule, then the lone pair of  $-\text{NH}_2$  reacts with the nitronium ion to form the electrophile character N-N. Step 2: the  $\text{H}_2\text{O}$  elimination of the intermediate cation to form 4-methylpyridine-2-diazonium, following the bromide nucleophilic attacks provided the target compound as a yellow liquid, 53% yield.

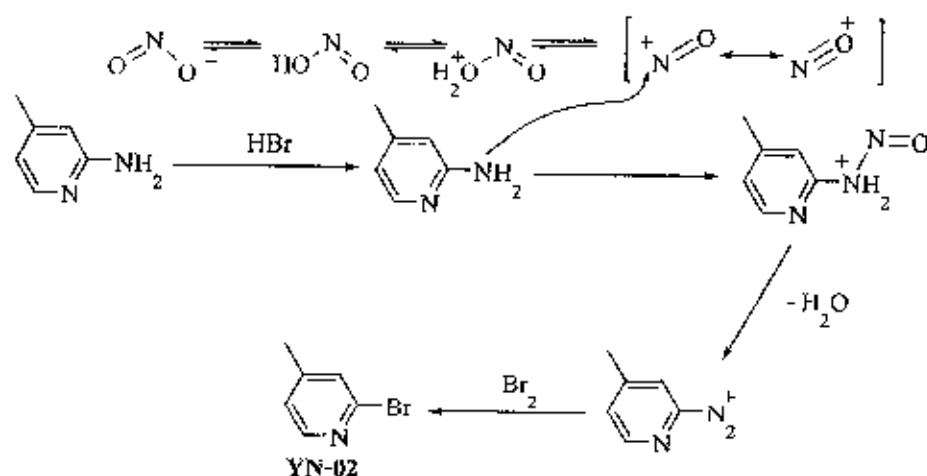


**Figure 4.5** The proposed mechanism of Sandmeyer reaction to form YN-02

The <sup>1</sup>H NMR spectra of YN-02 shows a signal at chemical shift 8.20 ppm (2H), 7.31 (2H) and 7.07 (2H) assigned as protons of aromatic ring, whereas the singlet signal at chemical shift 2.32 ppm (6H) assigned as proton of the methyl group. The <sup>13</sup>C NMR resonance of YN-02 displayed 12 spectra (Figure A.2, appendix A).

#### 4.1.2.2 The synthesis of 4,4'-dimethyl-2,2'-bipyridine (YN-03)

The synthesis pathway for YN-03 is shown in Figure 4.6. The homocoupling reaction of two equivalents of 2-bromo-4-methylpyridine (YN-02) was used to synthesize YN-03 using K<sub>2</sub>CO<sub>3</sub> and Pd(OAc)<sub>2</sub> as base and catalyst, respectively.

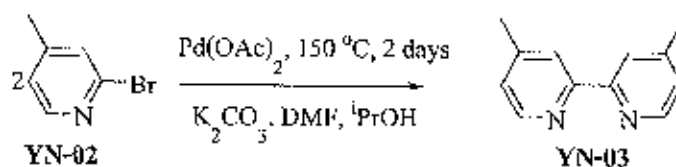


**Figure 4.6** The synthetic method of 4,4'-dimethyl-2,2'-bipyridine (YN-03)

The mechanism of the palladium catalyzed reaction is shown in Figure 4.7. The palladium(0) active catalyst species undergoes oxidative addition with bromo pyridine, followed by trans-metallation reaction and then reductive elimination to form the pyridine-pyridine carbon bond.

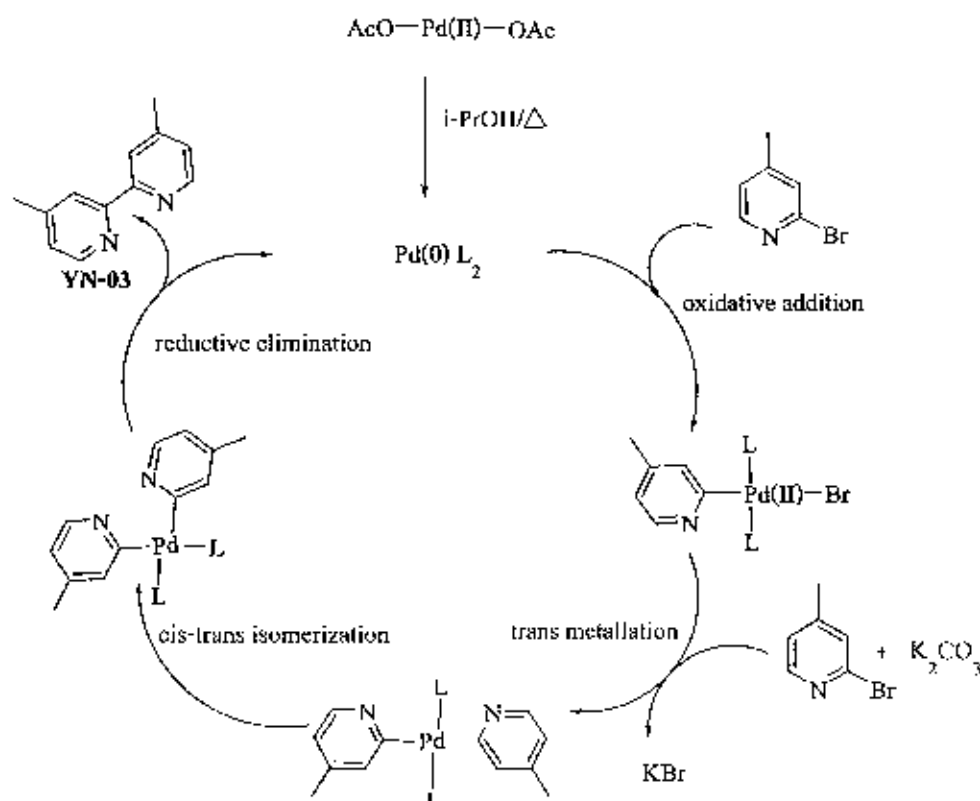
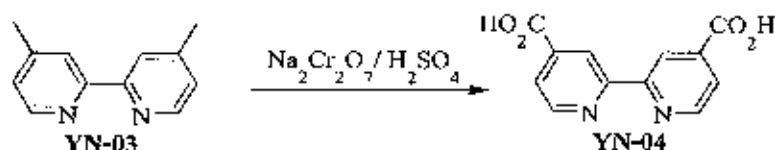


Figure 4.7 The propose mechanism of homocoupling reaction

The characterization of **YN-03** was investigated by FT-IR, melting point, FAB mass and NMR techniques. This compound has a  $C_2$  symmetrical molecular structure, as only half of the proton in the structure was observed in the  $^1\text{H}$  NMR spectra. The chemical shift at 8.53 ppm (2H), 8.22 (2H) and 7.13 (2H) was assigned as protons of the pyridine aromatic ring, and the singlet signal at  $\delta$  2.43 ppm (6H) assigned as the proton of  $\text{CH}_3$  (Figure A.3, appendix A). The  $^{13}\text{C}$  NMR spectra of **YN-03** show only 6 carbon signals which supported that it is a symmetric molecule.

#### 4.1.2.3 The synthesis of 4,4'-dicarboxylic-2,2'-bipyridine (YN-04)

The oxidation of YN-03 with oxidizing reagent, sodium dichromate ( $\text{Na}_2\text{Cr}_2\text{O}_7$ ), in acidic condition was used to synthesize the YN-04 ligand, shown in Figure 4.8.



**Figure 4.8** Synthetic method of 4,4'-dicarboxylic-2,2'-bipyridine (YN-04)

The mechanism of the oxidation reaction of 4,4'-dimethyl-2,2'-bipyridine (YN-03) shows in Figure 4.9. The dimethyl on bipyridine derivative, YN-03, was converted into aldehyde functional group, then it was oxidized to 4,4'-dicarboxylic-2,2'-bipyridine (YN-04) as white solid in quantitative yields by  $\text{Na}_2\text{Cr}_2\text{O}_7$ .

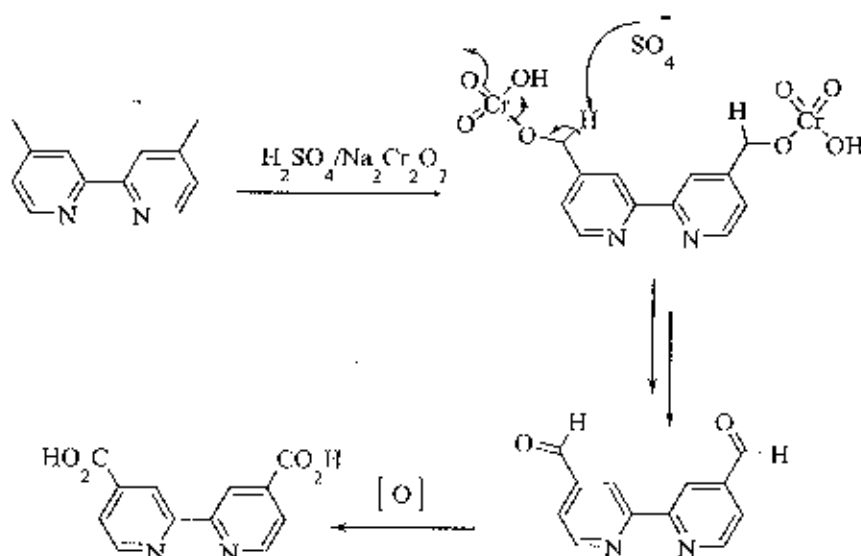


**Figure 4.9** The propose mechanism of oxidation reaction

The characterization of YN-04 was investigated by the same techniques as for YN-03. The YN-04 is a  $C_2$  symmetrical structure because the  $^1\text{H}$  NMR spectra was observed only 3 proton resonances (6H). The chemical shift at 8.90 ppm (2H), 8.80 (2H), and 7.89 (2H) are

assigned as protons of aromatic pyridine ring shown in Figure 4.10. The  $^{13}\text{C}$  NMR spectra of YN-04 show 5 carbon resonances for aromatic pyridine carbon and one signal for carboxylic group (see Figure A.4, appendix A).

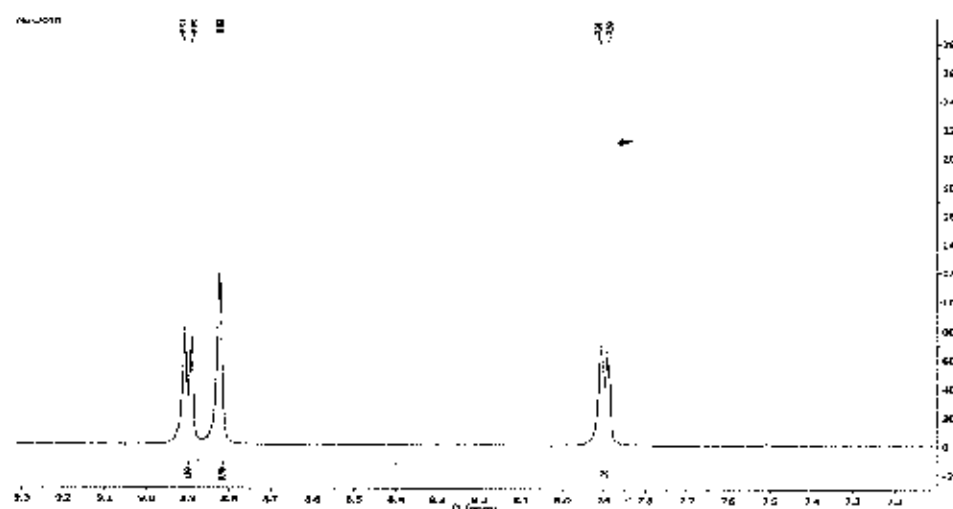
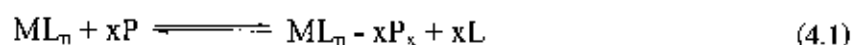


**Figure 4.10**  $^1\text{H}$  NMR in  $\text{DMSO-d}_6$  of 4,4'-dicarboxylic-2,2'-bipyridine (YN-04)

#### 4.1.3 The synthesis of homoleptic ruthenium(II) (YN-N3 (syn))

YN-N3 (syn) was synthesized by ligand substitution reaction (equation 4.1).



The YN-N3 (syn) was synthesized in a moderate yield by a one pot reaction. First, the reaction of  $[\text{RuCl}_2(p\text{-cymene})_2]$  with YN-04 according to 1:4 stoichiometry ratio in DMF at  $160^\circ\text{C}$  give the  $\text{RuCl}_2(4,4'\text{-dicarboxylic-2,2'-bipyridine})_2$  complex. Then the excessive  $\text{NiI}_2\text{SCN}$  was added to afford the final product, shown in Figure 4.11.

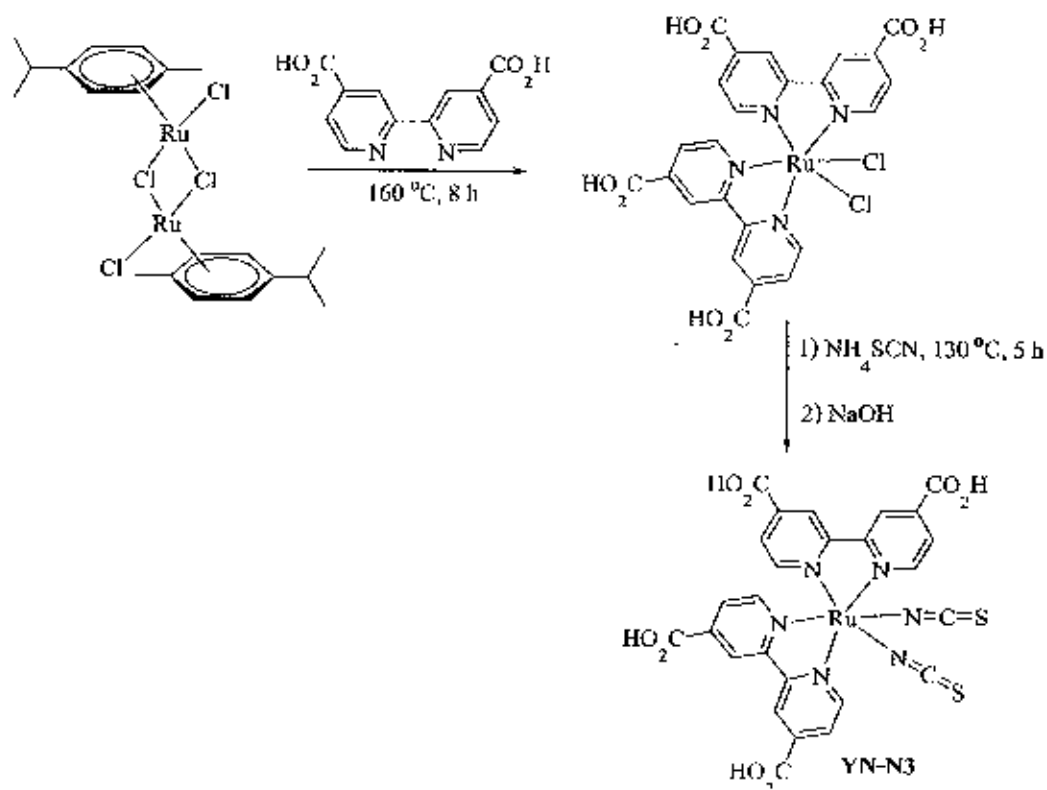


**Figure 4.11** The synthetic route of ligand substitution reaction to YN-N3 (syn) [70].

The molecular structure of YN-N3 (syn) was confirmed by NMR spectral data. The  $^1\text{H}$  NMR spectrum of YN-N3 (syn) suggested that the molecule is symmetrical. The signals at  $\delta$  9.62 ppm (2H), 9.09 (2H), 8.93 (2H), 8.35 (2H), 7.84 (2H), and 7.68 (2H) were assigned as the proton of bipyridine moieties, shown in Figure 4.12. These spectra are the same as that reported for the commercial standard complex characterization. Whereas, the  $^{13}\text{C}$  NMR signal of YN-N3 (syn) shows 13 signals, 10 signals of the aromatic pyridine carbon, two signals of the carboxylic group and one signal of the thiocyanate moiety.

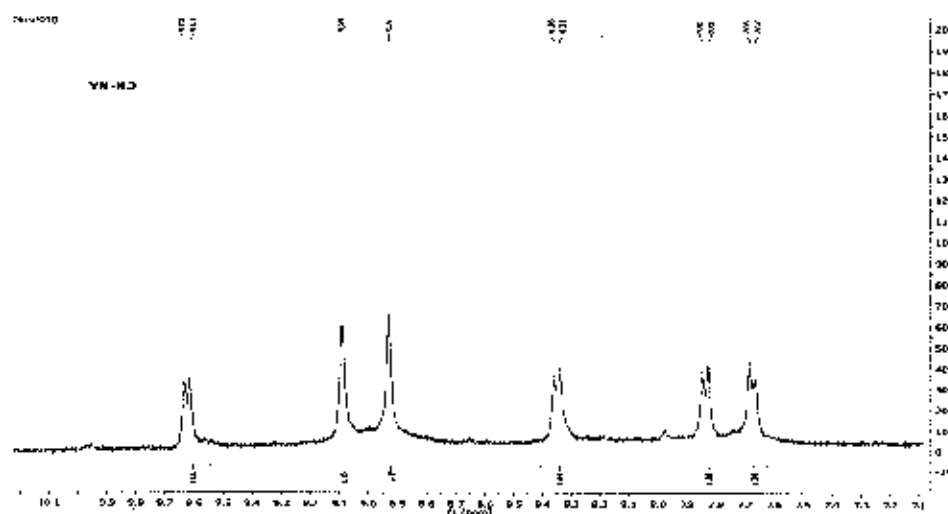


**Figure 4.12**  $^1\text{H}$  NMR of YN-N3 (syn) in  $\text{CD}_3\text{OD}$

#### 4.1.4 Characterization homoleptic ruthenium(II) complex dye without tetrabutyl ammonium salt

The homoleptic ruthenium(II) complex without the tetrabutyl ammonium salt in this study was fully characterized and then was fabricated as described in the experimental section 3.4.4. The photo and electrochemical properties were investigated as followed;

##### 4.1.4.1 Optical properties

UV-Vis absorption spectra of YN-N3 (syn) and N3 (std) complexes are shown in Figure 4.13, measured under the same experimental condition  $1 \times 10^{-5}$  M in DMF. The spectra of YN-N3 (syn) and N3 (std) complexes feature intense absorption bands in the UV region. The absorption band of both dyes shows nearly site, between 300 and 400 nm attributed to  $\pi-\pi^*$  transitions of the bipyridine ligand moieties. Both ruthenium(II) complex dyes show broad absorption band at longer wavelength around 450-650 nm region corresponding to the well known spin allowed metal to ligand charge transfer (MLCT) transition [71]. Notably, the molar extinction coefficient of the N3 (std) of the visible absorption bands at 400 and 550 nm are 20,972 and 19,386  $\text{M}^{-1}\text{cm}^{-1}$ , respectively, which are significantly higher than those of YN-N3 (syn) sensitizer, which posses about 13,247 and 12,016  $\text{M}^{-1}\text{cm}^{-1}$ . The N3 (std) give higher intensity compared with YN-N3 (syn). It should be noted that our YN-N3 (syn) is less soluble than that N3 (std) because the residue of  $\text{H}_2\text{O}$  and  $\text{CH}_3\text{OH}$  in the complex is responsible for this explanation (Falodthaisong,

C. et al. unpublished result). They found that the more residue of H<sub>2</sub>O and CH<sub>3</sub>OH in the complex, the higher power conversion efficiency. The absorption spectral properties of YN-N3 (syn) and N3 (std) are listed in Table 4.1.

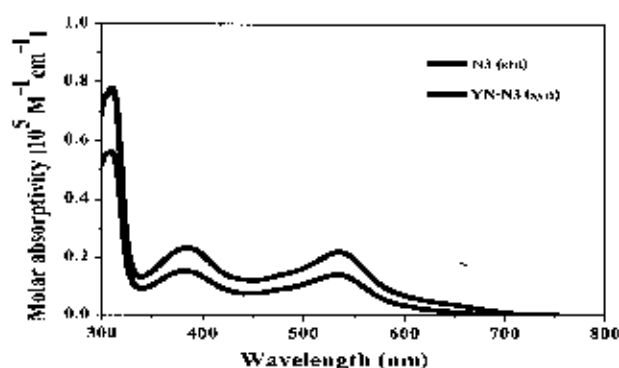


**Figure 4.13** UV-Vis absorption spectra of  $1 \times 10^{-5}$  M YN-N3 (syn) and N3 (std) solution in DMF at room temperature

**Table 4.1** The absorption of YN-N3 (syn) and N3 (std) solution in dry DMF

Dyes	$\lambda_{\text{max}}^{\text{obs}} / \text{nm} (\epsilon \times 10^5 / \text{M}^{-1} \text{cm}^{-1})$
YN-N3 (syn)	314 (0.59), 392 (0.13), 545 (0.12)
N3 (std)	314 (0.78), 399 (0.21), 551 (0.19)

#### 4.1.4.2 Electrochemical properties

The redox property of the similar structure YN-N3 (syn) and N3 (std) dyes were investigated using cyclic voltammetry (CV). The cyclic voltammogramme is shown in Figure 4.14 and summarized in Table 4.2. The measurement was performed with Autolab Metrohm PG11 on 0.1 mM solution of the complex in DMF with the presence of [Bu<sub>4</sub>N]PF<sub>6</sub> as supporting electrolyte. The cyclic voltammetry of YN-N3 (syn) and N3 (std) complexes solution in dry DMF shows the onset oxidation wave ( $E_{\text{onset}}^{\text{ox}}$ ) at 0.76 and 0.94 V vs. NHE, respectively. These values are more positive than the redox potential of iodide/triiodide pair (ca. 0.35 V vs NHE) [10] (see Figure 4.15), providing the thermodynamic driving force for efficient dye

regeneration. The oxidation potentials are due to the oxidation from Ru(II) to Ru(III). When scanning toward negative potential, the reversible waves of both dyes were observed,  $E_{red}$  at -0.75 and -0.72 V, respectively. These are assigned to the reduction of 2,2'-bipyridine-4,4'-dicarboxylic acid ligand. The reduction potentials of complexes are sufficiently more negative than the conduction band edge level of the  $TiO_2$  (anatase) at approximately ca. -0.57 V vs NHE and guarantee more efficient electron injection into  $TiO_2$  conduction band. The relationship of the redox potentials of YN-N3 (syn) is also similar to that of N3 (std). The ground state oxidation potential of complexes was calculated from the reduction potential and  $E_{00}$  (listed in Table 4.2). The  $E_{HOMO}$  and  $E_{LUMO}$  levels of the YN-N3 (syn) and N3 (std) are 1.08, -0.75 V and 1.07, -0.72 V, respectively. These  $E_{HOMO}$  and  $E_{LUMO}$  indicated that these complexes are expected to be excellent dyes for the application in dye sensitized solar cells.

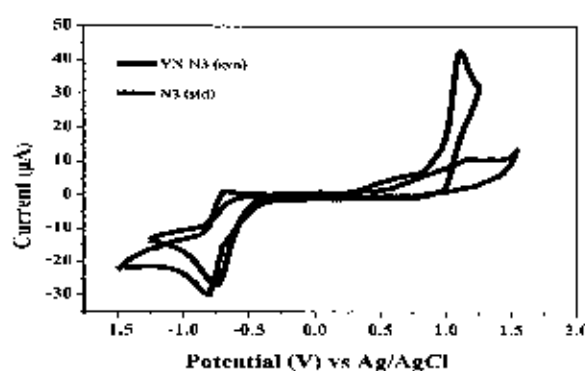


**Figure 4.14** Cyclic voltammogram for YN-N3 (syn) and N3 (std) in  $1 \times 10^{-4}$  M solution DMF at scan rate 100 mV/s with 0.1 M  $[Bu_4N]PF_6$  supporting electrolyte

**Table 4.2** Cyclic voltammetric for YN-N3 (syn) and N3 (std) [72]

Dyes	$\lambda_{\text{onset}}^{\text{abs}}$ (nm) <sup>a</sup>	$E_{\text{red}}$ (V) <sup>b</sup>	$E_{\text{onset}}^{\text{ox}}$ (V) <sup>b</sup>	$E_{\text{HOMO}}$ (V) <sup>c</sup>	$E_{0-0}$ (V) <sup>d</sup>
YN-N3 (syn)	643	-0.75	0.76	1.08	1.83
N3 (std)	670	-0.72	0.94	1.07	1.79

<sup>a</sup> Measured in diluted DMF solution

<sup>b</sup> Measure using a glass carbon as a working electrode, a Pt disk as a counter electrode, and Ag/AgCl as a reference electrode in DMF containing 0.1 M [Bu<sub>4</sub>N]PF<sub>6</sub> as a supporting electrolyte

<sup>c</sup> Calculated using the empirical equation:  $E_{\text{HOMO}} = E_{0-0} + E_{\text{red}}$

<sup>d</sup> Estimated from the onset of absorption ( $E_{0-0} = 1240/\lambda_{\text{onset}}$ )

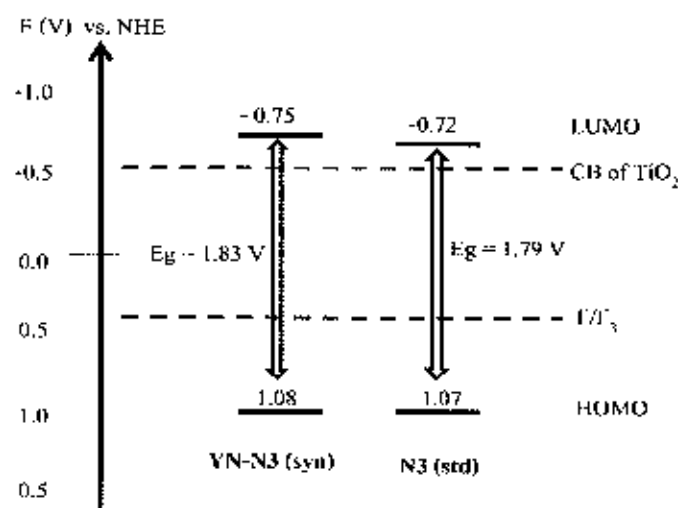


**Figure 4.15** Energy diagram for the YN-N3 (syn) and N3 (std) sensitized TiO<sub>2</sub> solar cells with iodine redox electrolyte

#### 4.1.4.3 Photovoltaic performance of DSSCs

The  $I-V$  characteristic and incident photon to current conversion efficiency (IPCE) of the two DSSCs, YN-N3 (*syn*) and N3 (*std*), were measured under identical experimental conditions. Figure 4.16A shows the  $I-V$  curve, and the resultant photovoltaic parameters under standard global AM 1.5 solar irradiation summarized in Table 4.3. YN-N3 (*syn*) DSSCs shows a lower short-circuit current density ( $J_{sc}$ ) than that of the N3 (*std*). It is believed that lower amount of YN-N3 (*syn*) dye adsorbed on  $TiO_2$  layer, causing from the lower absorption intensity and less solubility of YN-N3 (*syn*) in ethanol. The difference in solubility of both dyes was observed in DSSCs fabrication step. It was found from Talodthaisong, C et al. (unpublished result). The open-circuit voltage ( $V_{oc}$ ) of YN-N3 (*syn*) was decreased from 0.67 to 0.52 V and fill factor ( $ff$ ) increased from 0.67 to 0.71 V. Thus leading to a higher energy conversion efficiency of N3 (*std*) ( $\eta = 5.63$ ) compared to YN-N3 (*syn*) ( $\eta = 3.03$ ).

The incident photon to current conversion efficiency (IPCE) spectra would offer detailed information on the light harvesting ability of the DSSCs shown in Figure 4.16B. The IPCE spectra of the N3 (*std*) DSSCs shows a considerable increase over the entire range of light compared to that of YN-N3 (*syn*). In the longer wavelength region of 500 - 700 nm, the intense IPCE values of N3 (*std*) DSSCs is much higher than that of the YN-N3 (*syn*). The narrow IPCE spectra of YN-N3 (*syn*) dye is explained by the less amount of the dye adsorbed on  $TiO_2$  due to their slightly less soluble than YN-N3 (*syn*).

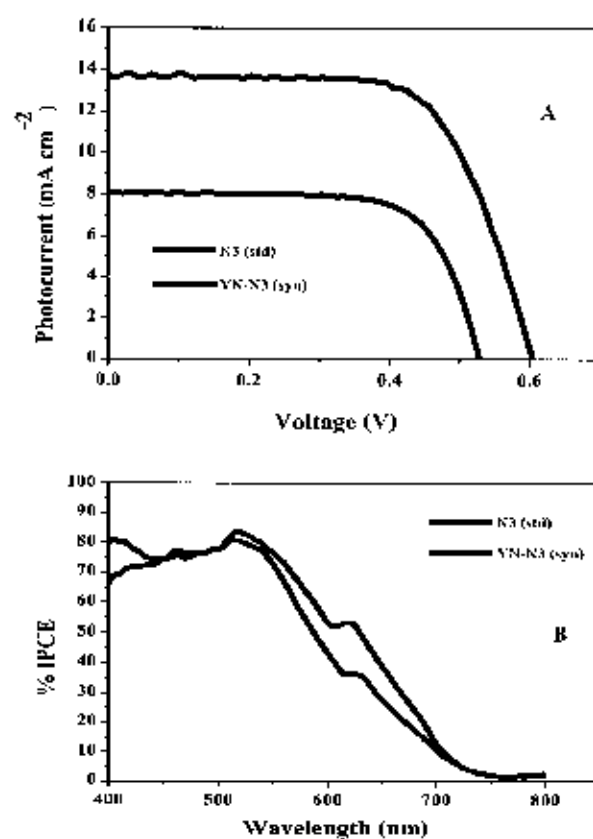


**Figure 4.16** A: IV characteristic of N3 (std) and YN-N3 (syn) under AM 1.5 G radiation ( $100 \text{ mW/cm}^2$ ) and B: incident photo to current conversion efficiency spectra for dye sensitized solar cells based on N3 (std) and YN-N3 (syn)

**Table 4.3** Solar light to electricity conversion efficiency of the YN-N3 (syn) and N3 (std) ruthenium(II) complexes

Dyes	$I_{\text{max}}$ (mA/cm <sup>2</sup> )	$V_{\text{max}}$ (V)	$V_{\text{oc}}$ (V)	$J_{\text{sc}}$ (mA/cm <sup>2</sup> )	$ff$	$\eta$ (%)
YN-N3 (syn)	7.31	0.41	0.52	8.09	0.71	3.03
N3 (std)	12.37	0.45	0.67	13.78	0.67	5.63

#### 4.2 The synthesis of heteroleptic pyridyl ruthenium(II) complexes with tetrabutyl ammonium salt

The molecular structure of both heteroleptic ruthenium(II) complexes, **YN-phen** and **YN-06**, are similar to the homoleptic ruthenium(II) complex (**YN-N3 (syn)**), composed of dithiocyanate, bipyridine ligand and carboxylic acid anchoring group. However, one of the pyridine carboxylic acid was replaced by phenanthroline ligand, whereas another carboxyl group was deprotonated by tetrabutyl ammonium salt. The structures of the ruthenium(II) complexes in this series are shown in Figure 4.17. For the synthesis of **YN-06**, the *N,N*-phenazine (**YN-01**) ligand was prepared and described in the next section.

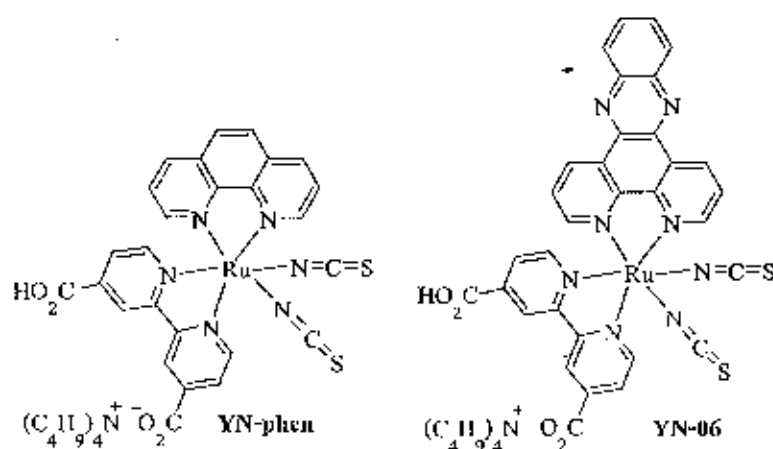


**Figure 4.17** Molecular structure of heteroleptic pyridyl ruthenium(II) complexes

##### 4.2.1 The synthesis of dipyrido[3,2-a:2',3'-c]phenazine (**YN-01**)

The dipyrido[3,2-a:2',3'-c]phenazine ligand was used for the synthesis of **YN-06** complex. The **YN-01** was synthesized as shown in Figure 4.18, whereas the ruthenium(II) precursor (**YN-05**) adopted from part 4.1 experimental result.

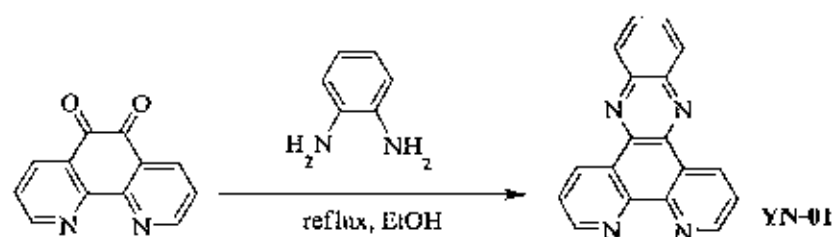


**Figure 4.18** Synthesis of dipyrido[3,2-a:2',3'-c]phenazine (YN-01) [73]

Cyclization reaction was used to synthesize YN-01 ligand. The mechanism of the cyclization reaction between 5,6-diketone-1,10-phenanthroline and *o*-phenyldiamine is shown in Figure 4.19. The cyclization reaction begins with the attack of the amine electron pair to the carbonyl group of 5,6-diketone-1,10-phenanthroline. Two  $\text{H}_2\text{O}$  molecules were then removed, followed by the delocalization provided dipyrido[3,2-a:2',3'-c]phenazine (YN-01) as a brown solid in moderate yield.

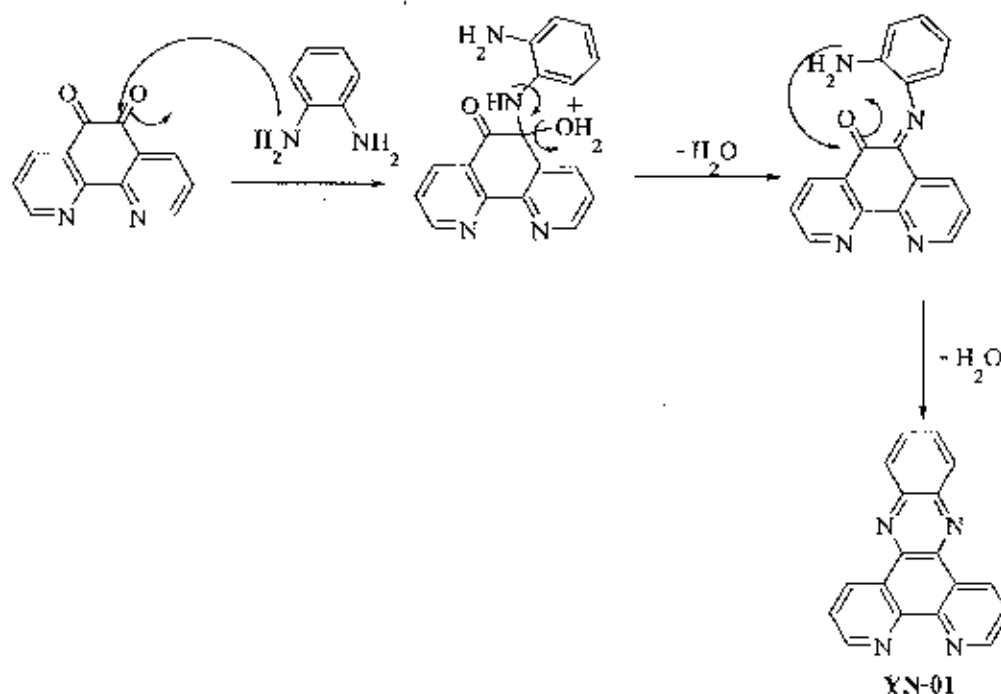


**Figure 4.19** The propose mechanism of cyclization reaction.

The chemical structure of **YN-01** was confirmed by FT-IR, NMR and FAB mass analyses. The **YN-01** is a symmetric molecule. The  $^1\text{H}$  NMR spectra show a signal at  $\delta$  9.64 ppm (2H), 9.27 (2H), 8.36 (2H), 8.01 - 7.93 (2H), and 7.82 - 7.78 (2H) assigned as aromatic protons (Figure 4.20).

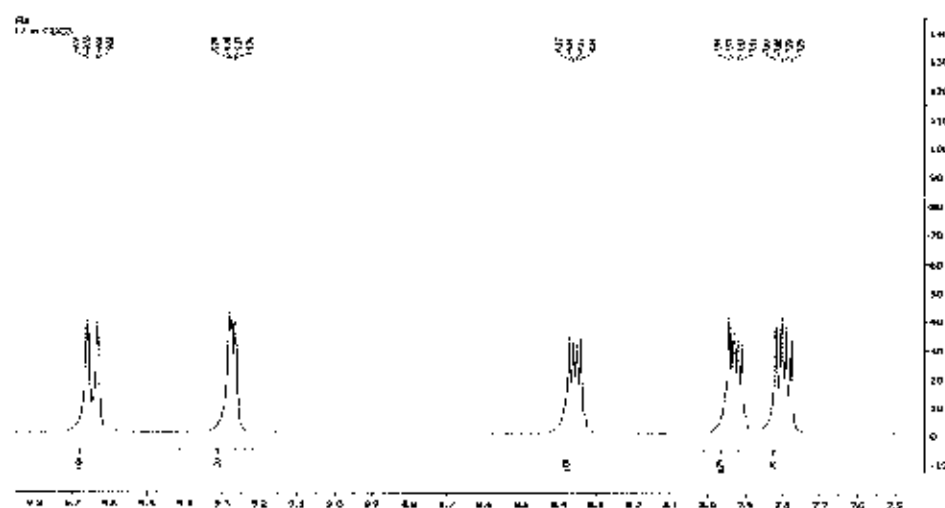
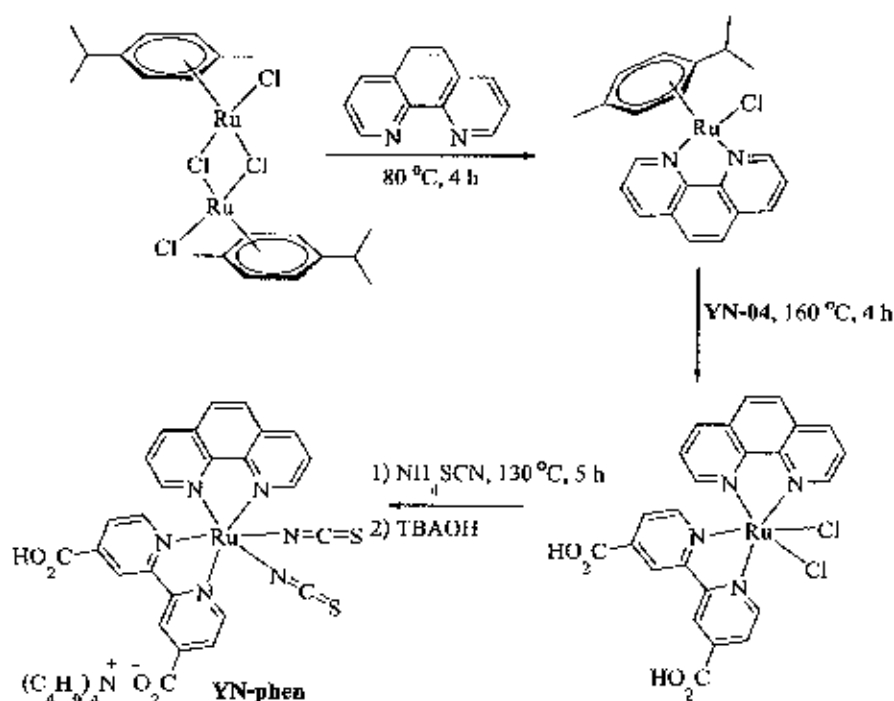


Figure 4.20  $^1\text{H}$  NMR of **YN-01** ligand in  $\text{CDCl}_3$

#### 4.2.2 The synthesis of heteroleptic ruthenium(II) (**YN-phen**)

The **YN-phen** ruthenium(II) complex was prepared according to the modified literature procedures [61]. Like the synthesis of **YN-N3 (syn)** procedure, the **YN-phen** dye was synthesized by a one pot reaction in a moderate yield. The synthetic route for this reaction is shown in Figure 4.21.



**Figure 4.21** The propose synthetic route of ligand substitution reaction of YN-phen

The  $^1\text{H}$  NMR spectrum of YN-phen shows 50-H signals as expected for an unsymmetrical structure (see Figure 4.22). The chemical shift at 9.76 ppm (1H), 9.03 (1H), 8.36 (1H), 7.93 (1H), 7.50 (1H) and 7.40 (1H) were assigned as the protons of the bipyridine ligand. The signal at  $\delta$  9.58 ppm (1H), 8.84 (1H), 8.72 (1H), 8.22 (3H) and 8.15 - 8.07 (2H) are attributed to the proton of the phenanthroline ligand. The proton of ammonium cation group exhibits a resonance at high field,  $\delta$  3.26 (8H), 1.75 - 1.60 (8H), 1.43 (8H) and 1.04 (12H). The integration ratio of  $^1\text{H}$  NMR in aromatic region (7 - 9 ppm) and aliphatic region (1.0 - 3.5 ppm) was found to be 1 : 8. This ratio supported that only one ammonium group in YN-phen complex was observed.



### 4.2.3 Characterization of heteroleptic pyridinyl ruthenium(II) complex dyes

#### 4.2.3.1 Optical properties

The absorption spectra of the new ruthenium complexes, **YN-phen** and **YN-06**, are comprised of difference N-N ligand moiety. The absorption bands of both ruthenium(II) complexes are dominated by  $\pi\text{-}\pi^*$  charge transfer (Figure 4.24), located at 370 nm. The peak position of the  $\pi\text{-}\pi^*$  band of **YN-06** sensitizer clearly shows ( $\epsilon_{\text{max}} \times 10^5 = 0.43 \text{ M}^{-1}\text{cm}^{-1}$ ) higher intensity than that of **YN-phen** ( $\epsilon_{\text{max}} \times 10^5 = 0.23 \text{ M}^{-1}\text{cm}^{-1}$ ), where as **YN-phen** shows broad absorption peak in this region. **YN-06** is expected to be more efficient solar light harvesting than **YN-phen**, because we observed high molar absorptivity although the slightly blue shifted about 6 nm of the MLCT broad band at 509 nm when extending  $\pi$ -conjugation with (dipyrido[3,2-a:2',3'-c]phenazine) ligand in **YN-06**. The UV-Vis absorption data of two new ruthenium(II) complexes are listed in Table 4.4.

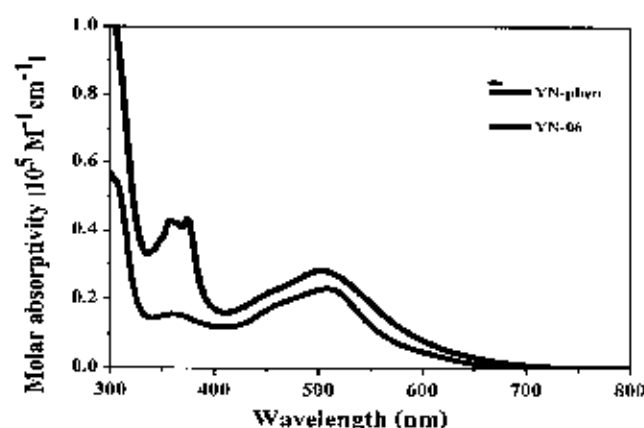


**Figure 4.24** UV-Vis absorption spectra of  $1 \times 10^{-5} \text{ M}$  **YN-phen** and **YN-06** solution in DMF at room temperature

**Table 4.4** The absorption of **YN-phen** and **YN-06** in DMF solution

Dyes	$\lambda_{\text{max}}^{\text{obs}} / \text{nm} (\epsilon \times 10^5 / \text{M}^{-1} \text{cm}^{-1})$
<b>YN-phen</b>	271 (0.57), 360 (0.23), 509 (0.15)
<b>YN-06</b>	280 (1.00), 379 (0.43), 503 (0.28)

#### 4.2.3.2 Electrochemical properties

The redox property and HOMO-LUMO energy levels of the **YN-phen** and **YN-06** were investigated using cyclic voltammetry (CV) (see Figure 4.25 for the voltammogramme). The measurement was performed using 0.1 mM solution of **YN-phen** and **YN-06** in dry DMF with the presence of  $[Bu_4N]PF_6$  as supporting electrolyte. For **YN-phen** and **YN-06** complexes, when scanning toward positive potentials, the anodic currents was observed,  $E_{onset}^{ox}$  at 0.78 and 0.75 V, due to the oxidation from Ru(II) to Ru(III). The irreversible oxidation waves of **YN-phen** closed to that **YN-06** have been ascribed to the presence of thiocyanate groups whose oxidation potential is very close to those for Ru(II) to Ru(III) of both dyes [74]. When scanning toward negative potential, the same reduction potential ( $E_{red}$ ) at -0.76 V of both dyes were observed.

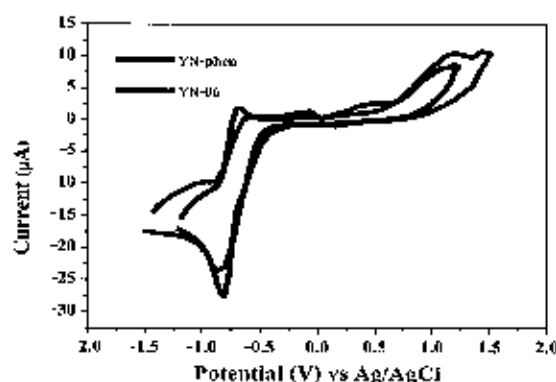


**Figure 4.25** Cyclic voltammogram for **YN-phen** and **YN-06** in  $1 \times 10^{-4}$  M DMF solution at scan rate 100 mV/s with 0.1 M  $[Bu_4N]PF_6$  supporting electrolyte

The resulting  $E_{LUMO}$  levels are calculated from  $E_{red}$  and  $E_{(D)}$  determined from the onset of the absorption spectrum listed in Table 4.5. The corresponding  $E_{HOMO}$  and  $E_{LUMO}$  energy levels were thus estimated to be 1.06 and -0.76 V for **YN-phen** and 1.00 and -0.76 V for **YN-06** vs NHE. As depicted in Figure 4.26, these results clearly show that the energy levels of the ground and excited state of complexes match well for the energetic requirements of a dye for DSSCs application.

**Table 4.5** Cyclic voltammetric result for **YN-phen** and **YN-06**

Dyes	$\lambda_{\text{onset}}^{\text{RDS}}$ (nm) <sup>a</sup>	$E_{\text{red}}$ (V) <sup>b</sup>	$E_{\text{onset}}^{\text{ox}}$ (V) <sup>b</sup>	$E_{\text{HOMO}}$ (V) <sup>c</sup>	$E_{\text{D-0}}$ (V) <sup>d</sup>
<b>YN-phen</b>	679	-0.76	0.78	1.06	1.82
<b>YN-06</b>	703	-0.76	0.75	1.00	1.76

<sup>a</sup>Measure in diluted DMF solution

<sup>b</sup>Measure using a glass carbon as a working electrode, a Pt disk as a counter electrode, and Ag/AgCl as a reference electrode in DMF containing 0.1 M  $[\text{Bu}_4\text{N}]\text{PF}_6$  as a supporting electrolyte

<sup>c</sup>Calculated using the empirical equation:  $E_{\text{HOMO}} = E_{\text{D-0}} + E_{\text{red}}$

<sup>d</sup>Estimated from the onset of absorption ( $E_{\text{D-0}} = 1240/\lambda_{\text{onset}}$ )

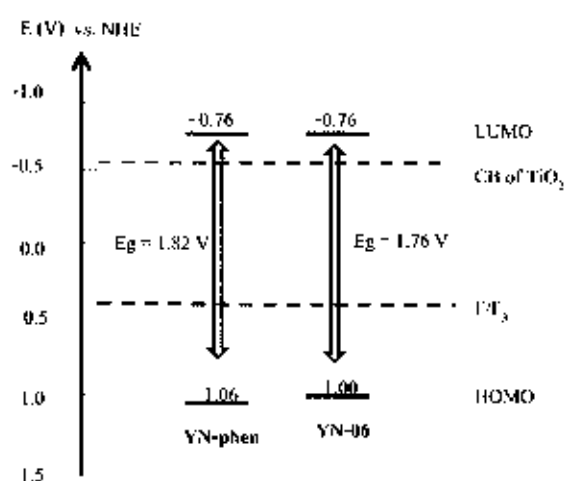


**Figure 4.26** Energy diagram for the **YN-phen** and **YN-06** sensitized  $\text{TiO}_2$  solar cells with iodine redox electrolyte

#### 4.2.3.3 Photovoltaic performance of DSSCs

The comparison  $I-V$  spectra of **YN-phen** and **YN-06** are shown in Figure 4.26A. The  $J_{sc}$ ,  $V_{oc}$ , fill factors ( $ff$ ) and overall cell efficiencies ( $\eta$ ) for each dye- $\text{TiO}_2$  electrode are summarized in Table 4.6. Compared between **YN-phen** and **YN-06**, it was found that the  $J_{sc}$  and  $V_{oc}$  are slightly increased, from 4.96 to 5.08  $\text{mA}/\text{cm}^2$  and 0.55 to 0.56 V, respectively, corresponding to an overall conversion efficiency ( $\eta = 1.86\%$  and 1.90% for **YN-phen** and

YN-06, respectively). These results show that the longer the  $\pi$ -conjugation of YN-01 ancillary ligand moiety of the YN-06 the higher the power conversion efficiency compared to that of YN-phen. This is supported with the higher intensity that observed in its absorption spectrum previously discussed. Figure 4.27B shows the IPCE spectra for the cells fabricated with YN-phen and YN-06 sensitizers. The IPCE values are plotted as a function of wavelength. Both dyes exhibit similar efficiency in the visible region and extending to the near IR region (ca. 750 nm). The YN-phen IPCE value shows of about 40% with the plateau region, where the IPCE value of YN-06 dye was slightly higher than YN-phen (60% in the region 480-450 nm).

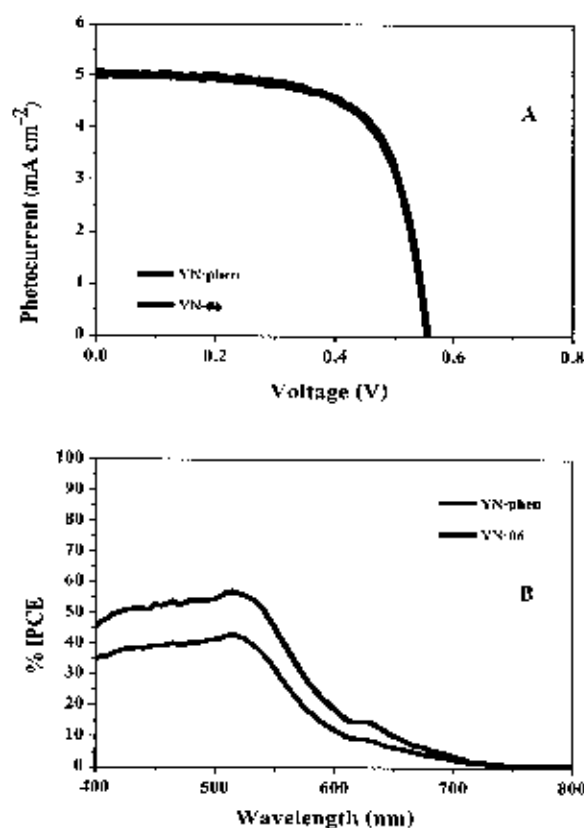


**Figure 4.27** A: IV characteristic of YN-phen and YN-06 under AM 1.5 G radiation ( $100 \text{ mW/cm}^2$ ) and B: incident photo to current conversion efficiency spectra for dye sensitized solar cells based on YN-phen and YN-06

**Table 4.6** Solar light to electricity conversion efficiency with the **YN-phen** and **YN-06** ruthenium(II) complexes

Dyes	$I_{max}$ (mA/cm <sup>2</sup> )	$V_{max}$ (V)	$V_{oc}$ (V)	$J_{sc}$ (mA/cm <sup>2</sup> )	$ff$	$\eta$ (%)
YN-phen	4.27	0.43	0.55	4.96	0.68	1.86
YN-06	4.26	0.44	0.56	5.08	0.67	1.90

#### 4.3 Synthesis homoleptic and heteroleptic ruthenium(II) complexes with tetrabutyl ammonium salt

To improve the conversion efficiency, we reported the synthesis and characterization of three ruthenium(II) sensitizers. The complexes short  $\pi$ -conjugation homoleptic **YN-719**, the heteroleptic **YN-07** and the extending  $\pi$ -conjugation homoleptic **YN-08** were synthesized and their structures are shown in Figure 4.28.

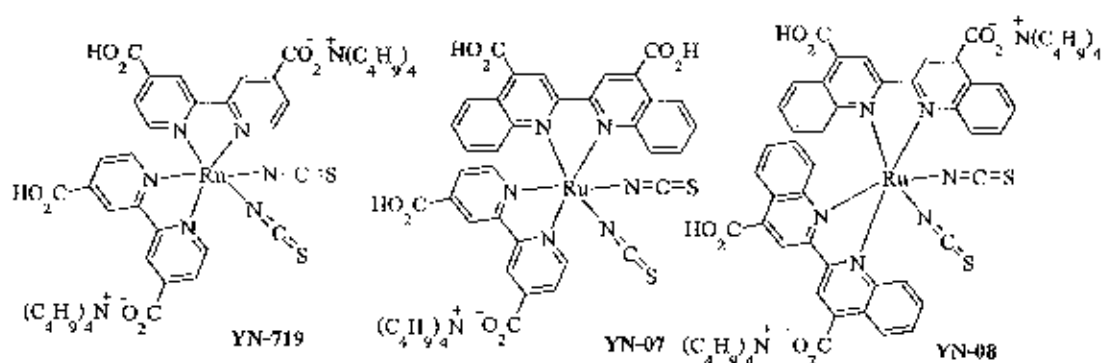


**Figure 4.28** Molecular structure of heteroleptic and homoleptic ruthenium(II) complexes

The synthetic route of homoleptic ruthenium(II) complexes (**YN-719**, **YN-08**) is similar to that of **YN-N3 (syn)** and the heteroleptic ruthenium(II) complex (**YN-07**) is the same as that of **YN-phen**. The synthesis methods of all complexes were reported in experimental section, see chapter 3.

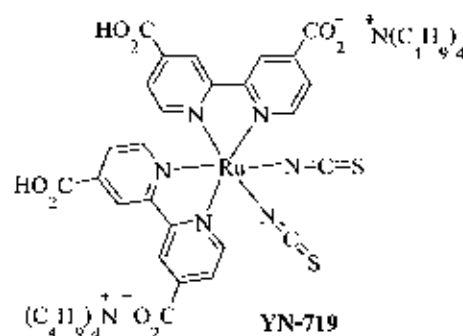


**Figure 4.29** The YN-719 ruthenium(II) complex structure

After we successfully synthesized the YN-719 ruthenium(II) complex, the molecular structure was investigated and characterized by FT-IR, FAB mass and NMR techniques. The  $^1\text{H}$  NMR spectra of YN-719 present 40 proton signals. We observed a similar NMR signal in the aromatic region as reported for YN-N3 (syn). 6 resonances of the pyridine ligand. Unlike YN-N3 (syn), 36 signals in aliphatic region assigned as  $\text{Bu}_4\text{N}^+$  cation group (see Figure 4.30) was observed, supporting the symmetrical structure of YN-719. The integration ratio of  $^1\text{H}$  NMR chemical shift for the aromatic and the aliphatic region is 1 : 8, confirming the presence of two tetrabutyl ammonium salt in the complex structures.

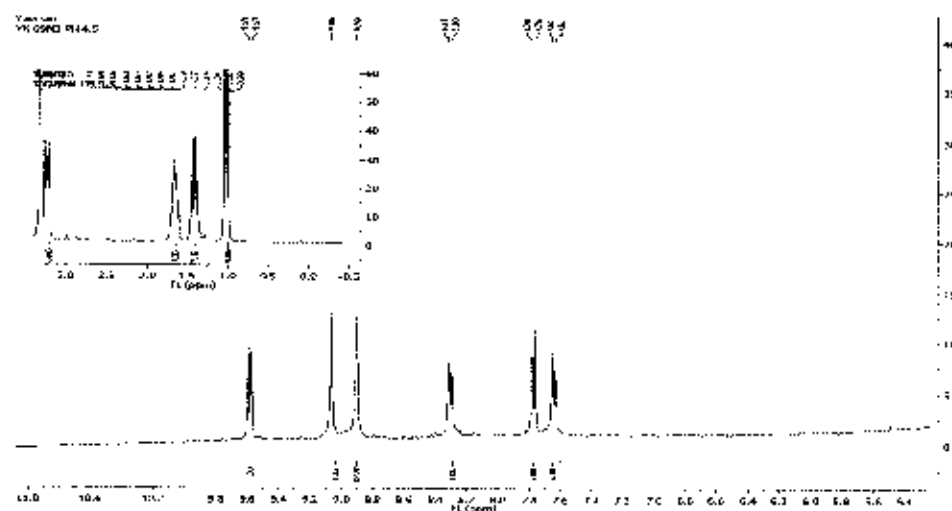


**Figure 4.30**  $^1\text{H}$  NMR in  $\text{DMSO-d}_6$  of homoleptic ruthenium(II) (YN-719)

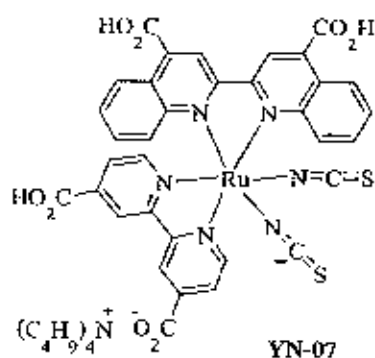


**Figure 4.31** Molecular structure of heteroleptic ruthenium(II) complex (YN-07)

The YN-07 molecular structure was confirmed by NMR, FT-IR and FAB mass analyses. YN-07 is an asymmetrical structure as it shows 52-H. The  $^1\text{H}$  NMR spectra of YN-07 shows 6 signals and 10 signals assigned as protons of the bipyridine and the biquinoline ligand, respectively. The proton signals of  $\text{Bu}_4\text{N}^+$  cation group present 36 resonances at aliphatic region. The YN-07 complex structure contained one tetrabutylammonium salt consistent with 1 : 8 the integration ratio of  $^1\text{H}$  NMR chemical shift as described in previously result.

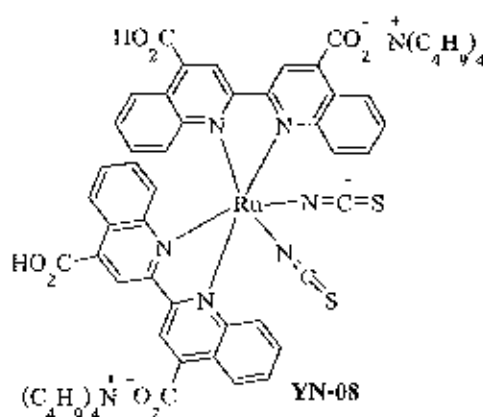


**Figure 4.32** Structural of homoleptic ruthenium(II) complex (YN-08)

The YN-08 ruthenium(II) complex was prepared according to the modified literature procedures [20]. The YN-08 dye was synthesized by a one pot reaction like the synthesis of YN-719 procedure as previously mentioned.

The  $^1\text{H}$  NMR spectra of **YN-08** show 5 characteristic protons of the biquinoline ligand (**dcbiq**). The integration ratio of the chemical shift of the aromatic region and  $\text{Bu}_4\text{N}^+$  cation group was found to be 1 : 4 supported that **YN-08** contains two tetrabutyl ammonium salt in the complex structure. The characterization of this complex, FT-IR,  $^1\text{H}$  and  $^{13}\text{C}$  NMR was shown in Figure A.11, in the appendix A.

#### 4.3.1 Characterization of homoleptic and heteroleptic Ru(II) complex dyes

##### 4.3.1.1 Optical properties

The UV-Vis absorption spectra of **YN-719**, **YN-07** and **YN-08** measured in  $1 \times 10^{-5}$  M ethanol are shown in Figure 4.31. The intense absorption bands in the UV region (300-450 nm), generated from the  $\pi-\pi^*$  ligand transitions were observed, furthermore a blue shifted is observed from **YN-08** to **YN-07** and **YN-719**. This result might be associated with the influent of the strong electron withdrawing group from **dcbiq** moieties for **YN-07** and **YN-08** dyes. Compared between **YN-719** (homoleptic ruthenium(II) complex) and **YN-07** (heteroleptic ruthenium(II) complex), the red shifted in the MLCT transition around 500 - 600 nm region with increasing  $\pi$ -conjugation ligand were clearly distinguished. The MLCT transition of **YN-08** is not clearly observed. This probable from the **YN-08** is less solubility in DMF. The UV-Vis absorption of **YN-719**, **YN-07** and **YN-08** are summarized in Table 4.7.

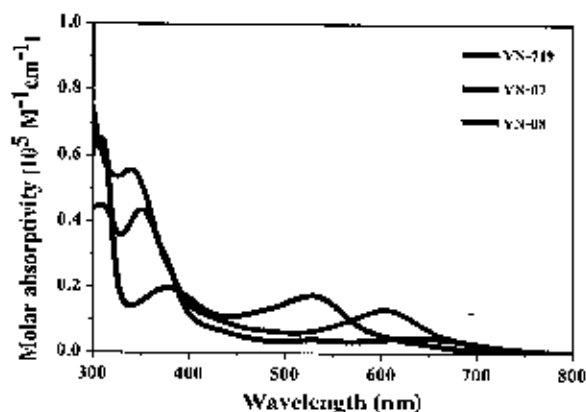


**Figure 4.33** UV-Vis absorption spectra of  $1 \times 10^{-5}$  M **YN-719**, **YN-07** and **YN-08** solution in DMF at room temperature

**Table 4.7** The absorption of YN-719, YN-07, YN-08 in DMF solution

Dyes	$\lambda_{\text{max}}^*/\text{nm}$ ( $\epsilon \times 10^5/\text{M}^{-1} \text{cm}^{-1}$ )
YN-719	310 (0.67), 389 (0.20), 542 (0.18)
YN-07	320 (0.45), 363 (0.43), 626 (0.12)
YN-08	353 (0.56), 637 (0.03)

#### 4.3.1.2 Electrochemical properties

To evaluate the feasibility of electron transfer from the excited state of the sensitizers to the conduction band of the  $\text{TiO}_2$  electrode, the cyclic voltammetry experiments was carried out using 0.1 M  $[\text{Bu}_4\text{N}]\text{PF}_6$  as supporting electrolyte and NHE reference electrode was carried out. The YN-719, YN-07 and YN-08 ruthenium(II) complexes showed the onset oxidation peak and reversible reduction peak, shown in Figure 4.34. The oxidation onset potential ( $E_{\text{onset}}^{\text{ox}}$ ) of YN-719, YN-07 and YN-08 are observed at 0.72, 0.76 and 0.74 V vs NHE, respectively, which are assigned to Ru(II)/Ru(III) couple. The irreversible oxidation waves of all complexes were described that the oxidation potential of thiocyanate groups is very close to those for Ru(II) to Ru(III) couple as previous mentioned. The reversible reduction potential ( $E_{\text{red}}$ ) peaks of the complexes are -0.79, -0.76 and -0.74 V, respectively, attributed to each of the reduction of the bipyridine ligands (YN-04 and **dcbiq**). The redox potential are summarized in Table 4.8. The oxidation and reduction potentials of YN-07 and YN-08 are slightly shifted to the anodic area presented more acceptor **dcbiq** compared to YN-719 [75], consistent with the UV visible absorption data. The  $E_{\text{HOMO}}$  levels of YN-719, YN-07 and YN-08 were calculated from  $E_{\text{red}}$  and  $E_{\text{onset}}^{\text{ox}}$  to be 0.95, 0.88, 0.90 V vs NHE, respectively. The  $E_{\text{HOMO}}$  and  $E_{\text{red}}$  clearly show that the energy levels of the ground and excited state of complexes are matched with the energetic requirements of the dye for efficient charge generation in DSSCs (see Figure 4.35).

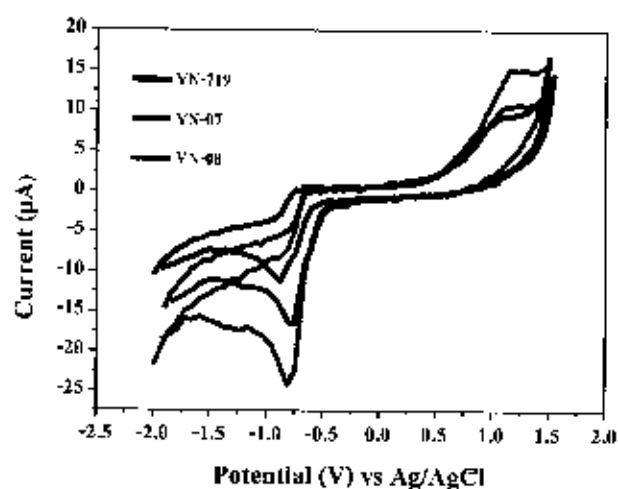


**Figure 4.34** Cyclic voltammogram of  $1 \times 10^{-4}$  M YN-719, YN-07 and YN-08 in DMF at scan rate 100 mV/s with 0.1 M  $[\text{Bu}_4\text{N}]\text{PF}_6$  supporting electrolyte

**Table 4.8** Cyclic voltammetric result for YN-719, YN-07 and YN-08

Dyes	$\lambda_{\text{onset}}^{\text{abs}}$ (nm) <sup>a</sup>	$E_{\text{red}}$ (V) <sup>b</sup>	$E_{\text{ox}}^{\text{onset}}$ (V) <sup>b</sup>	$E_{\text{HOMO}}$ (V) <sup>c</sup>	$E_{\text{H-L}}$ (V) <sup>d</sup>
YN-719	710	-0.79	0.72	0.95	1.74
YN-07	755	-0.76	0.76	0.88	1.64
YN-08	755	-0.74	0.74	0.90	1.64

<sup>a</sup>Measure in diluted DMF solution

<sup>b</sup>Measure using a glass carbon as a working electrode, a Pt disk as a counter electrode, and Ag/AgCl as a reference electrode in DMF containing 0.1 M  $[\text{Bu}_4\text{N}]\text{PF}_6$  as a supporting electrolyte

<sup>c</sup>Calculated using the empirical equation:  $E_{\text{HOMO}} = E_{\text{ox}} + E_{\text{red}}$

<sup>d</sup>Estimated from the onset of absorption ( $E_{\text{H-L}} = 1240/\lambda_{\text{onset}}$ )

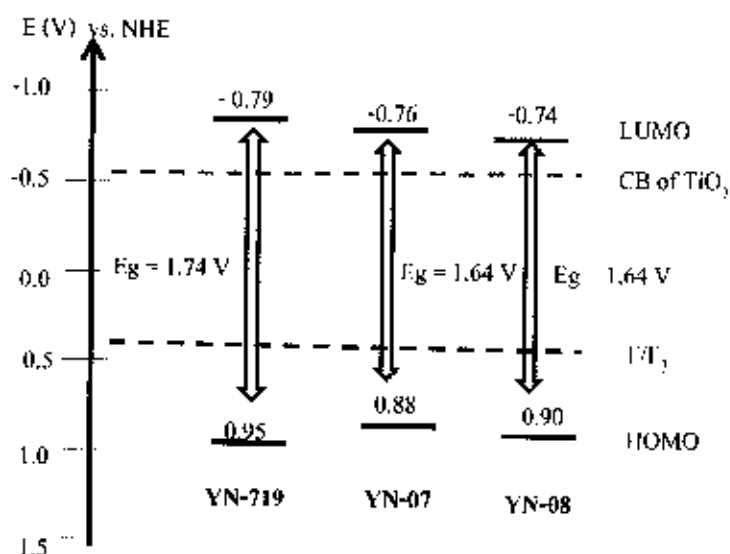


**Figure 4.35** Energy diagram for the YN-719, YN-07 and YN-08 sensitized  $\text{TiO}_2$  solar cells with iodine redox electrolyte

#### 4.3.1.3 Photovoltaic performance of DSSCs

To further understand the effect of the extending  $\pi$ -conjugation of the ligand to the photovoltaic performance of ruthenium dyes for the DSSCs application. The YN-719, YN-07 and YN-08 ruthenium(II) complex dyes were fabricated and investigated their power conversion efficiency. The YN-07 sensitized cell gave a  $J_{sc}$  of  $0.46 \text{ mA/cm}^2$ ,  $V_{oc}$  of 0.46 V, and a fill factor of 0.68, corresponding to an overall conversion efficiency of 0.14%. Under the same conditions, the YN-08 and YN-719 sensitized cell gave a  $J_{sc}$  of 0.35 and  $10.12 \text{ mA/cm}^2$ ,  $V_{oc}$  of 0.44 and 0.61 V, and a fill factor ( $ff$ ) of 0.54 and 0.74, corresponding to an overall conversion efficiency of 0.08% and 4.57% (listed in Table 4.9), respectively. From all three complexes, it was found that YN-08 which has the longest  $\pi$ -conjugation than those other two dyes (YN-07 and YN-719), but the overall conversion efficiency of the YN-08 DSSC is not 2-fold higher as expected. The YN-719 shows the highest photocurrent due to; 1) the YN-719 dye shows the highest intensity of MLCT from UV-Vis absorption data at, 2) the YN-719 dye show the best electron injection efficiency as described from the highest  $I_{inj}$  values, 3) the molecular structures of YN-08 and YN-07 are larger size than YN-719 sensitizer, responsible for preventing the penetration of the dye into the nanoporous film and 4) the  $V_{oc}$  values of YN-07 and YN-08 are

very low consistent with the increase of the dark current resulting from reverse electron transfer from  $\text{TiO}_2$  to  $\text{I}_3^-$ .

Figure 4.36B shows the IPCE action spectra for dye sensitized solar cells based on YN-719 dye alone. The IPCE of YN-719 presents a plateau of over 70%, from 400 to 550 nm, reaching the maximum of 85% at 520 nm. The photo-response of the cell extends up to 700 nm. The decline of the IPCE above 550 nm toward the red region is caused by the decrease in the extinction coefficient of YN-719. The IPCE of YN-07 and YN-08 ruthenium(II) complexes cannot be measured supporting the low power conversion efficiency ( $\eta$ ).

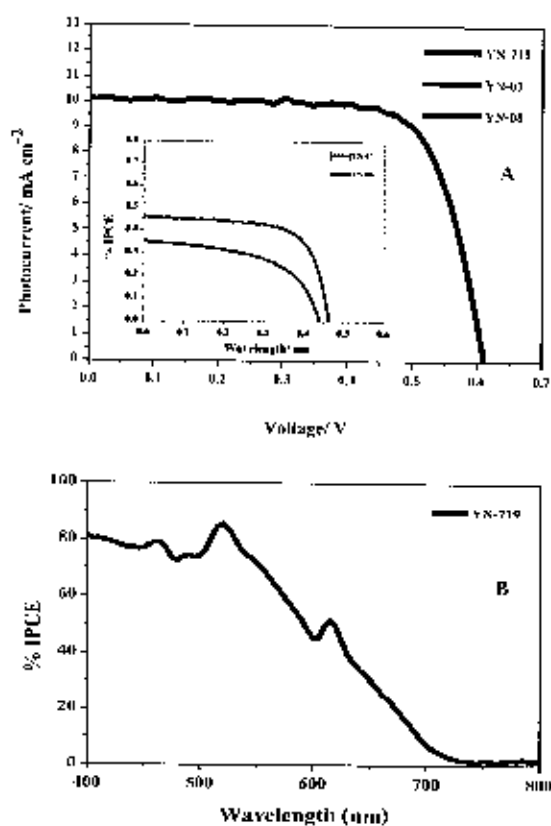


**Figure 4.36** A: IV characteristic of YN-719, YN-07 and YN-08 under AM 1.5 G radiation ( $100 \text{ mW/cm}^2$ ) and B: incident photo to current conversion efficiency spectra for dye sensitized solar cells based on YN07, YN-08 and YN-719

**Table 4.9** Solar light to electricity conversion efficiency with the YN-719, YN-07 and YN-08 ruthenium(II) complexes

Dyes	$I_{max}$ (mA/cm <sup>2</sup> )	$V_{max}$ (V)	$V_{oc}$ (V)	$J_{sc}$ (mA/cm <sup>2</sup> )	$\beta$	$\eta$ (%)
YN-719	9.40	0.48	0.61	10.12	0.74	4.57
YN-07	0.39	0.37	0.46	0.46	0.68	0.14
YN-08	0.26	0.32	0.44	0.35	0.54	0.08

## CHAPTER 5

### CONCLUSIONS

Novel ruthenium complex contained phenanthroline and bipyridine ligands with carboxylic anchoring group unit for using as dye sensitizers in DSSCs devices were successfully synthesized from ligand substitute reaction. The target molecules were characterized by NMR, FT-IR, UV-Vis spectroscopy, cyclic voltammetry, and mass spectroscopy. First, we studied the homoleptic ruthenium(II) complex dye without tetrabutylammonium salt YN-N3 (syn) and N3 (std) DSSCs. The N3 (std) shows a higher conversion efficiency ( $\eta$ ) than that YN-N3 (syn) causing from the difference amount of H<sub>2</sub>O and CH<sub>3</sub>OH in both complexes. Second, we studied heteroleptic pyridyl ruthenium(II) complex dyes with the tetrabutylammonium salt, YN-phen and YN-06. The extended  $\pi$ -conjugation ancillary ligand of YN-06 gives rise to molar absorptivity as well as relatively higher overall conversion efficiency with respect to YN-phen. Third, we reported the overall conversion efficiency of YN-719, YN-07, YN-08 sensitized DSSCs and examined the influence of the bulky ancillary ligand and extend  $\pi$ -conjugation. We can also see that with the longer  $\pi$ -conjugation from YN-08 > YN-07 > YN-719, the  $\eta$  of the YN-719 DSSCs shows the highest efficiency in this series. It is described to its high extinction coefficient and the highest  $V_{oc}$  due to the blocking effect of the charge recombination, which plays a crucial role in the electron-transfer process.

The photovoltaic performance of nanocrystalline oxide semiconductor solar cells sensitized for all ruthenium(II) complexes in this study are summarized in Table 5.1.

**Table 5.1** Solar light to electricity conversion efficiency with ruthenium(II) complexes

Dyes	$I_{max}$ (mA/cm <sup>2</sup> )	$V_{max}$ (V)	$V_{oc}$ (V)	$J_{sc}$ (mA/cm <sup>2</sup> )	$ff$	$\eta$ (%)
YN-N3 (syn)	7.31	0.41	0.52	8.09	0.71	3.03
N3 (std)	12.37	0.45	0.67	13.78	0.67	5.63
YN-phen	4.27	0.43	0.55	4.96	0.68	1.86
YN-06	4.26	0.44	0.56	5.08	0.67	1.90
YN-719	9.40	0.48	0.61	10.12	0.74	4.57
YN-07	0.39	0.37	0.46	0.46	0.68	0.14
YN-08	0.26	0.32	0.44	0.35	0.54	0.08

## REFERENCES

## REFERENCES

- [1] Promarak, V. et al. "Dye sensitized solar cells", Journal of Ubon Ratchathani University, 2(9): 1-18, 2007.
- [2] Chapin, D.M. et al. "A new silicon p-n junction photocell for converting solar radiation into electrical power", Journal of Applied Physics, 25(5): 676-677, 1954.
- [3] Mickey, C.D. et al. "Solar photovoltaic cells", Journal of Chemical Education, 58(5): 418, 1981.
- [4] Abdula, D. and Shim, M. "Performance and photovoltaic response of polymer-doped carbon nanotube p-n diodes", ACS Nano, 2(10): 2154-2159, 2008.
- [5] O'regan, B. and Grätzel, M. "A low-cost, high-efficiency solar cell based on dye-sensitized colloidal TiO<sub>2</sub> films", Letters to Nature, 353(6346): 737-740, 1991.
- [6] Grätzel, M. "Conversion of sunlight to electric power by nanocrystalline dye-sensitized solar cells", Journal of Photochemistry and Photobiology A: Chemistry, 164(1-3): 3-14, 2004.
- [7] Grätzel, M. "Dye-sensitized solar cells", Journal of Photochemistry and Photobiology C: Photochemistry Reviews, 4(2): 145-153, 2003.
- [8] Fan, S.-H. et al. "A triphenylamine-grafted imidazo[4,5-f][1,10]phenanthroline ruthenium(II) complex: acid-base and photoelectric properties", Inorganic Chemistry, 49(8): 3752-3763, 2010.
- [9] Guo, L. et al. "Synthesis and applications of 3,6-carbazole-based conjugated side-chain copolymers containing complexes of 1,10-phenanthroline with Zn(II), Cd(II) and Ni(II) for dye-sensitized solar cells", Dyes and Pigments, 92(3): 1062-1068, 2012.
- [10] Huang, W.-K. et al. "Design and characterization of heteroleptic ruthenium complexes containing benzimidazole ligands for dye-sensitized solar cells: the effect of fluorine substituents on photovoltaic performance", The Journal of Physical Chemistry Letters, 3(13): 1830-1835, 2012.

## REFERENCES (CONTINUED)

- [11] Kim, J.-J. et al. "Novel amphiphilic ruthenium sensitizer with hydrophobic thiophene or thieno(3,2-b)thiophene-substituted 2,2'-dipyridylamine ligands for effective nanocrystalline dye sensitized solar cells", *Chemistry of Materials*, 21(24): 5719-5726, 2009.
- [12] Wang, Z.-S. et al. "Significant efficiency improvement of the **Black Dye** sensitized solar cell through protonation of TiO<sub>2</sub> films", *Langmuir*, 21(10): 4272-4276, 2005.
- [13] Lai, L.-P. et al. "New fluorenone-containing organic photosensitizers for dye-sensitized solar cells", *Dyes and Pigments*, 98(3): 428-436, 2013.
- [14] Tan, H. et al. "Phenoxazine-based organic dyes with different chromophores for dye-sensitized solar cells", *Organic Electronics*, 14(11): 2795-2801, 2013.
- [15] Campbell, W.M. et al. "Porphyrins as light harvesters in the dye-sensitized TiO<sub>2</sub> solar cell", *Coordination Chemistry Reviews*, 248(13-14): 1363-1379, 2004.
- [16] Sirithip, K. et al. "Synthesis and characterization of  $\beta$ -pyrrolic functionalized porphyrins as sensitizers for dye-sensitized solar cells", *Tetrahedron Letters*, 54(19): 2435-2439, 2013.
- [17] Jitchati, R. et al. "A cheap synthetic route to commercial ruthenium N3 dye for sensitizing solar cell applications", *Advanced Materials Research*, 488-489(2012): 1049-1054, 2012.
- [18] Chen, C.-Y. et al. "A ruthenium complex with superhigh light-harvesting capacity for dye-sensitized solar cells", *Angewandte Chemie International Edition*, 45(35): 5822-5825, 2006.
- [19] Bencini, A. and Lippolis, V. "1,10-Phenanthroline: a versatile building block for the construction of ligands for various purposes", *Coordination Chemistry Reviews*, 254(17-18): 2096-2180, 2010.
- [20] Islam, A. et al. "Synthesis and photophysical properties of ruthenium(II) charge transfer sensitizers containing 4,4'-dicarboxy-2,2'-biquinoline and 5,8-dicarboxy-6,7-dihydro-dibenzo[1,10]-phenanthroline", *Inorganica Chimica Acta*, 322(1-2): 7-16, 2001.

## REFERENCES (CONTINUED)

- [21] Yu, Z. et al. "Investigation of iodine concentration effects in electrolytes for dye-sensitized solar cells", The Journal of Physical Chemistry C. 114(23): 10612-10620, 2010.
- [22] Lee, S.-H.A. et al. "Influence of different iodide salts on the performance of dye-sensitized solar cells containing phosphazene-based nonvolatile electrolytes", The Journal of Physical Chemistry C. 114(35): 15234-15242, 2010.
- [23] Wang, Z.-S. et al. "Efficient Eosin Y dye-sensitized solar cell containing  $\text{Br}^-/\text{Br}_3^-$  electrolyte", The Journal of Physical Chemistry B. 109(47): 22449-22455, 2005.
- [24] Oskam, G. et al. "Pseudohalogens for dye-sensitized  $\text{TiO}_2$  photoelectrochemical cells", The Journal of Physical Chemistry B. 105(29): 6867-6873, 2001.
- [25] Sapp, S.A. et al. "Substituted polypyridine complexes of cobalt(II/III) as efficient electron-transfer mediators in dye-sensitized solar cells", Journal of the American Chemical Society. 124(37): 11215-11222, 2002.
- [26] Cameron, P.J. et al. "Electrochemical studies of the  $\text{Co(II)/Co(II)(dbbip)}_2$  redox couple as a mediator for dye-sensitized nanocrystalline solar cells", Coordination Chemistry Reviews. 248(13-14): 1447-1453, 2004.
- [27] Shi, C. et al. "Silica nanoparticle doped organic ionic plastic crystal electrolytes for highly efficient solid-state dye-sensitized solar cells", ACS Applied Materials & Interfaces. 5(4): 1453-1459, 2013.
- [28] Gorlov, M. et al. "Electrolytes for dye-sensitized solar cells based on interhalogen ionic salts and liquids", Inorganic Chemistry. 46(9): 3566-3575, 2007.
- [29] Kim, S.-S. et al. "Electrodeposited Pt for cost-efficient and flexible dye-sensitized solar cells", Electrochimica Acta. 51(18): 3814-3819, 2006.
- [30] Kim, S.-S. et al. "Pt-NiO nanophase electrodes for dye-sensitized solar cells", Solar Energy Materials and Solar Cells. 90(3): 283-290, 2006.
- [31] Bertoz, M. "Dye-sensitizing solar cells", Fundamental Sciences Chemistry. 2(1): 1-16, 2010.
- [32] Justin Thomas, K.R. et al. "2,3-Disubstituted thiophene-based organic dyes for solar cells", Chemistry of Materials. 20(5): 1830-1840, 2008.

## REFERENCES (CONTINUED)

- [33] Zeng, W. et al. "Efficient dye-sensitized solar cells with an organic photosensitizer featuring orderly conjugated ethylenedioxythiophene and dithienosilole blocks", Chemistry of Materials. 22(5): 1915-1925, 2010.
- [34] Cheng, X. et al. "Organic dyes incorporating the cyclopentadithiophene moiety for efficient dye-sensitized solar cells", Dyes and Pigments. 92(3): 1292-1299, 2012.
- [35] Lee, D.H. et al. "Organic dyes incorporating low-band-gap chromophores based on  $\pi$ -extended benzothiadiazole for dye-sensitized solar cells", Dyes and Pigments. 91(2): 192-198, 2011.
- [36] Wang, Z.-S. et al. "Thiophene-functionalized coumarin dye for efficient dye-sensitized solar cells: electron lifetime improved by coadsorption of deoxycholic acid", The Journal of Physical Chemistry C. 111(19): 7224-7230, 2007.
- [37] Hara, K. et al. "Effect of additives on the photovoltaic performance of coumarin-dye-sensitized nanocrystalline TiO<sub>2</sub> solar cells", Langmuir. 20(10): 4205-4210, 2004.
- [38] Kuang, D. et al. "Co-sensitization of organic dyes for efficient ionic liquid electrolyte-based dye-sensitized solar cells", Langmuir. 23(22): 10906-10909, 2007.
- [39] Namuangruk, S. et al. "D-D- $\pi$ -A-type organic dyes for dye-sensitized solar cells with a potential for direct electron injection and a high extinction coefficient: synthesis, characterization, and theoretical investigation", The Journal of Physical Chemistry C. 116(49): 25653-25663, 2012.
- [40] Boschloo, G.K. and Goossens, A. "Electron trapping in porphyrin-sensitized porous nanocrystalline TiO<sub>2</sub> electrodes", The Journal of Physical Chemistry. 100(50): 19489-19494, 1996.
- [41] Barea, E.M. et al. "Porphyrin dyes with high injection and low recombination for highly efficient mesoscopic dye-sensitized solar cells", The Journal of Physical Chemistry C. 115(21): 10898-10902, 2011.
- [42] Liu, Y.-J. et al. "N-fused carbazole-zinc porphyrin-free-base porphyrin triad for efficient near-IR dye-sensitized solar cells", Chemical Communications. 47(13): 4010-4012, 2011.

## REFERENCES (CONTINUED)

- [43] Moonsin, P. et al. "Meso-multi(iodophenyl) porphyrins: synthesis, isolation, and identification", *Tetrahedron Letters*. 52(37): 4795-4798, 2011.
- [44] Nazeeruddin, M.K. et al. "Conversion of light to electricity by cis-X<sub>2</sub>bis(2,2'-bipyridyl-4,4'-dicarboxylate)ruthenium(II) charge-transfer sensitizers, X = Cl<sup>-</sup>, Br<sup>-</sup>, I<sup>-</sup>, CN<sup>-</sup>, and SCN<sup>-</sup> on nanocrystalline titanium dioxide electrodes", *Journal of the American Chemical Society*. 115(14): 6382-6390, 1993.
- [45] Robertson, N. "Optimizing dyes for dye-sensitized solar cells", *Angewandte Chemie International Edition*. 45(15): 2338-2345, 2006.
- [46] Meyer, G.J. "Molecular approaches to solar energy conversion with coordination compounds anchored to semiconductor surfaces", *Inorganic Chemistry*. 44(20): 6852-6864, 2005.
- [47] Nazeeruddin, M.K. et al. "Acid-base equilibria of (2,2'-bipyridyl-4,4'-dicarboxylic acid) ruthenium(II) complexes and the effect of protonation on charge-transfer sensitization of nanocrystalline titania", *Inorganic Chemistry*. 38(26): 6298-6305, 1999.
- [48] Nazeeruddin, M.K. et al. "Engineering of efficient panchromatic sensitizers for nanocrystalline TiO<sub>2</sub>-based solar cells", *Journal of the American Chemical Society*. 123(8): 1613-1624, 2001.
- [49] Yang, Y.S. et al. "Effects of anchoring groups in multi-anchoring organic dyes with thiophene bridge for dye-sensitized solar cells", *Synthetic Metals*. 161(9-10): 850-855, 2011.
- [50] Shang, H. et al. "The effect of anchoring group number on the performance of dye-sensitized solar cells", *Dyes and Pigments*. 87(3): 249-256, 2010.
- [51] Choi, H. et al. "High molar extinction coefficient organic sensitizers for efficient dye-sensitized solar cells", *Chemistry-A European Journal*. 16(4): 1193-1201, 2010.
- [52] Zhang, G. et al. "High efficiency and stable dye-sensitized solar cells with an organic chromophore featuring a binary [small pi]-conjugated spacer", *Chemical Communications*. 46(16): 2198-2200, 2009.

## REFERENCES (CONTINUED)

- [53] Zhang, X. et al. "A comparative theoretical investigation of ruthenium dyes in dye-sensitized solar cells", Journal of Photochemistry and Photobiology A: Chemistry. 185(2-3): 283-288, 2007.
- [54] Pack, S. et al. "New type of ruthenium sensitizers with a triazole moiety as a bridging group", Journal of Organometallic Chemistry. 695(6): 821-826, 2010.
- [55] Song, H.-K. et al. "Synthesis of ruthenium complex and its application in dye-sensitized solar cells", Journal of Industrial and Engineering Chemistry. 15(1): 62-65, 2009.
- [56] Wu, S.-J. et al. "An efficient light-harvesting ruthenium dye for solar cell application", Dyes and Pigments. 84(1): 95-101, 2010.
- [57] Luo, Y. et al. "Towards optimization of materials for dye-sensitized solar cells", Advanced Materials. 21(45): 4647-4651, 2009.
- [58] Kuang, D. et al. "High-efficiency and stable mesoscopic dye-sensitized solar cells based on a high molar extinction coefficient ruthenium sensitizer and nonvolatile electrolyte", Advanced Materials. 19(9): 1133-1137, 2007.
- [59] Kisserwan, H. and Ghaddar, T.H. "Enhancement of photovoltaic performance of a novel dye, "T18", with ketene thioacetal groups as electron donors for high efficiency dye-sensitized solar cells", Inorganica Chimica Acta. 363(11): 2409-2415, 2010.
- [60] Chen, C.-Y. et al. "Ruthenium sensitizer with thienothiophene-linked carbazole antennas in conjunction with liquid electrolytes for dye-sensitized solar cells", The Journal of Physical Chemistry C. 115(40): 20043-20050, 2011.
- [61] Reynal, A. et al. "Interfacial charge recombination between  $e^-$ -TiO<sub>2</sub> and the  $I^-/I_3^-$  electrolyte in ruthenium heteroleptic complexes: dye molecular structure-open circuit voltage relationship", Journal of the American Chemical Society. 130(41): 13558-13567, 2008.
- [62] Sun, Y. et al. "Viable alternative to N719 for dye-sensitized solar cells", ACS Applied Materials & Interfaces. 2(7): 2039-2045, 2010.

## REFERENCES (CONTINUED)

- [63] Thathong, Y. et al. "New family of ruthenium-dye-sensitized solar cells (DSSCs) with a high solar-energy-conversion efficiency". *Advanced Materials Research*. 770(45): 145-148, 2013.
- [64] Adams, R. and Miyano, S. "Condensation reactions of picoline 1-oxides", *Journal of the American Chemical Society*. 76(12): 3168-3171, 1954.
- [65] Justaud, F. et al. "Novel straightforward access to a 2,2'-bipyridine ligand bearing two " $(\eta^2\text{-dppc})(\eta^3\text{-C}_5\text{Me}_5)\text{FeC}=\text{C}$ " redox-active substituents by homocoupling of mononuclear organoiron(II) 2-bromopyridyl synthons", *Organometallics*. 27(16): 4260-4264, 2008.
- [66] LIU, K.-Y. et al. "Synthesis and characterization of cross-linkable ruthenium complex dye and its application on dye-sensitized solar cells", *Journal of Polymer Science*. 48(2): 366-372, 2010.
- [67] Bennett, M.A. and Smith, A.K. "Arene ruthenium(II) complexes formed by dehydrogenation of cyclohexadienes with ruthenium(III) trichloride", *Journal of the Chemical Society, Dalton Transactions*. 3(2): 233-241, 1974.
- [68] Sudyoadsuk, T. et al. "An organic dye using N-dodecyl-3-(3,6-di-tert-butylcarbazol-N-yl)carbazol-6-yl as a donor moiety for efficient dye-sensitized solar cells", *Tetrahedron Letters*. 54(36): 4903-4907, 2013.
- [69] Xue, G. et al. "Degradation mechanisms investigation for long-term thermal stability of dye-sensitized solar cells", *International Journal of Electrochemical Science*. 7(2): 1496-1511, 2012.
- [70] Fan, S.-H. et al. "A phenylcarbazole functionalized ruthenium dye for efficient dye-sensitized solar cells". *Solar Energy*. 85(10): 2497-2506, 2011.
- [71] Wang, P. et al. "Amphiphilic ruthenium sensitizers and their applications in dye-sensitized solar cells", *Inorganic Chemistry*. 43(14): 4216-4226, 2004.
- [72] Kim, J.-J. et al. "A new class of cyclometalated ruthenium sensitizers of the type CNN for efficient dye sensitized solar cells", *Inorganic Chemistry*. 50(22): 11340-11347, 2011.
- [73] Higgins, B. and DeGraff, B.A. "Luminescent transition metal complexes as sensors: structural effects on pII response", *Inorganic Chemistry*. 44(19): 6662-6669, 2005.

## REFERENCES (CONTINUED)

- [74] Yanagida, M. et al. "A new efficient photosensitizer for nanocrystalline solar cell: synthesis and characterization of cis-bis(4,7-dicarboxy-1,10-phenanthroline)dithiocyanato ruthenium(II)". Journal of the Chemical Society, Dalton Transactions. 39(16): 2817-2822, 2000.
- [75] Oner, I. et al. "Electroluminescence from two new ruthenium(II) complexes as phosphorescent dopant: positive effect of swallow-tail bipyridyl ligand". Dyes and Pigments. 95(1): 23-32, 2012.

## APPENDICES

**APPENDIX A**  
**Results of characterized studies**

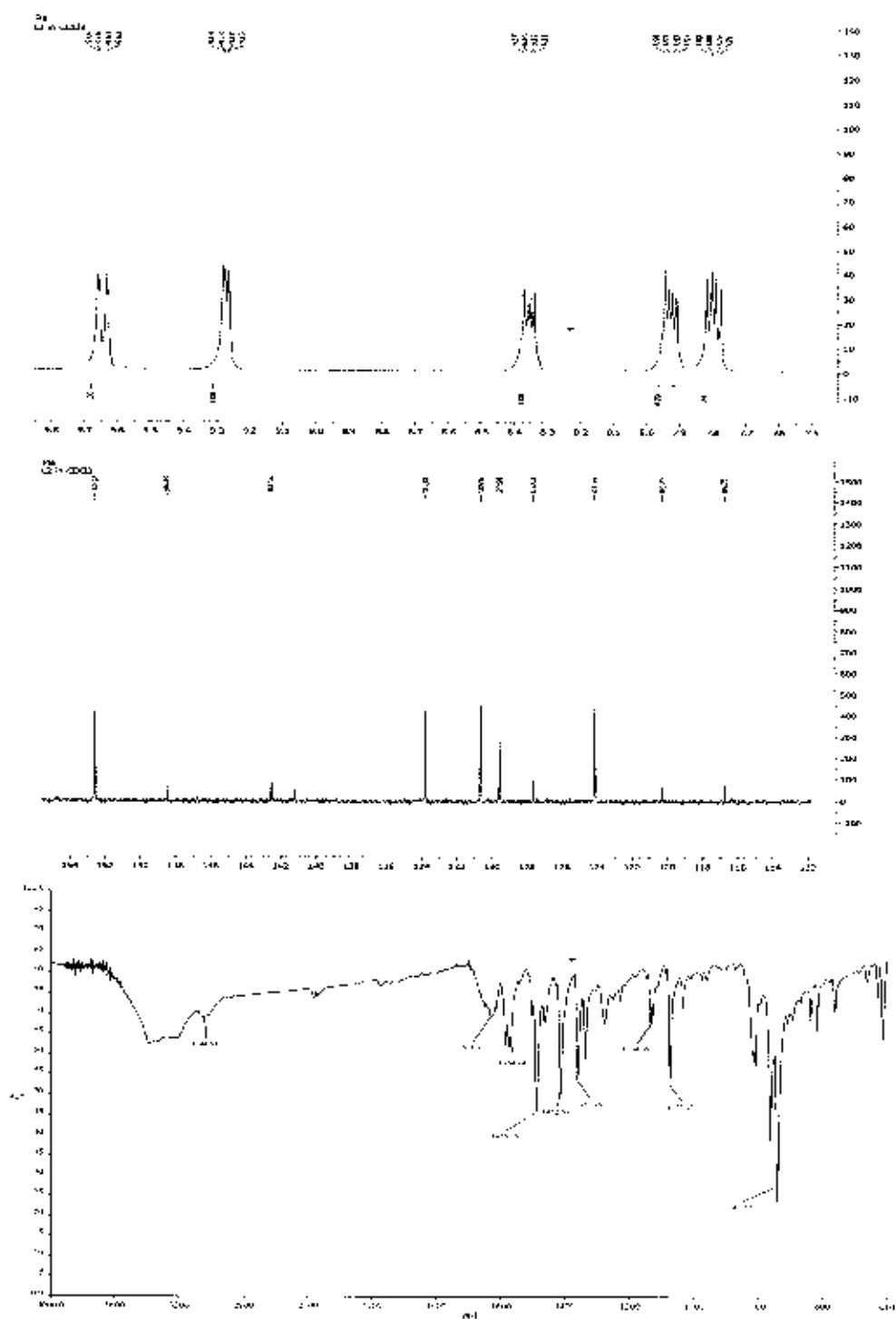
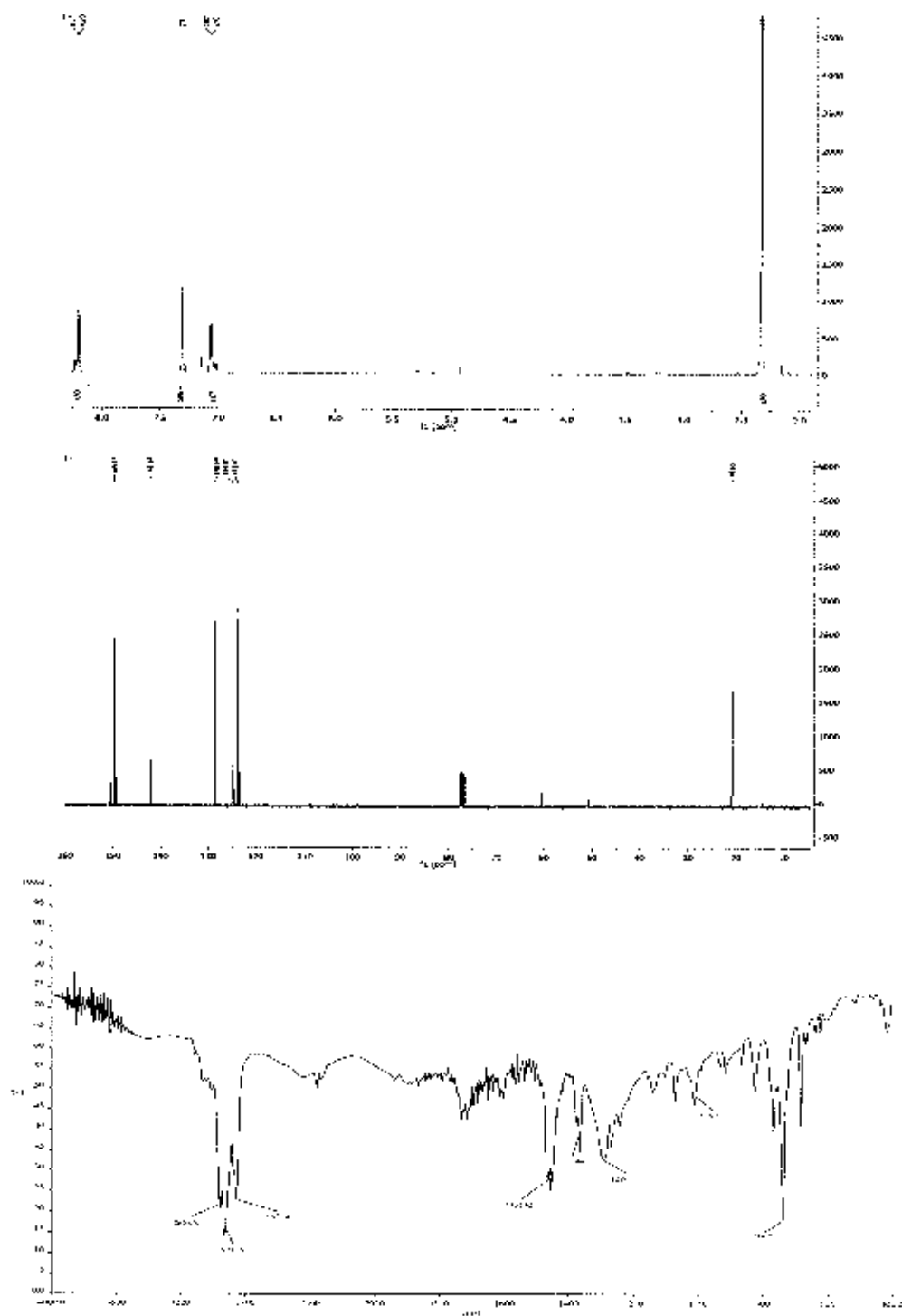
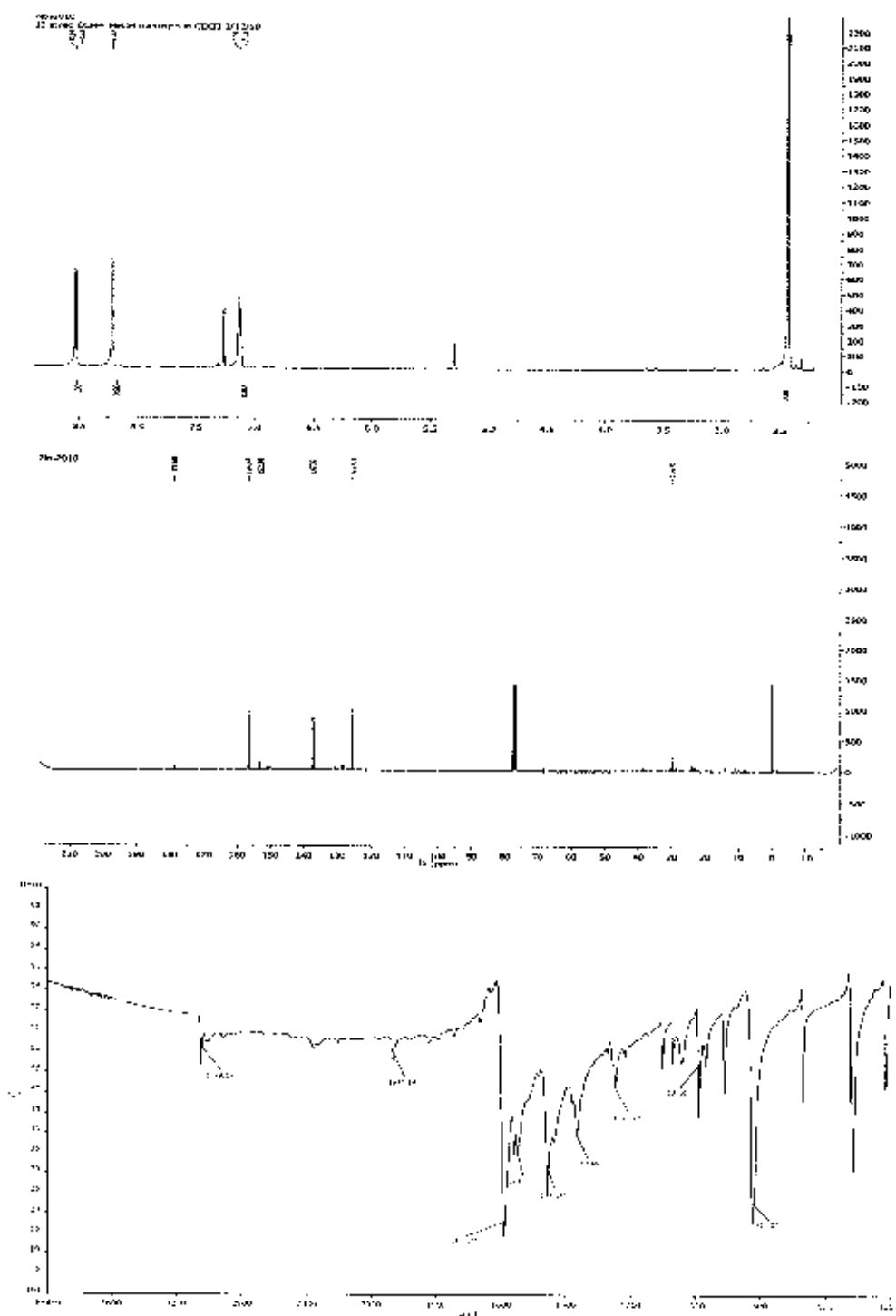


Figure A.1  $^1\text{H}$  NMR,  $^{13}\text{C}$  NMR in  $\text{CDCl}_3$  at room temperature and FT-IR spectra of dipyrido[3,2-a:2',3'-c]phenazine (YN-01)



**Figure A.2**  $^1\text{H}$  NMR,  $^{13}\text{C}$  NMR in  $\text{CDCl}_3$  at room temperature and FT-IR spectra of 2-bromo-4-methylpyridine (YN-02)



**Figure A.3**  $^1\text{H}$  NMR,  $^{13}\text{C}$  NMR in  $\text{CDCl}_3$  at room temperature and FT-IR spectra of 4,4'-dimethyl-2,2'-bipyridine (YN-03)

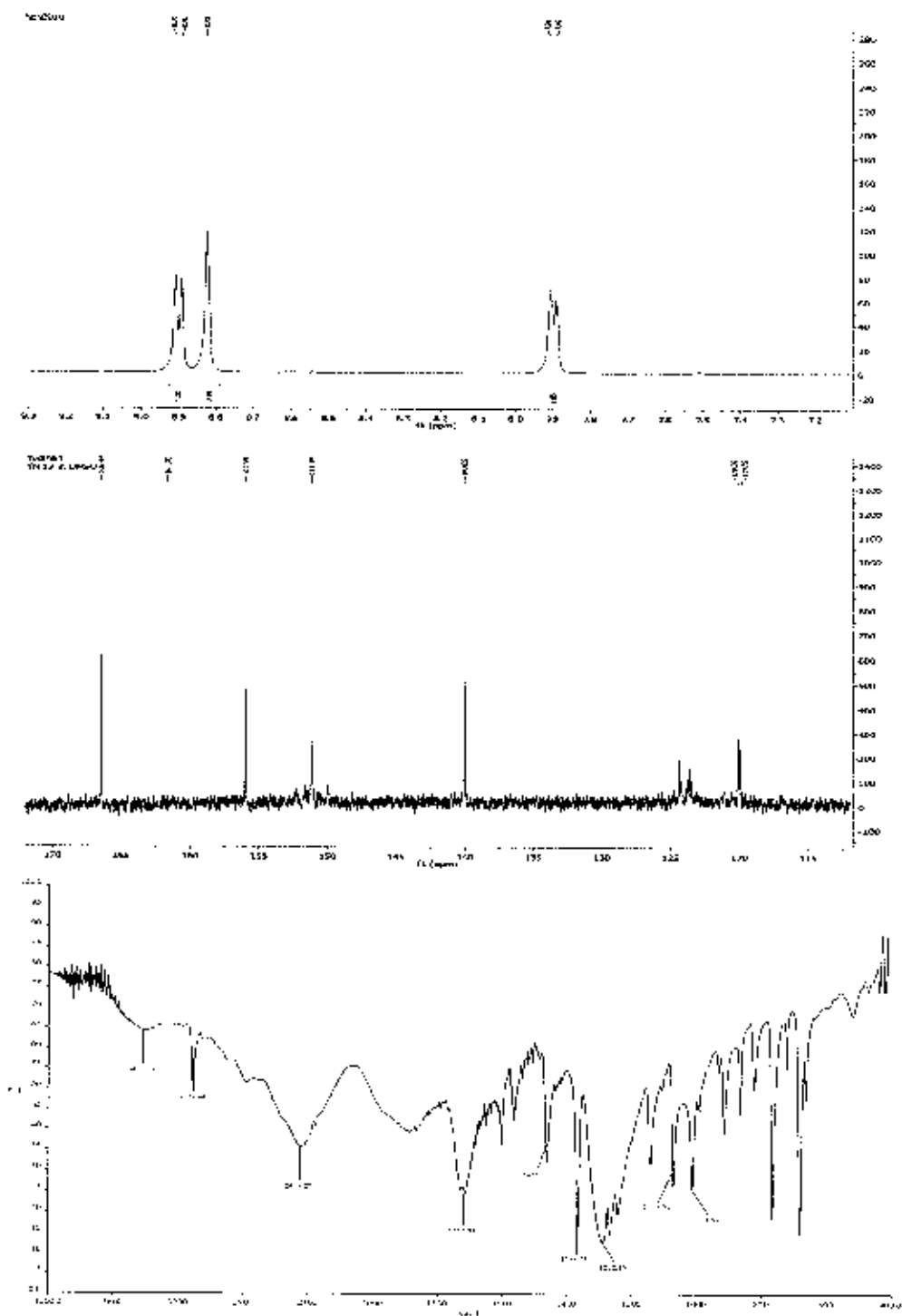


Figure A.4  $^1\text{H}$  NMR,  $^{13}\text{C}$  NMR in DMSO- $d_6$  at room temperature and FT-IR spectra of 4,4'-dicarboxylic-2,2'-bipyridine (YN-04)

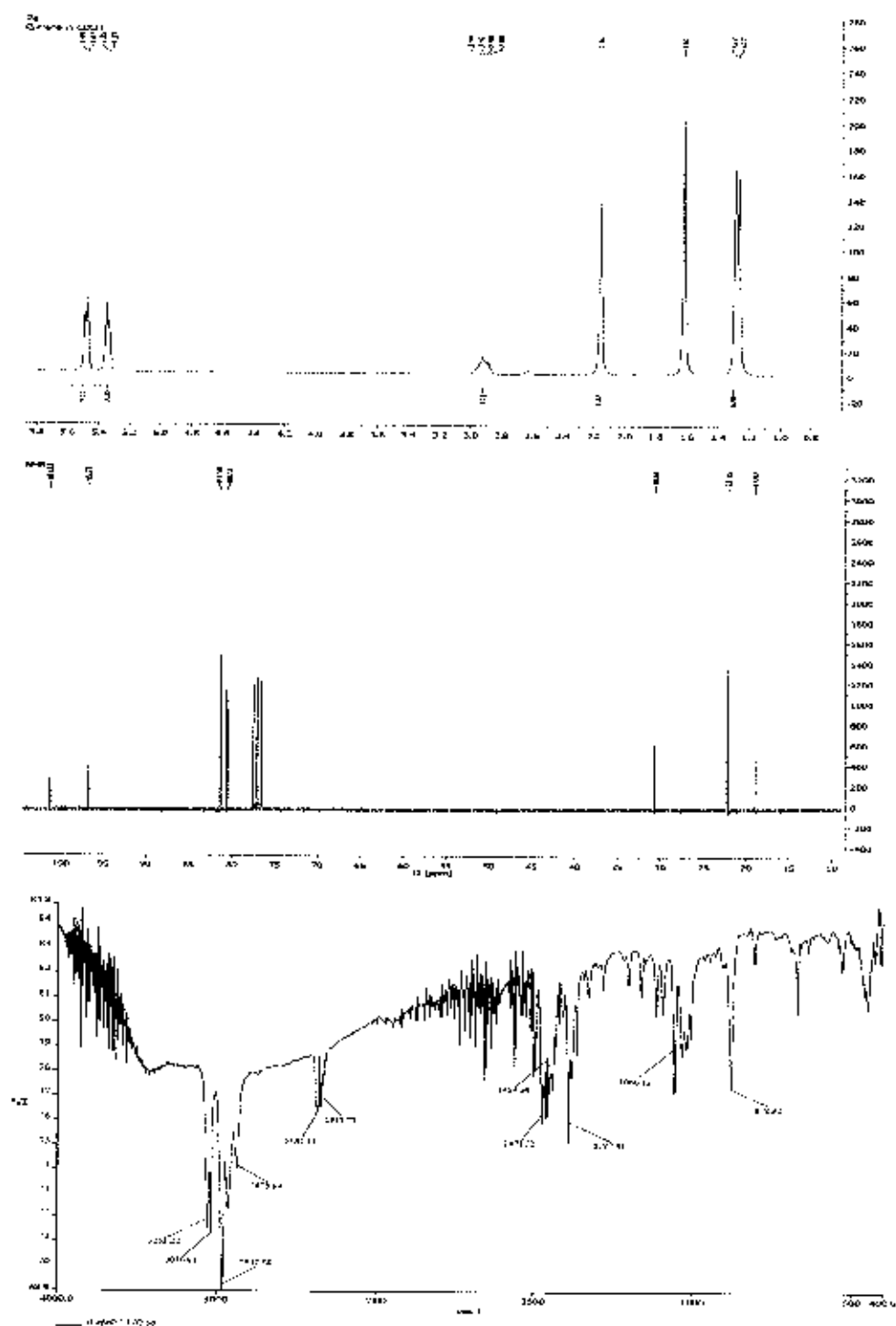
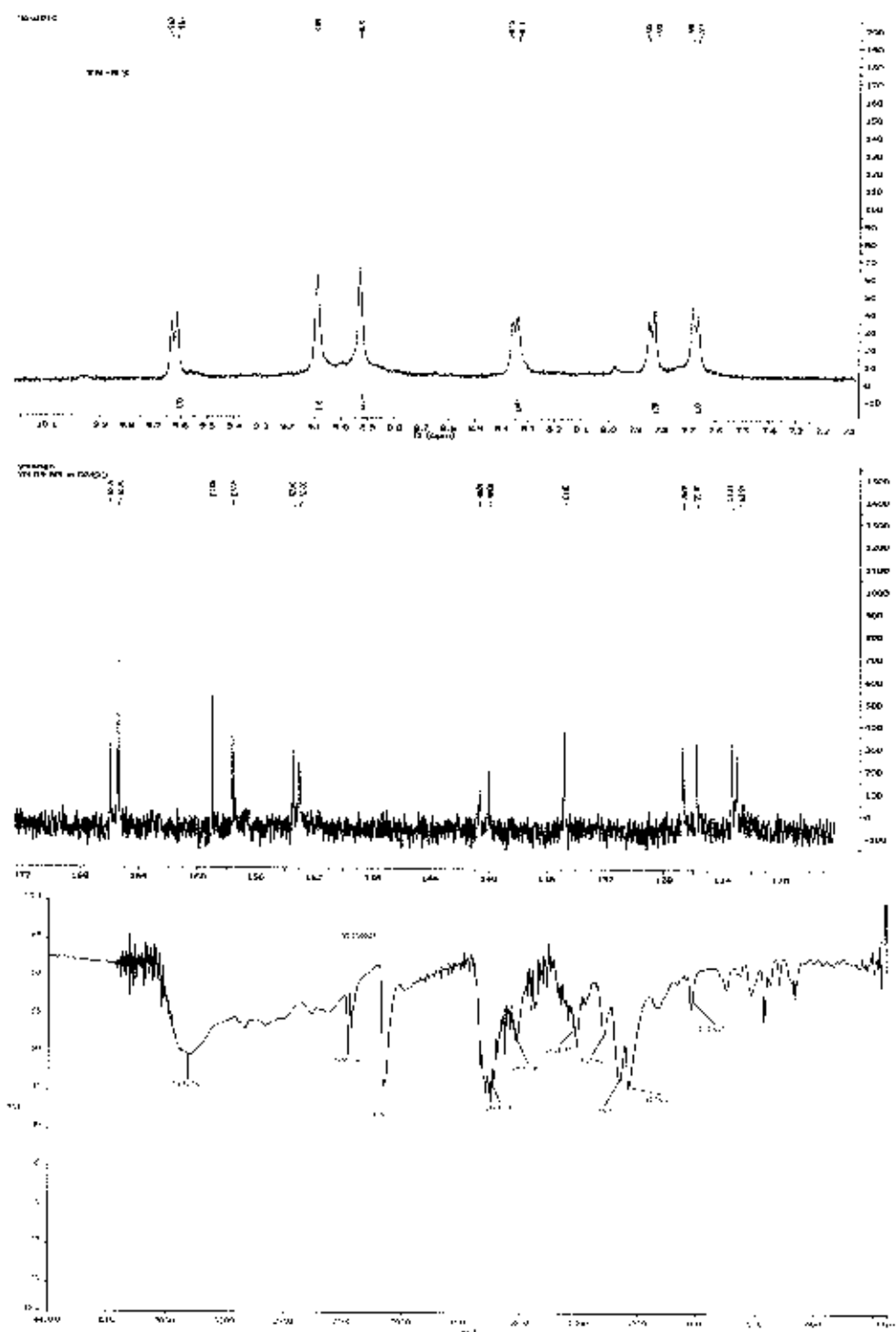
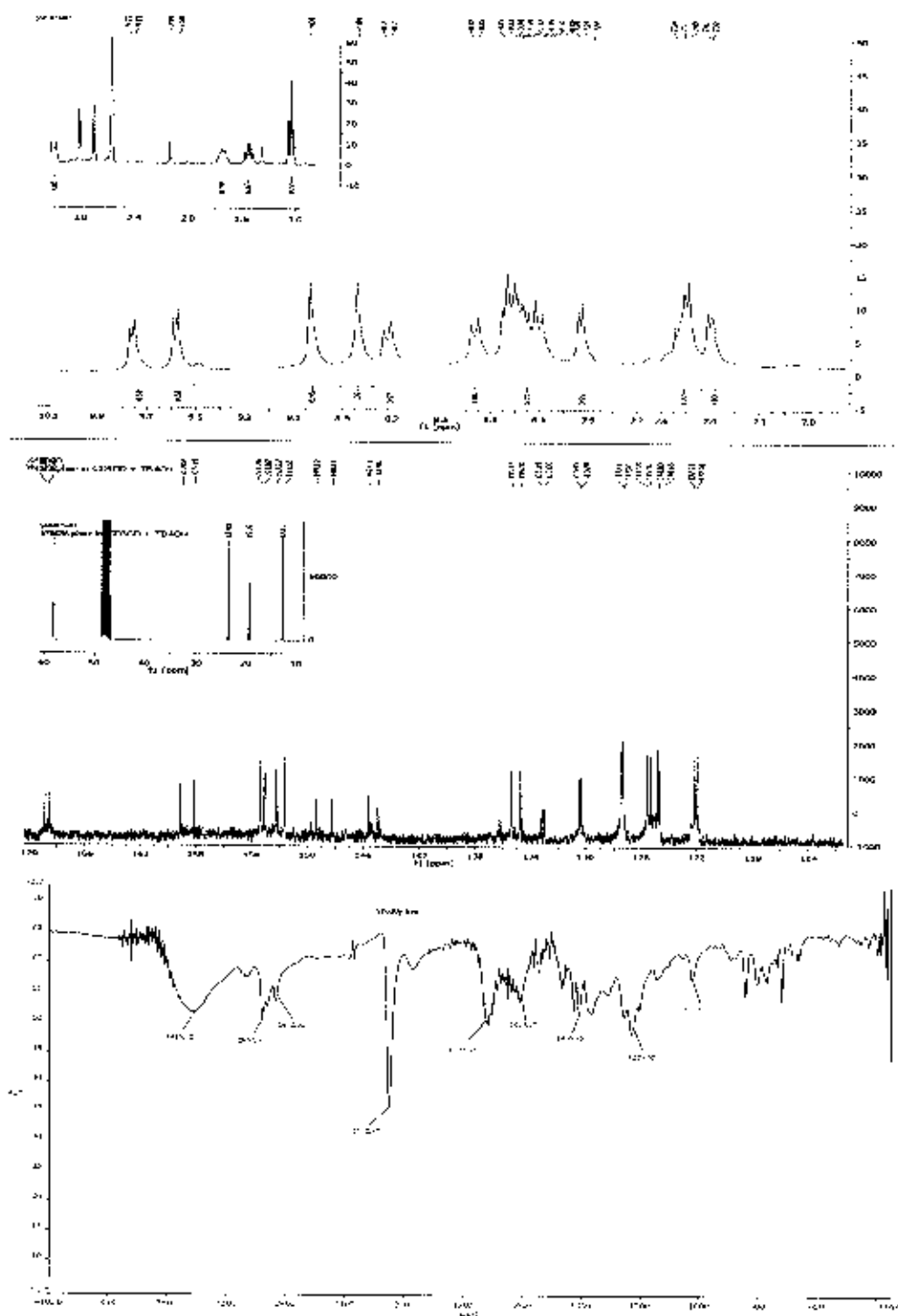


Figure A.5  $^1\text{H NMR}$ ,  $^{13}\text{C NMR}$  in  $\text{CDCl}_3$  at room temperature and FT-IR spectra of di- $\mu$ -chloro-bis( $\eta^6$ -benzene)chloro ruthenium(II) (YN-05)



**Figure A.6**  $^1\text{H}$  NMR,  $^{13}\text{C}$  NMR in  $\text{CD}_3\text{OD}$  at room temperature and FT-IR spectra of bis(4,4-dicarboxy-2,2'-bipyridine)dithiocyanatoruthenium(II), YN-N3 (syn)



**Figure A.7**  $^1\text{H}$  NMR,  $^{13}\text{C}$  NMR in DMSO- $d_6$  at room temperature and FT-IR spectra of tetrabutylammonium (1,10-phenanthroline)(4-carboxy-2,2'-bipyridine-4'-carboxylate)dithiocyanatoruthenium(II) ion (YN-phen)

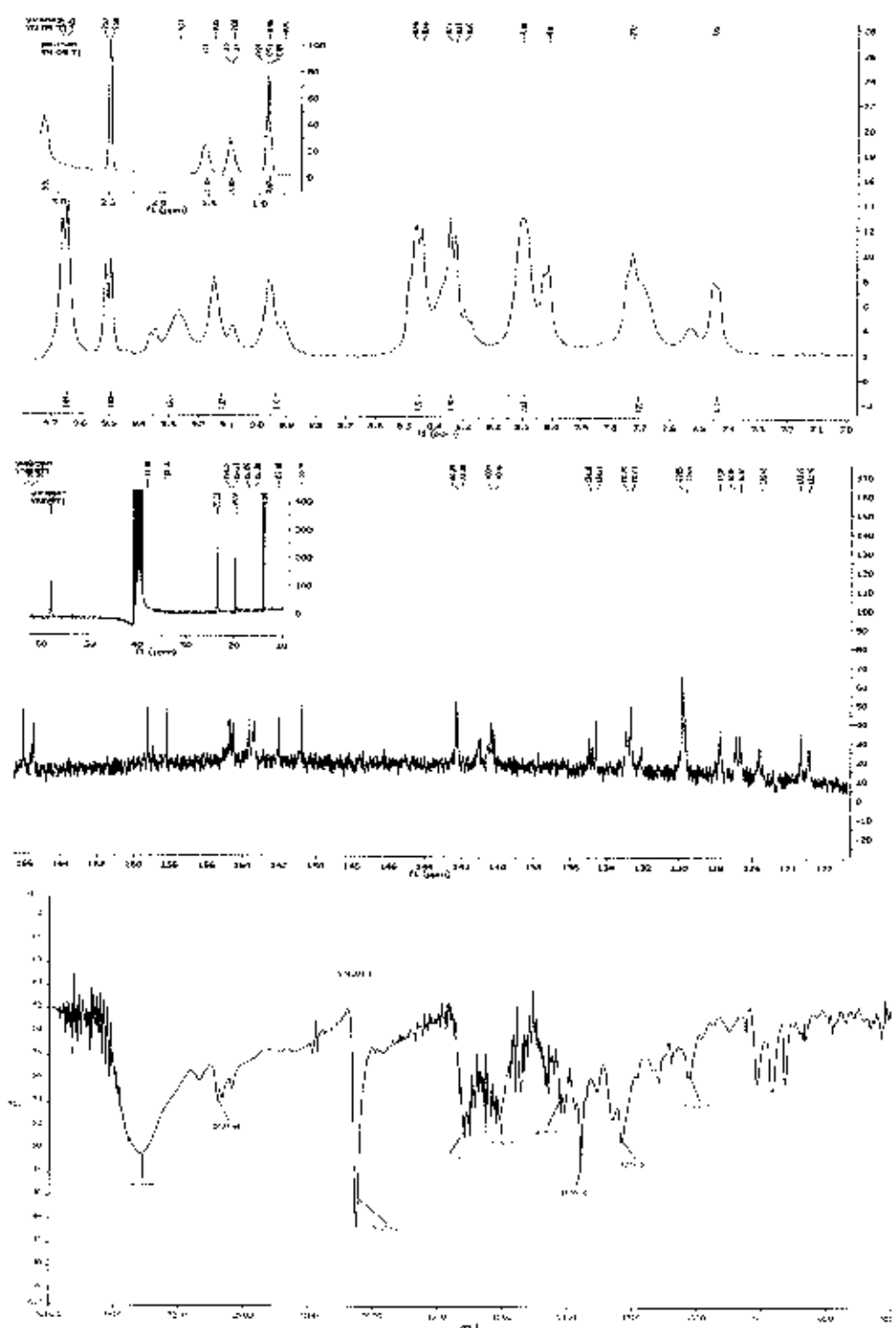


**Figure A.8**  $^1\text{H}$  NMR,  $^{13}\text{C}$  NMR in  $\text{DMSO-d}_6$  at room temperature and FT-IR spectra of tetrabutylammonium dipyrido[3,2-a:2',3'-c]phenazine(4-carboxy-2,2'-bipyridine-4'-carboxylate)dithiocyanatoruthenium(II) ion (YN-06)

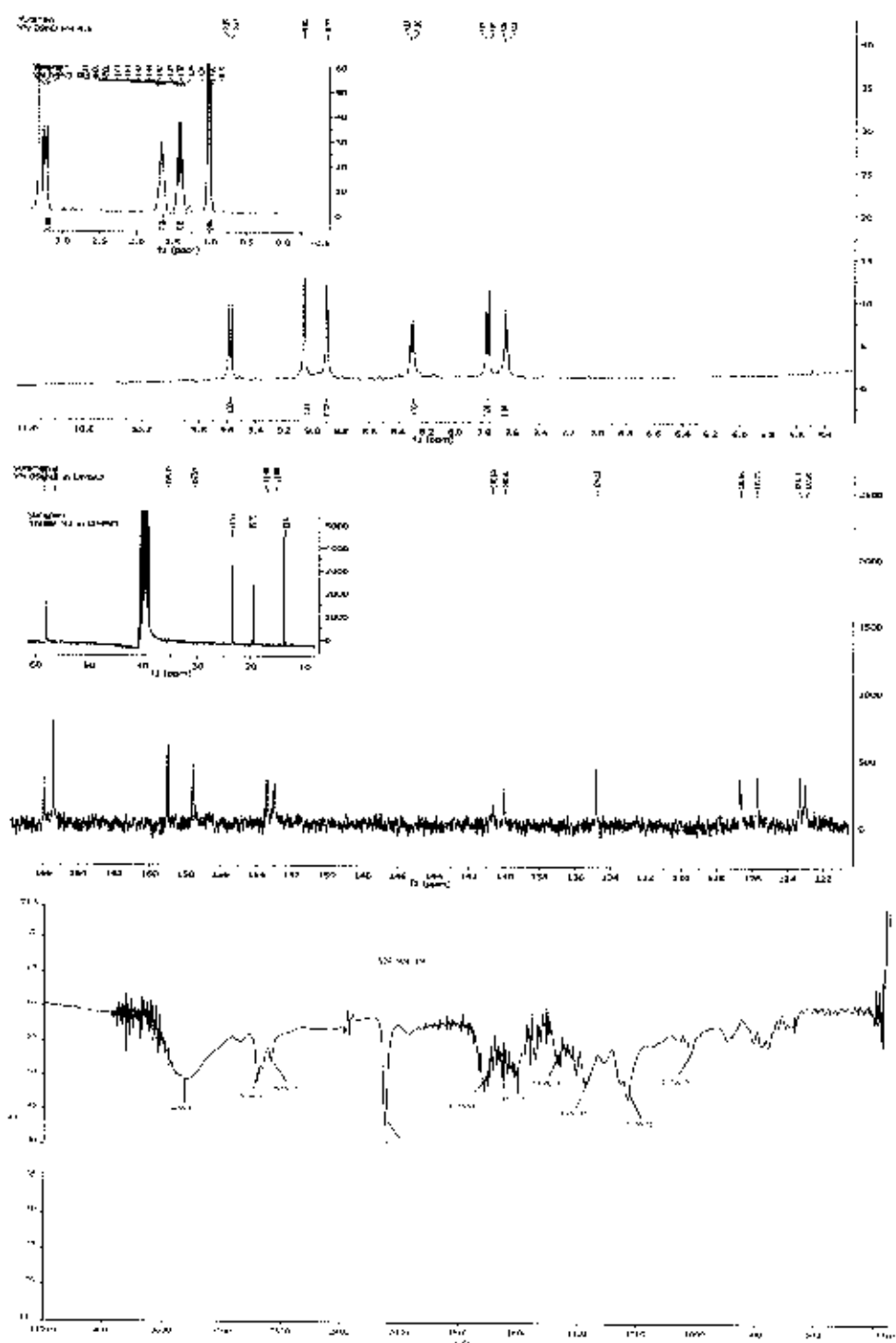


**Figure A.9**  $^1\text{H NMR}$ ,  $^{13}\text{C NMR}$  in  $\text{DMSO-}d_6$  at room temperature and FT-IR spectra of bis(tetrabutylammonium)bis(4-carboxy-2,2'-bipyridine-4'-carboxylate) dithiocyanatoruthenium(II) ion (YN-719)

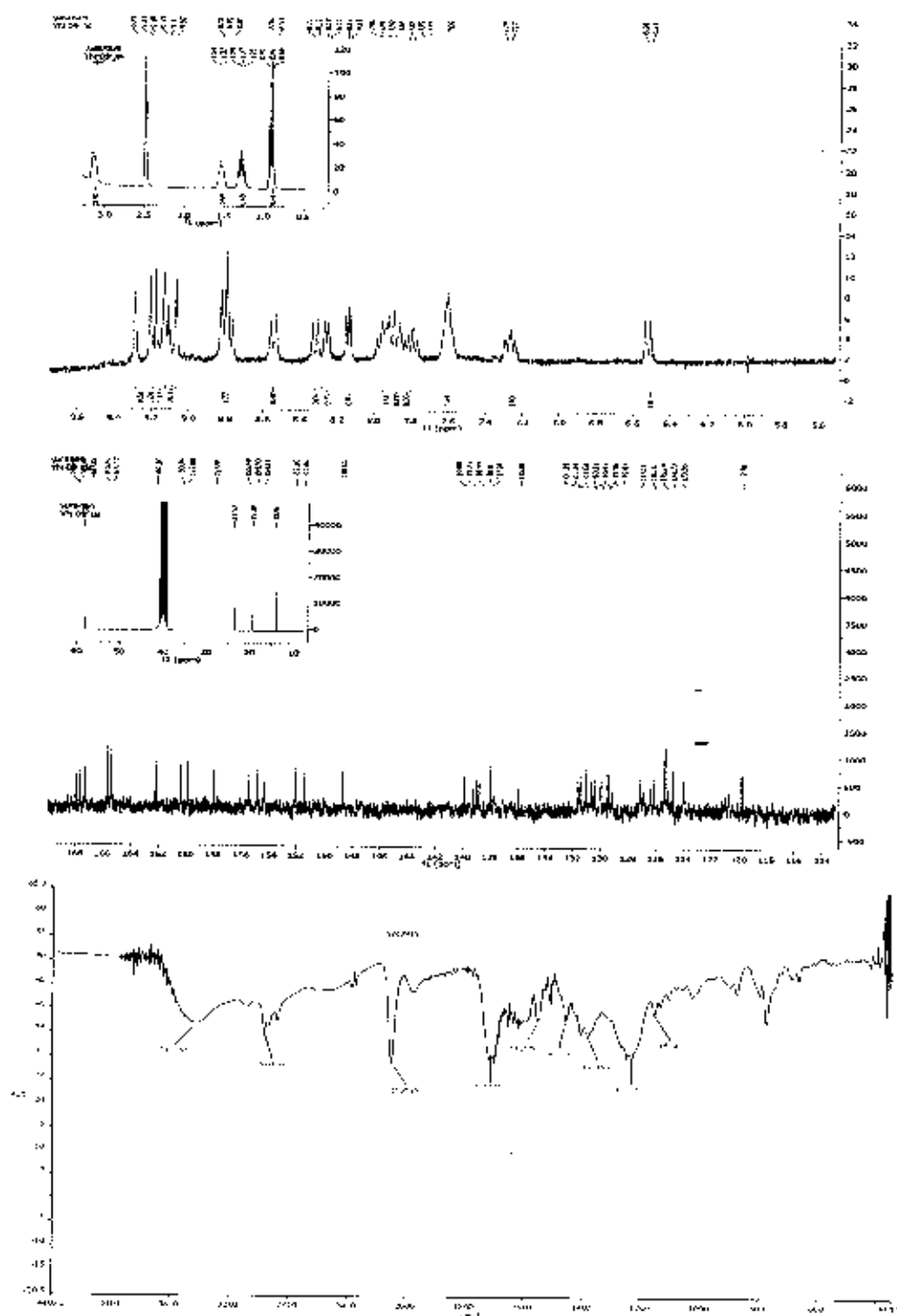


**Figure A.10**  $^1\text{H NMR}$ ,  $^{13}\text{C NMR}$  in  $\text{DMSO-d}_6$  at room temperature and FT-IR spectra of tetrabutylammonium (2,2'-biquinoline-4,4'-dicarboxylic acid)(4-carboxy-2,2'-bipyridine-4'-carboxylate)dithiocyanato ruthenium(II) ion (YN-07)



**APPENDIX B****Mass spectra of ligand and ruthenium(II) complexes**

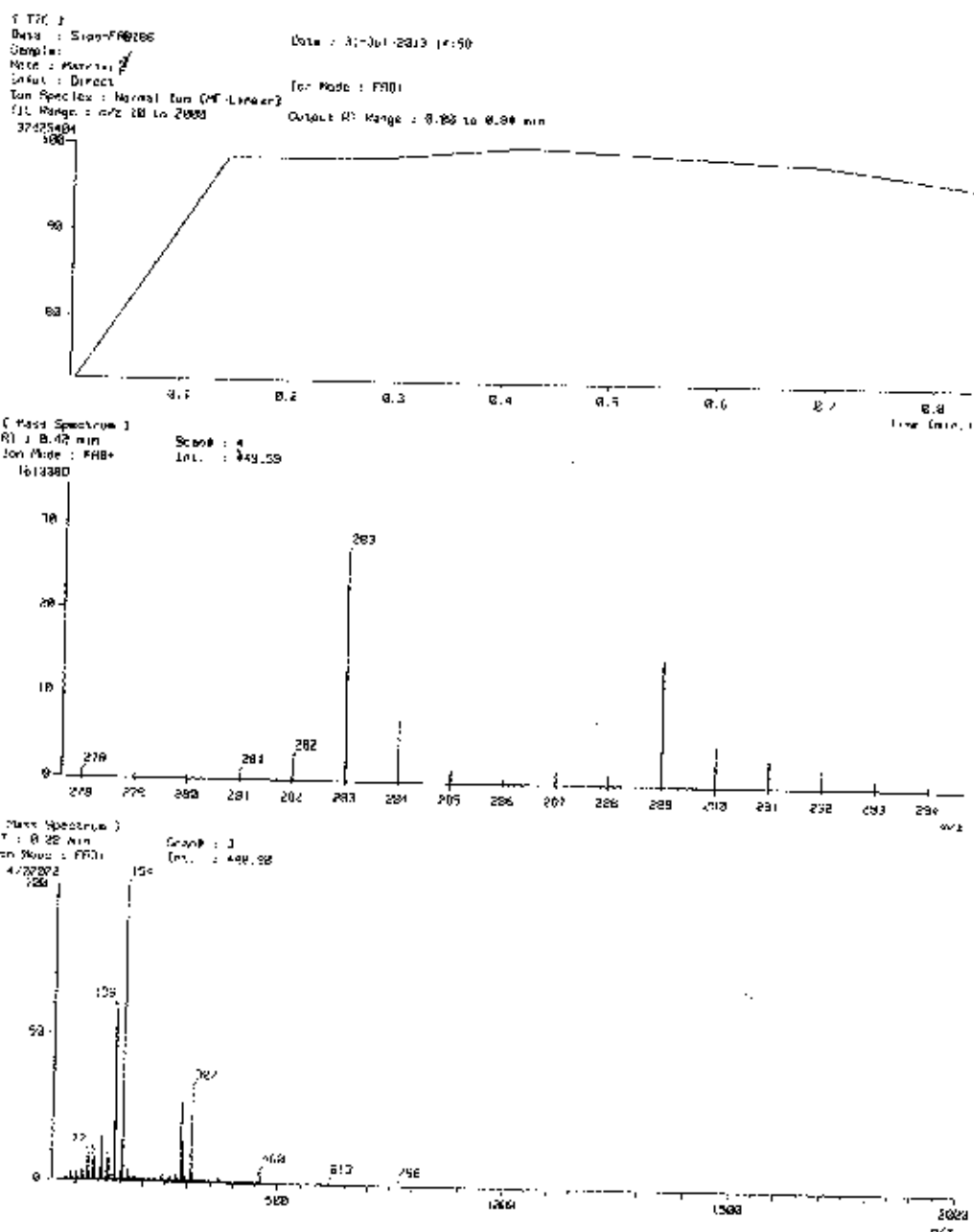


Figure B.1 Mass spectrum of dipyrido[3,2-a:2',3'-c]phenazine (YN-01)

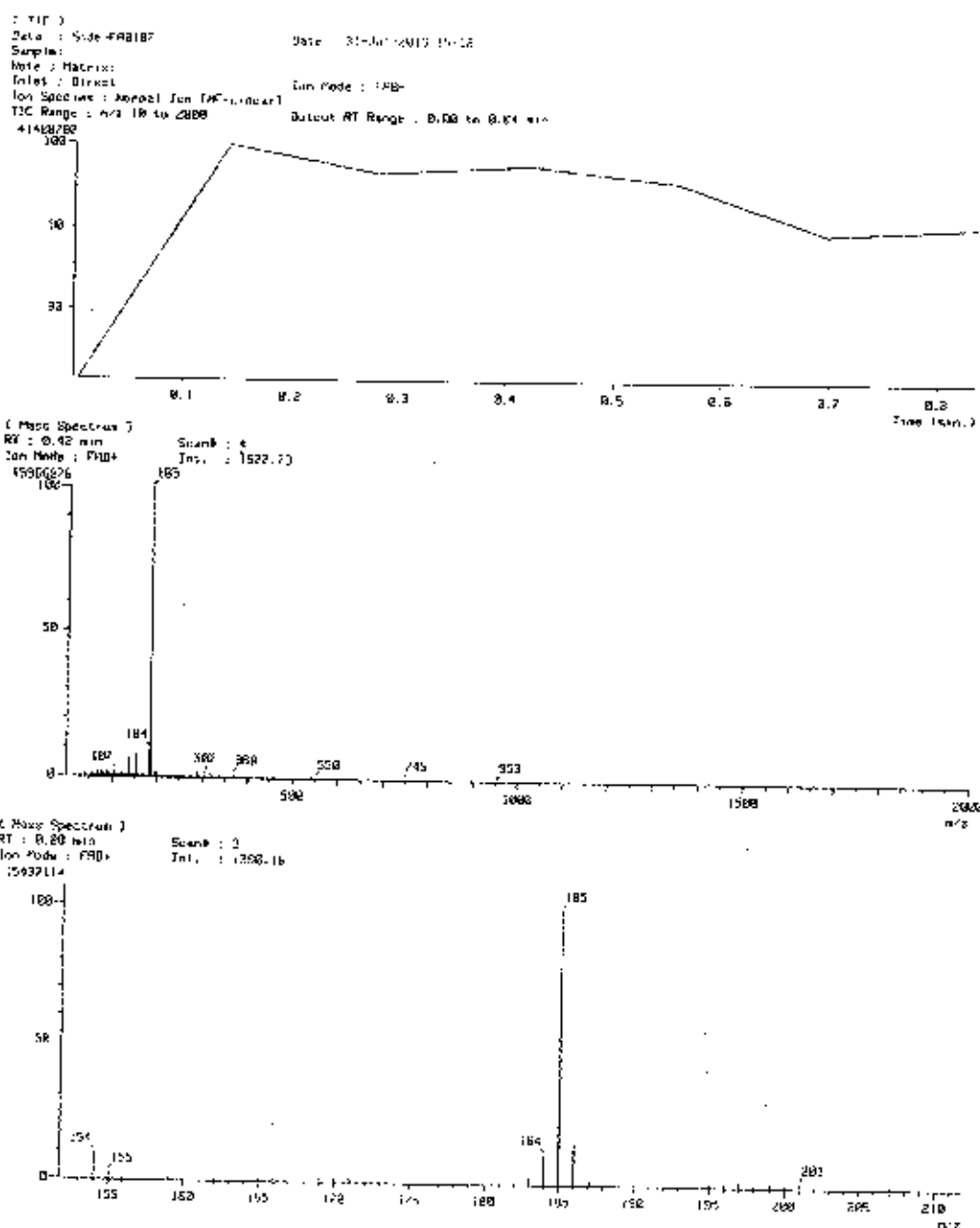


Figure B.2 Mass spectrum of 4,4'-dimethyl-2,2'-bipyridine (YN-03)

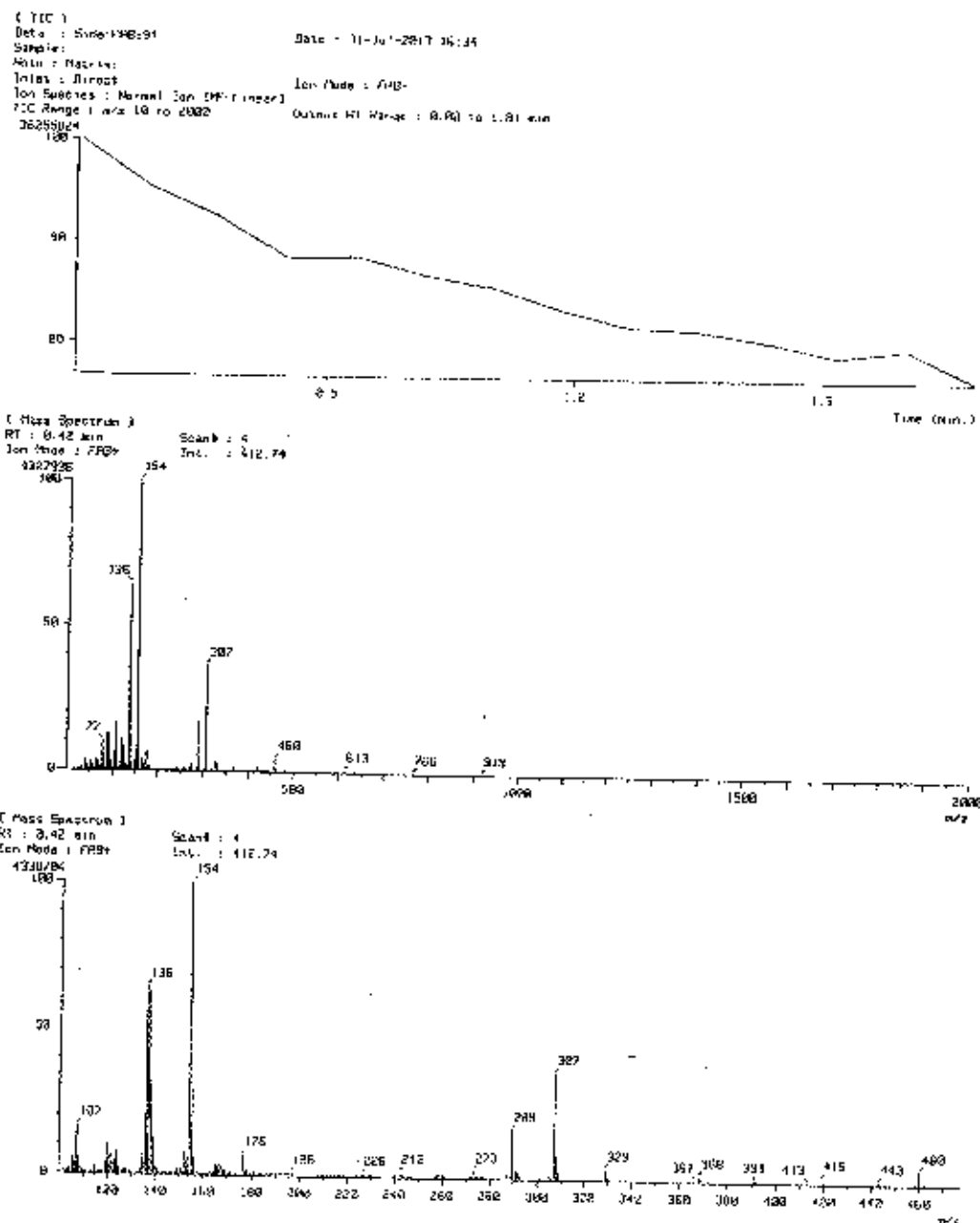


Figure B.3 Mass spectrum of 4,4'-dicarboxy-2,2'-bipyridine (YN-04)

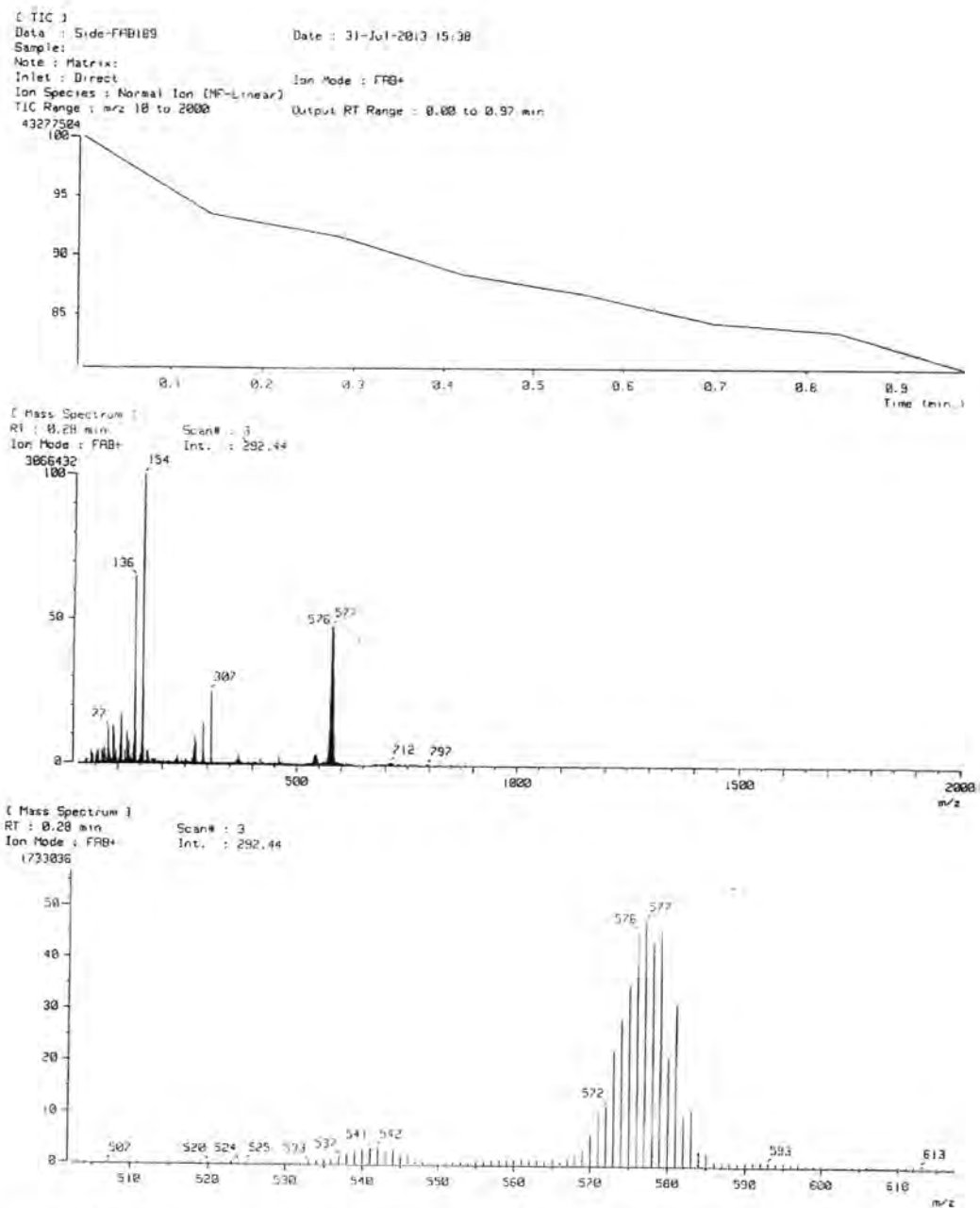


Figure B.4 Mass spectrum of di- $\mu$ -chloro-bis[( $\eta^6$ -benzene)chlororuthenium(II)] (YN-05)

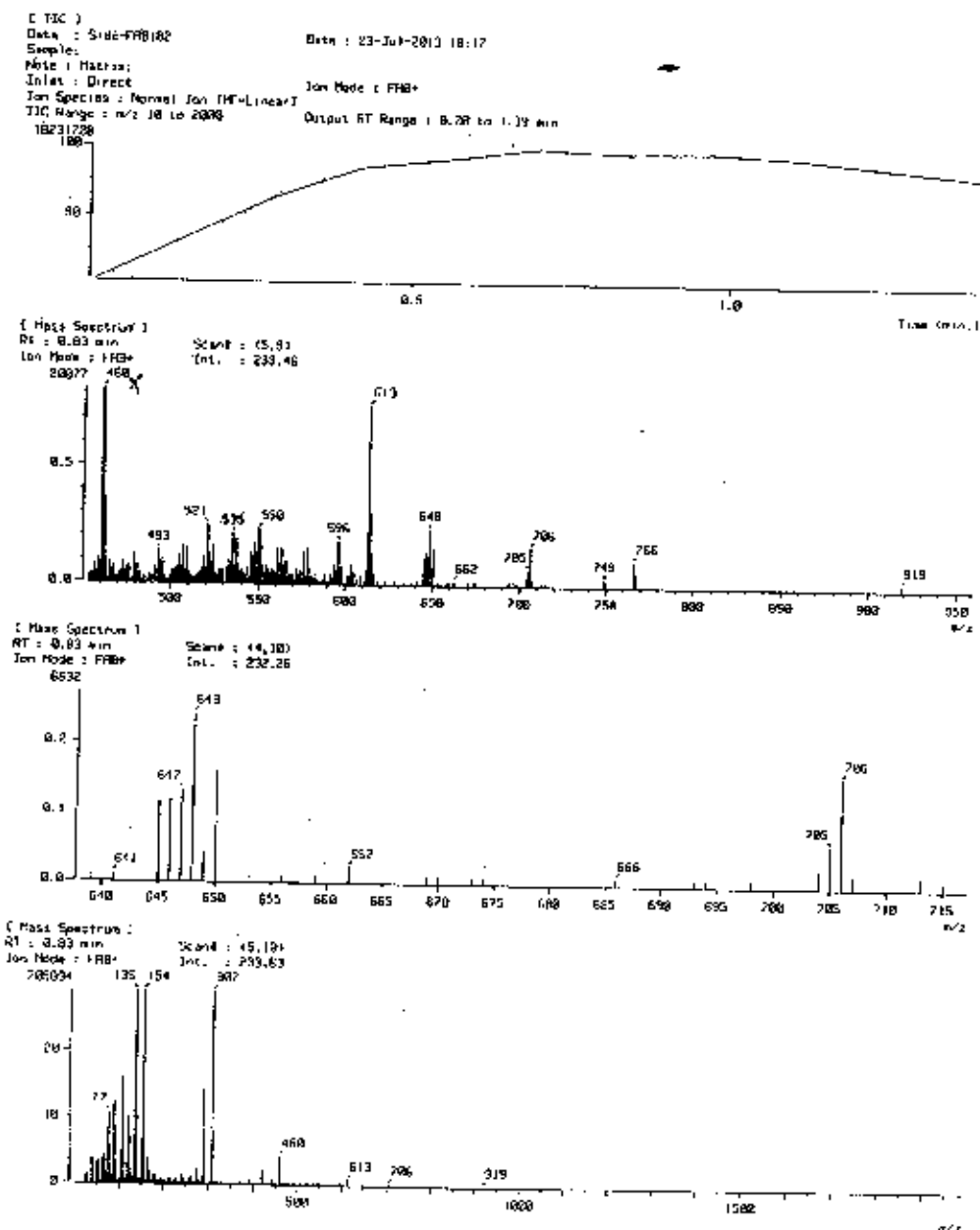
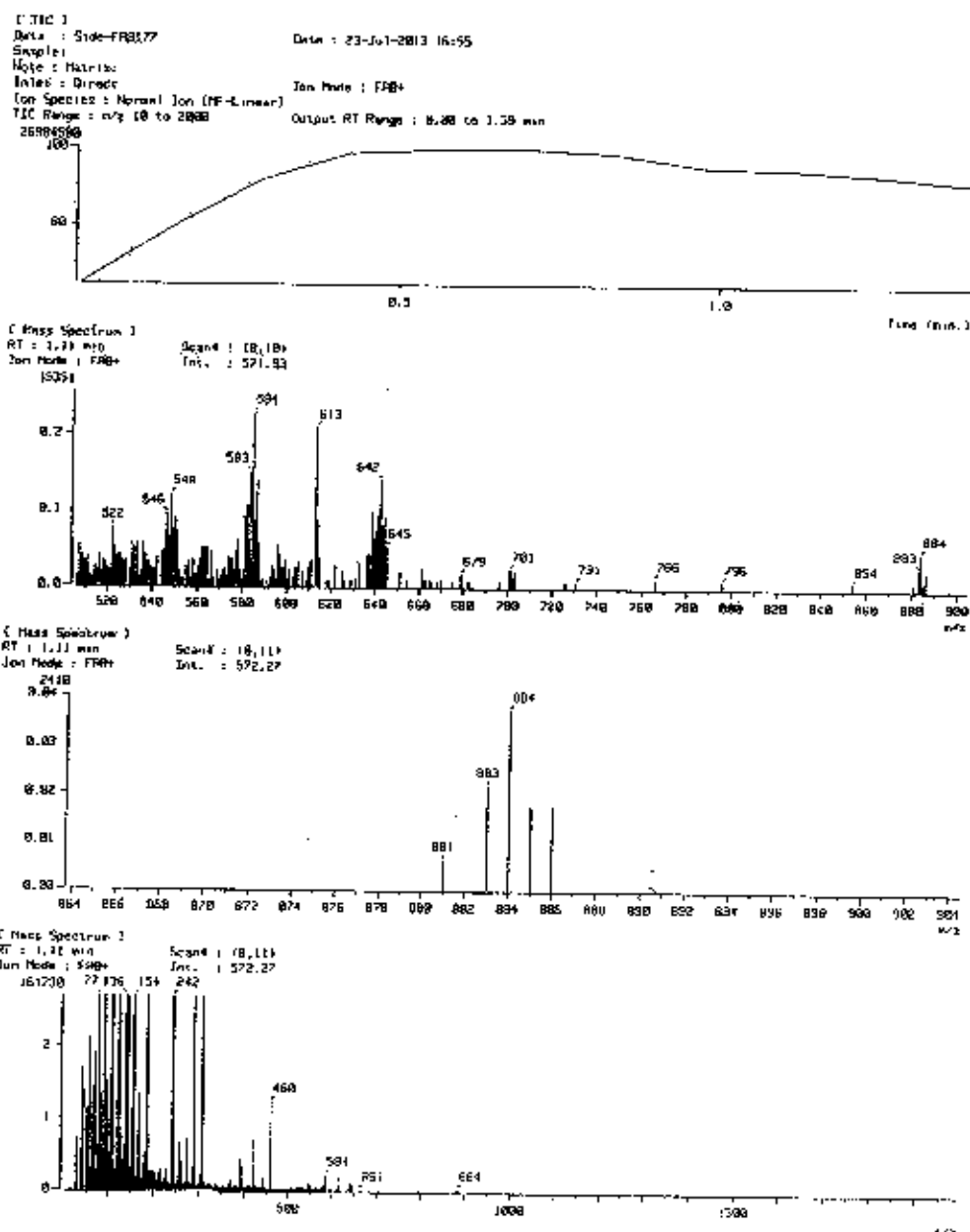


Figure B.5 Mass spectrum of bis(4,4'-dicarboxy-2,2'-bipyridine)dithiocyanatoruthenium(II)  
 (YN-N3 (syn))



**Figure B.6** Mass spectrum of tetrabutylammonium(1,10-phenanthroline)(4-carboxy-2,2'-bipyridine-4'-carboxylate)dithiocyanatoruthenium(II) ion (YN-phen)

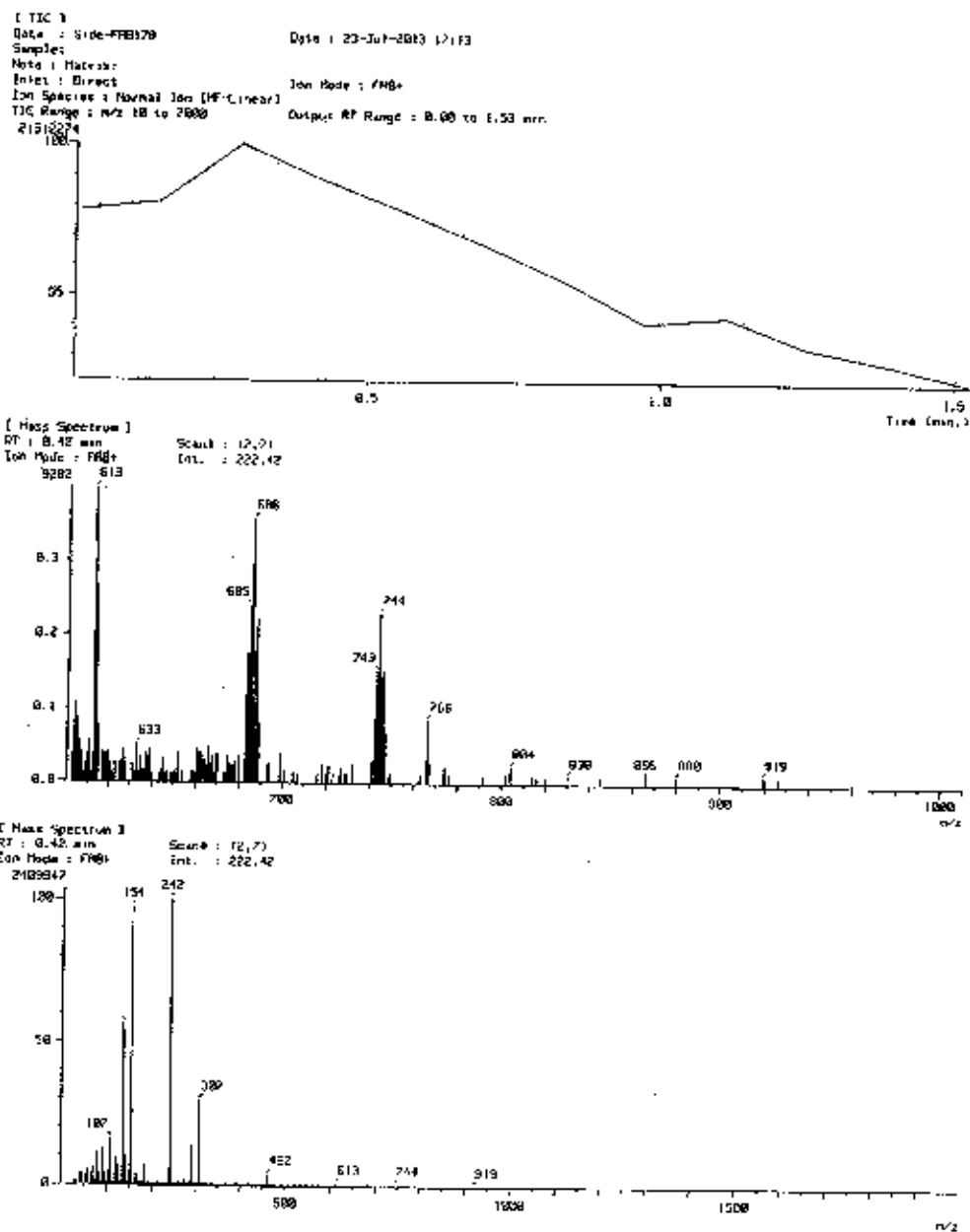
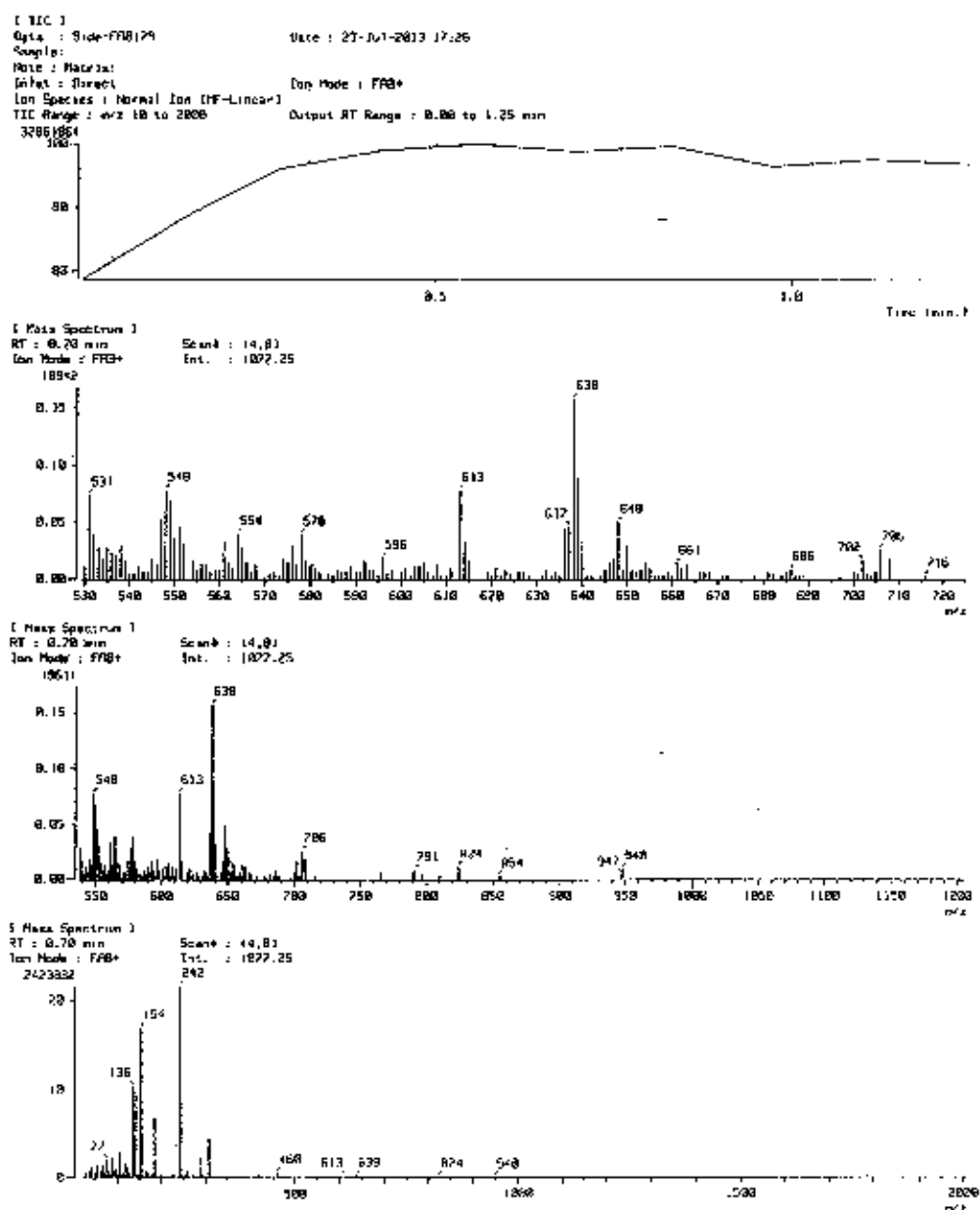


Figure B.7 Mass spectrum of tetrabutylammoniumdipyrido[3,2-a:2',3'-c]phenazine(4-carboxy-2,2'-bipyridine-4'-carboxylate)dithiocyanatoruthenium(II) ion (YN-06)



**Figure B.8** Mass spectrum of bis(tetrabutylammonium)bis(4-carboxy-2,2'-bipyridine-4'-carboxylate)dithiocyanatoruthenium(II) ion (YN-719)

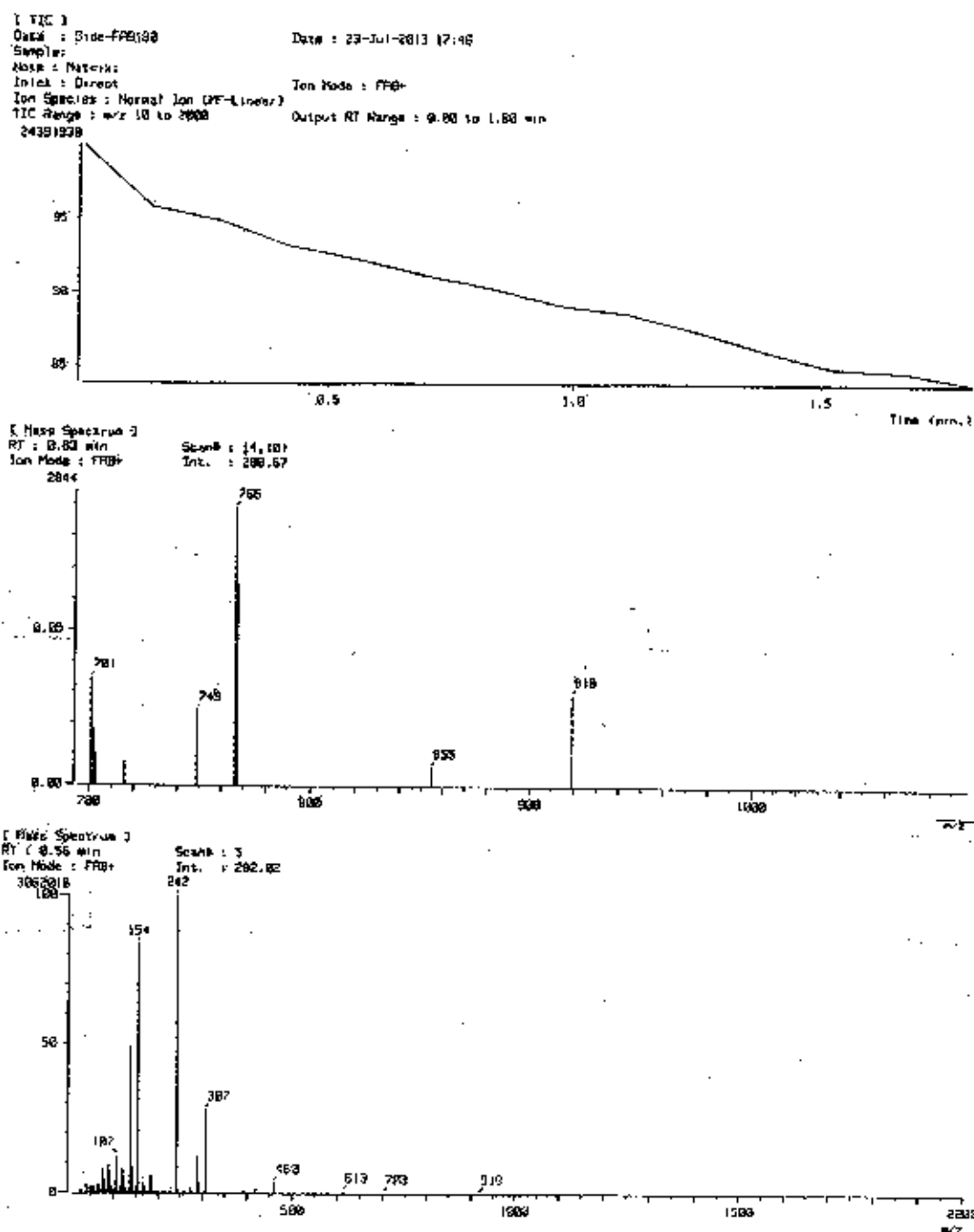
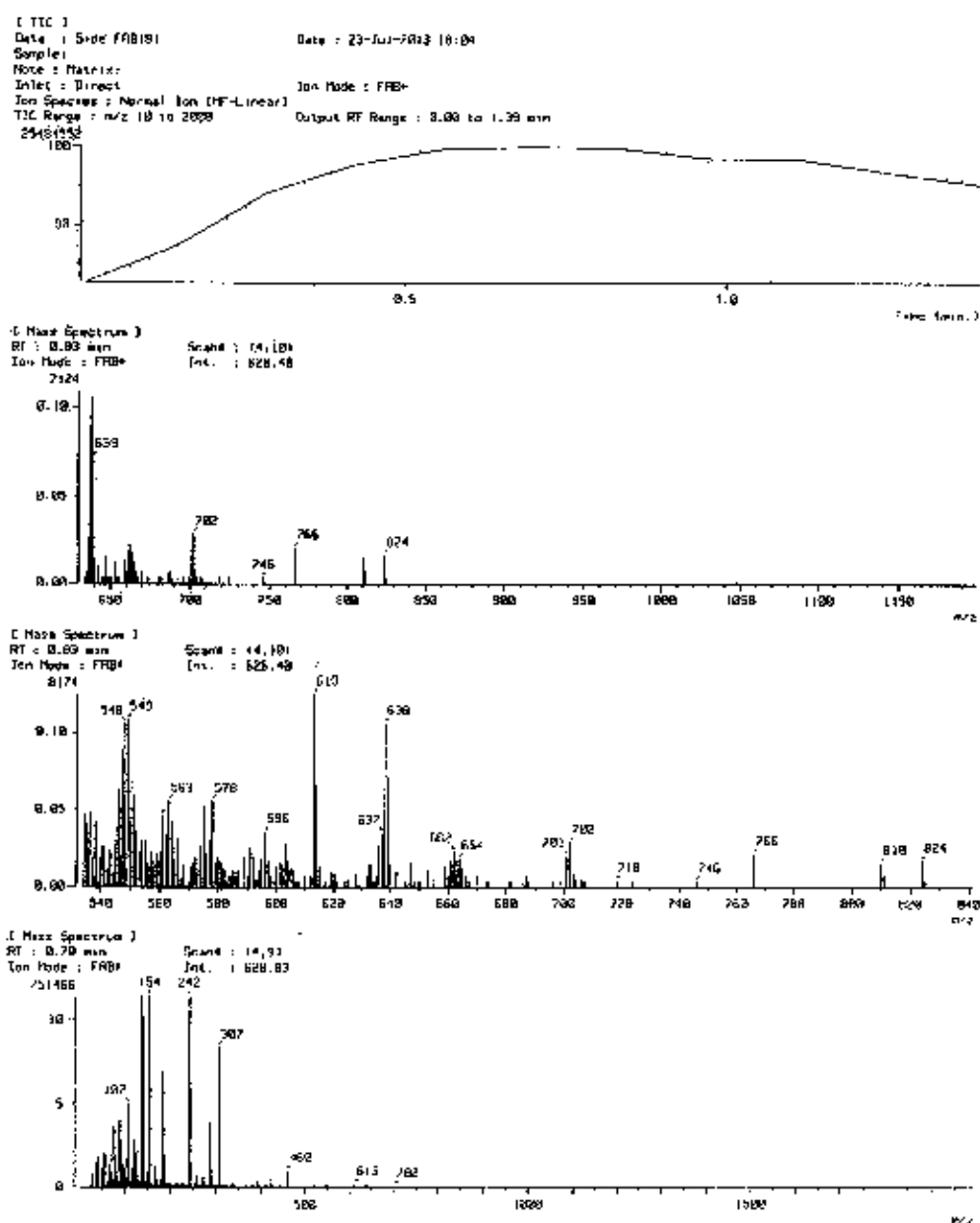


Figure B.9 Mass spectrum of tetrabutylammonium(4,4'-dicarboxy-2,2'-biquinoline)(4-carboxy-2,2'-bipyridine-4'-carboxylate)dithiocyanatoruthenium(II) ion (YN-07)



**Figure B.10** Mass spectrum of bis(tetrabutylammonium)bis(4-carboxy-2,2'-biquinoline-4'-carboxylate)dithiocyanatoruthenium(II) ion (YN-08)

**APPENDIX C**  
**Publication papers**



# THE SYNTHESIS AND CHARACTERIZATION OF RUTHENIUM COMPLEXES FOR DYE-SYNTHIZING SOLAR CELL APPLICATION

Yuragan Thairong<sup>1</sup>, Kitiya Wongkhan<sup>1</sup> and Rukkiat Jitcheal<sup>1\*</sup>

<sup>1</sup>Center for Organic Electronic and Alternative Energy (COEA), Department of Chemistry, Faculty of Science, Ubon Ratchathani University, Wankhumpap, Ubon Ratchathani Province, 34190, Thailand  
\*Corresponding author, rukkiat.j@hotmail.com

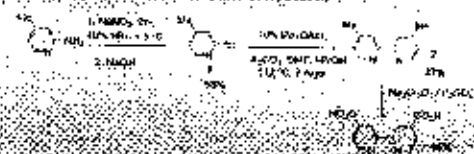


## Introduction

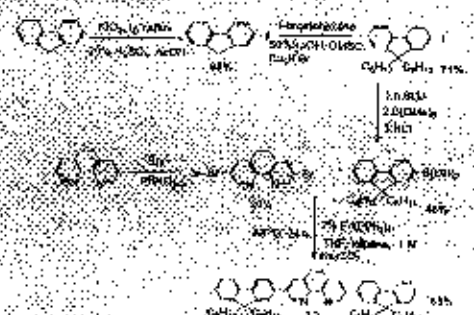
Since the dawn of oil, mankind has used energy from fossil fuel, whereas, the resource reserves of the earth will run out in the future. The increasing energy demands and shortage of fossil fuels have driven people to develop new types of clean and sustainable energy. So, the biggest challenge for our global society is to find ways to replace fossil fuels by renewable resources and, at the same time, avoid negative effects from the current energy system on climate, environment, and health. Now, the clean and renewable energy sources are wind, water and sun. However, the area of greatest promise is that of solar energy, which is generally referred to as "photovoltaic cells" (PV) [1]. However, a drawback to these most of PVs used today are inorganic thin film photovoltaic devices, i.e., CdTe and CuInGaSe, which contain highly toxic and expensive materials. For this reason, the rational generation of solar converters called dye-sensitized solar cells (DSSCs) has been developed [2] and proved to be the best alternative in the future [3].

## Synthetic Methodology

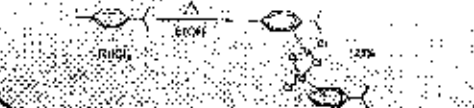
1,10-Phenanthroline (1) was synthesized in 85% yield, 2,2'-bipyridine (2) in 40% yield, and 2,2'-bipyridine (3) in 20% yield. The synthesis of 1,10-phenanthroline (1) is shown in Scheme 1. The synthesis of 2,2'-bipyridine (2) is shown in Scheme 2. The synthesis of 2,2'-bipyridine (3) is shown in Scheme 3.



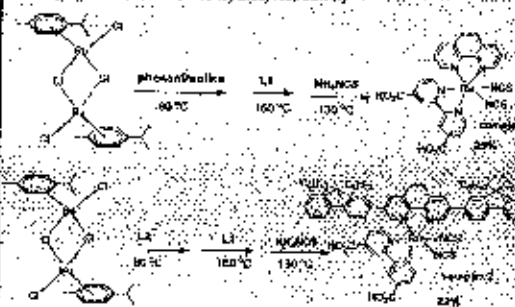
Complexes 1 and 2 were synthesized by reacting ruthenium(II) chloride with 1,10-phenanthroline (1) and 2,2'-bipyridine (2) respectively. The synthesis of complex 1 is shown in Scheme 4. The synthesis of complex 2 is shown in Scheme 5.



The dimeric ruthenium complex 3 was synthesized by reacting ruthenium(II) chloride and 2,2'-bipyridine in refluxing ethanol.



The two new ruthenium complexes were obtained by reacting a dimeric ruthenium with each of the ligands in dimethylacetamide (DMAc) under a nitrogen balloon in a typical dye-sensitization synthesis to get complex 1 and complex 2 in 24 and 22 percent yields, respectively.



## Results and Discussion

The two new ruthenium complexes were characterized and identified as 1,10-phenanthroline and bipyridine ruthenium(II) complexes by IR, UV-Vis, and NMR spectra. The complexes can be seen from 2D-bulk specific <sup>1</sup>H and <sup>13</sup>C NMR spectra. Complex 1 shows a typical spectrum with characteristic phenanthroline and bipyridine units. The <sup>13</sup>C NMR spectra show two carbonyl groups with a chemical shift of 177.2 and 178.8 ppm. In the case of complex 2, which was the complex with a dimeric structure, can be identified from the bulk and chain groups in the chemical shift range between 0 to 100 ppm and two carbonyl groups. The UV-Vis absorption spectra of the series of ruthenium complexes, complex 1 and 2 in DMAc solution, reveal of two main bands assigned as π-π\* transition and n-π\* transition.



UV-Vis absorption spectra of complex 1 (green line) and complex 2 (red line) in DMAc solution.

## Conclusions and Acknowledgements

We report the synthesis and characterization of two new ruthenium complexes. The difference in the UV-Vis absorption spectra demonstrates that a long and high absorption of complex 2 could be improved by bipyridine ligands in phenanthroline complexes. In a further development, both complexes are to be used as sensitizers in DSSCs in the future. The authors would like to acknowledge the financial support from the Ministry of Education and Learning (MOE), Food Ministry (NRI) & Microtechnology Center (MTC), NSTDA (P-10-11346) and Energy Policy and Planning Office (EPPO) (P-10-01-027).

## References

[1] Zohal, K., *Solar Eng. News* 1988, 14, 34-42 [2] Wang, Y., Zhang, L., Walker, D. M., *J. Phys. Chem. C* 2011, 115, 4226-4234 [3] O'Regan, B., Grätzel, M., *Nature* 1991, 353, 737-740 [4] Grätzel, M., K. Ray, A., Rodde, I., Humphry-Baker, M., Müller, E., Liska, S., Wasthouske, N., Grätzel, M., *J. Am. Chem. Soc.* 1998, 120, 6507-6509 [5] Grätzel, M., *Acc. Chem. Res.* 2009, 42, 1788-1798



ICCCP 2012: 5-6 May 2012, Kuala Lumpur, Malaysia

## Air-Stable Anthracene-Phosphine Oxide Adduct Ligand in Pd Catalysed Suzuki-Miyaura Reactions

Yurana Thathong<sup>a</sup>, Rukiat Jitchati<sup>a</sup>, Kittiya Wongkhan<sup>a\*</sup>

<sup>a</sup> Center for Organic Electronic and Alternative Energy (COEAE), Department of Chemistry, Faculty of Science, Ubon Ratchaburi University, Watischanong, Ubon Ratchaburi Province, 34199, Thailand

### Abstract

The palladium(0) and palladium(II) catalysed Suzuki-Miyaura cross-coupling reaction has been established. We found that the optimized conditions are 1% PdCl<sub>2</sub>(PPh<sub>3</sub>)<sub>2</sub>, 1 M aqueous Na<sub>2</sub>CO<sub>3</sub> (2.5 eq.) and anthracene-phosphine oxide adduct (3) as a noble ligand (0.1 eq.) in only 4 hours refluxing 1,3-dioxane. The reactions proceed in moderate to good yields with a diverse array of coupling partners as substrates.

© 2012 Published by Elsevier B.V. Selection and/or peer review under responsibility of Asia-Pacific Chemical, Biological & Environmental Engineering Society

**Keywords:** Anthracene adduct; Palladium-catalysed reaction; Phosphine oxide ligand; Suzuki-Miyaura reaction

### 1. Introduction

In recent decades, palladium-catalyzed coupling reactions have proven to be among the most powerful and versatile metal-mediated transformations in organic synthesis chemistry. Due to the excellent performance of these reactions, they have been used extensively, for example, in total synthesis and in the synthesis of conjugated materials and widespread used in many areas of organic chemistry, particularly in the synthesis of pharmaceuticals and compounds for materials chemistry applications [1,2,3]. Ideally, an efficient catalyst should have broad substrate activity under mild conditions at very low catalyst molar ratio. Initially, the substrates which were used in cross-coupling reactions were only reactive aryl bromides and iodides. However, aryl chlorides are more widely available and generally less expensive than the bromides and iodides. So the search for the suitable ligands showing higher reactivity and selectivity has been a field of enormous activity. The scope of this reaction has recently been enhanced by the addition of ligands, such as biphenyl phosphines [4,5,6] and NHC-ligands [7,8,9].

\* Corresponding author. Tel.: +66-45-253400 ext.4570. Fax: +66 45 258379  
 E-mail address: [kitti\\_w\\_2000@yahoo.se](mailto:kitti_w_2000@yahoo.se)

Recently, Doherty and co-workers reported that the phosphine adduct ligand namely, **KITPHOS** shows good properties as a co-catalyst in Suzuki-Miyaura cross-coupling reaction of the bulky and unreactive chlorobenzene with phenyl boronic acid using a catalyst ratio of only 1%mol [10]. However, the synthetic route to the phosphine anthracene adduct derivative ligand is difficult. From the applications point of view, phosphine ligands are affected by one problem: they are subject to oxidation. Therefore, reactions need to be carried out in an inert atmosphere. To overcome this problem, several stable phosphines have been reported [11,12,13,14]. Herein, we report the Pd-catalysed Suzuki-Miyaura cross-coupling reaction of aryl boronic acid and aryl halide with both reactive catalyst Pd(0) and stable Pd(II) complexes using various types of air stable ligand. The effect of cross- and homo coupling products when different ligand types, including our a stable anthracene phosphine oxide adduct, is also included.

## 2. Materials and Methods

All reactions were performed under a nitrogen balloon. Chemical reagents and solvents were purchased from commercial suppliers and used without further purification, unless noted. Methyl-2,3-(9,10-dihydroanthracenyl) propanoate (1) [15], mesityl boronic acid, 9,9-dihexyl-9H-fluoren-2-ylboronic acid [16], Pd(PPh<sub>3</sub>)<sub>4</sub>, PdCl<sub>2</sub>(PPh<sub>3</sub>) [17], 3-bromo-phenanthroline and 3,8-dibromo-phenanthroline [18] were synthesized as reported. Column chromatography was run on silica gel (100-200 mesh). <sup>1</sup>H and <sup>13</sup>C NMR spectra were recorded on a Bruker Avance 300 spectrometer. Chemical shifts are quoted downfield from internal standard TMS. IR spectra were measured on a Perkin-Elmer FT-IR spectroscopy spectrum RXI spectrometer as NaCl or KBr disc. Melting points were measured in open-end capillaries using a Büchi 530 melting point apparatus. The temperatures at the melting points were ramped at 2.5 °C/min and were uncorrected.

**Methyl 2,3-(9,10-dihydroanthracenyl)-2-(diphenylphosphoryl oxide)propanoate (3):** Diisopropylamine (3.90 ml, 27.60 mmole) was transferred by syringe to 100 ml round bottom flask in nitrogen system, followed by THF (40 ml). Subsequently, n-butyllithium (19.2 ml, 23.0 mmole) was slowly added at -78 °C and mixed at 0 °C for 1 hour. Methyl-2,3-(9,10-dihydroanthracenyl)propanoate (5.0 g, 19.1 mmole in THF 20 ml) was added to LDA solution at -78 °C. After the reaction was stirred at 0 °C for 2 hours, chlorodiphenyl phosphine (4.0 ml, 20.45 mmole) was added at -78 °C. The reaction was raised up to room temperature and kept for 6 hours. Then, the solution mixture was extracted with dichloromethane (3 x 50 ml). The organic content was dried with Na<sub>2</sub>SO<sub>4</sub>, then the crude reaction was evaporated to dryness and passed through silica column chromatography (10% EtOAc as the eluent) to obtain the target product; white solid (36% yield); m.p. 206-208 °C; <sup>1</sup>H NMR (CDCl<sub>3</sub>, 300 MHz): δ 2.47 (ddd, J = 21, 15, 3 Hz, 1H), 2.94 (ddd, J = 15, 9, 3 Hz, 1H), 3.10 (s, 3H), 4.31 (s, 1H), 3.56 (d, J = 6 Hz, 1H), 7.03-7.28 (m, 13H), 7.53-7.56 (m, 3H) 7.85-7.91 (m, 2H); <sup>13</sup>C NMR (CDCl<sub>3</sub>, 75 MHz): δ 33.8, 44.0, 49.6, 52.3, 58.1, 58.8, 123.0, 123.6, 124.1, 125.7, 125.8, 126.5, 126.7, 126.9, 127.7, 127.9, 128.1, 128.2, 131.1, 131.7, 131.8, 131.9, 132.0, 138.8, 140.6, 140.7, 143.9, 144.7, 171.7; IR (KBr) 536, 694, 706, 1193, 1217, 1434, 1732, 2946, 2960 cm<sup>-1</sup>; MS (ESI) 465.09 (MH<sup>+</sup>, 100%).

**General method for Suzuki-Miyaura cross-coupling reaction:** aryl boronic acid (2.7 g, 0.02 mol), aryl halide (2.7 g, 0.02 mol) and solvent (20 ml) were placed in a two necked round bottom flask, followed by base and palladium catalyst, respectively. Finally, the reaction was degassed several times with a nitrogen balloon. The reaction mixture was then heated to reflux until the reaction was completed. The mixture was cooled and extracted into dichloromethane (DCM). The organic part was dried with Na<sub>2</sub>SO<sub>4</sub>, then the crude reaction was evaporated to dryness and passed through silica column chromatography to obtain the pure product.

**2-Phenyl pyridine (6):** colorless liquid; <sup>1</sup>H NMR (300 MHz, CDCl<sub>3</sub>) δ 8.70 (s, 1H), 8.00 (d, J = 7.0 Hz, 2H), 7.74 (s, 2H), 7.53-7.58 (m, 4H), 7.24 (d, J = 6.4 Hz, 1H); <sup>13</sup>C NMR (75 MHz, CDCl<sub>3</sub>) δ 157.6, 149.5, 139.4, 136.8, 128.9, 128.7, 126.9, 122.1, 120.5; IR (NaCl) 692, 746, 800, 920, 993, 1020, 1076, 1152, 1292, 1423, 1449, 1465, 1587, 1960, 2358, 2857, 2929, 3064 cm<sup>-1</sup>.

**2-Thioyl pyridine (8):** white solid; m.p. 59-61 °C; <sup>1</sup>H NMR (300 MHz, CDCl<sub>3</sub>) δ 8.57 (d, J = 4.8 Hz,

1H), 7.78–7.63 (m, 3H), 7.59 (d,  $J = 3.5$  Hz, 1H), 7.40 (d,  $J = 5.2$  Hz, 1H), 7.20–7.07 (m, 2H);  $^{13}\text{C}$  NMR (75 MHz,  $\text{CDCl}_3$ )  $\delta$  152.6, 149.5, 136.6, 131.9, 130.8, 128.7, 128.0, 127.5, 124.5, 121.9, 118.78; IR(NaCl) 710, 779, 992, 1155, 1435, 1464, 1580, 3030  $\text{cm}^{-1}$ .

**2,4-Difluorophenyl pyridine (9)**; colourless liquid;  $^1\text{H}$  NMR (300 MHz,  $\text{CDCl}_3$ )  $\delta$  8.70 (d,  $J = 4.8$  Hz, 1H), 7.99 (dd,  $J = 15.7, 8.6$  Hz, 1H), 7.74 (d,  $J = 3.8$  Hz, 2H), 7.24 (dd,  $J = 8.8, 4.5$  Hz, 1H), 7.05–6.96 (m, 1H), 6.91 (t,  $J = 10.0$  Hz, 1H);  $^{13}\text{C}$  NMR (75 MHz,  $\text{CDCl}_3$ )  $\delta$  163.7 (dd,  $J = 253.0, 12.0$  Hz), 160.1 (dd,  $J = 253.0, 12.0$  Hz), 152.6 (d,  $J = 3.0$  Hz), 149.8 (s), 136.4 (s), 132.1 (dd,  $J = 10.0, 4.0$  Hz), 124.2 (d,  $J = 10.0$  Hz), 123.9–123.6 (m), 122.4 (s), 111.8 (dd,  $J = 21.1, 3.7$  Hz), 104.33 (dd,  $J = 27.0, 25.4$  Hz); IR(NaCl) 456, 514, 563, 586, 749, 780, 855, 970, 1107, 1144, 1264, 1502, 1613, 2924, 3070  $\text{cm}^{-1}$ .

**5-(Trifluoromethyl)-2-phenylpyridine (30)**; white solid; m.p. 60–62  $^\circ\text{C}$ ;  $^1\text{H}$  NMR (300 MHz,  $\text{CDCl}_3$ )  $\delta$  8.96 (s, 1H), 8.04 (dd,  $J = 7.6, 1.7$  Hz, 2H), 7.99 (dd,  $J = 8.4, 1.9$  Hz, 1H), 7.85 (d,  $J = 8.3$  Hz, 1H), 7.56–7.47 (m, 3H);  $^{13}\text{C}$  NMR (75 MHz,  $\text{CDCl}_3$ )  $\delta$  160.3 (s), 146.5 (dd,  $J = 13.7, 9.2$  Hz), 137.9 (s), 134.1–133.8 (m), 130.6–129.8 (m), 128.9 (s), 129.3–125.3 (m), 127.2 (s), 124.7, 120.4 (m), 119.9 (s); IR(NaCl) 695, 741, 790, 839, 861, 1012, 1088, 1123, 1335, 1603, 2929, 3100  $\text{cm}^{-1}$ .

**Trimethylphenylbenzene (11)**; colourless liquid;  $^1\text{H}$  NMR (300 MHz,  $\text{CDCl}_3$ )  $\delta$  7.70 (t,  $J = 7.3$  Hz, 2H), 7.61 (t,  $J = 7.3$  Hz, 1H), 7.46 (d,  $J = 7.0$  Hz, 2H), 7.26 (s, 2H), 2.66 (s, 3H), 2.35 (s, 6H);  $^{13}\text{C}$  NMR (75 MHz,  $\text{CDCl}_3$ )  $\delta$  141.2, 139.2, 136.6, 136.0, 129.4, 128.5, 128.2, 126.6, 21.1, 20.8.

**3-(9,9-Dihexyl-9H-fluoren-2-yl)-1,10-phenanthroline (12)**; viscous liquid;  $^1\text{H}$  NMR (300 MHz,  $\text{CDCl}_3$ )  $\delta$  7.72 (d,  $J = 6.9$  Hz, 2H), 7.58 (dd,  $J = 14.6, 7.9$  Hz, 2H), 7.42–7.24 (m, 9H), 6.87–6.77 (m, 2H), 2.04–1.87 (m, 4H), 1.21–0.97 (m, 12H), 0.78 (t,  $J = 6.7$  Hz, 6H), 0.71–0.62 (m, 4H);  $^{13}\text{C}$  NMR (75 MHz,  $\text{CDCl}_3$ )  $\delta$  155.3, 153.0, 150.7, 150.1, 141.1, 141.0, 134.3, 126.9, 126.6, 125.9, 122.8, 122.6, 120.5, 119.6, 118.7, 113.9, 110.1, 55.0, 55.1, 40.5, 40.4, 31.5, 31.4, 29.7, 29.6, 23.7, 23.6, 22.6, 22.5, 13.9; IR(NaCl) 741, 895, 1102, 1376, 1420, 1460, 2369, 2929, 3036  $\text{cm}^{-1}$ .

**3,8-bis(9,9-dihexyl-9H-fluoren-2-yl)-1,10-phenanthroline (13)**;  $^1\text{H}$  NMR ( $\text{CDCl}_3$ , 300 MHz):  $\delta$  0.75–0.81 (m, 20H), 1.00–1.27 (m, 24H), 2.06–2.09 (m, 8H), 7.36–7.42 (m, 5H), 7.71–7.81 (m, 5H), 7.90 (dd,  $J = 9, 6$  Hz, 2H), 7.97 (t,  $J = 6$  Hz, 2H), 8.45–8.50 (m, 3H), 9.23 (d,  $J = 3$  Hz, 1H), 9.52 (d,  $J = 3$  Hz, 1H), 9.54 (d,  $J = 0.5$  Hz, 1H);  $^{13}\text{C}$  NMR ( $\text{CDCl}_3$ , 75 MHz):  $\delta$  14.0, 22.5, 23.8, 29.7, 31.5, 40.3, 55.3, 119.7, 120.0, 120.4, 121.8, 123.0, 125.9, 126.5, 126.9, 127.0, 127.6, 128.2, 128.5, 129.6, 133.3, 136.0, 136.8, 137.5, 140.3, 140.4, 141.5, 141.7, 144.5, 149.7, 150.0, 151.1, 151.3, 152.0; IR(KBr) 941, 741, 1120, 1171, 1335, 1414, 1609, 2856, 2927, 3064, 3210  $\text{cm}^{-1}$ .

### 3. Results and Discussion

The synthesis of an anthracene-phosphine oxide adduct (3) shows in Fig 1. The known methyl acrylate-anthracene adduct [15] was phosphinated by LDA and chlorodiphenyl phosphine. The stable anthracene-phosphine oxide was afforded after separated by column chromatography. The pure product was characterized and confirmed the molecular structure by  $^1\text{H}$  and  $^{13}\text{C}$  and IR spectroscopy as well as molecular mass.

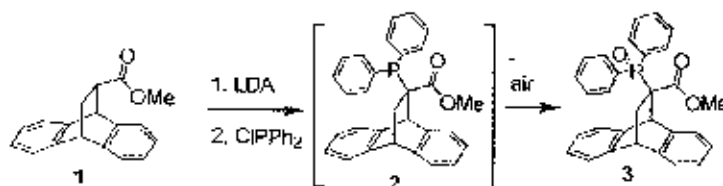


Fig. 1. The synthetic pathway to anthracene phosphine oxide adduct (3).

To determine the optimal reaction conditions, we began with the reaction of phenyl boronic acid (**4**) and 2-chloropyridine (**5**) under the following conditions: 1% mol stable Pd(II) catalyst, 1 M Na<sub>2</sub>CO<sub>3</sub> (aq.), without ligand in refluxing THF (Table 1, entry 1). However, the reaction gave both cross- and homo-coupling products with very low starting material conversion. After that the different type of ligands were added to the reaction utilizing the same protocol as in entry 1 with 10% mol ligands including **3**, PPh<sub>3</sub>, OPPh<sub>3</sub>, Phen, dpff, and dppe. We found that with the addition of the ligand, the efficiency of the Pd(II) catalysed reaction was improved (Table 1, entry 4-9). These results emphasize that the ligand is involved in the cross-coupling Pd(II) catalysed mechanism. It should be noted that the synthesized phosphine oxide adduct ligand **3** gave the best result in our Pd(II) series (Table 3, entry 4). We also studied an unstable Pd(0) complex. As we expected, the conversion proceeded faster than the Pd(II) catalysed reaction. After we added 0.1 eq. of **3** in Pd(0) catalysed process, the reaction gave poor conversion (Table 1, entry 3) unlike the Pd(II) catalysed protocol. With the positive result when using NaOH as base in Pd(II) catalysed reaction reported by Amatore and co-worker[19], we also tried this condition with our reaction (Table 3, entry 8). Unfortunately, a very low conversion was found. Furthermore, when Na<sub>2</sub>CO<sub>3</sub> solid base was used to reduce the reaction step, the low conversion was observed (Table 3, entry 9). This result is less efficient than that in the conventional protocol (entry 4). The 100% conversion of 2-chloropyridine is successfully achieved after the reaction was employed in refluxing 1,4-dioxane. Therefore, we concluded that the optimized condition for cross-coupling reaction is PdCl<sub>2</sub>(PPh<sub>3</sub>)<sub>2</sub> (1 mol%), aryl boronic acid (1 eq.), aryl halide (1 eq.), an aqueous 1 M Na<sub>2</sub>CO<sub>3</sub> (2.5 eq.) in refluxing 1,4-dioxane.

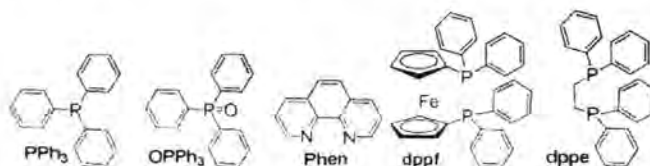
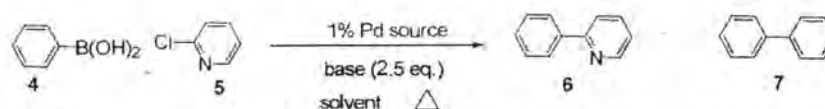
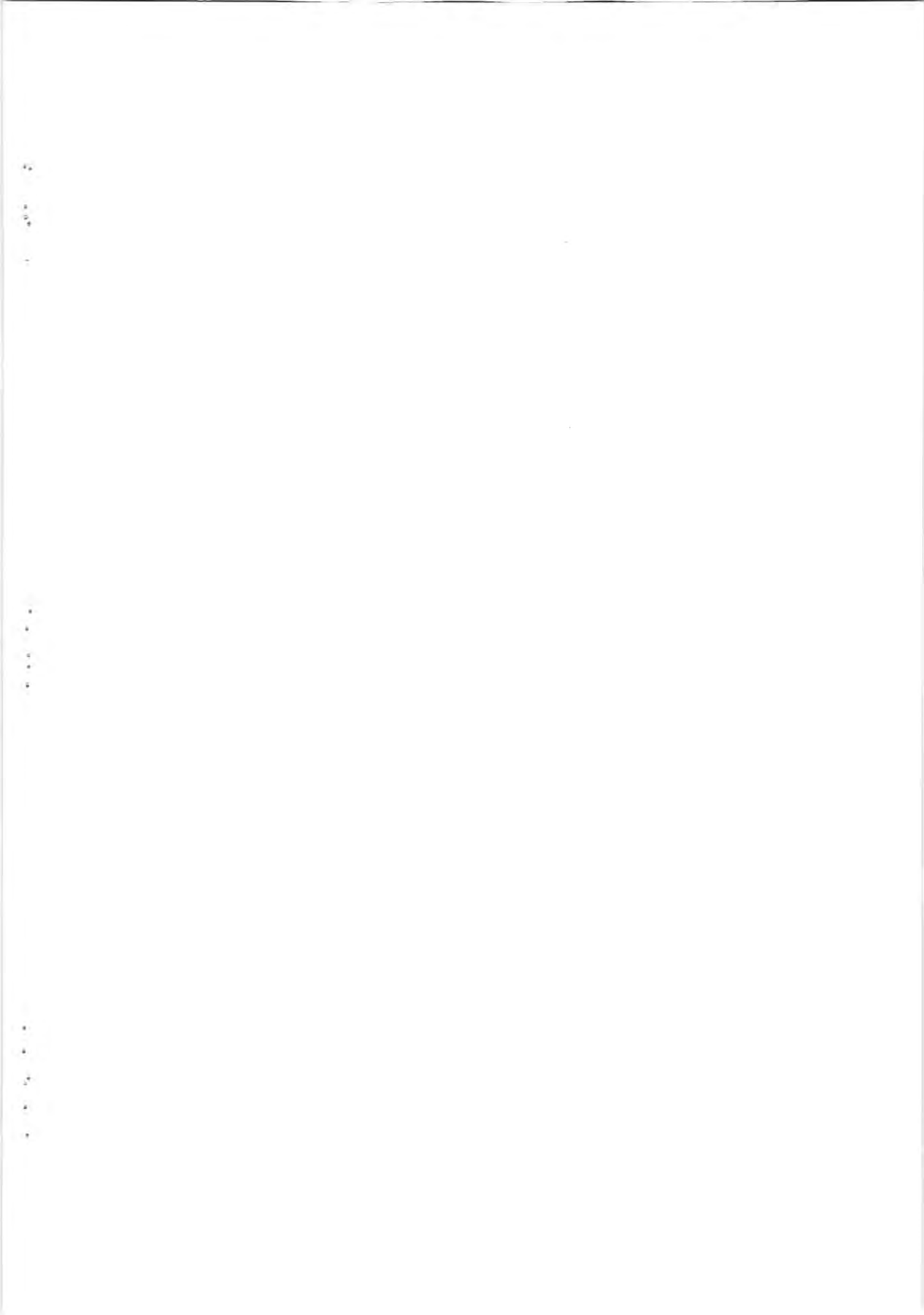


Fig. 2. The molecular structure of ligands using in Pd-catalysed Suzuki-Miyaura cross-coupling reactions

Table 1. Optimization of the Pd-catalysed reaction of phenyl boronic acid and 2-chloropyridine<sup>24</sup>



Entry	Pd source	Base	Solvent	Temp (°C)	Ligand	6/5 <sup>[b]</sup>	6/7 <sup>[b]</sup>
1	PdCl <sub>2</sub> (PPh <sub>3</sub> ) <sub>2</sub>	1 M Na <sub>2</sub> CO <sub>3</sub>	THF	65	-	0.1	1.2
2	Pd(PPh <sub>3</sub> ) <sub>4</sub>	1 M Na <sub>2</sub> CO <sub>3</sub>	THF	65	-	6.9	46.6
3	Pd(PPh <sub>3</sub> ) <sub>4</sub>	1 M Na <sub>2</sub> CO <sub>3</sub>	THF	65	10% <b>3</b>	0.5	12.3
4	PdCl <sub>2</sub> (PPh <sub>3</sub> ) <sub>2</sub>	1 M Na <sub>2</sub> CO <sub>3</sub>	THF	65	10% <b>3</b>	1.7	23.6
5	PdCl <sub>2</sub> (PPh <sub>3</sub> ) <sub>2</sub>	1 M Na <sub>2</sub> CO <sub>3</sub>	THF	65	10% PPh <sub>3</sub>	1.0	19.7
6	PdCl <sub>2</sub> (PPh <sub>3</sub> ) <sub>2</sub>	1 M Na <sub>2</sub> CO <sub>3</sub>	THF	65	10% OPPh <sub>3</sub>	0.04	0.5
7	PdCl <sub>2</sub> (PPh <sub>3</sub> ) <sub>2</sub>	1 M Na <sub>2</sub> CO <sub>3</sub>	THF	65	10% phen	0.04	0.3
8	PdCl <sub>2</sub> (PPh <sub>3</sub> ) <sub>2</sub>	1 M Na <sub>2</sub> CO <sub>3</sub>	THF	65	10% dpff	0.71	175.9
9	PdCl <sub>2</sub> (PPh <sub>3</sub> ) <sub>2</sub>	1 M Na <sub>2</sub> CO <sub>3</sub>	THF	65	10% dppe	0.03	0.15
10	PdCl <sub>2</sub> (PPh <sub>3</sub> ) <sub>2</sub>	1 M NaOH	THF	65	10% <b>3</b>	0.002	0.4

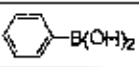
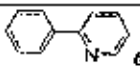
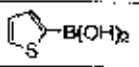
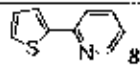
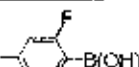
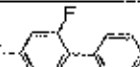
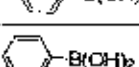
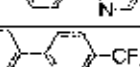
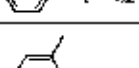
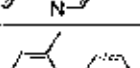
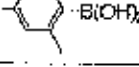
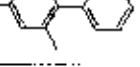
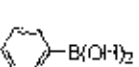
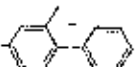
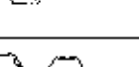
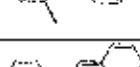


11	PdCl <sub>2</sub> (PPh <sub>3</sub> ) <sub>2</sub>	Na <sub>2</sub> CO <sub>3</sub> (s)	THF	65	10% 3	0.53	5.35
12	PdCl <sub>2</sub> (PPh <sub>3</sub> ) <sub>2</sub>	1 M Na <sub>2</sub> CO <sub>3</sub>	1,4-dioxane	101	10% 3	>1000	54.7

[a] Reaction conditions: Pd source (1 mol%), phenyl boronic acid (3.51 mmol), 3-chloropyridine (3.51 mmol), solvent (20 ml.), base (8.75 mmol); [b] determine by GC and calculated from peak area after 6 hours.

The scope of this reaction was next explored. Both electron-rich (thienyl) and electron poor (2,4-difluorobenzene) boronic acids were transformed into the desired cross-coupling products in moderate yields. This is a good result for the cross-coupling for both unstable boronic acids (Table 2, entries 2-3). Interestingly, the cross-coupling product was obtained in a very good yield from an electron-poor aryl halide (Table 2, entries 4). This could be explained from the oxidative step in Pd catalysed mechanism. Furthermore, a very bulky mesitylboronic acid proved to be an inefficient coupling partner in this reaction (Table 2, entry 5). However, the desired product was synthesized from indolizine methyl benzene and phenyl boronic acid in moderate yield. It is worth mentioning that the cross-coupling reaction works well with a bulky halobenzene moiety (Table 2, entries 6). The less reactive, mono- and dihalo phenanthroline, also proceed in the cross-coupling Suzuki-Miyaura reaction with fluorene boronic acid.

Table 2. Pd(II)-catalysed cross-coupling Suzuki-Miyaura reaction of aryl boronic acid and aryl halide.<sup>[a]</sup>

Entry	Aryl halide	Aryl boronic acid	Product	% Yield <sup>[b]</sup>
1				70
2				60
3				71
4				85
5				45
6				62
7				65
8[a]				54

[a] Reaction conditions: PdCl<sub>2</sub>(PPh<sub>3</sub>)<sub>2</sub> (1 mol), 0.05 mmol, aryl boronic acid (1.71 mmol), aryl halide (3.55 mmol), 1 M Na<sub>2</sub>CO<sub>3</sub> (8.75 mmol) in refluxing 1,4-dioxane (20 ml.) for 4 hours; [b] yield of purified product; [c] aryl boronic acid (1.7 mmol)

#### 4. Conclusion

## A Cheap Synthetic Route to Commercial Ruthenium N3 Dye for Sensitizing Solar Cell Applications

Rukkiat Jitchati<sup>1, a, \*</sup>, Yuranan Thathong<sup>1, b</sup>, and Kittiya Wongkhan<sup>1, c</sup>

<sup>1</sup> Center for Organic Electronic and Alternative Energy (COEA), Department of Chemistry, Faculty of Science, Ubon Ratchathani University, Warinchumrap, Ubon Ratchathani Province, 34190, Thailand

rukkiat\_j@hotmail.com<sup>a</sup>, su\_dkhobfa@hotmail.com<sup>b</sup>, kitt\_w\_2000@yahoo.ie<sup>c</sup>

**Keywords:** dye-sensitized solar cells (DSCs), ruthenium complexes dye, N3, one-pot reaction

**Abstract.** Dye-sensitized solar cells (DSCs) have received widespread attention owing to their low cost, easy fabrication, and relatively high solar-to-electricity conversion efficiency. Based on the TiO<sub>2</sub> electrode, ruthenium complex dye, liquid electrolyte, and Pt counter electrode, DSCs have already exhibited an efficiency above 11% and offer an appealing alternative to conventional solar cells. However, until now the commercial and well known standard dye is the ruthenium complex, namely, *cis*-bis(isothiocyanato)-bis(2,2'-bipyridyl-4,4'-dicarboxylato)ruthenium(II) (N3) which has been widely used around the world. In this article, N3 standard dye was synthesized and characterized by two synthetic routes. Grätzel's protocol and a one-pot reaction from cheap and easily prepared starting materials.

### Introduction

Since the distant past, mankind has used energy from fossil fuel, whereas, the resource reserves in the earth will run out in the future. The increasing energy demands and shortage of fossil fuels have driven people to develop new types of clean and sustainable energy. So, the largest challenge for our global society is to find ways to replace fossil fuels by renewable resources and, at the same time, avoid negative effects from the current energy system on climate, environment, and health. Now, the clean and renewable energy sources are wind, water and sun. However, the area of greatest promise is that of solar converters generally referred to as "photovoltaic cells" (PV) [1]. However a drawback is that, most of PVs used today are inorganic thin-film photovoltaic devices, i.e., CdTe [2] and CuIn(Sb)Se [3], which contain highly toxic and expensive materials. For that reason, the second generation of solar converters called "dye-sensitized solar cells (DSCs)" has been developed [4,5] and proved to be real PV materials in the future [6].

A large number of dyes have been developed; for example, ruthenium complex dyes [7,8], organic dyes [9], porphyrin dyes [10,11] and natural pigment dyes [12]. Among these the most efficient dye materials are the ruthenium complexes which have been developed by Grätzel's group [4]. The efficiency of ruthenium dyes has been improved since 1991. N3 dye showed  $\eta = 7.1-7.9\%$  and then afforded values up to  $\eta = 10\%$  in 1993 [5]. The same group reported the synthetic route to N3 dye from isolated expensive starting material: *cis*-di(chloro)-*N,N'*-bis(2,2'-bipyridyl-4,4'-dicarboxylic acid)-ruthenium(II) dihydrate (3.2H<sub>2</sub>O).

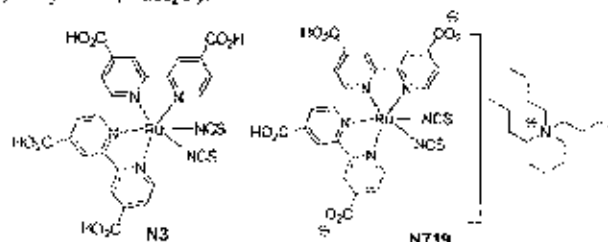


Fig 1. The known structure of N3 and N719

The N3 derivative called N719 has also been developed and has shown more promising efficiency of about 11% [13]. Until now, these two materials have been used as the standard complexes to benchmark other new synthetic dyes in the dye-sensitized solar cell system [7,14].

Herein, we report two synthetic routes: Grätzel's model and one-pot reaction of N3 from cheap materials and easily reproducible methods.

#### Materials and methods

4-Methylpyridin-2-amine, 48% hydrobromic acid, bromine, ammonium thiocyanate and Pd(OAc)<sub>2</sub> were purchased from Acros organic and used without further purification. Anhydrous dimethyl formamide (DMF) was distilled using calcium hydride. RuCl<sub>3</sub>·3H<sub>2</sub>O were purchased from Precious Metals Online PMO Pty Ltd. <sup>1</sup>H and <sup>13</sup>C NMR spectra were recorded on a Bruker Avance 300 spectrometer. Chemical shifts are quoted downfield from internal standard TMS. IR spectra were measured on a Perkin-Elmer FT-IR spectroscopy spectrum RXI spectrometer as KBr disc. Melting points were measured in open-end capillaries using a Büchi 530 melting point apparatus. The temperatures at the melting points were ramped at 2.5 °C/min and were uncorrected.

**2-Bromo-4-methylpyridine (1)** was synthesized as follows. 4-Methylpyridin-2-amine (2.7 g, 0.02 mol) and 48% hydrobromic acid (5 mL, 0.09 mol) were placed in an ice-salt bath with stirring. Then, 4 mL of bromine (0.07 mol) was added dropwise while the temperature was kept at 0 °C followed by aqueous solution of sodium nitrite (4 g in 6 mL). The controlling temperature of the reaction did not rise above 5 °C. After stirring for an additional 30 minutes to complete the reaction, yielding the dark brown solution, 2 mL sodium hydroxide (10 M) was added dropwise to the reaction mixture. The light yellow reaction was extracted by ethyl acetate followed by removal of the solvent. Then, the crude reaction was passed through silica column chromatography using 10% (v/v) ethyl acetate-hexane as the eluent. The product was obtained as the colourless liquid (2.29 g, 53%); <sup>1</sup>H NMR (CDCl<sub>3</sub>, 300 MHz): δ 2.32 (s, 3H), 7.07 (d, J = 6 Hz, 1H), 7.3 (s, 1H), 8.20 (d, J = 3 Hz, 1H); <sup>13</sup>C NMR (CDCl<sub>3</sub>, 75 MHz): δ 20.7, 123.8, 124.9, 128.7, 142.1, 149.6

**4,4'-Dimethyl-2,2'-bipyridine (2)**: The mixture of 3.76 g of 2-bromo-4-methylpyridine (20 mmol), 3.04 g K<sub>2</sub>CO<sub>3</sub> (20 mmol) and Pd(OAc)<sub>2</sub> (0.49 g, 1.8 mmol) was introduced in 30 mL of anhydrous DMF in a two necked round bottom flask. Then, 1 mL portion of anhydrous isopropanol was syringed at once to the reaction flask. The reaction mixture was then heated to reflux under nitrogen atmosphere at 150 °C for 2 days. The reaction mixture was cooled to room temperature and extracted into dichloromethane (DCM). The crude reaction was evaporated to dryness and then passed through silica column chromatography using 5% (v/v) methanol-DCM to get the target product as the white solid (0.89 g, 44%; m.p. 174-176 °C; <sup>1</sup>H NMR (CDCl<sub>3</sub>, 300 MHz): δ 2.43 (s, 3H), 7.13 (d, J = 6 Hz, 1H), 8.22 (s, 1H), 8.53 (d, J = 6 Hz, 1H); <sup>13</sup>C NMR (CDCl<sub>3</sub>, 75 MHz): δ 21.2, 76.6, 77.0, 77.4, 122.0, 124.7, 148.2, 148.9, 156.0; IR (KBr) 2924, 2851, 1591, 1457, 1365, 822, 514 cm<sup>-1</sup>

**2,2'-Bipyridine-4,4'-dicarboxylic acid (1.1)** was synthesized by the following steps. Sodium dichromate (1.35 g, 4.12 mmol) was added into a mixture of 25 mL concentrated sulfuric acid and 4,4'-dimethyl-2,2'-bipyridine (0.40 g, 2.06 mmol) with stirring. After 30 minutes, the reaction mixture was poured into 200 mL of cooled water to form a light yellow precipitate. After filtration and drying, the obtained clear yellow solid was dissolved by 10% sodium hydroxide aqueous solution followed by slow acidification (pH = 2) with 10% aqueous hydrochloric acid. After a second filtration, the crude product was dried under vacuum to afford a white solid (0.50 g, 95%); <sup>1</sup>H NMR (DMSO-d<sub>6</sub>, 300 MHz): δ 7.89 (d, J = 6 Hz, 1H), 8.80 (s, 1H), 8.90 (d, J = 6 Hz, 1H)

#### The synthesis method of N3

*The first method (Grätzel's model)*: RuCl<sub>3</sub>·3H<sub>2</sub>O (63 mg, 0.24 mmol) and 2,2'-bipyridine-4,4'-dicarboxylic acid (1.1) (120 mg, 0.48 mmol) were dissolved in 20 mL anhydrous DMF. The reaction mixture was then heated to reflux under nitrogen gas at 150 °C for 8 hours under

reduced light. The reaction mixture was cooled to room temperature. The solid was filtered to afford a red-black solid washed with mixture solvent (1:4 acetone-ether). After that, the residual solid was further refluxed with 0.10 M aqueous sodium hydroxide (7.50 mL) and ammonium thiocyanate (120 mg, 1.56 mmol) in 20 mL of DMF for 6 hours. The solvent of the cooled reaction mixture was removed by reduced pressure distillation. Then, the residual solid was dissolved with water and some of the impurity was filtered off. The filtrate was slowly added by 0.1 M aqueous nitric acid to pH = 2 to give the red-dark solid. The solid was filtered again to obtain a red-dark solid (N3) as the pure product (24 mg, 25%);  $^1\text{H NMR}$  ( $\text{CD}_3\text{OD}$ , 300 MHz):  $\delta$  7.68 (dd,  $J = 5.9, 1.7$  Hz, 1H), 7.84 (d,  $J = 5.9$  Hz, 1H), 7.98 (s, 1H), 8.35 (dd,  $J = 5.8, 1.7$  Hz, 1H), 8.94 (d,  $J = 1.2$  Hz, 1H), 9.10 (d,  $J = 1.2$  Hz, 1H), 9.62 (d,  $J = 5.8$  Hz, 1H). This  $^1\text{H NMR}$  spectrum is identical with the commercial standard complex.

*The second method (one-pot reaction);*  $\text{RuCl}_3 \cdot 3\text{H}_2\text{O}$  (100 mg, 0.38 mmol) and 2,2'-bipyridine-4,4'-dicarboxylic acid (L1) (190 mg, 0.77 mmol) were dissolved in 20 mL anhydrous DMF. The reaction mixture was then heated to reflux under nitrogen gas at 150 °C under reduced light for 8 hours. The reaction mixture was cooled to room temperature. The 0.10 M aqueous sodium hydroxide (8.3 mL, 0.82 mmol) and ammonium thiocyanate (0.13 g, 1.73 mmol) were added directly to the crude reaction mixture, which was then heated to reflux again for 6 hours as previously described. Then, DMF was removed by reduced pressure distillation to afford a red-dark residue solution, from which the red solid was dissolved with water and acidified by 0.1 M aqueous nitric acid to pH = 2. The precipitate was filtered again to obtain a red-dark solid (N3) (0.14 g, 58%). The  $^1\text{H NMR}$  spectra is identical with the product obtained by Grätzel's method.

## Results and discussions

### The synthesis of 4,4'-dicarboxylic-2,2'-bipyridine

4,4'-Dicarboxylic-2,2'-bipyridine which is the ligand in N3 ruthenium complex was synthesized from commercial cheaply available material, namely, 4-methylpyridin-2-amine with a method adopted from Adams and Miyano [15]. For this step, we found that the Sandmeyer reaction was successfully applied for the synthesis of **1** with the moderate to good yield in an undergraduate organic synthesis laboratory. From the student's product, the catalyzed homo-coupling reaction was applied using stable palladium(II) acetate to give 4,4'-dimethyl-2,2'-bipyridine (**2**) [16]. The last step of the ligand synthesis is to oxidize the dimethyl group on the bipyridine ring by cheap sodium dichromate oxidizing agent to afford the 4,4'-dicarboxylic-2,2'-bipyridine (L1) in quantitative yield, as shown in Figure 2 [17].

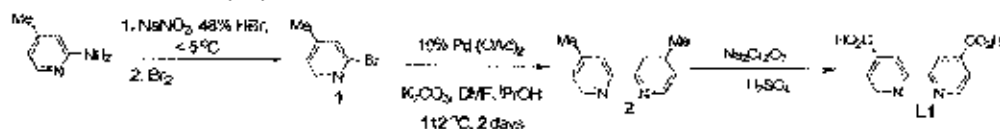


Fig. 2. The synthetic route of 4,4'-dicarboxylic-2,2'-bipyridine (L1)

### The synthesis of N3 ruthenium complex

The N3 ruthenium dye was synthesized from the cheap ruthenium source (ruthenium(III) chloride trihydrate:  $\text{RuCl}_3 \cdot 3\text{H}_2\text{O}$ ) under refluxing DMF conditions, followed by ligand exchange from ammonium thiocyanate to give the N3 dye as the target product, as shown in Figure 3.

For comparison, two approaches were designed; specifically isolated intermediate (**3**) as studied by Grätzel and a one-pot synthesis. Our result clearly suggested that N3 complex can be obtained as the target product from both methods. However, we found that the short and easily method (one-pot reaction) shows the better yield with 58%, whereas the separated intermediate (Grätzel's method) gave only 25% yield, respectively. It is noteworthy that by using Grätzel's protocol, we observed not only **3** but also found N,N'-tris(2,2'-bipyridyl)-4,4'-dicarboxylic acid-ruthenium(II) (**4**) [18] (see Fig. 3) as the intermediate after  $\text{RuCl}_3 \cdot 3\text{H}_2\text{O}$  and L1 were refluxed in DMF.

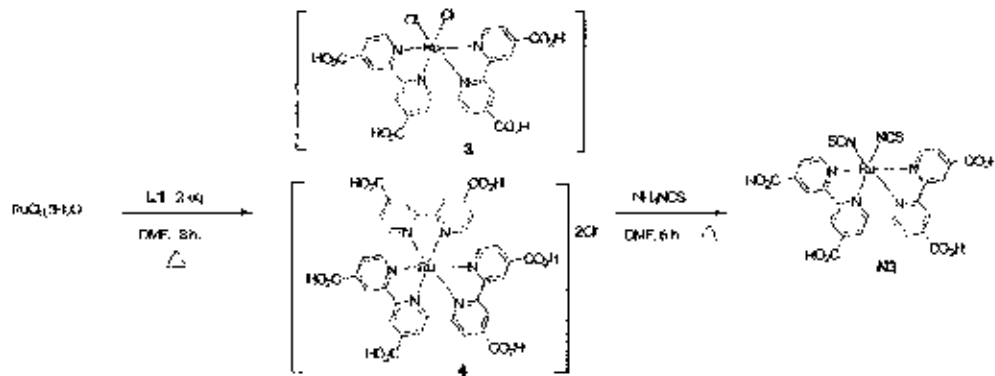


Fig. 3. The synthetic route of N3 ruthenium complex

<sup>1</sup>H NMR 300 MHz in CD<sub>3</sub>OD of synthesized N3 from both methods is shown in Figure 4 and the spectra are identical. These spectra are the same as the reported commercial standard complex spectra. The NMR result reveals that the target product is a symmetric molecule as we see only six protons from the bipyridine ring. Moreover, the <sup>1</sup>H NMR shows a single proton of carboxylic acid (-COOH) at the chemical shift 7.98 ppm.

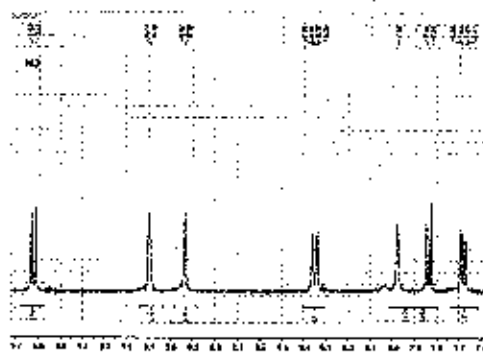
Fig. 4. <sup>1</sup>H NMR 300 MHz of synthesized N3

Table 1. Comparative cost of the two synthetic routes

Chemical names	Grätzel's model cost	One-pot cost
4-Methylpyridin-2-amine (2.7 g)	0.42	0.42
Reagents	~3	~3
Solvents	~7	~5
Catalyst	11.9	11.9
Ruthenium source	2.88	2.88
Total cost (USD)	~25.2	~23.2
N3 (overall yield)	26.9 mg (0.17%)	250.0 mg (1.68%)

All prices were checked from <http://www.sigmaaldrich.com>, (5 September 2011)

To gain insight into the price of the synthesis, the overall practical costs of 2.7 g of starting material; 4-methylpyridin-2-amine for both methods are shown in Table 1. We spent 25.2 and 23.2 USD for synthesized N3 dye which gave the overall yields of 26.9 mg (0.17%) and 250.0 mg (1.68%) for Grätzel's and one-pot reactions, respectively. It is clearly seen that for a similar cost our one-pot protocol gave nearly ten times higher yield than using Grätzel's protocol. It is worth mentioning that N3 can be bought from Sigma-Aldrich with the price of 293.50 USD for 250 mg (not included tax and serviced charge), whereas by using our one-pot procedure only 23.2 USD was spent.

### Conclusion

We have successfully synthesized and characterized the expensive N3 dye from cheap commercial available starting materials with total cost only 23 USD by using two straightforward synthetic routes. Nevertheless, the one-pot reaction route may be more practical due to the higher overall percent yield. Moreover, one reaction of the intermediate compound (2) was synthesized in the undergraduate's laboratory.

### Acknowledgment

The authors would like to acknowledge the financial support from the Research, Development and Engineering (RD&E) Fund through National Nanotechnology Center (NANO-TEC), National Science and Technology Development Agency (NSTDA), Thailand (Project P-10-11346). R.J. thanks to UBU for traveling money for ICKEM 2012.

### References

- [1] K. Zweibel: *Chem. Eng. News* Vol. 64 (1986), p. 34
- [2] Y. Wang, L. Wang and D. H. Waldeck: *J. Phys. Chem. C* Vol. 115 (2011), p. 18136
- [3] W. Liu, D. B. Mitzi, M. Yuan, A. J. Kellock, S. J. Chey and O. Guuawan: *Chem. Mater.* Vol. 22 (2009), p. 1010
- [4] B. O'Regan and M. Grätzel: *Nature* Vol. 353 (1991), p. 737
- [5] M. K. Nazeeeruddin, A. Kay, I. Rodicio, R. Humphry-Baker, E. Mueller, P. Liska, N. Vlachopoulos and M. Grätzel: *J. Am. Chem. Soc.* Vol. 115 (1993), p. 6382
- [6] M. Grätzel: *Acc. Chem. Res.* Vol. 42 (2009), p. 1788
- [7] A. Reynal, A. Forneli and E. Palomares: *Energy Environ. Sci.* Vol. 3 (2010), p. 805
- [8] X. Lv, F. Wang and Y. Li: *ACS Appl. Mater. Interfaces* Vol. 2 (2010), p. 1980
- [9] D. Kuang, S. Uchida, R. Humphry-Baker, Shaik M. Zakeeruddin and M. Grätzel: *Angew. Chem. Int. Ed.* Vol. 47 (2008), p. 1923
- [10] H. Imahori, T. Umeyama and S. Ito: *Acc. Chem. Res.* Vol. 42 (2009), p. 1809
- [11] H.-P. Lu, C.-L. Mai, C.-Y. Tsia, S.-J. Hsu, C.-P. Hsieh, C.-L. Chiu, C.-Y. Yeh and E. W.-G. Diau: *Phys. Chem. Chem. Phys.* Vol. 11 (2009), p. 10270
- [12] G. R. A. Kumara, S. Kaneko, M. Okuya, B. Onwona-Agyeman, A. Kouno and K. Tsumakone: *Sol. Energ. Mat. Sol. Cells* Vol. 90 (2006), p. 1220
- [13] Y. Luo, D. Li and Q. Meng: *Adv. Mater.* Vol. 21 (2009), p. 4647
- [14] Y. Sun, A. C. Onichtu, M. Myahkostupov and F. N. Castellano: *ACS Appl. Mater. Interfaces* Vol. 2 (2010), p. 2039
- [15] R. Adams and S. Miyano: *J. Am. Chem. Soc.* Vol. 76 (1954), p. 3168

## Three Synthetic Routes to a Commercial N3 Dye

R. Jitchati, Y. Thathong, and K. Wongkhan

**Abstract**—We present the synthesis and characterization of a commercial standard ruthenium dye namely, N3, by cheap and easily prepared starting materials from three synthetic routes: the Grätzel's protocol and the other two new methods designed in our laboratory, *i.e.*, the one-pot reaction and *via* the reaction of cymene complex.

**Index Terms**—Dye-sensitized solar cells (DSCs), N3, ruthenium complexes dye.

### I. INTRODUCTION

In the next few years, we will run out the fossil fuel energy so the scientists have tried to find the replace of energy source. Solar energy is one of the most promising future energy which referred as "photovoltaic cells" (PV) [1]. However, the first generation of PV is an inorganic thin-film photovoltaic devices, *i.e.*, CdTe [2] and CuIn(As)Se [3], which contain highly toxic and expensive materials. For that reason, the second generation of solar converters called "dye-sensitized solar cells (DSCs)" has been developed [4], [5]. This solar cell architecture has emerged as a promising candidate for practical photovoltaic applications by virtue of their low manufacturing costs and good conversion efficiencies [1], [2]. Numerous sensitizers have been prepared and their performance has been tested. DSSCs with power conversion efficiencies over 10% under AM 1.5 irradiation were initially demonstrated using prototype *cis*-di(thiocyanato)-*bis*[2,2'-bipyridyl]-4,4'-dicarboxylic acid] ruthenium(II) (N3), its *bis*-tetrabutylammonium (TBA) salt counterpart (N719), or the black dye [tri(thiocyanato)-(4,4',4''-[2,2':6',2''-terpyridine] tricarboxylic acid)ruthenium(II) as a sensitizers in combination with thicker titania films ( $\approx 12$ – $15 \mu\text{m}$ ) and volatile electrolytes [2]. In DSSCs, the sensitizer is one of the critical components because it absorbs sunlight and induces intramolecular charge transfer from the ancillary to the anchoring ligand with subsequent electron injection to the  $\text{TiO}_2$  *via* the carboxylic acid groups. Then, the electron is transported to and collected at an electrode. Subsequent hole transfer from the oxidized dye to  $\text{I}^-/\text{I}_3^-$  takes place, where the

hole is transported to and collected at the counter electrode [1].

Grätzel's group reported the synthetic route to N3 dye from isolated expensive starting material: *cis*-di(chloro)-*N,N'*-bis(2,2'-bipyridyl)-4,4'-dicarboxylic acid-ruthenium(II) dihydrate (3.2H<sub>2</sub>O).

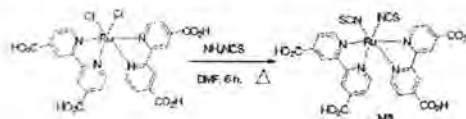


Fig. 1. The N3 synthetic route by Grätzel's group.

The N3 derivative called N719 has also been developed and has shown more promising efficiency of about 11% [6]. Until now, these two materials have been used as the standard complexes to benchmark other new synthetic dyes in the dye-sensitized solar cell system [7], [8].

Herein, we report three synthetic routes of N3: the Grätzel's protocol and two new methods designed from our laboratory, *i.e.*, the one-pot reaction and *via* the reaction of cymene complex where N3 can be synthesized from cheap starting material and easily producible methods.

### II. MATERIALS AND METHODS

2-Chloroisocinnamic acid,  $\alpha$ -phellandrene and  $\text{Pd}(\text{OAc})_2$  were purchased from Acros organic and used without further purification. Anhydrous dimethyl formamide (DMF) was distilled using calcium hydride.  $\text{RuCl}_3 \cdot 3\text{H}_2\text{O}$  were purchased from Precious Metals Online PMO Pty Ltd.  $^1\text{H}$  and  $^{13}\text{C}$  NMR spectra were recorded on a Bruker Avance 300 spectrometer. Chemical shifts are quoted downfield from internal standard TMS. IR spectra were measured on a Perkin-Elmer FT-IR spectroscopy spectrum RXI spectrometer as KBr disc. Melting points were measured in open-end capillaries using a Büchi 530 melting point apparatus. The temperatures at the melting points were ramped at  $2.5 \text{ }^\circ\text{C}/\text{min}$  and were uncorrected.

#### A. Methyl-2-Chloroisocinnate (2)

2-Chloroisocinnamic acid (2.5 g, 0.02 mol), methanol (50 mL) and  $\text{H}_2\text{SO}_4$  (2.5 mL) were placed in 100 mL round bottom flask. The reaction mixture was refluxed for 24 hours. The cooled reaction was extracted with dichloromethane (3–4 times), followed by the removed of organic solvent to afford the target product (2.1632 g, 81%).  $^1\text{H}$  NMR ( $\text{CDCl}_3$ , 300 MHz):  $\delta$  7.96 (s, 3H), 7.75 (d,  $J = 6 \text{ Hz}$ , 1H), 7.77 (d,  $J = 6 \text{ Hz}$ , 1H), 7.87 (s, 1H), 8.52 (d,  $J = 6 \text{ Hz}$ , 1H).  $^{13}\text{C}$  NMR ( $\text{CDCl}_3$ , 75 MHz):  $\delta$  53.0, 121.6, 124.1, 140.2, 150.5, 163.3.

Manuscript received February 20, 2012; revised March 30, 2012. This work was supported in part by the NASDA, Thailand under Grant P-10-11346.

R. Jitchati is with the Center for Organic Electronic and Alternative Energy (COEA), Department of Chemistry, Faculty of Science, Ubon Ratchathani University, Wana Chantrap, Ubon Ratchathani Province, 34190, Thailand (e-mail: rukkiat\_j@hotmail.com).

Y. Thathong and K. Wongkhan are with the Center for Organic Electronic and Alternative Energy (COEA), Department of Chemistry, Faculty of Science, Ubon Ratchathani University, Wana Chantrap, Ubon Ratchathani Province, 34190, Thailand (e-mail: su\_khobfa@hotmail.com and kitt\_w\_2000@yahoo.co.th respectively).

**B. Methyl 2-(4-(Methoxy Carbonyl)Pyridine-2-yl) Isonicotinate (3)**

The mixture of methyl-2-chloroisonicotinate (**2**) (0.5076 g, 3 mmol),  $K_2CO_3$  (3.04 g, 20 mmol) and  $Pd(OAc)_2$  (0.07 g, 0.3 mmol) was introduced in 15 mL of anhydrous DMF in a two necked round bottom flask. Then, 0.47 mL portion of anhydrous isopropanol was syringed at once to the reaction flask. The reaction mixture was then heated to reflux under nitrogen atmosphere at 150 °C for 2 days. After the reaction mixture was cooled to room temperature, the content was extracted into dichloromethane (DCM). The crude reaction was evaporated to dryness and finally passed through silica column chromatography using 5% (v/v) methanol/DCM to get the target product as a white solid (0.037 g, 9%), m.p. 130-135 °C;  $^1H$  NMR ( $CDCl_3$ , 300 MHz):  $\delta$  4.00 (s, 3H), 7.91 (dd,  $J = 5.0, 1.6$  Hz, 1H), 8.87 (dd,  $J = 5.0, 0.9$  Hz, 1H), 8.97 (dd,  $J = 1.6, 0.9$  Hz, 1H);  $^{13}C$  NMR ( $CDCl_3$ , 75 MHz):  $\delta$  68.2, 120.6, 128.8, 130.8, 138.7, 150.1, 165.6

**C. 2,2'-Bipyridine-4,4'-Dicarboxylic Acid (4)**

The 0.3 M sodium hydroxide (10 mL, 2.55 mmol) was added into methyl 2-(4-(methoxy carbonyl)pyridine-2-yl)isonicotinate (**3**) (0.28 g, 1.02 mmol) and methanol 25 mL with stirring. After the reaction was refluxed for 3 hours, the reaction mixture was poured into 50 mL of cooled water and slowly acidified to pH 2 with 10% aqueous hydrochloric acid. After filtration, the crude product was dried under vacuum to afford a white solid (0.25 g, 100%).  $^1H$  NMR ( $DMSO-d_6$ , 300 MHz):  $\delta$  7.89 (d,  $J = 6$  Hz, 1H), 8.80 (s, 1H), 8.90 (d,  $J = 6$  Hz, 1H)

**D. The Synthesis of Ruthenium Cymene Complex (6)**

$RuCl_3 \cdot 3H_2O$  (0.12 g, 0.45 mmol) was added to 50 mL two necked round bottom flask with stirring in ethanol (10 mL) under nitrogen balloon. After  $\alpha$ -phellandrene (0.70 mL, 4.30 mmol) was introduced, the reaction mixture was refluxed for 4 hours. The red precipitate in red solution was observed. The solvent was then removed under vacuum followed by filtration to obtain the red product (0.07 g, 25%), mp: 190 °C (decomposed);  $^1H$  NMR ( $CDCl_3$ , 300 MHz):  $\delta$  1.29 (d,  $J = 6$  Hz, 6H), 2.71 (s, 3H), 2.93 (q,  $J = 6$  Hz, 1H), 5.35 (d,  $J = 6$  Hz, 2H), 5.49 (d,  $J = 6$  Hz, 2H);  $^{13}C$  NMR ( $CDCl_3$ , 75 MHz):  $\delta$  18.9, 22.1, 30.6, 80.5, 81.3, 96.7, 101.2; IR (KBr) 878, 1387, 1471, 2364, 2873, 2957, 3053  $cm^{-1}$

**E. The Synthesis Method of N3**

**1) The First Method (Grätzel's Model)**

$RuCl_3 \cdot 3H_2O$  (63 mg, 0.24 mmol) and 2,2'-bipyridine-4,4'-dicarboxylic acid (**4**) (120 mg, 0.48 mmol) were dissolved in 20 mL anhydrous DMF. The reaction mixture was then heated to reflux under nitrogen gas at 150 °C for 8 hours under reduced light. The reaction mixture was cooled to room temperature. The solid was filtered to afford a red-black solid and then washed with the mixture solvent (1:4 acetone:ether). After that, the residual solid was further refluxed with 0.10 M aqueous sodium hydroxide (7.50 mL) and ammonium thiocyanate (120 mg, 1.56 mmol) in 20 mL of DMF for 6 hours. The solvent of the

cooled reaction mixture was removed by reduced pressure distillation. Then, the residual solid was dissolved with water and some of the impurity was filtered off. The filtrate was slowly added by 0.10 M aqueous nitric acid to pH 2 to give the red-dark solid. The solid was filtered again to obtain a red-dark solid (N3) as the pure product (24 mg, 25%).  $^1H$  NMR ( $CD_3OD$ , 300 MHz):  $\delta$  7.68 (dd,  $J = 5.9, 1.7$  Hz, 1H), 7.84 (d,  $J = 5.9$  Hz, 1H), 7.98 (s, 1H), 8.35 (dd,  $J = 5.8, 1.7$  Hz, 1H), 8.94 (d,  $J = 1.2$  Hz, 1H), 9.10 (d,  $J = 1.2$  Hz, 1H), 9.62 (d,  $J = 5.8$  Hz, 1H). This  $^1H$  NMR spectrum is identical with the commercial standard complex.

**2) The Second Method (the One-Pot Reaction)**

$RuCl_3 \cdot 3H_2O$  (100 mg, 0.38 mmol) and 2,2'-bipyridine-4,4'-dicarboxylic acid (**4**) (190 mg, 0.77 mmol) were dissolved in 20 mL anhydrous DMF. The reaction mixture was then heated to reflux under nitrogen atmosphere at 150 °C under reduced light for 8 hours. The reaction was cooled to room temperature. The 0.10 M aqueous sodium hydroxide (8.3 mL, 0.82 mmol) and ammonium thiocyanate (0.13 g, 1.73 mmol) were added directly to the crude reaction mixture, which was then heated to reflux again for 6 hours as previously described. Then, DMF was removed by reduced pressure distillation to afford a red-dark residue solution, from which the red solid was dissolved with water and acidified by 0.10 M aqueous nitric acid to pH 2. The precipitate was filtered again to obtain a red-dark solid product (N3) (0.14 g, 58%). The  $^1H$  NMR spectra is identical with the product obtained by Grätzel's method.

**3) The Third Method (via the Cymene Complex Reaction)**

Diruthenium(III) (**6**) (200 mg, 0.34 mmol), 2,2'-Bipyridine-4,4'-dicarboxylic acid (**4**) (165 mg, 0.68 mmol) was dissolved by 30 mL to 100 mL of DMF in two necked round bottom flask. The reaction mixture was stirred for 4 hours in the dark and heated to 160 °C under nitrogen balloon. Finally, an excess of  $NH_4SCN$  (206 mg) was added at 130 °C for 5 hour. The solvent was evaporated in a vacuum then water was added to get the insoluble dark red solid which was collected on the sintered glass crucible by suction filtration. The dark red solid product was obtained after purified by column chromatography (sephadex, MeOH) (40 mg, 17%). The  $^1H$  NMR spectra is identical with the product obtained by Grätzel's method.

III. RESULTS AND DISCUSSIONS

**A. The Synthesis of 4,4'-Dicarboxylic-2,2'-Bipyridine (4)**

4,4'-Dicarboxylic-2,2'-bipyridine (**4**) can be synthesized from commercially available compound **1**. With esterification reaction of compound **1**, the compound **2** was obtained in high yield. Then the Pd-catalyzed homo-coupling reaction of compound **2** was applied to yield compound **3**. Finally, compound **3** was then hydrolyzed in base to the target ligand **4** in quantitative yield, as shown in Fig 1.

**B. The Synthesis of N3 Ruthenium Complex**

N3 dye can be synthesized from the cheap ruthenium source, i.e., ruthenium(III) chloride trihydrate and 2

equivalents of 4,4'-dicarboxylic-2,2'-bipyridine (4). The synthesis of N3 dye can be established via 3 pathways. The first method called Grätzel's model; the second, one-pot reaction and the final reaction was called "by cyano complex".



Fig. 1. The synthetic route of 4,4'-dicarboxylic-2,2'-bipyridine (4).

The synthesis of N3 via the Grätzel's model was the reaction between ruthenium(III)chloride trihydrate and compound 4 in the refluxing DMF for 8 hours. By using this method, the intermediate content was isolated and followed by the ligand NH<sub>4</sub>SCN exchange as shown in Fig. 2. After the reaction was finished, 25% of N3 final product was obtained. The product was fully characterized by NMR spectroscopy.

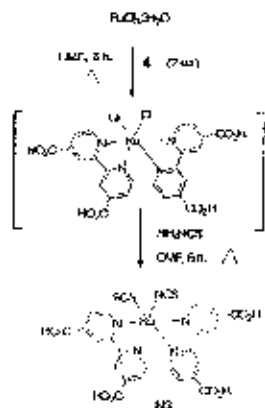


Fig. 2. The synthetic route of N3 via Grätzel's method.

The second protocol, the new one-pot reaction designed by our group was applied for the synthesis of N3. The protocol started with the reaction between ruthenium(III)chloride trihydrate and compound 4 under DMF refluxing shown in Fig. 3. This reaction step was the same as that in the Grätzel's model. However, after the content was refluxed, the reaction mixture was followed by the addition of NH<sub>4</sub>SCN for ligand exchange without any isolation. Then the intermediate reaction was continually refluxed in DMF for 6 hours. After the reaction was completed, the final pure product N3, confirmed by <sup>1</sup>H and <sup>13</sup>C NMR, was isolated in 58% yield via the simple filtration. As described, this one-pot reaction procedure not only short and easily for N3 preparation but also give a better yield (58%).

The last N3 synthetic route was created via ruthenium cyano precursor 6 synthesized by refluxing ruthenium chloride and n-phenanthroline (5). The synthesis of cyano 6 is

shown in Fig. 4. After the intermediate cyano 6 was separated, 2 equivalents of dicarboxylic pyridine ligand 4 was added and refluxed in DMF for 4 hours. Then, without any isolation, the excess of NH<sub>4</sub>NCS was added for ligand exchange. The reaction was continually refluxed for 5 hours. The final product N3 dye was obtained in 17% yield from column chromatography.

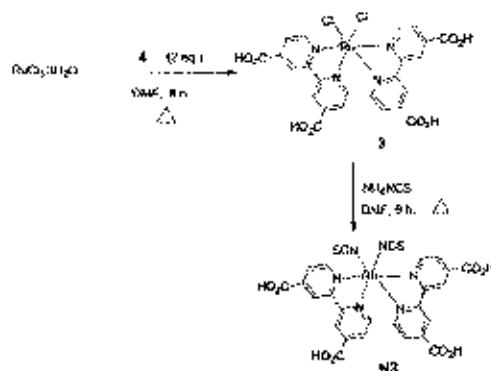


Fig. 3. The synthetic route of N3 via the one-pot reaction.

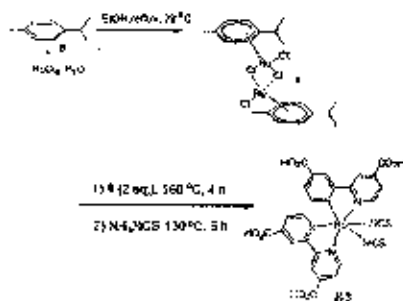


Fig. 4. The synthetic route of N3 via ruthenium cyano

#### IV. CONCLUSION

The N3 dye was successfully synthesized via three different pathways, i.e., the Grätzel's protocol, the one-pot reaction and via the reaction of cyano complex. Both one-pot reaction and the reaction via the cyano complex were developed in our laboratory. The highest yield N3 final product was obtained from the one-pot reaction.

#### ACKNOWLEDGMENT

Financial support from the Research, Development and Engineering (RD&E) Fund through National Nanotechnology Center (NANOTEC), National Science and Technology Development Agency (NSTDA), Thailand (Project P-10-21346).

#### REFERENCES

- [1] K. Zareba, "Photoactive Cells," *Chem. Eng. News*, pp. 34-48, 1986.
- [2] T. Wang, J. Weng and D. H. Waldeck, "Electrochemically Guided Photoactive Devices: A Protocent Study of the Charge Transfer

- Directionality between CdTe and CdSe Nanoparticles," *J. Phys. Chem. C*, pp. 18536-18541, 2011.
- [3] W. Liu, D. B. Mitzi, M. Yuan, A. J. Kellock, S. J. Chey, and G. Grumwiler, "1.2% Efficiency CuInS<sub>2</sub>/Si Photovoltaic Device Prepared Using a Hydrazine Solution Process," *Chem. Mater.*, pp. 1010-1014, 2009.
- [4] B. Oregan and M. Grätzel, "A low-cost, high-efficiency solar cell based on dye-sensitized colloidal TiO<sub>2</sub> films," *Nature*, pp. 737-740, 1991.
- [5] M. K. Nazareddin, A. Kay, I. Rogoju, R. Humphry-Baker, E. Mueller, P. Liska, N. Vlachopoulos, and M. Grätzel, "Conversion of light to electricity by cis-[Cr(big2-2'-bipyridyl)-4,4'-dicarboxylate] ruthenium(II) charge-transfer sensitizers (Cr = Cl, Br, I, CN, and SCN) on nanocrystalline titanium dioxide electrodes," *J. Am. Chem. Soc.*, pp. 6382-6390, 1996.
- [6] Y. Luo, D. Usuki, and Q. Meng, "Towards Optimization of Materials for Dye-Sensitized Solar Cells," *Adv. Mater.*, pp. 4647-4651, 2009.
- [7] A. Reynal, A. Fournil, and E. Palomares, "Dye structure-charge transfer process relationship in efficient ruthenium-dye based dye sensitized solar cells," *Energy Environ. Sci.*, pp. 805-812, 2010.
- [8] Y. Sun, A. C. Uchida, M. Mydlinski, and P. N. Gammel, "Viable Alternative to N719 for Dye-sensitized Solar Cells," *ACS Appl Mater Interfaces*, pp. 2039-2045, 2010.
- [9] K. Y. Jho, C. L. Bai, S. H. Chang, J. G. Chen, K. C. Ho, and K. P. Lin, "Synthesis and characterization of cross-linkable ruthenium complex dye and its application on dye-sensitized solar cells," *J. Polym. Sci., Part A: Polym. Chem.*, pp. 366-372, 2010.
- [10] O. Schwarz, D. Van Leyn, S. Jekusch, N. J. Turro, and H. Bässler, "Preparation and application of new ruthenium(II) polypyridyl complexes as sensitizers for nanocrystalline TiO<sub>2</sub>," *J. Photochem. Photobiol. A: Chem.*, pp. 91-98, 2000.



R. Jitchati (born 1957, Thailand) was appointed as a lecturer in Ubon Ratchasitani University in mid 1999. He received his B. Sc. (Chemistry) from Ubon Ratchasitani University (URU), M. Sc. (Organic chemistry) from Mahidul University, Thailand and Ph. D. (Chemistry) from Deleton University (UK) under the supervision of Prof. Dr. Martin R. Bryce. Currently, he is a lecturer at Chemistry Department of URU. His specific research interests are on the synthesis and the characterization of organometallic materials for organic-light emitting diodes (OLEDs) and dye sensitized solar cells (DSCs).



K. Wongsathan (born 1977, Thailand) has been working as a lecturer in Ubon Ratchasitani University since 1999. She received her B.Sc. (Chemistry) from Ubon Ratchasitani University, following a Master in Mahidul University and Ph.D. under the guidance of Prof. Dr. Todd E. Marder, studying the synthesis and the applications of palladium complexes, at Durham University, UK. She is currently a lecturer in Ubon Ratchasitani University. Her research is oriented toward the natural interface between organic, inorganic and physical chemistry. Key areas involve transition metal chemistry and the synthesis and application of palladium complexes with new types of ligand.



V. Thaitong was born in Amnatchaburi province, Thailand. She obtained her B.Sc. (Chemistry) from Ubon Ratchasitani University where she first studied organometallic under the guidance of Dr. R. Jitchati. She is currently doing her M.Sc. (chemistry) in the synthesis and characterization of organometallic materials for organic-light emitting diodes (OLEDs) and dye sensitized solar cells (DSCs).

## Two Ruthenium Complexes with Phenanthroline Ligand for Dye-Sensitized Solar Cells

Yuranan Thathong,<sup>1, a</sup> Kittiya Wongkhan<sup>1, b</sup> and Rukkiat Jitchati<sup>1, c</sup>

<sup>1</sup> Center for Organic Electronic and Alternative Energy (COEA), Department of Chemistry, Faculty of Science, Ubon Ratchathani University, Warinchumrap, Ubon Ratchathani Province, 34190, Thailand

su\_dkhobfa@hotmail.com,<sup>a</sup> kitt\_w\_2000@yahoo.ie,<sup>b</sup> rukkiat\_j@hotmail.com<sup>c</sup>

**Keywords:** dye-sensitized solar cells (DSCs), ruthenium complexes dya, phenanthroline

**Abstract.** We report the synthetic route of two ruthenium dye-sensitizers: namely, Ru (4,4'-dicarboxylic-2,2'-bipyridine) (1,10-phenanthroline) (NCS)<sub>2</sub> (6) and Ru (4,4'-dicarboxylic-2,2'-bipyridine) (1,10-phenanthroline-5-carboxylic acid) (NCS)<sub>2</sub> (7), which both complexes were characterized by <sup>1</sup>H NMR, <sup>13</sup>C NMR and UV-Vis spectroscopic techniques.

### Introduction

Dye-sensitized solar cells (DSCs) are attracting widespread interest for the conversion of sunlight into electricity because of their low cost and high efficiency [1]. In these cells, the sensitizer is one of the key components harvesting the solar radiation and converting it to electric current [2,3]. Over the last 17 years, ruthenium complexes endowed with thiocyanate ligands have maintained a clear lead in performance. Among these, the most efficient dye materials are the ruthenium complexes which have been developed by Grätzel's group. The efficiency of ruthenium dyes has been improved since 1991. The N3 dye showed  $\eta = 7.1-7.9\%$  and then afforded values up to  $\eta = 10\%$  in 1993 [4]. The N3 derivative called N719 has also been developed and has shown more promising efficiency of about 11% [5]. Until now, these two materials have been used as the standard complexes to benchmark other new synthetic dyes in the dye-sensitized solar cell system [6,7].

A new development for dyes applied to a ruthenium solar cell comes from the preparation of an amphiphilic heteroleptic N3-equivalent, coded Z907 in which the hydrophobic long chains interact laterally to form an aliphatic network to impede triiodide ions reaching the TiO<sub>2</sub> surface to give the power conversion efficiency more than 11% [8]. Recently, Nonomura and co-workers synthesized the ruthenium complex, coded YX360, which is incorporate a thiocyanate ligand in the molecule give the extended  $\pi$ -conjugation unit to the ruthenium complex. Correspondingly, the incident photon-to-current conversion efficiency (IPCE) spectra of solar cells show relatively higher values in the plateau region and a wider absorption spectrum [9].

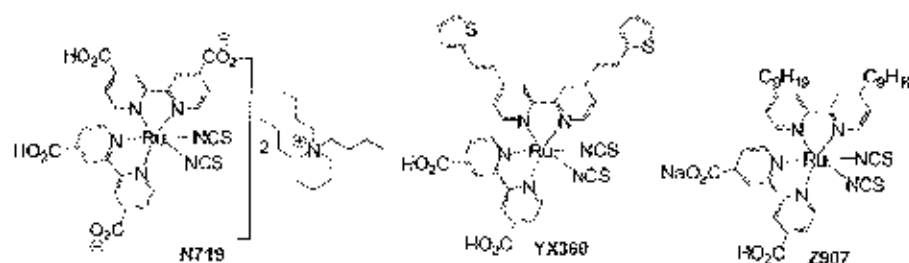


Fig 1. The structure of the highly efficient ruthenium sensitizer N719, Z907 and YX360 dyes

Herein, we report the synthesis of phenanthroline and bipyridine ligand where all starting materials and both complexes were characterized by <sup>1</sup>H and <sup>13</sup>C NMR.

**Materials and methods**

4,4'-Dicarboxylic-2,2'-bipyridine (**8**) and ruthenium cymene complex (**5**) were synthesized as reported [10,11]. Anhydrous dimethyl formamide (DMF) was distilled using calcium hydride before used.  $^1\text{H}$  and  $^{13}\text{C}$  NMR spectra were recorded on a Bruker Avance 300 spectrometer. Chemical shifts are quoted downfield from internal standard TMS. IR spectra were measured on a Perkin-Elmer FT-IR spectroscopy spectrum RX1 spectrometer as KBr disc. Melting points were measured in open-end capillaries using a Büchi 530 melting point apparatus. The temperatures at the melting points were ramped at 2.5 °C/min and were uncorrected.

**1,10-Phenanthroline-5,6-epoxide (2)**: Bleaching solution (Clorox) (140 mL, 110 mmol) and distilled water (70 mL) were mixed in 250 mL Erlenmeyer flask. Hydrochloric acid (conc) was added until the pH of 8–9 was achieved, followed by  $\text{Bu}_2\text{NH}_2\text{SO}_4$  (0.41 g, 1.20 mmol), 1,10-phenanthroline (1.03 g, 5.50 mmol) and  $\text{CHCl}_3$  (60 mL), respectively. The reaction mixture was stirred at room temperature for 17 hours and monitored the reaction by TLC (10% v/v MeOH:DCM; 1,10-phenanthroline-5,6-epoxide (**2**),  $R_f = 0.33$ ). The completed reaction was extracted with  $\text{CHCl}_3$  (10 mL $\times$ 3), dried with  $\text{Na}_2\text{SO}_4$  and then removed solvent under vacuum to afford a white solid 1,10-phenanthroline-5,6-epoxide (**2**) (1.04 g, 93%), mp: 150 °C;  $^1\text{H}$  NMR ( $\text{CDCl}_3$ , 300 MHz):  $\delta$  4.63 (s, 1H), 7.42 (dd,  $J = 6$  Hz,  $J = 9$  Hz, 1H), 8.02 (d,  $J = 6$  Hz, 1H), 8.92 (d,  $J = 6$  Hz, 1H);  $^{13}\text{C}$  NMR ( $\text{CDCl}_3$ , 75 MHz):  $\delta$  55.3, 123.7, 129.1, 138.2, 150.8, 151.6; IR (KBr) 755, 1046, 1429, 1563, 3058  $\text{cm}^{-1}$ .

**5-Cyano-1,10-phenanthroline (3)**: 1,10-Phenanthroline-5,6-epoxide (**2**) (0.50 g, 2.57 mmol), 0.3 M KCN (52 mL, 15.50 mmol) and distilled water (50 mL) were mixed in 250 mL round bottom flask. The reaction mixture was stirred at room temperature for 4 hours to afford a white precipitate, followed by filtration and washed with large amount of distilled water to get 5-cyano-1,10-phenanthroline (**3**) (0.15 g, 29%), mp: 160 °C (decomposed);  $^1\text{H}$  NMR ( $\text{CDCl}_3$ , 300 MHz):  $\delta$  7.74–7.84 (m, 2H), 8.34 (d,  $J = 6$  Hz, 2H), 8.64 (d,  $J = 6$  Hz, 1H), 9.30 (d,  $J = 6$  Hz, 2H);  $^{13}\text{C}$  NMR ( $\text{CDCl}_3$ , 75 MHz):  $\delta$  109.5, 116.3, 124.1, 124.3, 126.3, 126.8, 133.8, 134.9, 136.8, 145.7, 147.4, 151.8, 153.2; IR (KBr) 741, 1504, 1586, 2218, 3053  $\text{cm}^{-1}$ .

**1,10-Phenanthroline-5-carboxylic acid (4)**: 5-Cyano-1,10-phenanthroline (**3**) (0.63 g, 3.07 mmol) was added to 50 mL round bottom flask with stirring in 6 M NaOH (1.5 mL, 9.21 mmol). The reaction mixture was refluxed overnight. After that the reaction mixture was cooled to room temperature and extracted with DCM (10 mL $\times$ 3). The 6 M HCl was added to the collected aqueous until pH  $\approx$  5 and water was removed by rotary evaporator to give brown solid. After recrystallization, filtration and washed with hot water afforded a white solid (0.35g, 50%);  $^1\text{H}$  NMR (300 MHz, DMSO- $d_6$ ):  $\delta$  10.67 (s, 1H), 9.41 (d,  $J = 3.7$  Hz, 2H), 9.15 (d,  $J = 1.4$  Hz, 1H), 8.97 (d,  $J = 10.4$  Hz, 1H), 8.56 (dd,  $J = 5.6$ , 3.3 Hz, 2H), 8.30–8.12 (m, 3H), 7.93–7.79 (m, 2H); IR (KBr) 800, 965, 1076, 1633, 2935, 3422  $\text{cm}^{-1}$ .

**Ru(4,4'-dicarboxylic-2,2'-bipyridine)(1,10-phenanthroline)(NCS) $_2$  (6)**: ruthenium cymene complex (**5**) (200 mg, 0.32 mmol), phenanthroline (110 mg, 0.65 mmol) were dissolved by DMF (30 mL) in two necked round bottom flask. The reaction mixture was stirred for 4 hour in the dark at 80 °C under nitrogen balloon, followed by 4,4'-dicarboxylic-2,2'-bipyridine (150 mg, 0.65 mmol) at 160 °C for 4 hour and excess of  $\text{NH}_4\text{SCN}$  (190 mg) at 130 °C for 5 hour, respectively. The solvent was evaporated in a vacuum then water was added to get the insoluble dark red solid which was collected on the sintered glass crucible by suction filtration. The dark red solid product was obtained after purified by column chromatography (Sephadex LH-20, MeOH) (46 mg, 21%);  $^1\text{H}$  NMR (300 MHz, DMSO- $d_6$ ):  $\delta$  9.55 (d,  $J = 5.3$  Hz, 1H), 9.15 (s, 1H), 8.96 (s, 1H), 8.90 (d,  $J = 7.7$  Hz, 1H), 8.53 (d,  $J = 8.3$  Hz, 1H), 8.35 (d,  $J = 8.0$  Hz, 1H), 8.27 (dd,  $J = 21.3$ , 9.6 Hz, 2H), 7.91 (d,  $J = 5.2$  Hz, 1H), 7.69 (d,  $J = 5.9$  Hz, 1H), 7.62–7.55 (m, 1H), 7.46 (d,  $J = 5.9$  Hz, 1H).  $^{13}\text{C}$  NMR (75 MHz, DMSO- $d_6$ ):  $\delta$  182.3, 177.1, 165.8, 165.3, 159.6, 158.3, 153.4, 148.8, 147.6, 138.4, 137.5, 136.6, 135.9, 134.8, 134.3, 130.5, 130.2, 128.0, 126.5, 125.6, 123.0.

**Ru(4,4'-dicarboxylic-2,2'-bipyridine)(1,10-phenanthroline-5-carboxylic acid)(NCS)<sub>2</sub> (7):** This complex was prepared by using a similar procedure as described for complex 6. Diruthenium(III) (5) (200 mg, 0.32 mmol), phenanthroline carboxylic acid (140 mg, 0.65 mmol), 4,4'-dicarboxylic-2,2'-bipyridine (150 mg, 0.65 mmol) and NH<sub>4</sub>SCN (190 mg) to give the dark red solid product (30 mg, 13%); <sup>1</sup>H NMR (300 MHz, DMSO-d<sub>6</sub>): δ 9.55 (d, *J* = 5.3 Hz, 1H), 9.15 (s, 1H), 8.96 (s, 1H), 8.90 (d, *J* = 7.7 Hz, 1H), 8.53 (d, *J* = 8.3 Hz, 1H), 8.35 (d, *J* = 8.0 Hz, 1H), 8.27 (dd, *J* = 21.3, 9.6 Hz, 2H), 7.91 (d, *J* = 5.2 Hz, 1H), 7.69 (d, *J* = 5.9 Hz, 1H), 7.62-7.55 (m, 1H), 7.46 (d, *J* = 5.9 Hz, 1H)

### Results and Discussions

#### The synthesis of 1,10-phenanthroline-5-carboxylic acid (4)

1,10-phenanthroline (1) was used as a cheap starting material which was oxidized to give the epoxide product (2) in quantitatively yield. The following steps are the cyanation and base-hydrolysis reaction to provide the target ligand 4, shown in Fig. 2.

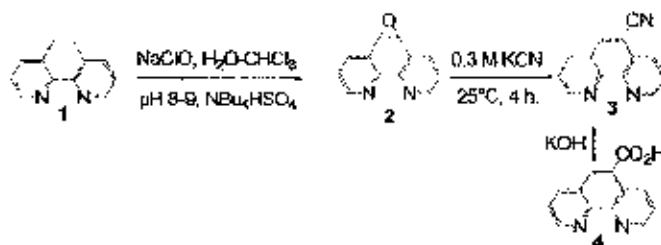


Fig. 2. The synthetic route of 1,10-phenanthroline-5-carboxylic acid (4)

#### The synthesis of ruthenium complexes

Two ruthenium complexes were synthesized by one-pot reaction with phenanthroline and ruthenium cymene complex, followed by bipyridine ligand (8) exchange to give our target product 6 and 7 in 21% and 13% yield, respectively, as shown in Figure 3. Both complexes were fully characterized by <sup>1</sup>H NMR and <sup>13</sup>C NMR in DMSO-d<sub>6</sub>.

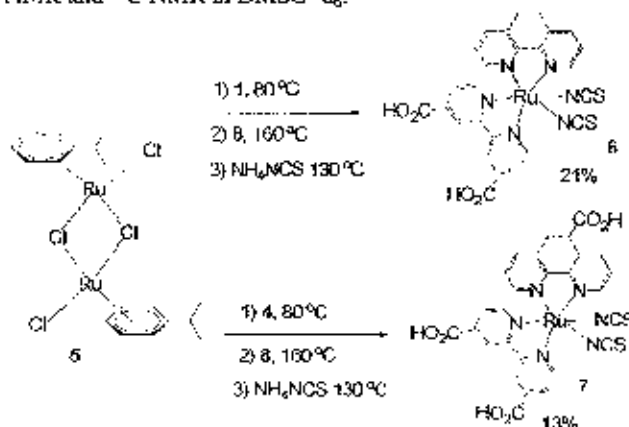


Fig. 3. The synthetic route of ruthenium phenanthroline 6 and 7

To study the electronic transition of the ruthenium complexes, the absorption spectra of the dyes in DMF solution are displayed in Figure 4. Three absorption bands are observed in the 300–800 nm region; the first band below 350 nm is attributed to the intraligand  $\pi-\pi^*$  transition of 4,4'-dicarboxylic acid-2,2'-bipyridine. The second band appeared from 360–390 nm is attributed to the  $\pi-\pi^*$  transition of the auxiliary phenanthroline ligand. The final band around 500–550 nm shows a

lower-energy MLCT band, that is the ruthenium  $d$  orbital to  $\pi^*$  orbital transition. As we expected, 1,10-phenanthroline-5-carboxylic acid ligand in complex 7 gives the high molar absorptivity and red shift compared with the parent complex. This result suggests that the high IPCE would be found in DSSC device.

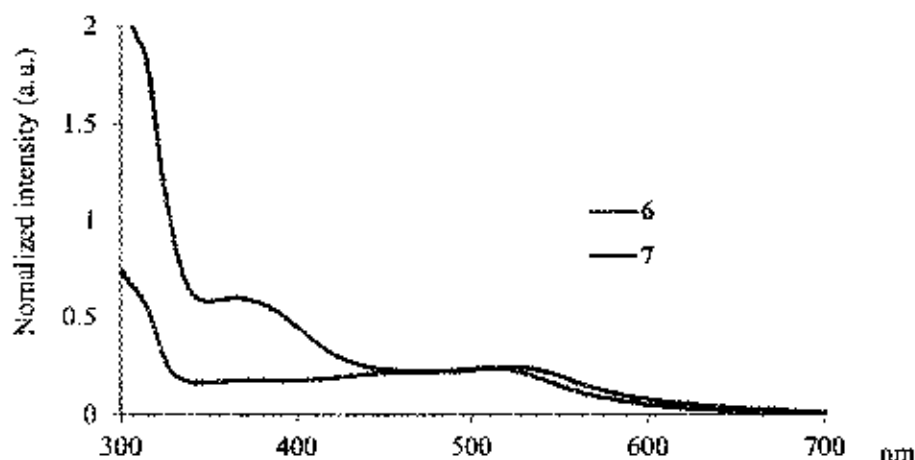


Fig. 4. Normalized absorption spectra of 6 and 7 in DMF ( $1.6 \times 10^{-4}$  M)

#### Conclusion

In conclusion, we have successfully synthesized and characterized the ruthenium dyes. Both complexes were characterized by  $^1\text{H}$  NMR,  $^{13}\text{C}$  NMR and UV-Vis spectroscopic techniques.

#### Acknowledgment

The authors would like to acknowledge the financial support from the Energy Policy and Planning Office (EPPO), Ministry of Energy, Thailand (07-01-53-027).

#### References

- [1] B. O'Regan, M. Grätzel, A low-cost, high-efficiency solar cell based on dye-sensitized colloidal  $\text{TiO}_2$  films, *Nature* 353 (1991) 737-740.
- [2] H. Imahori, T. Umeyama, S. Ito, Large p-aromatic molecules as potential sensitizers for highly efficient dye-sensitized solar cells, *Acc. Chem. Res.* 42 (2009) 1809-1818.
- [3] A. Mishra, M. Fischer, P. Bäuerle, Metal-free organic dyes for dye-sensitized solar cells: from structure-property relationships to design rules, *Angew. Chem. Int. Ed.* 48 (2009) 2474-2499.
- [4] M. K. Nazceruddin, A. Kay, I. Rodicio, R. Humphry-Baker, E. Mueller, P. Liska, N. Vlachopoulos, M. Grätzel, Conversion of light to electricity by cis- $\text{X}_2$ bis (2,2'-bipyridyl-4,4'-dicarboxylate) ruthenium(II) charge-transfer sensitizers ( $\text{X} = \text{Cl}^-$ ,  $\text{Br}^-$ ,  $\text{I}^-$ ,  $\text{CN}^-$ , and  $\text{SCN}^-$ ) on nanocrystalline titanium dioxide electrodes, *J. Am. Chem. Soc.* 115 (1993) 6382-6390.
- [5] Y. Luo, D. Li, Q. Meng, Towards optimization of materials for dye-sensitized solar cells, *Adv. Mater.* 21 (2009) 4647-4651.
- [6] A. Reynal, A. Fomeli, E. Palomares, Dye structure-charge transfer process relationship in efficient ruthenium-dye based dye sensitized solar cells, *Energy Environ. Sci.* 3 (2010) 805-812.

## New Family of Ruthenium-Dye-Sensitized Solar Cells (DSSCs) with a High Solar-Energy-Conversion Efficiency

Yuranan thathong, Kraisak Traipop,

Taweesak Sudyoadsuk and Rukkiat Jitchati\*

Center for Organic Electronic and Alternative Energy (COEA), Department of Chemistry, Faculty of Science, Ubon Ratchathani University, Warinchumrap, Ubon Ratchathani Province, 34190, Thailand

rukkiat\_j@hotmail.com

**Keywords:** Dye-sensitized solar cell (DSSCs); ruthenium complex; bipyridine; dipyrido phenazine

**Abstract.** Two ruthenium complexes (5 and 6) with bipyridine–dipyridophenazine auxiliary ligands have been synthesized in an attempt to increase the  $\pi$ -conjugated system as well as to increase the optical extinction coefficient. Structural characterization was determined by proton NMR spectra. The photophysical and electrochemical were studied by UV-Vis and cyclic voltammetry, respectively. The DSSCs fabrications of both ruthenium dyes were studied under 1.5 AM standard irradiation ( $100 \text{ mWcm}^{-2}$ ) and reported in the factor of solar-light-to-electricity conversion efficiency, a short-circuit current density, an open-circuit photovoltage, and a fill factor (compared with N3 dye).

### Introduction

The development of a new ruthenium complex have long been attractive which is considered as a material for solar cell as called dye-sensitized solar cells (DSSCs) [1,2]. The ruthenium dyes was studied in 1991 which named N3 [3]. The N3 derivative called N719 has also been developed and has shown more promising efficiency of about 11% [4]. Until now, these two materials have been used as the standard complexes to benchmark other new synthetic dyes in the dye-sensitized solar cell system [5,6].

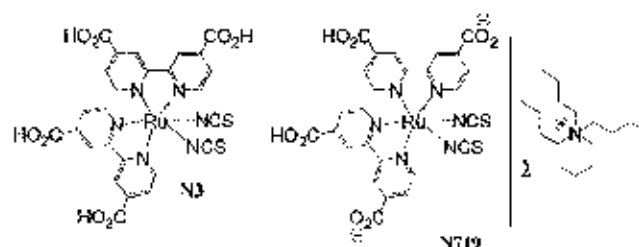


Fig. 1. The molecular structures of N3 and N719 dyes

Herein, we report the synthesis of two ruthenium complexes with dipyrido[3,2-a:2',3'-c]phenazine and bipyridine ligand which both complexes were characterized and studied for DSSC application.

### Materials and methods

4,4'-Dicarboxylic-2,2'-bipyridine (1) and ruthenium cymene complex (2) were synthesized as reported [7,8]. Anhydrous dimethyl formamide (DMF) was distilled using calcium hydride before used.  $^1\text{H}$  and  $^{13}\text{C}$  NMR spectra were recorded on a Bruker Avance 300 spectrometer. Chemical shifts are quoted downfield from internal standard TMS. IR spectra were measured on a Perkin-Elmer FT-IR spectroscopy spectrometry RX1 spectrometer as KBr or NaCl disc. Melting points were measured in open-end capillaries using a Büchi 530 melting point apparatus. The temperatures at the melting points were ramped at  $2.5^\circ\text{C}/\text{min}$  and were uncorrected.

**1,10-Phenanthroline-5,6-dione (3)** [9]: phenanthroline (1.00 g, 5 mmol) and potassium bromide (5.95 g, 50 mmol) were added to a mixture of sulfuric acid (20 ml) and nitric acid (10 ml) and refluxed for 4 hrs. After the reaction mixture was cooled to room temperature, the content was poured into 400 ml of ice water with added aq. NaOH. The pH was adjusted to 7 by adding sodium carbonate. The resulting product was extracted with dichloromethane. After removed solvent by rotary evaporator, the orange solid was then allowed to recrystallize from acetone. The target compound **3** was obtained (0.25 g, 24%), m.p. 240-249 °C;  $^1\text{H NMR}$  ( $\text{CDCl}_3$ , 300 MHz): 7.59 (dd,  $J = 7.9$  Hz,  $J = 4.7$  Hz, 1H), 8.51 (dd,  $J = 7.9$  Hz,  $J = 1.8$  Hz, 1H), 9.12 (dd,  $J = 4.7$  Hz,  $J = 1.8$  Hz, 1H);  $^{13}\text{C NMR}$  ( $\text{CDCl}_3$ , 75 MHz):  $\delta$  125.6, 137.3, 156.4, 178.7; IR (KBr) 736, 1423, 1566, 1646, 1690, 1703, 3048, 3436, 3563  $\text{cm}^{-1}$ .

**Dipyrido[3,2-a:2',3'-c]phenazine (4)**: 1,10-phenanthroline-5,6-dione (**3**) (0.25 g, 1.19 mmol) and *o*-phenyldiamine (0.26 g, 2.41 mmol) were dissolved in 10 ml ethanol. The reaction mixture was then refluxed for 1 hr. The target product was separated as a brown powder by vacuum filtration and washed by ethanol (0.28 g, 84%); mp 225-230 °C;  $^1\text{H NMR}$  (300 MHz,  $\text{CDCl}_3$ )  $\delta$  9.64 (dd,  $J = 8.1$ , 1.6 Hz, 2H), 9.27 (dd,  $J = 4.4$ , 1.6 Hz, 2H), 8.36 (dd,  $J = 6.5$ , 3.4 Hz, 2H), 8.01 - 7.92 (m, 2H), 7.92 - 7.73 (m, 2H); IR (NaCl) 521, 1075, 1363, 1493, 1639, 2335, 3365  $\text{cm}^{-1}$ .

**Di(isothiocyanato)(4,4'-dicarboxylic-2,2'-bipyridine)(dipyrido[3,2-a:2',3'-c]phenazine)ruthenium(II) (5)**: compound **1** (0.09 g, 0.34 mmol) and ruthenium cymene complex (**2**) (0.11 g, 0.17 mmol) were dissolved in DMF (25 ml). The reaction mixture was heated to 80 °C and stirred for 4 hrs in the dark under nitrogen balloon. Then, **4** (0.08 g, 0.34 mmol) was added to the reaction at 160 °C for 4 hrs. Finally, an excess of  $\text{Ni}(\text{L})_2\text{SCN}$  (190 mg) was added at 130 °C for 5 hrs. After the reaction was cooled to room temperature, the DMF solvent volume was removed by a rotary evaporator. The solid residue was dissolved with water and filtered with a sintered glass crucible. The resulting dark solid was dissolved by 1M NaOH in MeOH and further purified on a sephadex LH-20 column chromatography using MeOH as an eluent. The major band was concentrated and the residue was redissolved with water. The initial pH was adjusted to 3 by 0.02 M  $\text{HNO}_3$  then filtered on a sinter glass to collect the target complex as a red-brown solid (0.03 g, 25%);  $^1\text{H NMR}$  (300 MHz,  $\text{CD}_3\text{OD}$ )  $\delta$  9.86 (d,  $J = 7.7$  Hz, 1H), 9.77 (s, 1H), 9.63 (s, 1H), 9.52 (d,  $J = 12.7$  Hz, 2H), 9.11 (d,  $J = 8.0$  Hz, 2H), 8.94 (s, 1H), 8.49 (d,  $J = 13.7$  Hz, 2H), 8.36 (s, 2H), 8.09 (s, 2H), 7.94 (s, 1H), 7.83 (d,  $J = 5.6$  Hz, 1H), 7.78 - 7.63 (m, 2H), 7.30 (s, 1H); IR (NaCl) 1232, 1357, 1610, 1711, 2105, 2922, 3073, 3413  $\text{cm}^{-1}$ .

**Tetrabutylammonium di(isothiocyanato) (4'-carboxy-2,2'-bipyridine-4-carboxylate) (dipyrido[3,2-a:2',3'-c]phenazine)ruthenium(II) (6)**: this complex was prepared by using a similar procedure as described for complex **5**. However, in the final step, the resulting solid was dissolved with 1M TBAOH instead of 1M NaOH and purified by a sephadex LH-20 to give the dark red solid as a target product **6** (0.16 g, 62%);  $^1\text{H NMR}$  (300 MHz, MeOD)  $\delta$  9.83 (dd,  $J = 11.0$ , 7.1 Hz, 2H), 9.68 (d,  $J = 5.6$  Hz, 1H), 9.46 (d,  $J = 8.1$  Hz, 1H), 9.10 (d,  $J = 14.7$  Hz, 1H), 8.90 (s, 1H), 8.58 - 8.39 (m, 2H), 8.34 (dd,  $J = 12.1$ , 4.2 Hz, 2H), 8.07 (dd,  $J = 9.0$ , 5.2 Hz, 2H), 7.98 (s, 1H), 7.81 (d,  $J = 5.8$  Hz, 1H), 7.78 - 7.70 (m, 1H), 7.66 (dd,  $J = 11.6$ , 6.2 Hz, 1H), 7.51 (d,  $J = 5.5$  Hz, 1H), 3.23 (d,  $J = 9.1$  Hz, 8H), 1.65 (d,  $J = 7.1$  Hz, 8H), 1.50 - 1.31 (m, 8H), 1.02 (t,  $J = 7.2$  Hz, 12H); IR (NaCl) 1030, 1115, 1357, 1628, 2105, 2927, 3440  $\text{cm}^{-1}$ .

**Fabrication of DSSC**: The transparent (Ti-Nanoxide 20T/SP, Solaronix) and a scattering (Ti-Nanoxide R/SP, Solaronix)  $\text{TiO}_2$  layer were prepared by a screen-printing method on a transparent FTO glass (8  $\Omega/\text{sq}$ , Solaronix) and then sintered at 450 °C for 30 minute and cooled to 80 °C. The nanocrystalline  $\text{TiO}_2$  films were coated with dyes by dipping the film in  $3 \times 10^{-4}$  M dye solutions in ethanol overnight. The dye-coated  $\text{TiO}_2$  electrode was incorporated into a thin-layer sandwich-type cell with a Pt-coated FTO as counter electrode, a spacer film, and an organic electrolyte solution to measure the solar cell performance. The Pt counter electrode was prepared by spin-coating a 7 mM  $\text{H}_2\text{PtCl}_6$  in 3-methoxyethanol solution on FTO glass followed by sintering at 385 °C for 30 minute. The electrolyte contained 0.05M  $\text{I}_2$ , 0.1M LiI, 0.4 M *t*-butylpyridine (tBPY), and 0.6 M tetrapropyl ammonium iodide (TPAI) in 85:15v/v acetonitrile/valeronitrile solvent was used.

Light-to-electricity conversion efficiency values were measured using Newport sun simulator 96000 equipped with an AM 1.5 G filter. The current density-voltage of DSSCs was measured by Keithley 2400 source meter unit in a terminal sense configuration.

### Results and discussions

All ligands were synthesized in our laboratory as described in the experiment section. Two ruthenium complexes were synthesized by a similar method from 4,4'-dicarboxylic-2,2'-bipyridine (**1**) and dipyrido[3,2-a:2',3'-c]phenazine (**4**) to give our target products **5** and **6** in 25% and 62% yield, respectively. Both complexes were fully characterized by  $^1\text{H}$  NMR and IR spectra.

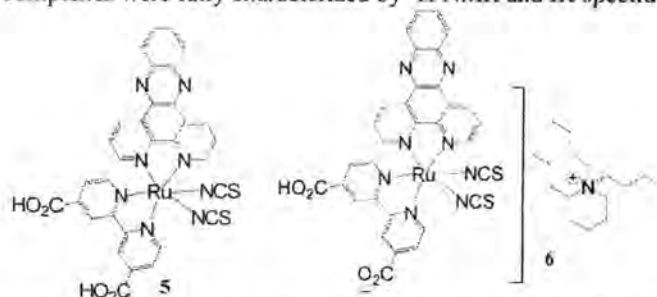


Fig. 2. The molecular structure of ruthenium phenazine **5** and **6**

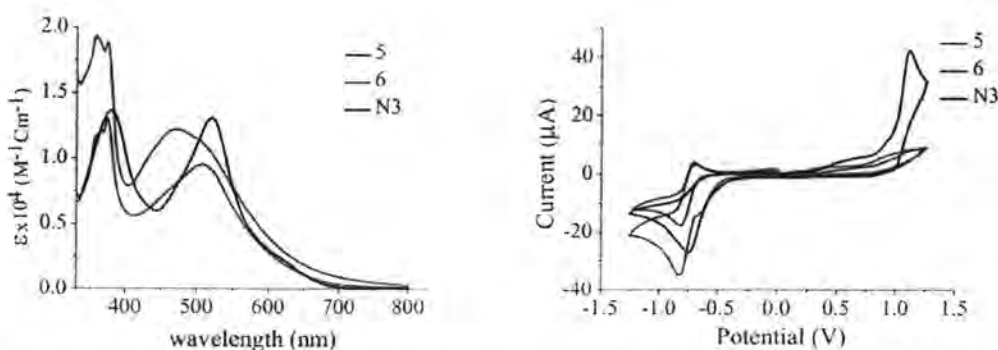


Fig. 3. a)  $1.6 \times 10^{-4}$  M solution absorption spectra b)  $1 \times 10^{-3}$  M cyclic voltammograms of **5**, **6** and **N3** (in DMF)

Both complexes were studied the UV-Vis absorption spectra in DMF solution as the spectra shown in Fig. 3. The two major absorption bands are observed around 400 and 500 nm. The first band is attributed to the  $\pi-\pi^*$  of ligand bipyridine. The second band appeared the  $\pi-\pi^*$  transition of the phenazine ligand and MLCT transition of the ruthenium  $d$  to  $\pi^*$  orbital. We should note that the UV-Vis absorption of our ruthenium complexes are red-shifted to 500 nm compared with the parent **N3** dye. The cyclic voltammograms of **5** and **6** in a DMF solution containing 0.1 M TBAPF<sub>6</sub> as supporting electrolyte, scan rates at  $100 \text{ mVs}^{-1}$ , when the potential is scanned between  $-1.25$  and  $1.25$  V. Both **5** and **6** complexes show chemically reversible oxidation waves at 1.08, which can be attributed to the one electron oxidation of ruthenium center in both dyes. Compared to the standard **N3** dye, the metal center oxidation of **5** and **6** is cathodically shifted by 30 mV indicating the electron-rich character of the pyrazine units. We then fabricated DSSCs using **5**, **6** and **N3** complexes with composed of  $0.25 \text{ cm}^2$  dye-adsorbed  $\text{TiO}_2$  film, 0.05 M  $\text{I}_2$ , 0.1 M LiI, 0.4 M tBPY, and 0.6 M TPAI as the electrolyse under AM 1.5 G illumination ( $100 \text{ mWcm}^{-2}$ ). The preliminary results suggested that the maximum efficiency for the **6**-sensitized  $\text{TiO}_2$  solar cell was calculated to be 1.84%, with a short-circuit current ( $J_{sc}$ ) of  $4.52 \text{ mAcm}^{-2}$ , an open-circuit photovoltage ( $V_{oc}$ ) of 0.51 V, and a fill factor (FF) of 0.71. To be able to make a fair comparison, the DSSC performance of **N3** was also optimized in the current study. As a result, the efficiency for the **N3** was 5.97%, with a  $J_{sc}$  of

13.78  $\text{mAcm}^{-2}$ , a  $V_{oc}$  of 0.67 V, and a FF of 0.64. In another approach, the conversion efficiency of the 5-sensitized solar cell was apparently lower, with a  $J_{sc}$  of 1.18  $\text{mAcm}^{-2}$ , a  $V_{oc}$  of 0.50 V, a FF of 0.63, and consequently an energy-conversion efficiency of only 0.38% was deduced. It should be noted that the very low conversion efficiency of both ruthenium 5 and 6 dyes could be explained by the low solubility in ethanol solvent in the dipping step. However, we can further optimize our DSSCs in the future.

### Conclusion

In conclusion, we have successfully synthesized and characterized the ruthenium dyes. Both ruthenium 5 and 6 complex structures were characterized by  $^1\text{H}$  NMR and IR spectra. We found that both complexes show similar cyclic chromatogram and UV-Vis spectra. The preliminary data of the conversion efficiency show 1.84% and 0.38% for 5 and 6, respectively.

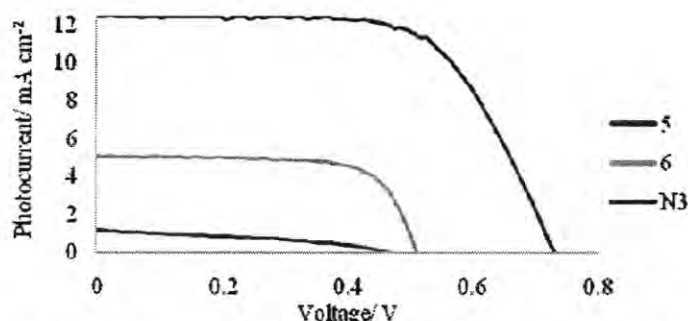


Fig. 4. Photocurrent density–voltage ( $J$ - $V$ ) characteristics of a device using 5 and 6 as sensitizer

### Acknowledgment

The authors would like to acknowledge the financial support from energy policy and planning office (EPPO), Ministry of Energy, Thailand (07-01-53-027).

### References

- [1] B. O'Regan, M. Grätzel, A low-cost, high-efficiency solar cell based on dye-sensitized colloidal  $\text{TiO}_2$  films, *Nature* 353 (1991) 737-740.
- [2] Y. Thathong, K. Wongkhan, R. Jitchati, Two Ruthenium Complexes with Phenanthroline Ligand for Dye-Sensitized Solar Cells, *Adv. Mat. Res.* 651 (2013) 115-119.
- [3] M. K. Nazeeruddin, A. Kay, I. Rodicio, R. Humphry-Baker, E. Mueller, P. Liska, N. Vlachopoulos, M. Grätzel, Conversion of light to electricity by cis- $\text{X}_2\text{bis}(2,2'$ -bipyridyl-4,4'-dicarboxylate)ruthenium(II) charge-transfer sensitizers ( $\text{X} = \text{Cl}^-$ ,  $\text{Br}^-$ ,  $\text{I}^-$ ,  $\text{CN}^-$ , and  $\text{SCN}^-$ ) on nanocrystalline titanium dioxide electrodes, *J. Am. Chem. Soc.* 115 (1993) 6382-6390.
- [4] Y. Luo, D. Li, Q. Meng, Towards optimization of materials for dye-sensitized solar cells, *Adv. Mater.* 21 (2009) 4647-4651.
- [5] A. Reynal, A. Forneli, E. Palomares, Dye structure-charge transfer process relationship in efficient ruthenium-dye based dye sensitized solar cells, *Energy Environ. Sci.* 3 (2010) 805-812.
- [6] Y. Sun, A. C. Onicha, M. Myahkostupov, F. N. Castellano, Viable alternative to N719 for dye-sensitized solar cells, *ACS Appl. Mater. Interfaces* 2 (2010) 2039-2045.
- [7] R. Jitchati, Y. Thathong, K. Wongkhan, A cheap synthetic route to commercial ruthenium N3 dye for sensitizing solar cell applications, *Adv. Mat. Res.* 488-489 (2012) 1049-1054.
- [8] R. Jitchati, Y. Thathong, K. Wongkhan, Three synthetic routes to a commercial N3 dye, *Int. J. App. Phy Mat.* 2 (2012) 107-110.
- [9] S. Goswami, R. Chakrabarty, Highly Selective Colorimetric Fluorescent Sensor for  $\text{Pb}^{2+}$ , *Eur. J. Org. Chem.* 2010 (2010) 3791-3795.